PRENTICE-HALL EE SERIES

Blackwell and Kotzebue

Semiconductor-Diode Parametric Amplifiers

INTERNATIONAL SERIES IN ENGINEERING

Semiconductor-Diode
Parametric Amplifiers

PRENTICE-HALL INTERNATIONAL SERIES IN ENGINEERING

BLACKWELL AND KOTZEBUE *Semiconductor-Diode Parametric Amplifiers*
DRESHER *Games of Strategy: Theory and Application*
EDMUNDSON, ED. *Proceedings of the National Symposium on Machine Translation*
KOLK *Modern Flight Dynamics*
STANTON *Numerical Methods for Science and Engineering*

PRENTICE-HALL, INC.
PRENTICE-HALL INTERNATIONAL, INC., UNITED KINGDOM AND EIRE
PRENTICE-HALL OF CANADA, LTD., CANADA
BERLINER UNION, WEST GERMANY AND AUSTRIA

Semiconductor-Diode Parametric Amplifiers

LAWRENCE A. BLACKWELL

Texas Instruments, Inc.

KENNETH L. KOTZEBUE

Watkins-Johnson Co.

Prentice-Hall, Inc., Englewood Cliffs, N. J.

1961

PRENTICE-HALL ELECTRICAL ENGINEERING SERIES

WILLIAM L. EVERITT, *Editor*

ANNER *Elements of Television Systems*
BALABANIAN *Network Synthesis*
BENEDICT *Introduction to Industrial Electronics*
BLACKWELL AND KOTZEBUE *Semiconductor-Diode Parametric Amplifiers*
DAVIS AND WEED *Industrial Electronic Engineering*
DEKKER *Electrical Engineering Materials*
DUNN AND BARKER *Electrical Measurements Manual*
EVANS *Experiments in Electronics*
FETT *Feedback Control Systems*
FICH *Transient Analysis in Electrical Engineering*
FICH AND POTTER *Theory of A-C Circuits*
FLORES *Computer Logic: The Functional Design of Digital Computers*
GOLDMAN *Information Theory*
GOLDMAN *Transformation Calculus and Electrical Transients*
HERSHBERGER *Principles of Communication Systems*
JORDAN *Electromagnetic Waves and Radiating Systems*
LO, ET AL *Transistor Electronics*
MARTIN *Electronic Circuits*
MARTIN *Physical Basis for Electrical Engineering*
MARTIN *Ultra High Frequency Engineering*
MOSKOWITZ AND RACKER *Pulse Techniques*
NIXON *Handbook of Laplace Transformation: Tables and Examples*
NIXON *Principles of Automatic Controls*
PARTRIDGE *Principles of Electronic Instruments*
PUMPHREY *Electrical Engineering*, 2nd
PUMPHREY *Fundamentals of Electrical Engineering*, 2nd
REED *Electric Network Synthesis*
REED *Foundation for Electric Network Theory*
RIDEOUT *Active Networks*
RYDER, F. L. *Creative Engineering Analysis*
RYDER, J. D. *Electronic Engineering Principles*, 3rd
RYDER, J. D. *Electronic Fundamentals and Applications*, 2nd
RYDER, J. D. *Networks, Lines and Fields*
SHEDD *Fundamentals of Electromagnetic Waves*
SKODER AND HELM *Circuit Analysis by Laboratory Methods*, 2nd
SOOHOO *Theory and Application of Ferrites*
STOUT *Basic Electrical Measurements*, 2nd
THOMSON *LaPlace Transformation*, 2nd
VAIL *Circuits in Electrical Engineering*
VAN DER ZIEL *Noise*
VAN DER ZIEL *Solid State Physical Electronics*
VAN VALKENBURG *Network Analysis*
VON TERSCH AND SWAGO *Recurrent Electrical Transients*
WARD *Introduction to Electrical Enginnering*, 3rd
WARFIELD *Introduction to Electronic Analog Computers*
WEED AND DAVIS *Fundamentals of Electron Devices and Circuits*

Library of Congress Catalog Card Number: 61-12978

PRINTED IN THE UNITED STATES OF AMERICA

80619

Preface

The tempo of technological progress today is undeniably swift and at times rather startling. Often, before we are fully able to grasp the consequences of one development, another has made its appearance. The progress made in recent years on the achievement of low-noise amplification at microwave frequencies is certainly a good example. Up to a few years ago, it was largely a struggle for one tenth-decibel improvement in noise figure here and another there. Then, almost without warning, a deluge of low-noise devices was upon us. The "old" traveling-wave tube began to achieve noise figures comparable with the best resistive mixers, and soon achieved noise figures well below the supposed theoretical minimum. Quantum mechanics became a must for the aspiring electrical engineer with the introduction of "microwave amplification by stimulated emission"—the maser. Here was a device with a noise figure so low that it was some time before this quantity could even be measured! Close on the heels of the maser came the parametric amplifier. Not as low in noise as the maser, the parametric amplifier nevertheless quickly achieved a position of prominence—mainly because of its rather unbelievable simplicity.

The writing of a book in such an atmosphere of swift and unyielding progress is certainly not without its hazards. A "comprehensive" book is out of the question. A compilation of all the current literature runs the risk of having significant omissions by the time of publication. Today's statements of finality can become tomorrow merely historical curiosities. The present book will make no pretense as to completeness. The emphasis instead will be on the presentation of such basic information as will be of interest to the average design engineer who wants to know how and why parametric amplifiers work, and when they can be employed to advantage.

Further boundaries to the discussion can be summed up by the following three phrases: (1) semiconductor diodes; (2) low noise; and (3) microwave devices. Parametric devices can be based on electron beam and ferrite phenomena. Other embodiments will, no doubt, be forthcoming. The semiconductor-diode parametric amplifier, however, has the advantage of being the simplest device both in concept and construction, and currently is the most popular form of parametric amplifier. Many of the concepts presented here are by no means limited to diode devices: the concepts of energy transfer and general noise properties are, for example, of universal application. The emphasis on the low-noise aspects of these devices is mainly dictated by the fact that this characteristic is the major reason for the employment of parametric amplifiers. Because of this, and because of some confusion regarding the peculiar noise properties of parametric amplifiers, a fairly complete discussion of noise is incorporated. Finally, since it is largely in the microwave region that low-noise performance is both very useful and very difficult to obtain, whenever reference is made to actual devices, it will be made in the context of microwave devices.

The authors would like to express their sincere appreciation for the assistance and encouragement provided by Texas Instruments Incorporated during the writing of this book. We wish to especially thank Dr. J. R. Baird, T. M. Hyltin, and B. T. Vincent, Jr. for many helpful discussions and suggestions. It is also a pleasure to acknowledge the help of R. E. Allan, T. Pedersen, and Mrs. Betty Chupik for much of the computational work. Special thanks are also due Dr. J. J. Spilker, Jr. for his assistance in the analysis of the noise characteristics of degenerate parametric amplifiers.

L. A. Blackwell
K. L. Kotzebue

Los Angeles, California

Contents

1

Introduction to Parametric Devices

The name *parametric amplifier* has become associated with a class of amplifying and frequency-converting devices which utilize the properties of nonlinear or time-varying reactances. Other names have also been proposed and used in connection with these devices, such as variable-parameter amplifiers, reactance amplifiers, and MAVAR's (Microwave Amplification, by VAriable Reactance). While these alternative names may have their merits in being possibly more descriptive, it appears that the term parametric amplifier is in preferred use today. To repeat, the distinguishing feature of a parametric device is the presence of a nonlinear or time-varying reactance. This reactance can be either electrical or mechanical; that is, it can store either electromagnetic energy or mechanical energy. The function of this reactance is to channel energy from an a-c source to a useful load. In this sense, a parametric amplifier is similar to a vacuum tube amplifier. The vacuum tube is essentially a variable *resistance* which converts d-c energy to useful a-c energy. Perhaps this analogy can even be stretched to suggest that a parametric amplifier is capable of lower-noise amplification than a vacuum tube. The essential feature of a vacuum tube is a *resistance*, and we know that any resistor at a non-zero temperature exhibits noise properties. The essential feature of a parametric amplifier, however, is a nonlinear *reactance*, and we know that reactance does not contribute thermal noise to a circuit. We might anticipate then, that parametric amplifiers can be low-noise devices.

As is the case of almost all inventions, the "discovery" of the parametric amplifier came much later than the discovery of the basic principles of operation. Many of the essential properties of nonlinear energy-storage systems, including instability (a so-called negative-resistance effect) were described by Faraday[40] as early as 1831 and by Lord Rayleigh[123] in 1883. R. V. L. Hartley[49] in 1936 discussed in great detail an electro-mechanical nonlinear capacitance device very similar to today's negative-resistance parametric amplifier. In a sense, H. Q. North[98] discovered the semiconductor parametric amplifier during World War II when he observed a crystal mixer with net conversion gain instead of the usual conversion loss. With the passing of time, various experimental and theoretical papers were published describing circuits with nonlinear reactive elements. Manley and Peterson[92] described negative resistance effects in circuits containing saturable reactors; Landon[81] analyzed and gave experimental results of such circuits used as converters, amplifiers, and oscillators; and van der Ziel[139] analyzed circuits containing nonlinear capacitance. In his paper, van der Ziel first mentioned that such a circuit might be useful as a low-noise amplifier.

The ingredients were all there, but it was almost ten years after the publication of van der Ziel's paper that the parametric amplifier was "discovered." The age of *solid-state electronics* dawned, and microwave engineers and scientists dreamed of a solid-state microwave amplifier to replace their noisy and fragile electron-beam devices. The maser had already been born, but had failed to satisfy completely the appetites of the microwave designer. What was needed was a device with the low-noise properties of the maser, but the mechanical simplicity of the transistor. It was at this point that H. Suhl[125] proposed a microwave solid-state amplifier using ferrite. Shortly later M. T. Weiss[147] announced the experimental verification of Suhl's proposal. These two announcements supplied the needed catalyst, and the parametric amplifier was at last "discovered."

The parametric amplifier has become a useful device largely because of its low-noise properties. It has made possible for the first time the construction of receiving systems, without the use of cryogenic techniques, which are so sensitive that the antenna noise now often will equal or exceed the total receiver noise contribution. In the succeeding chapters of this book, we will explore the operating principles of these devices, present a few design criteria for their construction, make some comments regarding specific areas of application, and describe the characteristics of several typical operating units.

1.1 Some Principles of Nonlinear and Time-varying Reactances

A reactance may be defined as a circuit element that stores and transfers electromagnetic energy, as opposed to a resistance which is an element that dissipates energy. If the stored energy is predominantly in the electric field, the reactance is said to be capacitive; if the stored energy is predominantly in the magnetic field, the reactance is said to be inductive. In many applications, even at microwave frequencies, it is most convenient to speak in terms of voltages and currents rather than electric or magnetic fields. A capacitive reactance may then be defined as an element for which a functional relation between charge q and voltage v can be written

$$q = f(v). \tag{1.1}$$

Similarly, an inductive reactance may be defined as an element for which a functional relation between flux ϕ and current i can be written

$$\phi = f(i). \tag{1.2}$$

Note that, for a resistive element, the functional relation involves the *time derivative* of charge or flux and the voltage or current. Thus, for example, we can write for a resistive element

$$\dot{q} = f(v). \tag{1.3}$$

A reactance is said to be *linear* if the particular functional relationship happens to be a linear one. For example, a linear capacitance implies a linear relation between charge and voltage.

$$q = Cv \tag{1.4}$$

where C is defined as the capacitance of the reactive element. Similarly, a *linear* inductance implies a linear relation between flux and current. Therefore,

$$\phi = Li \tag{1.5}$$

where L is defined as the inductance of the reactive element.

If these relations are *not* linear, the reactance is said to be *nonlinear*. For example, if the relation between charge and voltage happens to be

$$q = av^2 \tag{1.6}$$

the element is said to be a nonlinear capacitance. In this case, it is convenient to define capacitance as the partial derivative of charge with respect to voltage.

$$C = \frac{\partial q}{\partial v}. \tag{1.7}$$

The analogous definition of inductance is

$$L = \frac{\partial \phi}{\partial i}. \tag{1.8}$$

Since there is no essential difference in the analysis of circuits containing nonlinear inductances rather than capacitances, no further mention of the inductance case will be made, it always being assumed that the two are interchangeable by duality.

If the relation between charge and voltage is linear, as in (1.4), but the coefficient C happens to be a function of time, the resulting capacitance is said to be linear, but time-varying. For example, if we were to have a parallel-plate capacitor whose plate spacing were varied in time by some external means, we would have such a time-varying linear capacitance.

Mathematically speaking, there is a great deal of difference between circuits containing nonlinear reactances and those containing time-varying linear reactances. In the latter case, the principle of superposition holds, and powerful analytical techniques are available, such as Fourier analysis and the theory of Mathieu's and Hill's equations. In the case of nonlinear circuits, superposition fails and the difficulty of exact analysis is substantially increased. From the standpoint of circuit performance, however, the two cases yield quite similar results. Both will cause frequency mixing, and as will be shown later, both will be capable of creating a transfer of power from one frequency to another.

1.2 The Manley-Rowe Power Relations

Manley and Rowe[93] have derived a very general set of equations relating power flowing into and out of an ideal nonlinear reactance. These relations are a powerful tool in predicting whether or not power gain is possible in a given situation, and in predicting the maximum gain that can be achieved.

To help picture the problem which they analyzed, consider Fig. 1.1. Here we have two voltage generators at frequencies f_1 and f_2 together with associated series resistances and band-pass filters, placed across a nonlinear capacitor. These filters are designed to reject power at all frequencies other than their respective signal frequencies. In addition to the two signal generators, an infinite array of load resistances and band-pass filters are also connected to the nonlinear capacitor. These filters are tuned to the various sum and difference frequencies which will arise because of the nonlinear reactance. The sign convention will be used that power flowing *into* the nonlinear capacitance is positive (*e.g.*, the power coming from the two signal generators), while power flowing *from* the capacitance (*e.g.*, the power flowing into the load resistances) will be negative in sign.

The equations they obtained (derived in the Appendix) are

$$\sum_{m=0}^{\infty} \sum_{n=-\infty}^{\infty} \frac{mP_{m,n}}{mf_1 + nf_2} = 0 \tag{1.9}$$

$$\sum_{n=0}^{\infty} \sum_{m=-\infty}^{\infty} \frac{nP_{m,n}}{mf_1 + nf_2} = 0 \tag{1.10}$$

where $P_{m,n}$ is the power flow into the reactance at frequency mf_1 and nf_2. These relations are remarkable in that they are independent of the shape of the nonlinear characteristic and the power levels involved.

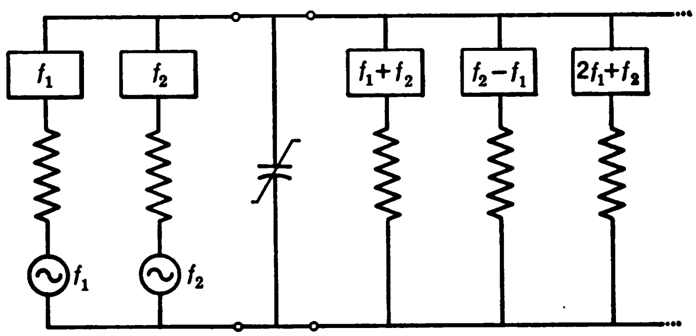

Figure 1.1. Circuit model for Manley-Rowe derivation

The usefulness of the Manley-Rowe power relations can be illustrated by several cases in which power flow at only three frequencies is allowed. Let the signal generator at f_1 represent a signal source, and the generator at f_2 the so-called pump source. Consider first the case where power flow is allowed at a frequency f_3 which is the sum of f_1 and f_2. Then (1.9) reduces to

$$\frac{P_1}{f_1} + \frac{P_3}{f_3} = 0 \tag{1.11}$$

and (1.10) reduces to

$$\frac{P_2}{f_2} + \frac{P_3}{f_3} = 0. \tag{1.12}$$

Since we are supplying energy to the nonlinear reactance at frequency f_1, P_1 is positive. Eq. (1.11) thus tells us that the power P_3 is negative; that is, P_3 flows *from* the reactance and to our resistive termination at f_3. We can define a gain which is the ratio of the power delivered by the reactance at frequency f_3 to that absorbed by the reactance at frequency f_1. From (1.11), this gain is seen to be

$$\text{gain}_{1-3} = \frac{f_3}{f_1}. \tag{1.13}$$

Here we have the first example of a so-called parametric device, variously called a sum-frequency amplifier or up-converter. The maximum transducer gain that can be obtained with such a device is precisely as given by (1.13) regardless of the circuit configuration or shape of nonlinearity. In practice, circuit reactance and loss influences the operating characteristics, and a detailed analysis is necessary for a complete description; nevertheless, some of the general characteristics are readily deduced from the Manley-Rowe relations.

As a second example, let the signal frequency be the sum of pump frequency and output frequency. Equation (1.11) predicts that the device will have a gain of

$$\text{gain}_{3-1} = \frac{f_1}{f_3} \tag{1.14}$$

which, in this case, will be a loss.

For a third example, let power flow at a frequency equal to the difference between pump and signal. That is, now let f_1 be the signal frequency, f_2 the output frequency, and f_3 the pump frequency with $f_1 + f_2 = f_3$. We are now supplying power at f_3, hence P_3 is positive. In this case, *both* P_1 and P_2 are negative. That is, the reactance delivers power to the signal generator at f_1 rather than absorbing it. If we define a gain which is the ratio of power supplied to the generator resistance at f_1 by the nonlinear reactance to that supplied by the signal generator itself, we see that infinite gain is possible, for the reactance can deliver power at f_1 regardless of whether a signal generator at f_1 is delivering power or not. That is, the Manley-Rowe relations predict that such a device is potentially unstable and is capable of oscillation both at f_1 and f_2. This is another example of a parametric device, often called a negative-resistance parametric amplifier.

1.3 Methods of Analysis

The analysis of parametric devices often involves the analysis of nonlinear circuits. While there is, in general, no method by which exact solutions can be obtained, various approximate methods give results which are quite satisfactory in most applications. Perhaps the most well-known method is the so-called small-signal approximation. In this approximation, it is assumed that the signal voltage is small compared to the pump voltage. (In the theory of resistive mixers, it would be said that the signal level is small relative to the local oscillator.) Another method, which will be shown to be equivalent to the small-signal approach, is that of replacing the nonlinear reactance with a time-varying linear reactance. A third method, which for lack of a better name will be called the large-signal approach, is to expand the nonlinear characteristic in a Taylor series about a d-c point and consider only the first few terms. While mathematically similar to the usual small-signal theory, the signal voltage need not be small compared to the pump voltage, and hence some saturation effects are predictable.

Small-signal Method

In the analysis of parametric devices, we are interested in computing the mixing effects that occur when voltages at two or more different frequencies are impressed on a nonlinear reactance. As a simple example, let us consider the case when two voltages are present, one at a frequency $\omega = 2\pi f$, and one at a frequency 2ω. One quantity of interest is the resultant current at frequency ω, for by dividing this current by the assumed voltage at ω we can obtain an equivalent linear admittance which the remainder of the circuit sees at ω. Once this admittance is determined, the significant properties of the parametric device can be obtained by linear analysis.

The so-called *small-signal* analysis applies when one r-f voltage (the signal voltage) is small compared to another r-f voltage (the pump voltage). In the study of low-noise amplifiers, for example, the small-signal approach is certainly justified since we are interested in signal voltages which are typically more than 100 db below the level of the pump. Let the two voltages be

$$v_1 = V_1 \cos \omega t, \qquad v_2 = V_2 \cos 2\omega t \tag{1.15}$$

where $V_1 \ll V_2$. Because $V_1 \ll V_2$, we can expand the charge on the capacitor in a Taylor series about v_2 and consider only the first two terms.

$$q(v) \approx q(v_2) + \frac{dq}{dv}(v_2)v_1. \tag{1.16}$$

For convenience, let us define a *capacitance* by

$$C(v_2) = \frac{dq}{dv}(v_2). \tag{1.17}$$

The current through the capacitor is given by the time derivative of the charge.

$$i = \frac{dq}{dt} = \frac{d}{dt}q(v_2) + \frac{d}{dt}[C(v_2)V_1 \cos \omega t]. \tag{1.18}$$

Since $C(v_2)$ is periodic with a fundamental frequency of 2ω, we can also expand it in a Fourier series. Assuming that we choose our time reference to make $C(v_2)$ an even function, we obtain

$$C(v_2) = \sum_{n=0}^{\infty} C_n \cos 2n\omega t. \tag{1.19}$$

We can interpret $C(v_2)$ as a time-varying *linear* capacitance in this approximation, for we see that the second term of Eq. (1.18) is of the form

$$\frac{d}{dt}[C(t)v(t)]$$

which was shown in Section 1.1 to be the result obtained for a linear but time-varying capacitance. The C_n coefficients can be interpreted as the magnitude of each harmonic of this time-varying capacitance. That is, C_0 gives the magnitude of the constant capacitance, C_1 the magnitude of the capacitance variation at 2ω, etc.

Using Eq. (1.18) and (1.19), the current component at the frequency ω can be computed to be

$$\begin{aligned} i(\omega) &= \frac{d}{dt}[(C_1 \cos 2\omega t)(V_1 \cos \omega t)] \\ &= \frac{d}{dt}\left[\frac{C_1V_1}{2}\cos \omega t\right] = -\frac{\omega C_1 V_1}{2}\sin \omega t. \end{aligned} \tag{1.20}$$

From the foregoing analysis it is seen that insofar as small-signal effects at the *signal* frequency are involved, a circuit containing a *nonlinear* reactance can be replaced by a time-varying *linear* reactance.

Large-signal Method

The preceeding small-signal approach cannot be used to predict saturation effects since the signal level must remain small relative to the pump level. However, if we choose to expand our relation for charge about a d-c point rather than an a-c point, we need not restrict the magnitude of one r-f voltage relative to another. We do need to specify, however, that the a-c excursions be relatively small so that again only a few terms in the Taylor series expansion will be necessary to adequately represent the circuit. Expanding the charge about a bias voltage V_0,

$$q(v) \approx q(V_0) + \frac{dq}{dv}(V_0)[v_1 + v_2] + \frac{1}{2}\frac{d^2q}{dv^2}(V_0)[v_1 + v_2]^2. \tag{1.21}$$

Here no restriction is placed on the magnitude of the signal voltage relative to the pump voltage. Let

$$\begin{aligned} \frac{dq}{dv}(V_0) &= C_0, \qquad & v_1 &= V_1 \cos \omega t \\ \frac{d^2q}{dv^2}(V_0) &= C_1', \qquad & v_2 &= V_2 \cos 2\omega t. \end{aligned} \tag{1.22}$$

The current component due to the nonlinear mixing is

$$i = \frac{d}{dt}[\tfrac{1}{2}C_1'(v_1 \cos \omega t + v_2 \cos 2\omega t)^2]. \tag{1.23}$$

The component of this at frequency ω is

$$i(\omega) = \frac{d}{dt}\left[\frac{C_1'V_1V_2}{2}\cos \omega t\right] = -\frac{\omega_1 C_1' V_2}{2} V_1 \sin \omega t. \tag{1.24}$$

Comparing this result with that obtained by the small-signal analysis, we see that at *frequency* ω the results are identical if

$$C_1'V_2 = C_1. \tag{1.25}$$

C_1' may be interpreted as the slope of the capacitance-versus-voltage curve and therefore $C_1'V_2$ may be interpreted as the amplitude of the capacitance change at the pump frequency.

In addition to yielding information about mixing effects at frequency ω, this *large-signal* approach also yields similar information at the pump frequency 2ω. It is this additional information, not obtainable from the small-signal approach, which is useful in predicting the effects of signal voltage on the remainder of the circuit. One such effect will be shown to be a gain-limiting phenomena which contributes to saturation in a negative-resistance parametric amplifier.

The Small-signal Linearized Admittance Matrix

In many types of parametric circuits we are interested in determining current flow through a nonlinear capacitor when it is assumed that small signal voltages are allowed to exist across the capacitor only at two or three frequencies. Usually these frequencies will be:

1. the impressed signal frequency,
2. the difference between pump and signal frequencies,
3. the sum of pump and signal frequencies.

Because this situation occurs so frequently in analysis, it is convenient to evaluate these currents as a function of the voltage, obtaining an equivalent linearized admittance matrix. The nonlinear element can then be replaced in our circuit by this matrix whenever we wish to compute the small-signal characteristics of a parametric device (assuming that no other frequencies are of significance).

To construct this matrix, we will deal with real quantities in complex form. For example, the capacitance variation will be expressed as

$$C(t) = C_0(1 + 2\gamma_1 \cos \omega_3 t) = C_0 + \overset{C_0}{\wedge}\gamma_1[e^{j\omega_3 t} + e^{-j\omega_3 t}] \tag{1.26}$$

where C_0 and γ_1 are real quantities. In a similar manner the small-signal voltages and currents at frequencies ω_1, ω_2, and ω_4 will be expressed as

$$v = V_1e^{j\omega_1 t} + V_1{}^*e^{-j\omega_1 t} + V_2e^{j\omega_2 t} + V_2{}^*e^{-j\omega_2 t} + V_4e^{j\omega_4 t} + V_4{}^*e^{-j\omega_4 t}$$

$$i = I_1e^{j\omega_1 t} + I_1{}^*e^{-j\omega_1 t} + I_2e^{j\omega_2 t} + I_2{}^*e^{-j\omega_2 t} + I_4e^{j\omega_4 t} + I_4{}^*e^{-j\omega_4 t} \tag{1.27}$$

W_1 : signal

where

$$\omega_1 + \omega_2 = \omega_3$$

W_3 : pump

$$\omega_1 + \omega_3 = \omega_4.$$

The coefficients V_1, V_2, V_4, I_1, I_2, I_4 are complex quantities containing phase information. The overall expressions for v and q at any given frequency, however, are real since they consist of the sum of a quantity and its complex conjugate.

The small-signal current and voltage are related according to the following equation, as was indicated in the previous discussion:

$r_n = \frac{C_n}{2C_0}$

$$i = \frac{d}{dt}[C(t)v(t)]. \tag{1.28}$$

Substituting the values of voltage, Eq. (1.27), into Eq. (1.28), three equations for current are obtained, one for each frequency. These resulting equations can be expressed in the following matrix form:

$C = C_0 - C_1 \cos \omega t$
$+ C_2 \cos 2\omega t$
$- C_3 \cos 3\omega t$

$$\begin{bmatrix} I_2{}^* \\ I_1 \\ I_4 \end{bmatrix} = \begin{bmatrix} -j\omega_2 C_0 & -j\omega_2\gamma_1 C_0 & 0 \\ j\omega_1\gamma_1 C_0 & j\omega_1 C_0 & j\omega_1\gamma_1 C_0 \\ 0 & j\omega_4\gamma_1 C_0 & j\omega_4 C_0 \end{bmatrix} \begin{bmatrix} V_2{}^* \\ V_1 \\ V_4 \end{bmatrix}. \tag{1.29}$$

+

If the capacitance variation is assumed to have a second harmonic component (as will usually be the case) of form shown below,

$$C = C_0(1 + 2\gamma_1 \cos \omega_3 t + 2\gamma_2 \cos 2\omega_3 t) \tag{1.30}$$

pump frequency

the matrix will become

$$\begin{bmatrix} I_2^* \\ I_1 \\ I_4 \end{bmatrix} = \begin{bmatrix} -j\omega_2 C_0 & -j\omega_2\gamma_1 C_0 & -j\omega_2\gamma_2 C_0 \\ j\omega_1\gamma_1 C_0 & j\omega_1 C_0 & j\omega_1\gamma_1 C_0 \\ j\omega_4\gamma_2 C_0 & j\omega_4\gamma_1 C_0 & j\omega_4 C_0 \end{bmatrix} \begin{bmatrix} V_2^* \\ V_1 \\ V_4 \end{bmatrix}. \tag{1.31}$$

In many practical situations, it is assumed that only two frequencies have signals of significant voltage. The so-called up-converter is described by the matrix obtained by setting $V_2^* = 0$.

How to make $V_2^* = 0$ in circuit simulation...

$$\begin{bmatrix} I_1 \\ I_4 \end{bmatrix} = \begin{bmatrix} j\omega_1 C_0 & j\omega_1\gamma_1 C_0 \\ j\omega_4\gamma_1 C_0 & j\omega_4 C_0 \end{bmatrix} \begin{bmatrix} V_1 \\ V_4 \end{bmatrix}. \tag{1.32}$$

The negative-resistance parametric amplifier is described by the matrix obtained by setting $V_4 = 0$

$$\begin{bmatrix} I_1 \\ I_2^* \end{bmatrix} = \begin{bmatrix} j\omega_1 C_0 & j\omega_1\gamma_1 C_0 \\ -j\omega_2\gamma_1 C_0 & -j\omega_2 C_0 \end{bmatrix} \begin{bmatrix} V_1 \\ V_2^* \end{bmatrix}. \tag{1.33}$$

We have said that these matrices are useful when only two or three voltages are assumed to be of significant magnitude, which in turn implies that all unwanted harmonics are short-circuited. When a semiconductor diode is used as the nonlinear element, however, the inevitable series resistance means that in practice a perfect short circuit can never be obtained. We may obtain another set of matrices which correspond to a condition ~~of *open*~~-circuited harmonics (a condition which is obtained in the pres~~ence of series resistance~~) by considering several additional voltages which give rise to other mixing effects which may be significant. The complete set of frequencies which we will now consider are:

$$\begin{aligned} &\omega_1 \\ &\omega_2 = \omega_3 - \omega_1 \\ &\omega_4 = \omega_3 + \omega_1 \\ &\left.\begin{aligned} \omega_5 &= 2\omega_3 - \omega_1 \\ \omega_6 &= 2\omega_3 + \omega_1. \end{aligned}\right\} \text{intermodulation} \end{aligned} \tag{1.34}$$

The last two frequencies need to be included since they can mix with the dominant fundamental capacitance variation at ω_3 and give rise to currents at ω_2 or ω_4. (We need not include any other voltages since they cannot give rise to components at ω_1, ω_2, ω_4 through mixing with the fundamental capacitance variation.)

To evaluate the effect of these additional voltages let us first construct an admittance matrix similar to that of Eq. (1.29). Using the same procedure as in the construction of Eq. (1.29), and keeping only the fundamental and second harmonic capacitance variations, we obtain the following matrix:

$$\begin{bmatrix} I_1 \\ I_2^* \\ I_4 \\ I_5^* \\ I_6 \end{bmatrix} = \begin{bmatrix} j\omega_1 C_0 & j\omega_1\gamma_1 C_0 & j\omega_1\gamma_1 C_0 & j\omega_1\gamma_2 C_0 & j\omega_1\gamma_2 C_0 \\ -j\omega_2\gamma_1 C_0 & -j\omega_2 C_0 & -j\omega_2\gamma_2 C_0 & -j\omega_2\gamma_1 C_0 & 0 \\ j\omega_4\gamma_1 C_0 & j\omega_4\gamma_2 C_0 & j\omega_4 C_0 & 0 & j\omega_4\gamma_1 C_0 \\ -j\omega_5\gamma_2 C_0 & -j\omega_5\gamma_1 C_0 & 0 & -j\omega_5 C_0 & 0 \\ j\omega_6\gamma_2 C_0 & 0 & j\omega_6\gamma_1 C_0 & 0 & j\omega_6 C_0 \end{bmatrix} \begin{bmatrix} V_1 \\ V_2^* \\ V_4 \\ V_5^* \\ V_6 \end{bmatrix} \tag{1.35}$$

Now, instead of assuming that the unwanted harmonics are short-circuited, let us assume that they are open-circuited. This we accomplish by setting the unwanted currents equal to zero. As an example, let us assume that $I_2^* = I_5^* = I_6 = 0$, which will give us a matrix analogous to Eq. (1.32). Since the effect of the second harmonic capacitance variation will be small, we may use perturbation methods in the solution to Eq. (1.35). With γ_2 first set equal to zero, we obtain the following equations from Eq. (1.35):

$$\begin{aligned} V_2^* &= -\gamma_1 V_1 - \gamma_1 V_5^* \\ V_5^* &= -\gamma_1 V_2^* \\ V_6 &= -\gamma_1 V_4. \end{aligned} \tag{1.36}$$

From Eq. (1.36) we see that our assumption of no significant voltage at unwanted harmonics is not grossly in error *even when these harmonics are actually open-circuited*, for they are of order γ_1 or γ_1^2 times the wanted voltages, V_1 and V_4. Let us now insert these values into the complete matrix of Eq. (1.35) and solve for I_1 and I_4, neglecting terms of order γ_1^4, $\gamma_1^2\gamma_2$, or higher. The result is:

$$\begin{bmatrix} I_1 \\ I_4 \end{bmatrix} = \begin{bmatrix} j\omega_1 C_0(1-\gamma_1^2) & j\omega_1 C_0\gamma_1(1-\gamma_2) \\ j\omega_4 C_0\gamma_1(1-\gamma_2) & j\omega_4 C_0(1-\gamma_1^2) \end{bmatrix} \begin{bmatrix} V_1 \\ V_4 \end{bmatrix}. \tag{1.37}$$

Comparing this result with that of Eq. (1.32), we see that very little difference exists between the case of open-circuited harmonics and short-circuited harmonics. As we shall see in Chapter 3, the calculated difference in amplifier performance using these two alternatives is quite small.

The analogous matrix for open-circuited harmonics at ω_4, ω_5, and ω_6 is

$$\begin{bmatrix} I_1 \\ I_2{}^* \end{bmatrix} = \begin{bmatrix} j\omega_1 C_0(1 - \gamma_1^2) & j\omega_1 C_0 \gamma_1(1 - \gamma_2) \\ -j\omega_2 C_0 \gamma_1(1 - \gamma_2) & -j\omega_2 C_0(1 - \gamma_1^2) \end{bmatrix} \begin{bmatrix} V_1 \\ V_2{}^* \end{bmatrix}. \tag{1.38}$$

These linearized small-signal matrices will be used extensively in the analysis of parametric devices to follow.

What are γ_1 and γ_2 ?

2

Noise Considerations

Much of the interest in parametric amplifiers is the result of their ability to yield extremely low-noise amplification. It seems in order, therefore, to consider the subject of noise and its influence on system performance in some detail before beginning a study of the devices themselves. This subject is a complex one and a complete and rigorous treatment of it is far beyond the scope and intent of this book. Instead, it will be the purpose of this chapter to present an elementary statement of the problems involved with primary emphasis on the practical consequences of the inevitable thermal noise on a system.

We may broadly classify noise according to its source as either external or internal to the receiver. Both sources lead to a degradation of the signal quality and put a lower limit on the sensitivity of any system. Internal noise has been characterized for some time by the noise figure of a receiver. This chapter will begin with a review of those concepts necessary for a quantitative discussion of thermal noise, followed by a careful examination of the noise figure concept. A discussion of external noise, the application of these ideas to system design, and a section on noise figure measurement will conclude this chapter.

2.1 Thermal Noise

Intuition would suggest that a resistor at a finite temperature would exhibit a small fluctuating voltage at its terminals because of the random motion of the large number of free electrons present. From fundamental thermodynamic considerations, Nyquist was able to show, in fact, that any two-terminal network in thermal equilibrium at an absolute temperature T and total resistance R could be replaced (as far as its noise generating properties in the frequency interval df are concerned) by a noiseless resistor in series with a noise generator of emf e_n as shown in Fig. 2.1 (a) where e_n is given by

$$\overline{e_n^2} = 4kTRp(f)\, df \tag{2.1}$$

where k is the Boltzmann constant ($k = 1.38 \times 10^{-16}$ erg deg^{-1} °K), $p(f)$ is the Planck factor

$$p(f) = \frac{hf}{kT}\,(e^{hf/kT} - 1)^{-1} \tag{2.2}$$

and h is Planck's constant ($h = 6.63 \times 10^{-27}$ erg sec).

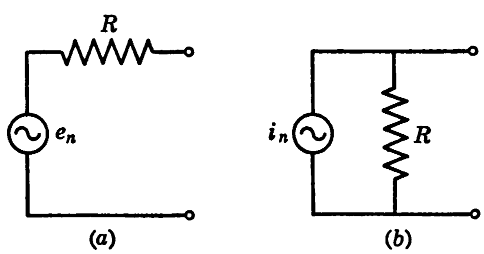

Fig. 2.1. (*a*) Equivalent series and (*b*) shunt representation of noise sources.

At room temperature and for frequencies well into the microwave region, the quantity hf/kT is very much smaller than unity and Eq. (2.1) reduces to

$$\overline{e_n^2} = 4kTR\, df. \tag{2.3}$$

Sometimes it is more convenient to represent thermal noise by a current generator of infinite impedance connected in parallel with a noiseless resistor as shown in Fig. 2.1 (b), in which case

$$\overline{i_n^2} = \frac{4kTp(f)\, df}{R}. \tag{2.4}$$

Generally, one is not so much interested in the voltage appearing across the terminals of a resistor as in the noise power which is available at these terminals. Remembering that a generator of internal resistance R_g developing an emf of e volts will deliver $e^2R_l/(R_g + R_l)^2$ watts of power into a load resistor of R_l ohms; when $R_g = R_l$, the power delivered is a maximum and is equal to $e^2/4R_g$. This quantity is independent of the impedance to which the generator is connected and is called the available power of the generator. The available gain of a two-port network may be defined as the ratio of the available signal power at the output to the available signal power at the input of the network. We are assuming here that the output and input impedances of the network have positive real parts. We thus see that while the available power at the output terminals is independent of the load, it is not independent of the way in which the signal generator is coupled to the network.

We may now write down the available noise power from a resistor:

$$N = \frac{e_n^2}{4R} = \frac{4RkT\,df}{4R} = kT\,df. \tag{2.5}$$

It is interesting to note that the available noise power is independent of the resistance R. If this resistor is connected to the input terminals of an ideal amplifier which introduces no additional noise of its own and which has a rectangular bandpass characteristic of width B, the total available noise power at the output will be

$$N_o = g_a kTB \tag{2.6}$$

where g_a is the available power gain of the network. In general, however, the gain characteristic of an amplifier will not be flat but will be a function of frequency. In this case, the total available noise power at the output will be

$$N_o = \int g_a(f)kT\,df. \tag{2.7}$$

The effective bandwidth of an ideal network of mid-band gain g which gives the same noise output is given by Eq. (2.8) below.

$$gkTB = \int g(f)kT\,df$$

$$B = \frac{1}{g}\int g(f)\,df. \tag{2.8}$$

2.2 Noise Figure

Definition

We are now in a position to define the *noise figure* of a two-port network. The noise figure at a specified input frequency is the ratio of the total noise power per unit bandwidth (at a corresponding output frequency) available at the output, to that portion of this power engendered at the input frequency by the input termination *at the standard* *noise temperature of 290°K.** The noise temperature at a pair of terminals is the absolute temperature of a resistance having an available thermal noise power per unit bandwidth equal to that available at the actual terminals. Therefore,

$$\text{noise figure} = F = \frac{N_o}{g_a k T_0 B}. \tag{2.9}$$

By this definition, the noise figure is a precisely defined measure of the noisiness of any network. In terms of the degradation of signal-to-noise ratio by a receiver, we may write, for a linear transducer

$$F = \frac{N_o}{(S_o/S_i)kT_0B} = \frac{S_i/kT_0B}{S_o/N_o} \tag{2.10}$$

where S_i and S_o are the available input and output signal powers respectively. We see, therefore, that noise figure is the ratio of the signal-to-noise ratio at the input to signal-to-noise ratio at the output of a linear transducer *when and only when the input noise temperature is 290°K.*

It is worthwhile to point out that noise figure can also be evaluated in terms of the *transducer gain* of a network. Transducer gain is defined as the ratio of the power delivered to the load to the available power of the source. If N_o' is the actual noise power delivered to the load and g_t is the transducer gain, we may write

$$\frac{N_o'}{N_o} = \frac{g_t}{g_a}. \tag{2.11}$$

Therefore,

$$F = \frac{N_o}{g_a k T_0 B} = \frac{N_o'}{g_t k T_0 B}. \tag{2.12}$$

Effective Input Noise Temperature

An expression which is often used in place of noise figure, especially when referring to low-noise amplifiers, is the *effective input noise temperature* of a network. Effective input noise temperature is defined as the temperature of the input termination which results in output noise power per unit bandwidth double that which would occur if the input termination were at absolute zero. We may, therefore, replace our receiver and noise source at a temperature T by the equivalent system of a noiseless receiver and a voltage noise generator at the effective input noise temperature of the receiver in series with the original input generator.

* "IRE Standards on Electron Tubes: Definition of Terms, 1957," *Proc IRE*, vol. 45, p. 1000; July 1957.

In order to derive a relation between effective input noise temperature and noise figure, consider the circuit of Fig. 2.2 in which we have a noise generator of temperature T_0 matched into a network of available power gain g_a. By our definition of noise figure, the noise temperature of our output terminals will be $g_a F T_0$. Replacing our network by an ideal noiseless one, and referring the output noise temperature to the input terminals, we get a total noise temperature of FT_0 at these terminals. Of this, T_0 is due to the source. The remainder, $(F - 1)\,T_0$, is due to the receiver and is what we have defined as the effective input noise temperature. Therefore,

$$T_e = T_0(F - 1) \tag{2.13}$$

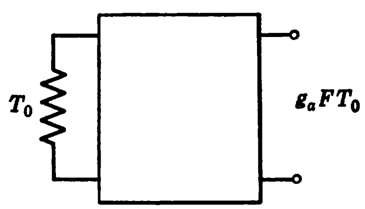

Fig. 2.2. Equivalent circuit relating noise figure to effective input noise temperature.

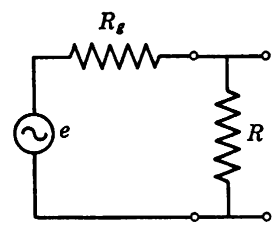

Fig. 2.3. Equivalent circuit of a signal generator and a simple network.

Noise Figure of a Resistor

As an illustration of the concepts of available gain and noise figure, let us calculate these quantities for the simplest network we can think of, a resistor at 290°K, as shown in Fig. 2.3.

With the generator connected, the open circuit voltage across the output terminals is $eR/(R_g + R)$ and the output impedance is $RR_g/(R_g + R)$; therefore, the available output power is

$$P_a = \frac{1}{4}\left(\frac{eR}{R_g + R}\right)^2\left(\frac{R + R_g}{RR_g}\right) = \frac{e^2R}{4(R_g + R)R_g}. \tag{2.14}$$

Since the available power from the generator is $e^2/4R_g$, the available gain of the network is

$$g_a = \frac{R}{R_g + R} \tag{2.15}$$

and by definition, the noise figure is

$$F = \frac{N_o}{g_a k T_0 B} = \frac{kT_0B}{\dfrac{R}{R_g + R}\,kT_0B} = 1 + \frac{R_g}{R}. \tag{2.16}$$

It is worth noting that when a resistor at the standard temperature is matched to the noise generator, $R = R_g$ and the noise figure is equal to 3 db. If the resistor R is at some temperature other than the standard temperature, its noise figure becomes

$$F = 1 + \frac{R_g}{R}\frac{T}{T_0} \tag{2.17}$$

where T is the absolute temperature of the resistor.

Noise Figure of an Attenuator

Let us now compute the noise figure of an attenuator at some temperature $\bar{T}$. This result will allow us to quantitatively predict the effect of circuit losses on the noise figure of a system. Let the attenuator be repre-

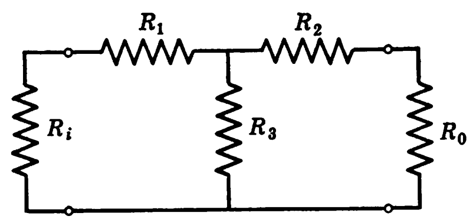

Fig. 2.4. Equivalent circuit of a lossy network.

sented by an equivalent "T" network as shown in Fig. 2.4. If the loss ratio of the network is L, then R_1, R_2 and R_3 are given by

$$R_1 = R_i\left[\frac{L+1}{L-1}\right] - R_3 \tag{2.18}$$

$$R_2 = R_o\left[\frac{L+1}{L-1}\right] - R_3 \tag{2.19}$$

$$R_3 = \frac{2\sqrt{LR_iR_o}}{L-1}. \tag{2.20}$$

where $L = 1/g_t$.

Now, if each of the resistors R_1, R_2 and R_3 are considered noise generators of open-circuited voltage $\overline{e_j^2} = (4R_jk\bar{T}B)^{1/2}$ we may compute the excess noise power delivered to R_0 due to each of these generators.

$$N_o'' = \frac{e_1^2R_3^2R_o + e_2^2(R_i + R_1 + R_3)^2R_o + e_3^2(R_i + R_1)^2R_o}{[(R_i + R_1 + R_3)(R_o + R_2 + R_3) - R_3^2]^2}$$

$$= 4k\bar{T}BR_o\frac{R_1R_3^2 + R_2(R_i + R_1 + R_3)^2 + R_3(R_i + R_1)^2}{[(R_i + R_1 + R_3)(R_o + R_2 + R_3) - R_3^2]^2}. \tag{2.21}$$

Substituting Eqs. (2.18) to (2.20) for R_1, R_2 and R_3 and simplifying the excess noise is found to be

$$N_o'' = k\bar{T}B\left(\frac{L-1}{L}\right). \tag{2.22}$$

The total noise power is then

$$N_o' = \frac{kT_0B}{L} + \frac{(L-1)k\bar{T}B}{L}. \tag{2.23}$$

The noise figure of this attenuator is, therefore,

$$F = \frac{N_o'}{g_t k T_0 B} = 1 + (L-1)\frac{\bar{T}}{T_0}. \tag{2.24}$$

The corresponding effective input noise temperature is

$$T_e = T_0(F-1) = \bar{T}(L-1). \tag{2.25}$$

Noise Figure of Cascaded Networks

Let us now consider a cascade of two networks of noise figures F_1 and F_2 and with available gains g_1 and g_2 respectively as shown in Fig. 2.5. The total noise power available at the output terminals will be made up of the output noise of the first stage amplified by the second stage, plus the excess noise power due to the second stage:

$$N_{12} = F_1 g_1 g_2 k T_0\, df + (F_2 - 1) g_2 k T_0\, df.$$

The overall noise figure is

$$F_{12} = \frac{N_{12}}{g_1 g_2 k T_0\, df}.$$

Therefore,

$$F_{12} g_1 g_2 k T_0\, df = F_1 g_1 g_2 k T_0\, df + (F_2 - 1) g_2 k T_0\, df.$$

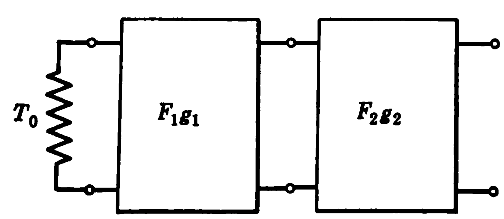

Fig. 2.5. Equivalent circuit of two cascaded networks.

Rearranging, we obtain

$$F_{12} = F_1 + \frac{F_2 - 1}{g_1}. \tag{2.26}$$

This method may be generalized to include n stages with the result

$$F_{1\cdots n} = F_1 + \frac{F_2 - 1}{g_1} + \frac{F_3 - 1}{g_1 g_2} + \cdots + \frac{F_n - 1}{g_1 g_2 \cdots g_{n-1}}. \tag{2.27}$$

From the relation between noise figure and effective input noise temperature, we may write for the effective input noise temperature of n cascaded networks

$$T_{e_{1\cdots n}} = T_{e_1} + \frac{T_{e_2}}{g_1} + \frac{T_{e_3}}{g_1 g_2} + \cdots. \tag{2.28}$$

Transmission Line Losses

Like most other losses in receiver systems, transmission line losses become important when dealing with extremely low-noise amplifiers, and may contribute a significant amount to the noise figure. For convenience, we may speak of the noise figure of the transmission line which is given by Eq. (2.24)

$$F_l = 1 + (L - 1)\frac{\bar{T}}{T_0} \tag{2.29}$$

or its effective input noise temperature

$$T_l = (L - 1)\bar{T}. \tag{2.30}$$

By reducing the temperature of the loss, its contribution to the overall noise figure may be minimized. Even if its physical temperature is reduced to zero, however, it degrades the signal-to-noise ratio and consequently the noise figure of the system, as may be seen by examination of Eq. (2.31), which follows directly from Eq. (2.28).

$$T_e = T_l + LT_r = (L - 1)\bar{T} + L(F_r - 1)T_0. \tag{2.31}$$

The contribution from the first term of Eq. (2.31) amounts to 7° for a 0.1 db loss at room temperature, only 2° if the loss is at 77°K, and about 0.1° if it is at liquid helium temperatures. For frequencies in the microwave region where waveguide attentuation is of the order of tenths of a decibel per meter, transmission lines between the antenna feed and the amplifier should be kept as short as possible and operated at reduced temperatures if convenient. The nomograph of Fig. 2.6 is that of Eq.

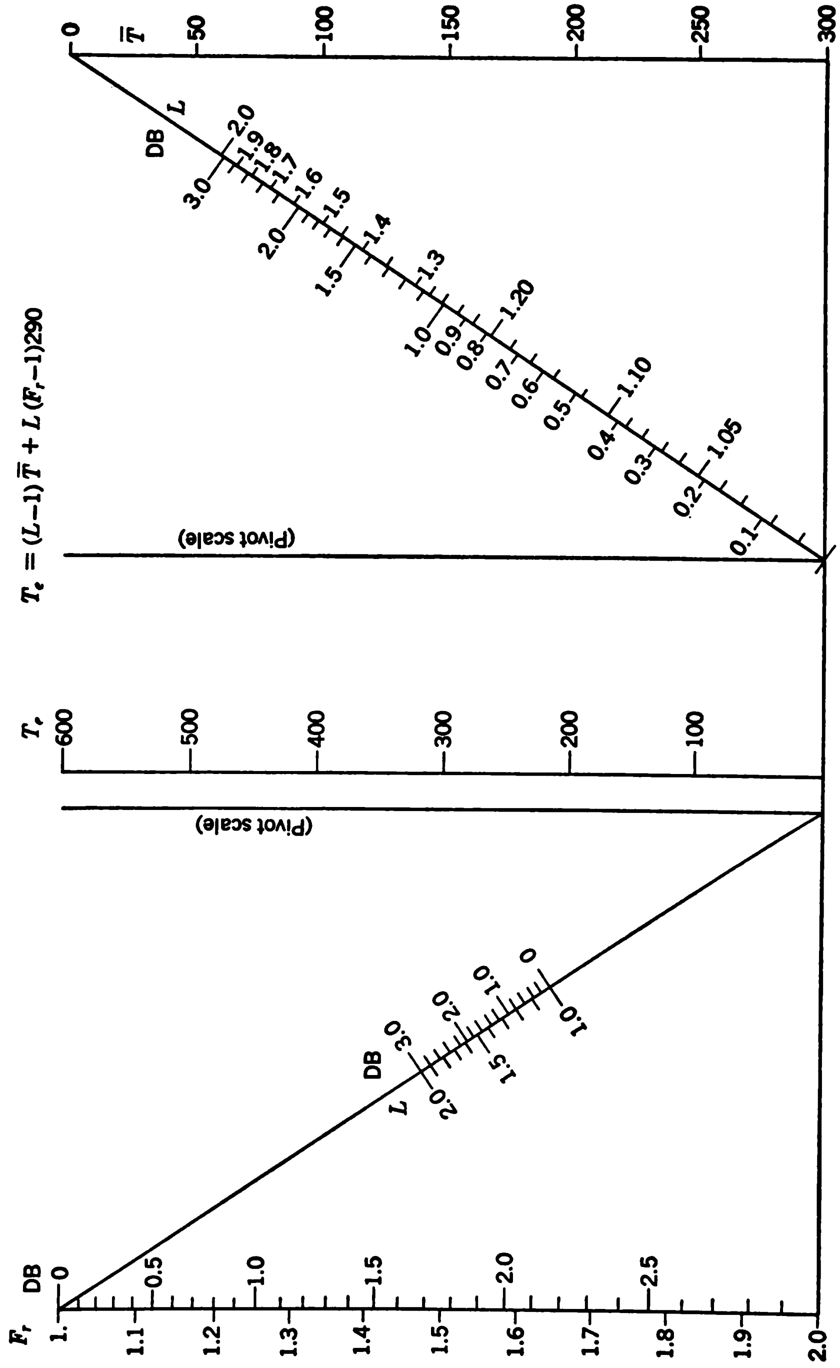

Fig. 2.6. Nomograph for determining the effect of transmission line losses on the noise performance of a receiver.

(2.31) and affords a simple and rapid method for determining the effective input noise temperature of a receiver following a loss L at a temperature $\bar{T}$.

Circulators, which are often used with negative-resistance parametric amplifiers may be treated in much the same way as transmission lines, where the losses are now the arm-to-arm insertion losses of the device. In practice, this may be the order of a few tenths of a db. The problems associated with keeping insertion losses this low over an appreciable bandwidth such as might be required in a radiometric application are severe, however.

Generally, commercial circulators and isolators cannot be cooled much below room temperature without mechanical failure. In addition, some ferrites become excessively lossy even at liquid nitrogen temperatures. Using single crystal yttrium iron garnet, however, circulators have been operated at liquid helium temperatures with excellent results.

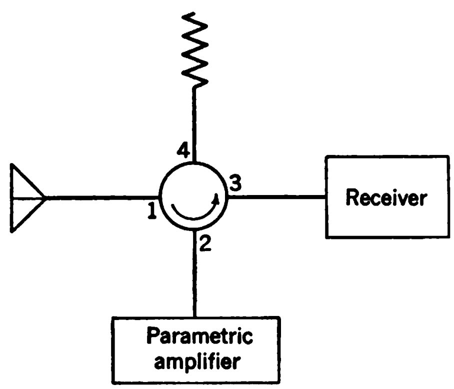

Fig. 2.7. Schematic circuit of a parametric amplifier, using a circulator.

As an example of the noise contributions from a non-ideal circulator, consider the receiving system shown in Fig. 2.7. For the sake of simplicity, we will assume that the system is at the standard temperature T_0. If L is the total loss between the antenna terminals and the input of the parametric amplifier, and g is the gain of the parametric amplifier, we may write for the overall effective input noise temperature

$$T_e = T_{la} + (L - 1)T_0 + L(T_{rp} + T_{lp} + T_p) + \frac{LT_r}{g} \quad (2.32)$$

T_{la} = effective noise temperature at the antenna terminals due to noise emitted by the load and reflected at the antenna because of the finite VSWR;

T_{rp} = effective noise temperature at the input of the parametric amplifier due to receiver noise transmitted directly through the circulator due to the finite isolation between arms 3 and 2;

T_{lp} = effective noise temperature due to the load noise and the finite isolation between arms 4 and 2;

T_p = the effective input noise temperature of the parametric amplifier;

T_r = the effective input noise temperature of the receiver including all losses between ports 2 and 3.

In a well-designed circulator, the isolation between arms 3 and 2 and 4 and 2 may exceed 30 db in which case T_{lp} and T_{rp} would be about 1° and, therefore, negligible with respect to T_p. If the VSWR at the antenna can be kept to 1.1 or less, T_{la} will also be of the order of 1°, assuming the load is at room temperature. In cases where either the antenna cannot be matched or the desired circulator performance cannot be obtained, either cooling the matched load or the whole circulator should be considered.

2.3 Antenna Temperature and System Sensitivity

Before the advent of extremely low-noise amplifiers such as the maser and the parametric amplifier, external noise could usually be neglected with respect to internal noise in most applications. One notable exception is in the science of radio astronomy where a portion of the external noise is actually the information of interest. In fact, much of the quantitative information we have on this topic is the result of many years of research in the field of astronomy, one of the "purest" of all sciences. Much of the recent work on low-noise amplifiers may be justified, on the other hand, by the significant improvements in the sensitivity and range of radio telescopes expected when the use of these amplifiers becomes widespread. It would be difficult to find a better example of the interdependence of pure and applied research.

There are a number of external noise sources which influence the performance of a receiving system. Some of the most important are galactic noise, solar noise, absorption and re-radiation by the ionosphere, oxygen and water vapor absorption in the atmosphere, and finally man-made interference. Losses degrade system performance both by attenuating the signal and by radiating noise power proportional to their temperatures. Before considering each of these contributions in detail, it will be helpful to introduce the idea of *brightness temperature*.

A quantitative measure of the radiation from any distributed source (for example, the sky) is the brightness b. The power in the frequency interval Δf per unit area is defined as the flux density S. If we consider a solid angle whose vertex is at the receiving point, enclosing a line in the direction under consideration, the brightness in this direction is defined as:

$$b = \lim_{\Delta\Omega \to 0} \frac{\Delta S}{\Delta\Omega}, \tag{2.33}$$

where ΔS is the flux density at the point from that part of the source within the angle $\Delta\Omega$.

It is usually more convenient to speak in terms of brightness temperature T_b, which is defined as the temperature in degrees Kelvin of an ideal black body which would give the same brightness as observed. This does not necessarily imply that the radiation being measured is thermal in origin, and, therefore, brightness temperature will generally depend on frequency and the polarization of the antenna.

In order to relate brightness temperature for a black body to frequency, we remember that the Planck radiation law gives the energy emitted per unit frequency interval per stearadian by a unit area of black body:

$$b = \frac{2hc}{\lambda^3}\left(\frac{1}{e^{hc/k\lambda T} - 1}\right). \tag{2.34}$$

For $hf \ll kT$ this leads to the Rayleigh-Jeans approximation

$$b = \frac{2kT}{\lambda^2}. \tag{2.35}$$

The flux density S from a solid angle Ω of uniform temperature is therefore

$$S = b\Omega = \frac{2kT\Omega}{\lambda^2}. \tag{2.36}$$

Antenna Temperature

Unless our antenna is ideal, the quantity of real interest in determining system sensitivity is the antenna temperature T_a. The antenna temperature may be defined as

$$T_a = \frac{P_a}{k\,\Delta f} \tag{2.37}$$

where P_a is the available noise power at the antenna terminals. In any real system, it has contributions from antenna losses and side and back lobes, in addition to the brightness temperature in the direction in which the antenna is aimed.

Brightness temperature or sky temperature, as it is sometimes called, may be related to the antenna temperature of an ideal antenna. If we consider an antenna looking at n radiators, each at a brightness temperature T_n and each contributing a fraction α_n of the incident power, we may write

$$P_a = k\Delta f \sum_n \alpha_n T_n = k\Delta f T_a$$

so that

$$T_a = \sum_n \alpha_n T_n. \tag{2.38}$$

Alternatively, we may write

$$T_a = \frac{\iint T_b(\theta, \varphi) g(\theta, \varphi)\, d\Omega}{\iint g(\theta, \varphi)\, d\Omega} \tag{2.39}$$

where $g(\theta, \varphi)$ is the gain in the direction of the angle element $d\Omega$, and T_b is the brightness temperature in this direction.

Sources of External Noise

Atomspheric absorption. Up to now, we have not discussed the source of brightness temperature or, in particular, sky temperature in the usual case where the antenna is directed above the horizon. It is of interest to determine how atmospheric absorption affects this quantity as the beam makes various angles with the zenith. Let us consider the situation of Fig. 2.8 where the antenna is again looking at a black body at temperature T_b but with an absorbing medium at the same temperature having a fractional absorption α between the two. At thermal equilibrium, the power at the antenna is still $kT_b\Delta f$; however, it is made up of a contribution $(1 - \alpha)kT_b\Delta f$ from the black body and $\alpha kT_b\Delta f$ from the absorber. By a logical extension of this argument, we find that if the absorber is at a temperature $\bar{T}$ then the antenna temperature of an ideal antenna would be

$$T_a = \alpha\bar{T} + (1 - \alpha)\, T_b. \tag{2.40}$$

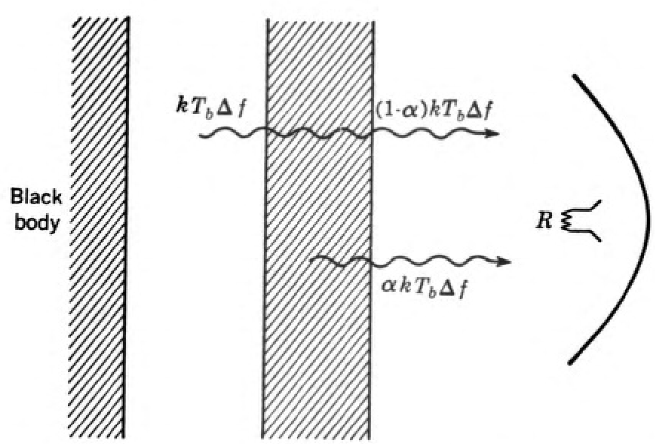

Fig. 2.8. Illustration of the contributions to the brightness of an absorber.

In terms of loss factor $L = 1/(1 - \alpha)$,

$$T_a = \frac{T_b}{L} + \left(1 - \frac{1}{L}\right)\bar{T} \tag{2.41}$$

which is in agreement with Eq. (2.23). The quantity α is a strong function of both frequency and elevation angle.

Information on atmospheric absorption, which is useful in calculating antenna temperatures in the microwave region, is rare and often unreliable. The most comprehensive data which has been published to date are those of Hogg[60] and are the results of calculations done on a simple but rather accurate model. The absorption is assumed to be totally due to the pressure-broadened water and oxygen lines at 22.5 and 60 kmc respectively. The dependence of temperature and pressure on altitude is essentially that of the International Standard atmosphere and the water vapor content is assumed to vary linearily from 12 g/m^3 at the surface to 0 at 5 km. The calculation was based on a generalization of Eq. (2.41).

$$T_a = T_b \exp\left[-\int_0^\infty \alpha(x)\,dx\right] + \int_0^\infty \alpha(x)\,T(x)\,\exp\left[-\int_0^x \alpha(x)\,dx\right] dx \tag{2.42}$$

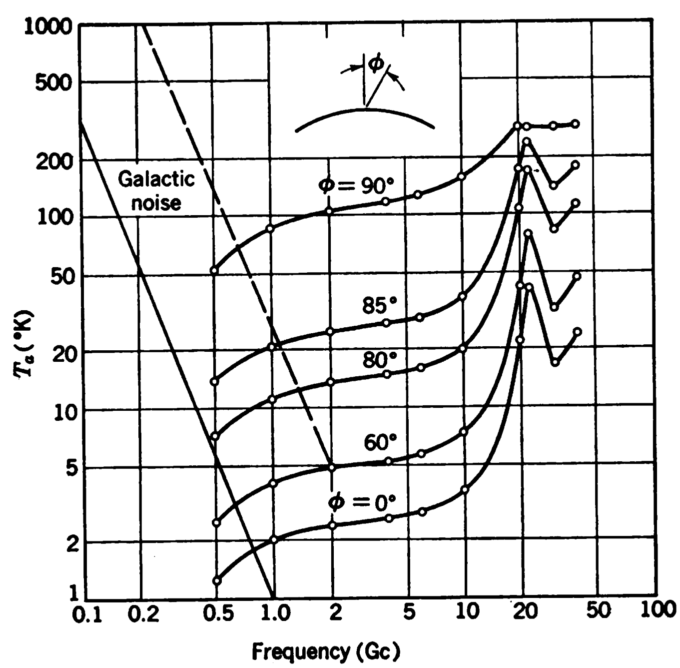

Fig. 2.9. Brightness temperature of the sky as a function of frequency (after Hogg).

The results of these calculations, where we have taken T_b to be zero and the absorption coefficient α to be small so that $1 - e^{-\alpha x} \approx -\alpha x$ are shown in Fig. 2.9. Here we have a plot of the antenna temperature for an ideal antenna having a delta function response from 0.5 to 40 kmc. Zenith angle is the parameter. For convenience, the contribution from galactic noise, both perpendicular and in galactic plane, is also shown. It can be seen that the optimum frequencies for communication against a sky background lie between 2 and 10 kmc if noise is the most important consideration.

The atmosphere contains other absorbers, especially at the higher altitudes; these include ozone and various ionic species. Their concentration, however, is low and they may generally be neglected above 100 mc.

Extraterrestrial noise. Radio noise originating outside of the atmosphere may be divided into two classes. The first type, which is solar in origin, is extremely time-dependent. This component includes flares, noise storms, slow and fast drift bursts, and corpuscular radiation influencing the upper ionosphere. Its effect, while generally limited to UHF fre-

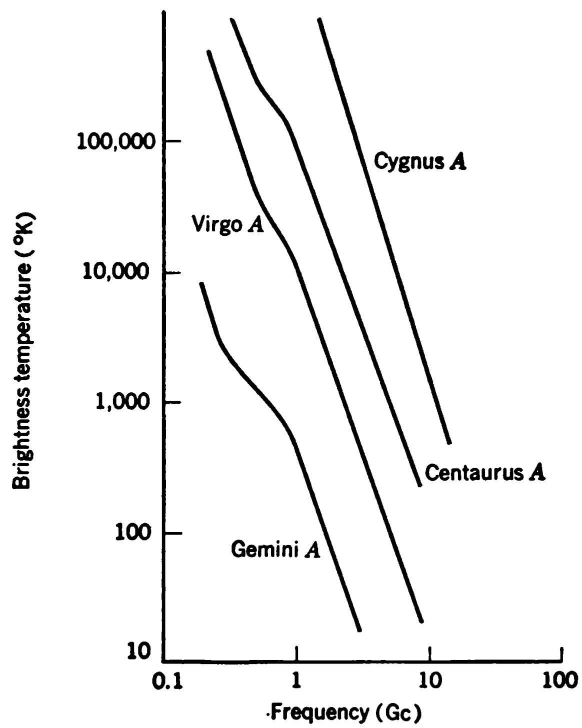

Fig. 2.10. Brightness temperature spectra of several of the most intense radio sources. (After Ewen)

quencies and below, may be severe enough to completely disrupt radio communications.

Noise storms which are caused by localized disturbances in the solar corona above active sunspot regions consist of a long series of short bursts continuing over hours or days, superimposed on a slowly varying continuum. Although usually spread over a wide frequency band, the noise is generally limited to frequencies below 250 mc.

Slow and fast drift bursts are characterized by a narrow band of intense radiation which drifts towards lower frequencies. The slow bursts have a duration of the order of several minutes and occur at a rate of about 50 per year. The fast bursts have a duration of only seconds, occuring at a rate of about 1000 per year. The cause of these disturbances is unknown at this time.

The second type of noise, originating from without the solar system, is sometimes called the galactic background. It does not vary with time but does depend on the partidular area of the galaxy viewed by the antenna. This celestial noise, which is the most important at microwave frequencies, has the spectrum shown in Fig. 2.9. Fig. 2.10 gives the brightness temperature of several of the strongest radio sources.[39] When in the antenna beam, these sources can contribute significantly to the antenna temperature. The galactic background composed of similar but less intense sources shows the same $1/f^{2.5}$ frequency dependence both in and perpendicular to the galactic plane. It is believed that this radiation originates partly in hot ionized interstellar gas and partly in stellar atmospheres.

System Sensitivity

In any consideration of low-noise receivers, we are ultimately interested in the minimum signal we can detect and use. We may arbitrarily define sensitivity as the available signal power at the antenna terminals when the *predetection* signal-to-noise power ratio is unity. This quantity is independent of the effect of nonlinear detectors or any signal enhancement or correlation techniques we might want to use. We have also lumped together everything on the receiver side of the antenna terminals and will call this the receiving system. This includes transmission line losses, circulator losses, etc.

It is convenient now to define a temperature which we will call the *operating noise temperature* T_{op}.

$$T_{op} = \frac{N_o}{g_a k B} \tag{2.43}$$

where N_o is the noise power available at the receiver output terminals, and g_a is the receiver system available gain. When the ouput signal-to-noise ratio is unity, the sensitivity is

$$S_i = kBT_{op} \tag{2.44}$$

so that the system sensitivity is proportional to T_{op}.

Examination of the definition of operating noise temperature will show that, for linear transducers, it may be written as the sum of the effective input noise temperature of the receiver and the antenna temperature.

$$T_{op} = T_0(F - 1) + T_a. \tag{2.45}$$

It will be shown later in Sections 3.3 and 4.2 that somewhat different expressions must sometimes be used in connection with parametric amplifiers. This is because the nonlinear mixing process creates a situation in which the magnitude of the so-called internal noise is actually a function of the antenna temperature. Operating noise temperature is sometimes normalized and called operating noise figure:

$$F_{op} = F - 1 + t_a. \tag{2.46}$$

where

$$t_a = \frac{T_a}{T_0}.$$

Fig. 2.11 is a plot of noise figure versus operating noise figure with antenna temperature as a parameter. This figure vividly illustrates how, for low antenna temperatures, a moderate decrease in noise figure may

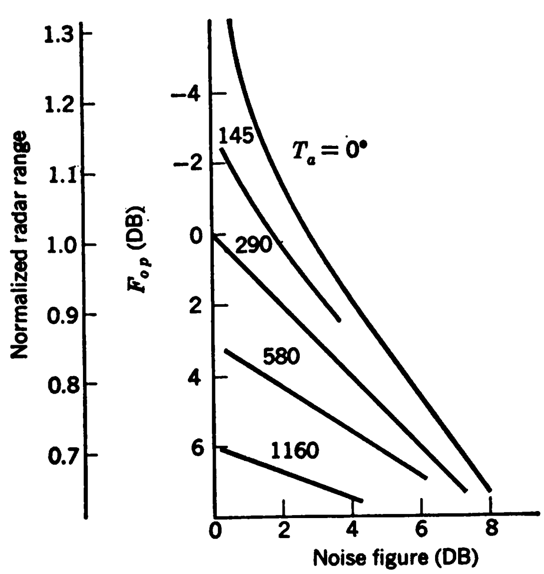

Fig. 2.11. Operating noise figure versus noise figure with antenna temperature as the parameter.

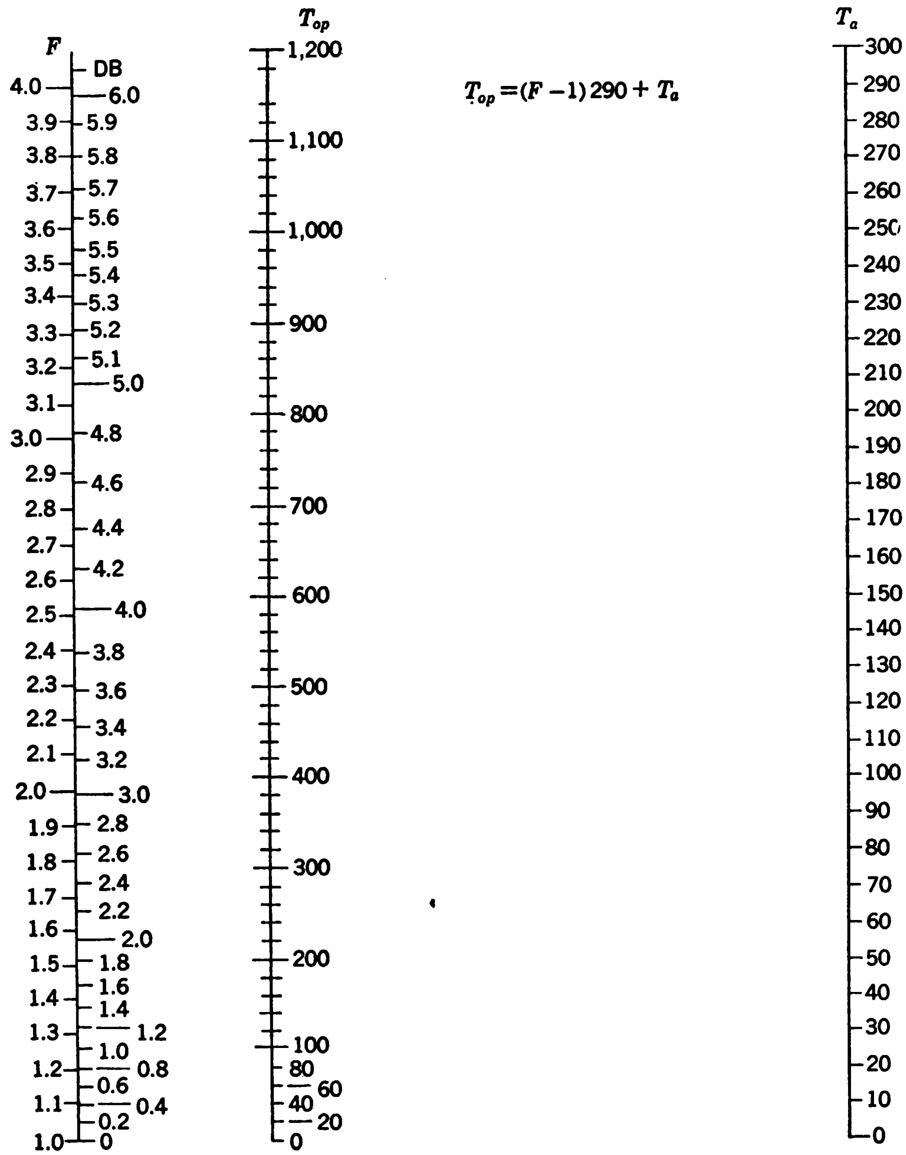

Fig. 2.12. Nomograph for determining operating noise temperature.

improve sensitivity considerably. Eq. (2.45) may be put into convenient nomographic form as shown in Fig. 2.12 with which one may quickly find the operating noise temperature for a given noise figure and antenna temperature.

As an example of how atmospheric absorption affects the operating noise temperature and hence the sensitivity of a receiver, let us consider the situation shown schematically in Figure 2.13 which represents a receiver looking at background brightness temperature T_b through an atmosphere of loss L at an effective temperature $\bar{T}$. Let us assume that the signal originates between the background and the loss. This would be the situation when communicating with a space vehicle outside of the atmosphere, where T_b would be the galactic background. The identical situation would exist when operating an airborne radiometer at frequencies or altitudes where atmospheric absorption is significant. In this case T_b represents the brightness temperature of the ground. F_r is the noise figure of the receiver, including all internal losses. Let us now define F as the over-all noise figure of the two networks, L and F_r.

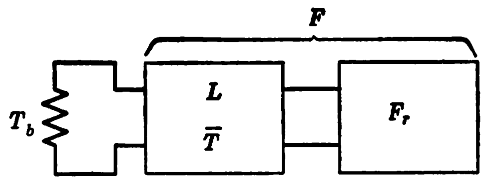

Fig. 2.13. Schematic of a receiver looking at a brightness temperature T_b through a loss of temperature of $\bar{T}$.

In other words, we are referring all noise temperatures back to the point where the signal is introduced. The operating noise temperature for this case is:

$$T_{op} = T_b + T_0(F - 1) \tag{2.47}$$

where

$$F = F_l + L(F_r - 1) \tag{2.48}$$

and F_l is the noise figure of the loss. Using Eq. (2.24) for the noise figure of a lossy pad at an average temperature $\bar{T}$, T_{op} becomes

$$T_{op} = T_b + T_0\left[(L - 1)\frac{\bar{T}}{T_0} + L(F_r - 1)\right]. \tag{2.49}$$

The actual antenna temperature which the receiver sees is as given by Eq. (2.41)

$$T_a = \frac{T_b}{L} + \left(1 - \frac{1}{L}\right)\bar{T} = \frac{T_b + (L - 1)\bar{T}}{L}. \tag{2.50}$$

Solving for T_b and substituting into Eq. (2.49), we obtain:

$$\begin{aligned} T_{op} &= LT_a - \bar{T}(L - 1) + T_0\left[(L - 1)\frac{\bar{T}}{T_b} + L(F_r - 1)\right] \qquad (2.51) \\ &= L(T_a + T_e) \end{aligned}$$

where T_e is the effective input noise temperature of the receiver alone. The sensitivity of a system operating under these conditions is, therefore, proportional to the atmospheric loss L.

2.4 The Measurement of Noise Figure

Noise figure measurements on unilateral low-noise parametric amplifiers present special problems largely to the extent that one is dealing with numerically small values where small errors can have a significant effect.

There are two commonly used techniques for this measurement: the signal generator method and the noise source method. In the first method, an accurately calibrated signal generator is connected to the input of the receiver under test as shown in Fig. 2.14.

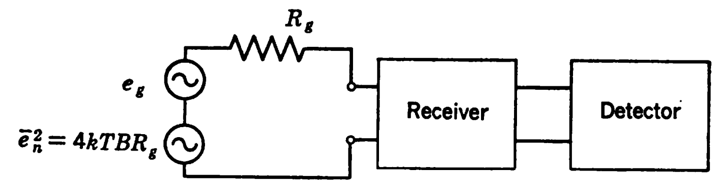

Fig. 2.14. Circuit arrangement for noise figure measurements.

The procedure is to introduce a known amount of power and to compare the resulting output with that which existed before the introduction of the signal. This is usually done as follows:

With the signal generator off, the noise power output of the receiver is observed. The signal level is then increased until either the power output, as read on the detector is doubled, or the gain of the receiver is decreased 3 db and the detector returned to its original setting. The noise figure is then:

$$F = \frac{S_i/N_i}{S_o/N_o} = \frac{S_i}{kT_0B}. \tag{2.52}$$

Since, under these conditions, $S_o = N_o$, S_i is the available power of the signal generator $e_g^2/4R_g$. It is worth noting that the signal generator is not necessarily matched to the receiver. (If this measurement were made under matched conditions, the minimum noise figure obtainable if the input resistance were effectively at T_0 would be 3 db as given by Eq. (2.16).) In order to use this method, it is clear by Eq. (2.52) that the noise bandwidth B as defined by Eq. (2.8) must be known. Often an accurate measurement of this quantity is not easy. For this reason and because accurately calibrated signal generators are often not available, this method is not recommended except for high noise figures.

The noise-source method is more accurate and simpler if calibrated noise sources are available, because a separate determination of noise bandwidth is unnecessary. At frequencies below 1000 mc, a noise diode is commonly used; above this frequency, a gas tube noise generator similar to an ordinary fluorescent lamp is used. One measurement technique involves connecting an adjustable waveguide attenuator between the source and the receiver under measurement, recording the receiver output with the attenuator at its maximum setting, and then decreasing its setting until the output power is doubled. The excess noise power may be found from Eq. (2.50).

$$P_n = kB\left[\frac{T_2 + (L-1)\bar{T}}{L} - T_0\right] \tag{2.53}$$

and noise figure is

$$F = \frac{P_n}{kT_0B} = \frac{T_2 + (L - 1)\bar{T} - LT_0}{LT_0} \tag{2.54}$$

where T_2 is the effective temperature of the discharge, $\bar{T}$ is the temperature of the attenuator and L is its loss factor. For $\bar{T} = T_0$, Eq. (2.54) reduces to

$$F = \frac{T_2 - T_0}{LT_0}. \tag{2.55}$$

A slightly different technique is to connect the noise lamp directly to the receiver under test. With the noise lamp off, a reading is made of the output power of the receiver. The noise lamp is then turned on and the output power is again read. (In practice, it is more accurate to introduce attenuation prior to the detector which is sufficient to bring the power output to the same level as when the noise lamp is off. The detector characteristic is thus eliminated as a possible source of error.) With the noise lamp on, the output noise power is

$$P_2 = gkT_2B + gkT_eB. \tag{2.56}$$

With the noise lamp off and at temperature T_1, the output noise power is

$$P_1 = gkT_1B + gkT_eB. \tag{2.57}$$

The ratio is then

$$\frac{P_2}{P_1} = \frac{T_2 + T_e}{T_1 + T_e}.$$

Solving for T_e, we obtain

$$T_e = \frac{T_2 - YT_1}{Y - 1} \tag{2.58}$$

where $Y = P_2/P_1$. Expressing this in terms of noise figure we have

$$T_e = T_0(F - 1) = \frac{T_2 - YT_1}{Y - 1} \tag{2.59}$$

so

$$F = 1 + \frac{\dfrac{T_2}{T_0} - Y\dfrac{T_1}{T_0}}{Y - 1}$$

$$= \frac{\left(\dfrac{T_2}{T_0} - 1\right) - Y\left(\dfrac{T_1}{T_0} - 1\right)}{Y - 1}. \tag{2.60}$$

For the special case of $T_1 = T_0$, Eq. (2.60) becomes

$$F = \frac{\frac{T_2}{T_0} - 1}{Y - 1}. \tag{2.61}$$

In so using a noise lamp for the measurement of noise figure, it is sometimes possible to introduce significant errors because of an error in the estimate of the temperature of the noise lamp, T_2. While the *intrinsic* noise power from such a device can be closely controlled, the matching of this noise power to the transmission line presents some difficulty. In addition, it is not an easy matter to calibrate such a noise source with commonly available equipment. Because of such uncertainties, alternative schemes have been developed which involve cooled terminations as well as hot terminations. For example, a termination can be cooled to the temperature of liquid nitrogen to form a cold load at T_1. The hot load can simply be a load at room temperature or somewhat hotter. One advantage of such a scheme is that it is possible to measure the actual temperatures involved quite accurately. Good matched loads can be obtained at such temperatures and, therefore, the effective temperature of the noise lamp can be directly measured to within a fraction of a degree Kelvin. Transmission losses between loads and the receiver must be included, but in practice such corrections can be kept small.

Another method uses a fixed attenuator at a reduced temperature between a calibrated noise lamp and the receiver, in which case the available noise temperature at the receiver is

$$T_{av} = \frac{T_2}{L} + \left(1 - \frac{1}{L}\right) \bar{T}. \tag{2.62}$$

If the insertion loss of the attenuator is assumed to be 30 db and at a temperature of 77°K, for example, with the noise lamp off the available temperature is

$$T_{av} = (0.999)77 + (0.001)290 = 77.2°\text{K}.$$

Assuming a noise lamp temperature of 11,000°K, the available noise temperature with the noise lamp on is

$$T_{av} = (0.999)77 + (0.001)(11{,}000) = 87.9°\text{K}.$$

The effective input noise temperature may be then found by the method described above. One advantage of this technique over that using switched loads at different temperatures is that it offers a relatively constant impedance to the amplifier by virtue of the 30 db isolation. On the other hand, the small differences in available noise power means that only amplifiers of very low noise figure can be accurately measured.

The methods outlined above are useful in the determination of the overall system noise figure of a receiver, which is usually the quantity of interest in specifying, for example, the range of a radar receiver. Often, however, it is desirable to know the noise figure of the preamplifier only. This may in principle be found by measuring the noise figure of the second stage r-f amplifier or mixer i-f amplifier combination, the available gain of the preamplifier, and using Eq. (2.26) for the noise figure of cascaded amplifiers. The measurement of the available gain of a parametric amplifier is not straightforward, however, when the input and output are at different frequencies. The absolute calibration between two different signal generators used at the input and output may be quite poor and may introduce substantial error in the insertion gain measurement. There is an indirect method which has been successfully used that is based on the measurement of noise figure. In this method a precision attenuator is inserted between the parametric preamplifier and the r-f amplifier or mixer and the overall noise figure measured as a function of the insertion loss of the attenuator L. From Eq. (2.27), which gives the noise factor for n networks in cascade, we can write

$$F = F_1 + \frac{L-1}{g_1} + \frac{(F_3 - 1)L}{g_1} = \left(F_1 - \frac{1}{g_1}\right) + \frac{F_3 L}{g_1} \qquad (2.63)$$

where F_1 is the noise figure of the parametric amplifier and F_3 the noise figure of that portion of the receiver following the attenuator. If one now plots the overall noise figure F against the attenuation L, a straight line is obtained given by Eq. (2.63). When F_3 is measured, the available gain g_1 may be determined since the slope of the line is F_3/g_1. The noise figure of the parametric amplifier alone can then be found from the intercept which is equal to $F_1 - 1/g_1$. This method has the further advantage of smoothing out measurement errors.

3

Up-converter and Negative-resistance Parametric Amplifier Theory

The great majority of parametric devices are closely related to two basic types of parametric amplifiers: the *up-converter* and the *negative-resistance parametric amplifier*. In this chapter, we will develop an approximate small-signal theory of operation for these devices with particular attention to their noise performance. The special form of the negative-resistance amplifier known as the degenerate amplifier will be treated separately in some detail as it possesses some unusual features not found in any other practical amplifying device.

3.1 The Up-converter

As a matter of definition, we will say that an up-converter is characterized by the following properties:

1. The output frequency is equal to the sum of the input frequency and the pump frequency.
2. There is no power flow in the device at frequencies other than the input, output, and pump frequencies.

When these two conditions are satisfied, the Manley-Rowe relation of Eq. (1.13) is applicable, showing there is a maximum possible power gain for this device numerically equal to the ratio of output frequency to input frequency.

To compute the detailed operating characteristics of the up-converter, the circuit model shown in Fig. 3.1 will be used. Since the analysis will be restricted to the small-signal case, the nonlinear capacitance has been replaced by a linear time-varying capacitance. A resistance in series with the time-varying capacitance is indicated to provide a loss mechanism for the nonlinear element. It will be shown later that such a series resistance representation is useful when the nonlinear capacitor is a semiconductor *p-n* junction. (A practical semiconductor diode will also have

Why is there no pump signal in the circuit model?

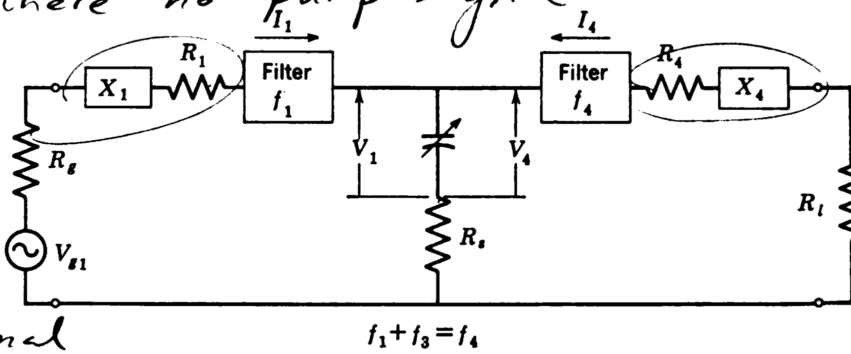

f_1 : signal
f_3 : pump

Fig. 3.1. Circuit model used in the analysis of the up-converter.

series lead inductance and shunt cartridge capacitance. These elements will not affect mid-band gain since they will be in resonance. They may affect bandwidth, however, increasing circuit Q by increasing the stored energy in the circuit.) A signal circuit at f_1 is indicated by X_1, together with a filter which allows current to flow only at frequency f_1. A similar circuit $X_4 + R_l$ is shown for the output frequency. In practice, the frequency filters will usually be replaced by resonant circuits.

The small-signal admittance matrix of either Eq. (1.32) or Eq. (1.37) can be used for this analysis, depending upon whether the unwanted harmonics are more nearly short-circuited or open-circuited. In practical microwave circuits it is difficult to control this condition, so we cannot *a priori* say that one is more correct than the other. Fortunately, the analysis is exactly the same for both cases, with the only differences being in the numerical values assigned to certain parameters. For completeness we will analyze both cases.

To include the effects of the series resistance in the semiconductor diode, we must first invert the admittance matrix of Eq. (1.32) or (1.37) to obtain an impedance matrix. For either case the resulting matrix is

$$\begin{bmatrix} V_1 \\ \\ V_4 \end{bmatrix} = \begin{bmatrix} \dfrac{1}{j\omega_1 C} & -\dfrac{\gamma}{j\omega_4 C} \\ \\ -\dfrac{\gamma}{j\omega_1 C} & \dfrac{1}{j\omega_4 C} \end{bmatrix} \begin{bmatrix} I_1 \\ \\ I_4 \end{bmatrix}. \tag{3.1}$$

For the case of short-circuited harmonics, we have

What's γ ?

$$\begin{aligned} \gamma &= \gamma_1 \\ C &= C_0(1 - \gamma_1^2). \end{aligned} \tag{3.2}$$

What's the meaning of short-circuited and open-circuited harmonics.

while for open-circuited harmonics we have

$$\begin{aligned} \gamma &= \gamma_1(1 + \gamma_1^2)(1 - \gamma_2) \\ C &= C_0(1 - 2\gamma_1^2). \end{aligned} \tag{3.3}$$

Equation (3.3) is valid for γ_1^2 small compared to unity, a condition satisfied by semiconductor diodes. The maximum value that γ_1 is likely to reach in low-noise amplification is about $\frac{1}{3}$. When γ_1 does equal $\frac{1}{3}$, the difference in γ and C as predicted by Eqs. (3.2) and (3.3) is less than 10 per cent. The resulting difference in amplifier performance is even less, for as we shall show, amplifier performance is in general related to the ratio γ/C.

Up-converter Transducer Gain

For conceptual purposes, the circuit model of Fig. 3.1 can be replaced by the linear four-terminal representation of Fig. 3.2. We can compute the transducer gain between input and output by standard linear circuit techniques. It will be recalled that transducer gain is defined as the ratio of the actual power output to the available power input. The actual power output is

$$\text{power output} = |I_4|^2 R_l \tag{3.4}$$

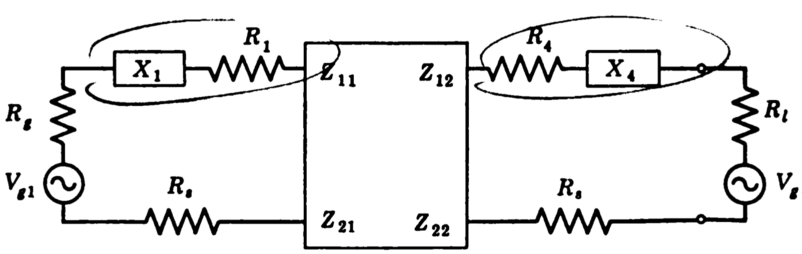

Fig. 3.2. Linear four-terminal representation of the up-converter.

and the available input power is

$$\text{available input power} = |V_g|^2/4R_g. \tag{3.5}$$

To compute these quantities, it is necessary to express I_4 in terms of V_{g1}. This is easily accomplished in the matrix formulation by adding the external circuit impedances to the effective self-impedances of the nonlinear element. That is, we can write the following matrix equation:

$$\begin{bmatrix} V_{g1} \\ V_{g4} \end{bmatrix} = \begin{bmatrix} Z_{11} + Z_{T1} & Z_{12} \\ Z_{21} & Z_{22} + Z_{T4} \end{bmatrix} \begin{bmatrix} I_1 \\ I_4 \end{bmatrix} \tag{3.6}$$

Z_{T1} = total external circuit impedance at f_1

$$= X_1 + \underbrace{R_g + R_s + R_1}_{R_{T1}}$$

Z_{T4} = total external circuit impedance at f_4

$$= X_4 + \underbrace{R_l + R_s + R_4}_{R_{T4}}$$

The current I_4 can be easily obtained by re-inverting the matrix of Eq. (3.6), or by using Cramer's Rule. Setting $V_{g4} = 0$, we obtain

$$I_4 = -\frac{V_{g1}Z_{21}}{(Z_{11} + Z_{T1})(Z_{22} + Z_{T4}) - Z_{12}Z_{21}}. \tag{3.7}$$

The transducer gain then becomes

$$g_t = \frac{4R_gR_l\,|I_4|^2}{|V_{g1}|^2} = \frac{4R_gR_l\,|Z_{21}|^2}{|(Z_{11} + Z_{T1})(Z_{22} + Z_{T4}) - Z_{12}Z_{21}|^2}. \tag{3.8}$$

This is the familiar expression for the transducer gain of a linear four-terminal network.

To investigate the mid-band gain, let us arbitrarily impose the tuning conditions

$$-X_1 = Z_{11}, \qquad -X_4 = Z_{22}. \tag{3.9}$$

At resonance then, the gain becomes

$Z_{21} = -\dfrac{\gamma}{j\omega_1 C}$

$Z_{12} = -\dfrac{\gamma}{j\omega_4 C}$

$$g_t = \frac{4R_gR_l\gamma^2}{(\omega_1 C)^2} \frac{1}{\left[R_{T1}R_{T4} + \dfrac{\gamma^2}{\omega_1\omega_4 C^2}\right]^2}. \tag{3.10}$$

The Manley-Rowe power relations predict a maximum gain of ω_4/ω_1 for this device, a fact not too obvious from Eq. (3.10). To show that this prediction is verified, let us choose the correct values for R_g and R_l to maximize g_t. As a simplification, assume

$$R_{T1} = R_g + R_s, \qquad R_{T4} = R_l + R_s. \tag{3.11}$$

why is related →

This is equivalent to saying that circuit losses are negligible compared to diode losses. With these assumptions, the transducer gain becomes

$$g_t = \frac{4R_gR_l}{\left[(R_g + R_s)(R_l + R_s)\dfrac{\omega_1 C}{\gamma} + \dfrac{\gamma}{\omega_4 C}\right]^2}. \tag{3.12}$$

This expression is symmetric in R_g and R_l; therefore, whatever value of R_g maximizes g_t, it follows that the identical value of R_l also maximizes g_t. For this case, then, $R_g = R_l$ for maximum gain. The value of R_g which maximizes g_t is found by standard methods of differential calculus. This value is

$$R_g = R_s\sqrt{1 + \frac{\gamma^2}{\omega_1\omega_4 C^2 R_s^2}}. \tag{3.13}$$

We can define $1/\omega CR_s$ as the effective Q of the nonlinear element at ω. With this definition, Eq. (3.13) becomes

$$R_g = R_s\sqrt{1 + \frac{\omega_1}{\omega_4}(\gamma Q)^2} \tag{3.14}$$

where $Q = 1/\omega_1 CR_s$. Substituting this value of R_g (and R_l) into Eq. (3.12), we obtain after some algebraic manipulation:

$$g_t = \frac{\omega_4}{\omega_1}\frac{x}{[1 + \sqrt{1 + x}]^2} \tag{3.15}$$

where $x = (\omega_1/\omega_4)(\gamma Q)^2$.

We can easily obtain from Eq. (3.15) an upper bound on the gain of the up-converter when a diode of finite Q is used. As $\omega_4/\omega_1 \to \infty$, the gain will increase to the limiting value of

$$(g_t)_{\max} = \tfrac{1}{4}(\gamma Q)^2. \tag{3.16}$$

A plot of the function $x/[1 + \sqrt{1 + x}]^2$ is shown in Fig. 3.3. Note that it is always less than unity, approaching unity as x approaches

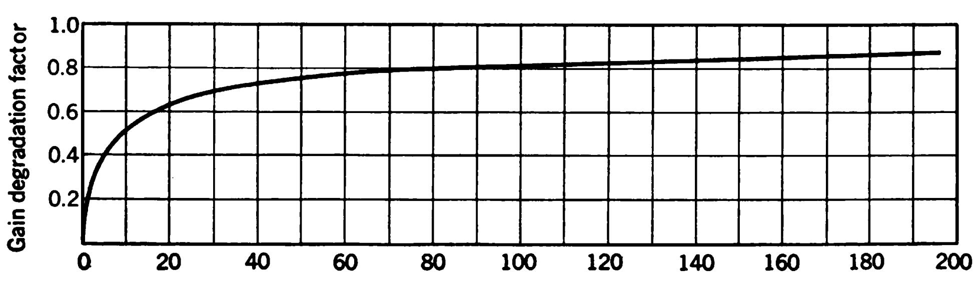

Fig. 3.3. Plot of gain degradation factor $\dfrac{x}{(1 + \sqrt{1 + x})^2}$

infinity. Since γ is bounded, an infinite value of x can be obtained only by making $Q \to \infty$, which implies a lossless nonlinear element. This is in agreement with the Manley-Rowe power relations.

We should also note that x is a function only of frequency and the parameters of the nonlinear capacitance. A good figure of merit for this capacitor is then:

$$\text{Figure of merit} = \gamma Q. \tag{3.17}$$

Referring to Eqs. (3.2) and (3.3), we see that a convenient approximation to use for design purposes is

$$\gamma \approx \gamma_1$$

$$C \approx C_0 \tag{3.18}$$

where the capacitance variation is of the form

$$C_0(1 + 2\gamma_1 \cos \omega t). \tag{3.19}$$

Down-converter Transducer Gain

What happens if we attempt to operate the up-converter in reverse? For example, we might be tempted to replace our microwave resistive mixer by such a parametric down-converter in hope of obtaining frequency conversion to i-f frequencies with gain instead of loss. Unfortunately, the Manley-Rowe relations tell us that an up-converter operated in reverse (that is, putting power *in* at f_4 and removing it at f_1) will produce loss instead of gain. The minimum loss we can have is simply f_1/f_4. We can immediately show this by examining the expression for the up-converter transducer gain, Eq. (3.8). This expression is symmetric with respect to generator and load except for the term $|Z_{21}|^2$. Thus to evaluate down-conversion gain, we only have to replace $|Z_{21}|^2$ by $|Z_{12}|^2$. This is equivalent to interchanging ω_1 and ω_4, a change which seems intuitively obvious. The down-conversion gain (actually a loss) can then be immediately written as

$$g_t = \frac{\omega_1}{\omega_4} \frac{x}{[1 + \sqrt{1 + x}]^2}. \tag{3.20}$$

Input and Output Impedance of the Nonlinear Capacitor

The up-converter is a stable device with positive input and output impedance. The previous discussion has indicated the degree of sta-

See equ 3.15

bility, for even if the output terminals are shorted so as to reflect all output power, oscillation cannot occur since the reverse loss is always greater than the forward gain.

To evaluate the effective impedance which the nonlinear capacitor and associated terminations present to the circuits at f_1 and f_4, standard relations from the theory of linear four-terminal networks can be used. For example, the effective impedance which the nonlinear capacitor presents to the input circuit is given by the following standard equation:

$$Z_{\text{in}} = Z_{11} - \frac{Z_{12}Z_{21}}{Z_{22} + Z_{T4}}$$

$$= \frac{1}{j\omega_1 C} + \frac{\gamma^2}{\omega_1\omega_4 C^2\left(Z_{T4} + \dfrac{1}{j\omega_4 C}\right)}. \tag{3.21}$$

At resonance we have

$$R_{\text{in}} = \frac{\gamma^2}{\omega_1\omega_4 C^2 R_{T4}} \tag{3.22}$$

which is a positive quantity. By use of symmetry the effective impedance which the nonlinear capacitor presents to the ouput circuit at resonance is given by

$$R_{\text{out}} = \frac{\gamma^2}{\omega_1\omega_4 C^2 R_{T1}}. \tag{3.23}$$

which is again positive.

Bandwidth

To discuss the frequency response of the up-converter, it will be necessary to specify the input and output circuits. For simplicity, we will assume that the input and output circuits are simple single-tuned series resonant circuits. The use of single-tuned circuits does not necessarily yield the maximum bandwidth, but it at least is a condition which can be readily analyzed. Using the high-Q approximation, the circuit impedances become

$$Z_{11} + Z_{T1} = R_{T1}(1 + j2\delta_1 Q_1)$$

$$Z_{22} + Z_{T4} = R_{T4}(1 + j2\delta_4 Q_4) \tag{3.24}$$

where R_{T1} = total resistive loading at f_1, including R_g,

R_{T4} = total resistive loading at f_4, including R_l,

Q_1 = loaded circuit Q at f_1,

Q_4 = loaded circuit Q at f_4,

$\delta_1 = (\omega_{\text{in}} - \omega_1)/\omega_1$,

$\delta_4 = (\omega_{\text{out}} - \omega_4)/\omega_4$.

Substituting these values into the expression for transducer gain, Eq. (3.8), we obtain

$$g_t = \frac{\dfrac{4\gamma^2 R_g R_l}{(\omega_1 C R_{T1} R_{T4})^2}}{\left\{1 + \dfrac{\gamma^2}{\omega_1\omega_4 C^2 R_{T1} R_{T4}} - (2\delta_1 Q_1)^2 \dfrac{\omega_1}{\omega_4}\dfrac{Q_4}{Q_1}\right\}^2 + (2\delta_1 Q_1)^2 \left\{1 + \dfrac{\omega_1}{\omega_4}\dfrac{Q_4}{Q_1}\right\}^2}. \tag{3.25}$$

When the optimum source and load impedances for maximum gain are inserted into Eq. (3.25), the maximum transducer gain as a function of frequency becomes the rather formidable expression of Eq. (3.26).

$$g_{t(\max)} = \frac{4\dfrac{\omega_4}{\omega_1}\dfrac{x(x+1)}{[1+\sqrt{1+x}]^4}}{\left\{1 + \dfrac{x}{[1+\sqrt{1+x}]^2} - (2\delta_1 Q_1)^2 \dfrac{\omega_1}{\omega_4}\dfrac{Q_4}{Q_1}\right\}^2 + (2\delta_1 Q_1)^2 \left\{1 + \dfrac{\omega_1}{\omega_4}\dfrac{Q_4}{Q_1}\right\}^2}. \tag{3.26}$$

Note that the gain-degradation factor $x/[1 + \sqrt{1 + x}]^2$ appears in this expression. When the gain degradation is small, the gain can be written in the following simplified form.

$$g_{t(\max)} \approx \frac{4\dfrac{\omega_4}{\omega_1}}{\left\{2 - (2\delta_1 Q_1)^2 \dfrac{\omega_1}{\omega_4}\dfrac{Q_4}{Q_1}\right\}^2 + (2\delta_1 Q_1)^2 \left\{1 + \dfrac{\omega_1}{\omega_4}\dfrac{Q_4}{Q_1}\right\}^2}. \tag{3.27}$$

In the general case, the bandwidth of the up-converter can be computed from Eq. (3.26). Setting the denominator of (3.26) equal to twice its resonant value, we obtain the following quadratic equation:

$$c^2s^2 + (c^2 - 2ac + 1)s - (1 + a)^2 = 0 \tag{3.28}$$

where

$$s = (2\delta_1 Q_1)^2$$

$$a = \frac{\gamma^2}{\omega_1 \omega_4 C^2 R_{T1} R_{T4}}$$

$$c = \frac{\omega_1}{\omega_4} \frac{Q_4}{Q_1}.$$

Note that the fractional bandwidth of the up-converter is $2\delta_1$, while the fractional bandwidth of the input resonant circuit is $1/Q_1$. Therefore the parameter s is the square of the ratio of up-converter bandwidth to input circuit bandwidth.

$$\sqrt{s} = \frac{B}{B_1} \tag{3.29}$$

where B = up-converter bandwidth

B_1 = input resonant circuit bandwidth.

When the up-converter is adjusted for maximum gain, the parameter a becomes equal to the gain degradation factor, and is therefore less than unity. The parameter c is equal to the ratio of input circuit bandwidth to output circuit bandwidth. For wide amplifier bandwidths at maximum gain, it is desirable to have the output bandwidth larger than the input bandwidth, a situation not difficult to obtain in practice since the output frequency will be much higher than the input frequency.

We can estimate the maximum bandwidth obtainable from an up-converter when such single-tuned circuits are used. Assuming that the parameter c is small compared to unity, we can approximate Eq. (3.28) by

$$c^2s^2 + s - (1 + a)^2 = 0 \tag{3.30}$$

the approximate solution to this equation is

$$s = (1 + a)^2 \tag{3.31}$$

therefore,

$$b = \frac{1}{Q_1}(1 + a) \tag{3.32}$$

Since the parameter a is equal to the gain-degradation factor, it will always be less than unity. We can thus state that for an up-converter optimized for maximum gain, the bandwidth is limited by

$$b \leq \frac{2}{Q_1} \tag{3.33}$$

which states that the fractional bandwidth will be less than or equal to *twice* the bandwidth of the input circuit.

We can also evaluate the minimum value of Q_1 under conditions of small gain degradation.

$$Q_1 = \frac{1}{\omega_1 C R_{T1}} \tag{3.34}$$

where $$R_{T1} = R_s + R_g = R_s\left[1 + \sqrt{1 + \frac{\omega_1}{\omega_4}(\gamma Q)^2}\right].$$

Assuming that $(\omega_1/\omega_4)(\gamma Q)^2 \gg 1$, the condition for small gain degradation, we obtain

$$Q_1 \approx \frac{1}{\gamma\sqrt{\omega_1/\omega_4}}. \tag{3.35}$$

Therefore,

$$b \leq 2\gamma\sqrt{\omega_4/\omega_1}. \tag{3.36}$$

Note that Eq. (3.36) predicts quite large bandwidths for the up-converter. With $\omega_4/\omega_1 = 10$ and $\gamma = 0.25$, we have

$$b = 1.58$$

which is so large that the high-Q approximation which was used in the derivation of Eq. (3.28) is really not valid. We can still, perhaps, use Eq. (3.36) as an indication of what measure of bandwidth should be obtainable.

It might seem unreasonable that the up-converter is capable of bandwidths in excess of the bandwidth of the associated input circuit. This apparent paradox can be resolved by remembering that energy is transferred from the signal circuit to the ouput circuit by the action of the variable capacitance. This energy transfer at f_1 can be looked upon as an additional positive resistance in the input circuit, which lowers the Q and hence raises the bandwidth. For the case of the negative-resistance amplifier to be discussed next, there appears an equivalent *negative* resistance in the input circuit, *raising* the circuit Q and greatly *restricting* the bandwidth.

Noise Figure

A parametric device is capable of low-noise amplification since in theory a pure reactance does not contribute thermal noise to the circuit.

In practice, the pure reactance does not exist; it is inevitable that loss will accompany the nonlinear reactance. Additional non-thermal noise may be introduced by the nonlinear element; the evaluation of such noise, however, cannot be made without referring to a specific nonlinear device. For the present purpose, all non-thermal noise sources will be neglected. For the case of the back-biased semiconductor diode, such an approximation seems experimentally justifiable.

The up-converter was shown to be a stable, unilateral amplifier with positive input and output impedances. It is therefore a straightforward matter to evaluate the noise figure according to the standard IRE definition. We must evaluate the noise power delivered to the load when R_g is at the temperature of 290°K, and divide this noise power by $g_l k T_0 B$. The matrix equation of Eq. (3.6) is useful for this purpose. Replacing V_{g1} by the noise voltage e_1, and setting $V_{g4} = 0$, we obtain for the output noise power due to thermal sources at f_1:

$$N_1 = \frac{e_1^2 R_l \mid Z_{21} \mid^2}{\mid (Z_{11} + Z_{T1})(Z_{22} + Z_{T4}) - Z_{12}Z_{21} \mid^2}. \tag{3.37}$$

Similarly for the noise sources at f_4:

$$N_4 = \frac{e_4^2 R_l \mid Z_{11} + Z_{T1} \mid^2}{\mid (Z_{11} + Z_{T1})(Z_{22} + Z_{T4}) - Z_{12}Z_{21} \mid^2}. \tag{3.38}$$

The total output noise power is the sum of N_1 and N_4.

$$N_o = N_1 + N_4 \tag{3.39}$$

The noise figure then is

$$F = \frac{N_1 + N_4}{g_l k T_0 B} = \frac{1}{4kT_0BR_g}\left[e_1^2 + \frac{\mid Z_{11} + Z_{T1} \mid^2}{\mid Z_{21} \mid^2} e_4^2\right]. \tag{3.40}$$

The thermal noise voltages at f_1 and f_4 are given by

$$\begin{aligned} e_1^2 &= 4kB(T_0R_g + T_dR_s + TR_1) \\ e_4^2 &= 4kB(T_dR_s + TR_4) \end{aligned} \tag{3.41}$$

where $T_0 = 290°\mathrm{K}$

T = amplifier circuit temperature

T_d = diode temperature

R_1 = circuit losses at ω_1

R_4 = circuit losses at ω_4.

Therefore, the noise figure becomes

$$F = 1 + \frac{T_d R_s + T R_1}{T_0 R_g} + \frac{|Z_{11} + Z_{T1}|^2}{|Z_{21}|^2} \frac{T_d R_s + T R_4}{T_0 R_g}. \tag{3.42}$$

At resonance, we have

$$F = 1 + \frac{T_d R_s + T R_1}{T_0 R_g} + \frac{(\omega_1 C R_{T1})^2}{\gamma^2} \frac{T_d R_s + T R_4}{T_0 R_g}. \tag{3.43}$$

If we assume that circuit losses are negligible compared to diode losses, the expression for noise figure can be somewhat simplified.

$$F \approx 1 + \frac{T_d}{T_0} \frac{R_s}{R_g} \left[1 + \left(\frac{R_g}{R_s} + 1 \right)^2 \frac{1}{(\gamma Q)^2} \right] \tag{3.44}$$

when $R_{T1} = R_g + R_s$.

It is of interest to determine what value of R_g minimizes the noise figure. By differentiating Eq. (3.44) with respect to R_g, the following values are obtained.

$$\begin{aligned} F_{\min} &\approx 1 + \frac{T_d}{T_0} \left[2 \frac{1}{(\gamma Q)^2} + 2 \sqrt{\frac{1}{(\gamma Q)^2} \left(1 + \frac{1}{(\gamma Q)^2} \right)} \right] \\ &\approx 1 + \frac{2 T_d}{T_0} \left[\frac{1}{\gamma Q} + \frac{1}{(\gamma Q)^2} \right] \end{aligned}$$

when $$R_g = R_s \sqrt{1 + (\gamma Q)^2}. \tag{3.45}$$

It is possible to estimate the magnitude of this minimum noise figure under typical operating conditions. Assuming a value of $\gamma Q = 10$, and $\omega_4/\omega_1 = 10$ the minimum noise figure according to Eq. (3.45) will be for $T_d = 290°K$, $F_{\min} = 1.22$ (or 0.86 db). Since the generator resistance used to obtain this minimum noise figure is not the same as that used to obtain maximum gain, it is of interest to evaluate the gain for this value of R_g. For the optimum load impedance, the calculated gain is 6 db. When R_g is adjusted for maximum gain, the calculated gain is 7.3 db and the calculated noise figure is 1.3 db.

In practice, it is desirable to minimize the overall system noise figure. For two stages in cascade, the expression for overall noise figure is

$$F_{12} = F_1 + \frac{F_2 - 1}{g_1} \tag{2.26}$$

where
F_{12} = overall noise figure
F_1 = first-stage noise figure
F_2 = second-stage noise figure
g_1 = first-stage available gain.

When the second-stage noise figure is high, the minimum overall noise figure is obtained by sacrificing some first-stage noise figure in exchange for increased gain. When the second-stage noise figure is low, first-stage gain is not as important, and it is then desirable to minimize first-stage noise figure. It is possible to compute the exact value of R_g necessary to achieve minimum F_{12}, however this minimum is very close to that computed on the basis of either maximum gain or minimum first-stage noise figure. In Table 3.1 is shown a summary of overall noise figure for the two up-converters examples treated. A second-stage noise figure of 7 db is assumed.

TABLE 3.1

	Maximum gain condition	*Minimum first-stage noise figure*
Gain	7.3 db	6 db
F_1	1.3 db	0.9 db
F_{12}	3.2 db	3.5 db

3.2 The Negative-resistance Parametric Amplifier

Let us now consider the case in which significant power flow occurs only at the signal frequency, pump frequency, and the so-called idler frequency, which is the difference between the pump frequency and the signal frequency. As was briefly discussed in Section 1.2, this leads to a regenerative condition with the possibility of oscillation at both the signal frequency and the idler frequency. When operated below the oscillation threshold, such a device behaves as a bilateral negative-resistance amplifier.

For this mode of operation, the matrix of either Eq. (1.33) or (1.38) is applicable, depending upon whether the unwanted harmonics are more nearly short-circuited or open-circuited. As in the analysis of the up-converter, we will invert the appropriate matrix and add a series resistance to represent loss in the nonlinear capacitor. The inverted matrix becomes

$$\begin{bmatrix} V_1 \\ \\ V_2^* \end{bmatrix} = \begin{bmatrix} \dfrac{1}{j\omega_1 C} & \dfrac{\gamma}{j\omega_2 C} \\ \\ \dfrac{-\gamma}{j\omega_1 C} & \dfrac{-1}{j\omega_2 C} \end{bmatrix} \begin{bmatrix} I_1 \\ \\ I_2^* \end{bmatrix} \tag{3.46}$$

where as before we have

$$\gamma = \gamma_1$$
$$C = C_0(1 - \gamma_1^2) \tag{3.2}$$

for short-circuited hamonics, and

$$\gamma = \gamma_1(1 + \gamma_1^2)(1 - \gamma_2)$$

$$C = C_0(1 - 2\gamma_1^2) \tag{3.3}$$

for open-circuited harmonics.

The procedure used to determine the transducer gain of the negative resistance amplifier will be similar to that used in the previous section for the analysis of the up-converter. In the present case, we have a choice of obtaining an amplified output at either ω_1 or ω_2; both transducer gains will be evaluated.

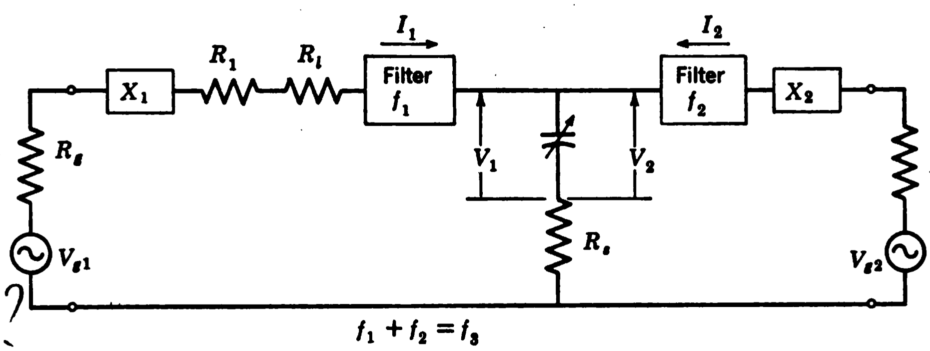

Fig. 3.4. Circuit model used in the analysis of the negative resistance parametric amplifier.

How to add the pump signal? Where is f_3 in the model

Transducer Gain at ω_1

The circuit model to be analyzed is indicated in Fig. (3.4). Again series impedance and band-pass filters are used. As in the case of the up-converter, series resonant circuits could be used in practice to approximate this circuit model.

The matrix equation for this circuit becomes

$$\begin{bmatrix} V_{g1} \\ V_{g2}^* \end{bmatrix} = \begin{bmatrix} Z_{11} + Z_{T1} & Z_{12} \\ Z_{21} & Z_{22} + Z_{T2}^* \end{bmatrix} \begin{bmatrix} I_1 \\ I_2^* \end{bmatrix} \tag{3.47}$$

where $$Z_{T1} = X_1 + R_g + R_l + R_s + R_1$$

$$Z_{T2} = X_2 + R_s + R_2.$$

Computing the current I_1 as a function of V_{g1} with V_{g2}^* set equal to zero, we obtain

$$I_1 = \frac{V_{g1}(Z_{22} + Z_{T2}^*)}{(Z_{11} + Z_{T1})(Z_{22} + Z_{T2}^*) - Z_{12}Z_{21}}. \tag{3.48}$$

The transducer gain at frequency ω_1 is given by the ratio of the power dissipated in R_l to the power available at ω_1.

$$g_t = \frac{4R_gR_l|\cancel{V_2}|^2}{|V_{g1}|^2} \quad (I_1)^2$$

$$= \frac{4R_gR_l\,|\,(Z_{22} + Z_{T2}^*)\,|^2}{|\,(Z_{11} + Z_{T1})(Z_{22} + Z_{T2}^*) - Z_{12}Z_{21}\,|^2}. \tag{3.49}$$

At resonance, the transducer gain becomes

$$g_t = \frac{4R_gR_l}{\left[R_{T1} - \dfrac{\gamma^2}{\omega_1\omega_2C^2R_{T2}}\right]^2} \tag{3.50}$$

gain is not related to taylor expansion coefficient of C ?

when R_{T1} = total series resistance at ω_1

R_{T2} = total series resistance at ω_2.

This expression for the gain of the negative resistance amplifier is reminiscent of that obtained for the up-converter. However, there is one significant difference: the negative sign in the denominator. Now the gain can be made arbitrarily large; in fact, oscillation can occur. This form is characteristic of a circuit containing a negative resistance; the equivalent negative resistance is

$$-R = -\frac{\gamma^2}{\omega_1\omega_2C^2R_{T2}}. \tag{3.51}$$

In practice, a negative-resistance amplifier of this type would be ~~operated~~ close to the point of oscillation in order to achieve significant ~~gain. As an~~ example, let us suppose that $R_g = R_l$ and that $R_{T1} = R_g + R_l$. Then, from Eq. (3.50) we see that in order to achieve 20 db gain, $|R| = 0.9\ R_{T1}$. At this value of gain a three per cent decrease in R_{T1} would cause a 3 db increase in gain. A similar increase in $|R|$ would also produce the same effect. Thus, we can see that gain stability can be a serious problem with the negative-resistance parametric amplifier. At microwave frequencies, non-reciprocal devices such as isolators and circulators can be of great help in stabilizing the input and output impedance, and hence in stabilizing R_{T1}. The magnitude of the negative resistance must also be held constant, which imposes stability criteria upon the pump source.

Another property of such a negative-resistance amplifier is its bilateral gain characteristic. We can look upon the negative resistance as a power generator within the amplifier. In the circuit which has been considered above, this ~~power will be~~ dissipated ~~in~~ both R_g and R_l. It therefore follows that either R_g or R_l could be considered as the output of the amplifier. In the above example the power gain from input to output would be identical to that from output to input. Again at microwave frequencies this property can be altered by employing a circulator to separate the incident energy from the internally generated and reflected energy. (We shall shortly see that the use of a circulator also improves the bandwidth and noise figure of the negative-resistance parametric amplifier.)

Transducer Conversion Gain from ω_1 to ω_2

If we choose to utilize the power dissipated in the resistance R_2 at ω_2 instead of the resistance R_l at ω_1, we have a negative-resistance frequency converter. Again setting $V_{g2}^* = 0$, we can solve for I_2^*:

$$I_2^* = \frac{-Z_{21}V_{g1}}{(Z_{11} + Z_{T1})(Z_{22} + Z_{T2}^*) - Z_{12}Z_{21}}. \tag{3.52}$$

The transducer conversion gain becomes

$$g_{tc} = \frac{4R_gR_2|I_2|^2}{|V_{g1}|^2}$$

$$= \frac{4R_gR_2 \mid Z_{21} \mid^2}{\mid (Z_{11} + Z_{T1})(Z_{22} + Z_{T2}^*) - Z_{12}Z_{21} \mid^2}. \tag{3.53}$$

At resonance the gain becomes

$$g_{tc} = \frac{\omega_2}{\omega_1} \frac{4R_gR_2(R/R_{T2})}{[R_{T1} - R]^2}. \tag{3.54}$$

The similarity to the up-converter can be noted by again introducing the parameter a, which becomes in this case

$$a = \frac{R}{R_{T1}}. \tag{3.55}$$

Then

$$g_{tc} = 4\frac{\omega_2}{\omega_1} \frac{R_gR_2}{R_{T1}R_{T2}} \frac{a}{[1 - a]^2}. \tag{3.56}$$

This expression is identical to that obtained for the up-converter except that the factor $1 + a$ has been replaced by $1 - a$ for the negative-resistance case. Again, this brings out the fact that in one case we have a *positive*-resistance converter, while in the other case we have a *negative*-resistance converter.

Bandwidth

The variation of gain with frequency in the negative-resistance amplifier will depend greatly on the form of the tuned circuits at signal and idler frequencies. In the following section, we will analyze the case of simple single-tuned circuits at both signal and idler frequencies. While this does not yield the optimum circuit for maximum bandwidth, it does give expressions which are at least capable of analysis without resorting to the use of a computer. In Section 4.1 an approach will be discussed for increasing the bandwidth of negative-resistance amplifiers by the use of multiple-tuned circuits.

Assuming series resonant circuits and employing the high-Q approximation, we can write the passive circuit impedances as

$$\begin{aligned} Z_{11} + Z_{T1} &= R_{T1}(1 + j2\delta_1 Q_1) \\ Z_{22} + Z_{T2}^* &= R_{T2}(1 - j2\delta_2 Q_2) \end{aligned} \tag{3.57}$$

where

$$\begin{aligned} R_{T1} &= \text{total resistive loading at } \omega_1 \\ R_{T2} &= \text{total resistive loading at } \omega_2 \\ Q_1 &= \text{loaded circuit } Q \text{ at } \omega_1 \\ Q_2 &= \text{loaded circuit } Q \text{ at } \omega_2 \\ \delta_1 &= \frac{\omega_{\text{signal}} - \omega_1}{\omega_1} \\ \delta_2 &= \frac{\omega_{\text{idler}} - \omega_2}{\omega_2} = -\frac{\omega_1}{\omega_2}\delta_1. \end{aligned}$$

The expression for transducer gain at ω_1 thus becomes

$$g_t = \frac{4R_g R_l}{\left[R_{T1}(1 + j2\delta_1 Q_1) - \dfrac{R}{1 - j2\delta_2 Q_2}\right]^2}. \tag{3.58}$$

Let $a = R/R_{T1}$ as before. The gain may then be written as

$$g_t = \frac{4R_g R_l/R_{T1}^2}{\left[1 + j2\delta_1 Q_1 - \dfrac{a}{1 + j2\delta_1 \dfrac{\omega_1}{\omega_2} Q_2}\right]^2} \tag{3.59}$$

$$= \frac{4R_g R_l/R_{T1}^2}{\left\{1 - \dfrac{a}{1 + \left(2\delta_1 Q_2 \dfrac{\omega_1}{\omega_2}\right)^2}\right\}^2 + (2\delta_1 Q_1)^2 \left\{1 + \dfrac{a \dfrac{\omega_1}{\omega_2} \dfrac{Q_2}{Q_1}}{1 + \left(2\delta_1 Q_2 \dfrac{\omega_1}{\omega_2}\right)^2}\right\}^2}.$$

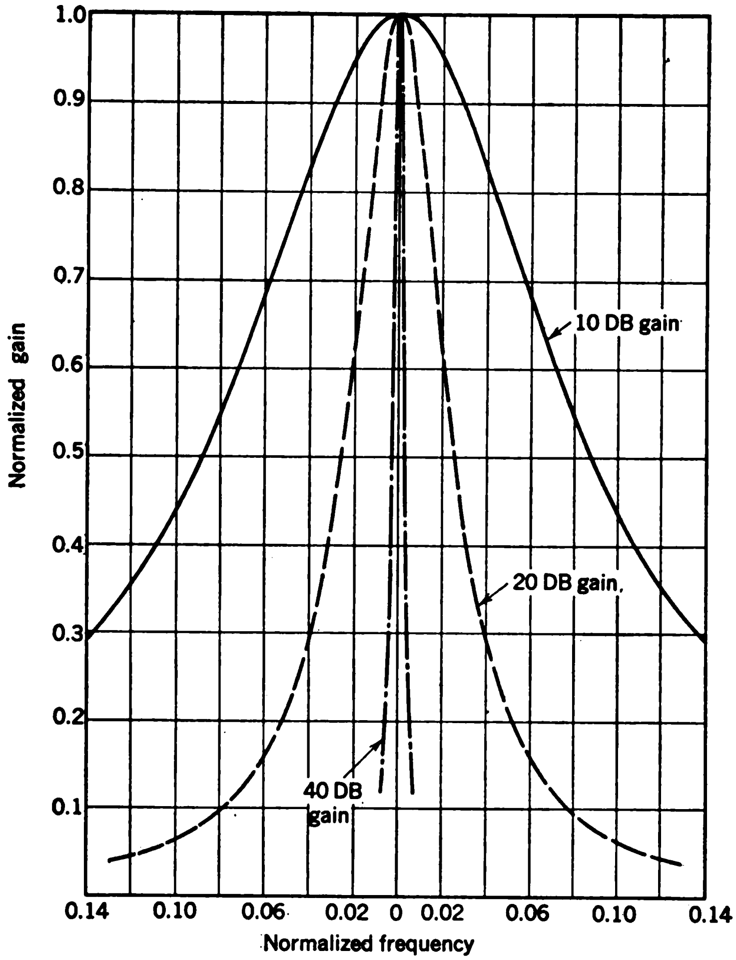

Fig. 3.5. Gain characteristics of a negative-resistance parametric amplifier.

A plot of this gain function in normalized form for several values of gain is shown in Fig. 3.5. The response is more sharply peaked than an ordinary single-tuned circuit. This results in a noise bandwidth which is somewhat greater than the 3 db bandwidth, which is of significance since it is the extent of the noise bandwidth that determines the receiver sensitivity. (See Section 2.3.) Shown in Fig. 3.6 is a plot of noise bandwidth as a function of gain when $R_T = R_g + R_l$.

To quantitatively determine the relation between gain and bandwidth, the denominator of Eq. (3.59) is set equal to twice its resonant value. The resulting equation may be expressed in the following quadratic form:

$$c^2s^2 + [c^2 + 2ac + 1 - 2(1 - a)^2]s - (1 - a)^2 = 0 \tag{3.60}$$

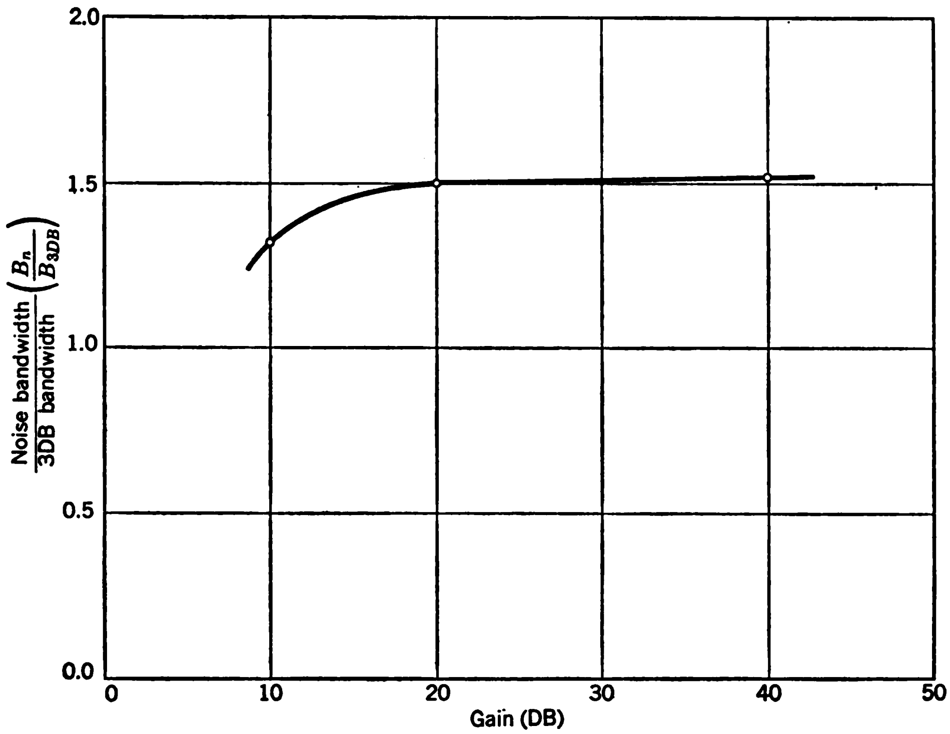

Fig. 3.6 Normalized noise bandwidth as a function of gain for a negative-resistance parametric amplifier.

where

$$a = \frac{R}{R_{T1}}$$

$$c = \frac{\omega_2}{\omega_1}\frac{Q_1}{Q_2}$$

$$s = \left(2\delta_1 Q_2 \frac{\omega_1}{\omega_2}\right)^2.$$

To simplify matters, an approximate solution will be used. It will almost always be true that

$$[c^2 + 2ac + 1 - 2(1 - a)^2]^2 \gg 4c^2(1 - a)^2. \tag{3.61}$$

If so, the solution to the quadratic equation becomes

$$s \approx \frac{(1 - a)^2}{(a + c)^2 + (1 - a)(3a - 1)}. \tag{3.62}$$

We can obtain a gain-bandwidth product by multiplying Eqs. (3.50) and (3.62) together.

$$g_t b^2 = \frac{\dfrac{4R_g R_l}{R_{T1}^2}\left(\dfrac{\omega_2}{\omega_1 Q_2}\right)^2}{\left(a + \dfrac{\omega_2}{\omega_1}\dfrac{Q_1}{Q_2}\right)^2 + (1 - a)(3a - 1)}. \tag{3.63}$$

where b is fractional bandwidth. For high gain, $a \approx 1$, the gain-bandwidth product becomes

$$g_t b^2 \approx \frac{4R_g R_l / R_{T1}^2}{\left[Q_1 + \dfrac{\omega_1}{\omega_2} Q_2\right]^2}. \tag{3.64}$$

It is interesting to compare the approximate gain-bandwidth expression just developed with the analogous expression for a hypothetical linear negative-resistance amplifier whose negative resistance is constant and pure real, independent of frequency. The gain-bandwidth product for this case can be easily shown to be

$$g_t b^2 = \frac{4(R_g R_l / R_T^2)}{Q^2}. \tag{3.65}$$

The expressions are almost identical except that in the case of the parametric amplifier an additional Q, the idler circuit Q, is involved. We might thus talk about an effective circuit Q at the signal frequency which is equal to the actual Q plus the *transformed* idler Q, the transformation ratio being the frequency ratio, ω_1/ω_2.

Equation (3.64) indicates that the single-tuned negative-resistance amplifier is a narrow-band device. To give an estimate of the maximum possible gain-bandwidth product consistent with reasonable gain, let us assume that $R_g = R_l = \frac{1}{2}R_{T1}$. The minimum attainable circuit Q's will be

$$Q_1 = \frac{1}{\omega_1 C R_{T1}}, \qquad Q_2 = \frac{1}{\omega_2 C R_{T2}}. \tag{3.66}$$

For significant gain, we require that $a \approx 1$. Therefore, we have

$$\gamma^2 Q_1 Q_2 \approx 1. \tag{3.67}$$

The maximum gain-bandwidth product can then be written as

$$(g_t b^2)_{\max} = \frac{1}{\left[Q_1 + \dfrac{\omega_1/\omega_2}{\gamma^2 Q_1}\right]^2}. \tag{3.68}$$

This expression has a maximum when $\gamma Q_1 = \sqrt{\omega_1/\omega_2}$. Inserting this value for Q_1 in Eq. (3.68), we obtain

$$(g_t^{1/2} b)_{\max} = \frac{\gamma}{2}\sqrt{\frac{\omega_2}{\omega_1}}. \tag{3.69}$$

×10

As an example, let us assume a gain of 20 db, an idler frequency four times the signal frequency, and $\gamma = 0.25$. The maximum possible bandwidth for single-tuned circuits (assuming that no circulator is used) will then be $b_{\max} = \frac{1}{40} = 2.5\%$. It is difficult to achieve this maximum bandwidth in practice, for the nonlinear reactance will usually have stored energy in excess of that required to resonate with C_0. However, it will be shown that the gain-bandwidth product can be improved by:

1. Using a circulator.
2. Using more complex circuits.

Amplifier Performance with Isolators and Circulators

When negative-resistance parametric amplifiers are used at microwave frequencies, it becomes practical to use such non-reciprocal circuit elements as isolators and circulators. An ideal isolator is a circuit element which transmits energy in one direction without loss, but absorbs all energy transmitted in the opposite direction. An ideal circulator is a circuit element which transmits energy without loss from port 1 to port 2 (see Fig. 2.7), from port 2 to port 3, etc. In contrast with the isolator, the ideal circulator never *absorbs* energy, only *directs* it.

Let us first consider the effect of a circulator on the performance of a negative-resistance parametric amplifier. We will at the same time compare its performance with that of the transmission or two-port amplifier previously treated. Fig. 3.7 shows a circuit for the negative-resistance parametric amplifier with circulator. It is sufficient for our present purpose to represent the parametric amplifier by a simple negative resistance.

The transducer gain for the amplifier with circulator will be equal to the power reflected from the amplifier divided by the power available from the source (assuming a matched ideal circulator). The available

Why do we need the circulator in neg-res paramp?

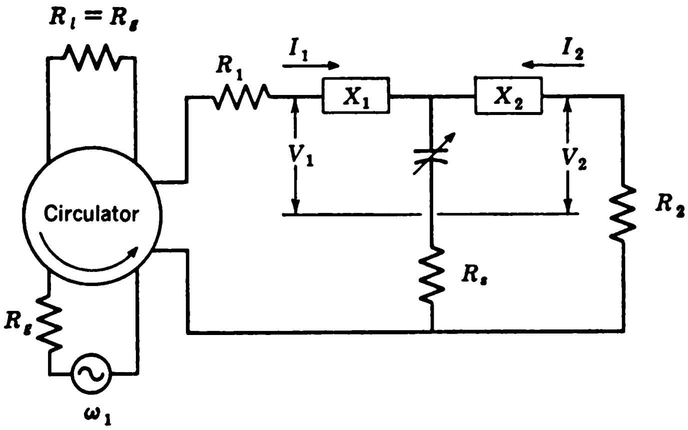

Fig. 3.7. Circuit model for the negative-resistance parametric amplifier operated with circulator.

power is equal to the *incident* power in this case; therefore, the transducer gain becomes simply the ratio of reflected power to incident power. For equal input and output line impedances the transducer gain becomes simply the square of the voltage reflection coefficient.

$$g_t = \rho^2 = \left| \frac{Z_l - Z_o}{Z_l + Z_o} \right|^2. \tag{3.70}$$

For our negative-resistance amplifier, this becomes at resonance:

$$g_t = \left(\frac{R_1 + R_s - R - R_g}{R_1 + R_s - R + R_g} \right)^2 = \frac{(R_{T1} - R - 2R_g)^2}{(R_{T1} - R)^2} \tag{3.71}$$

where $R_g = Z_o$ = generator and load impedance. When the gain is high, $R \approx R_{T1}$. Under this condition the gain becomes

$$g_t = \frac{4R_g^2}{(R_{T1} - R)^2}. \tag{3.72}$$

We can now compare this with the gain of our two-port amplifier, Fig. 3.4. From Eq. (3.50) we have

$$g_t = \frac{4R_g R_l}{(R_{T1} - R)^2}. \tag{3.73}$$

It might appear at first glance that we have only succeeded in discovering a difficult way to make the load impedance equal the generator impedance. In reality, we have improved the gain by at least 6 db for a given bandwidth. To see this, we need to point out that with a given diode, there is a certain maximum negative resistance which can be obtained. From Eq. (3.51), we see that

$$-R_{\max} = -\frac{\omega_1}{\omega_2}(\gamma Q)^2 \tag{3.74}$$

since

$$R_{T2} \geq R_s. \tag{3.75}$$

Under conditions of high gain, we have $R_{T1} \approx R$. Therefore,

$$R_{T1} \approx \frac{\omega_1}{\omega_2}(\gamma Q)^2 \tag{3.76}$$

regardless of whether we use a circulator or not. Eq. (3.76) thus tells us that R_{T1} is the quantity to keep constant in our present comparison. In each case let us assume the optimum loading and zero circuit loss. For the circulator amplifier, the total external passive loading is only R_g. Hence, the gain becomes

$$g_t = \frac{4R_{T1}^2}{(R_{T1} - R)^2}. \tag{3.77}$$

For the two-port amplifier, $R_{T1} = R_g + R_l$. The optimum will be $R_g = R_l = \frac{1}{2}R_{T1}$. For this case the gain becomes

$$g_t = \frac{R_{T1}^2}{(R_{T1} - R)^2} \tag{3.78}$$

which is only *one-fourth* the gain of the circulator amplifier. Thus by the use of a circulator we have doubled the *voltage*-gain-bandwidth product.

As an extra bonus, the stability of the parametric amplifier is greatly improved through the use of a circulator. Regardless of how the generator or load impedances may change, the amplifier will always see a match (no reflected wave) looking into the circulator. Considering the circulator as an integral part of the amplifier, we can thus transform the potentially unstable negative-resistance amplifier into a relatively well-behaved unilateral amplifier with positive input and output impedances.

So far we have been speaking about an ideal circulator. In practice, it is well to keep several things in mind. First, an actual circulator will have some insertion loss. Since this loss occurs before amplification, the noise figure will be directly affected. (See Section 2.2.) If extremely low-noise performance is desired, it may be necessary to cool the circulator to very low temperatures, or else not use one at all. Another problem is imperfect isolation between ports. This will cause a feedback of some of the amplified signal, perhaps to the extent of instability.

The use of isolators in the input and output of a two-port negative-resistance amplifier does not significantly improve the operating characteristics of the amplifier other than by increasing stability. The gain-bandwidth product does not change; noise figure may be either slightly improved or degraded. An improvement in noise performance will occur if load noise is significant and *if* the introduction of an isolator lowers the effective noise temperature of the output termination. One way to lower this temperature is to physically cool the isolator. If load noise is not significant in the first place, introduction of isolators will slightly degrade noise performance (because of the finite forward loss). Isolators *will* reduce amplifier sensitivity to external impedance changes; for this reason their use would probably be recommended when a circulator is not available.

Noise Figure and Operating Noise Temperature

Let us consider first the noise performance of the negative-resistance amplifier operated in conjunction with an ideal circulator. We have already seen that a circulator will improve the gain-bandwidth product of a negative-resistance amplifier; we shall now see that a similar improvement in noise figure is possible.

A negative-resistance amplifier operated with a circulator becomes a unilateral amplifier with positive input and output impedances. Therefore, it is a relatively simple matter to compute the noise figure or effective noise temperature according to IRE standards. For convenience in making the calculations, we will use the high-gain approximation. Using this approximation, the available gain (which in this case is equal to the transducer gain) becomes

$$g_a = \frac{4R_g^2}{(R_{T1} - R)^2}. \tag{3.79}$$

As in the calculation of the noise characteristics of the up-converter, only noise of thermal origin will be considered. Experimental evidence indicates that this approximation is good when diodes are used, as long as they are not driven significantly into conduction, or into reverse breakdown. Of course, when thermal noise is substantially reduced by cooling, the non-thermal sources of noise may begin to be significant.

There are two sources of thermal noise in the negative-resistance parametric amplifier: One is noise from the internal amplifier loss at frequencies near the signal frequency, and another is similar noise at frequencies near the idler frequency. It is this so-called "idler noise" which often complicates and confuses the situation.

To compute noise figure or effective noise temperature, we must obtain the available noise power at the output of the amplifier. Since the high-gain approximation is being used, we can use the matrix approach, being careful to note that $R_l = R_g$ and $R_{T1} = R_s + R_1 + R_g$. We will represent thermal noise by voltage generators at both the signal and idler frequencies, as shown in Fig. 3.4. (Even though a non-reciprocal circulator is actually present, we can still use these same analytical methods in this high-gain approximation if we remember to let R_g and R_l be physically identical.) Using techniques identical with those used to determine gain, we obtain for the noise power output

$$N_1 = \frac{e_1^2 R_g \mid Z_{22} + Z_{T2}^* \mid^2}{\mid (Z_{11} + Z_{T1})(Z_{22} + Z_{T2}^*) - Z_{12}Z_{21} \mid^2}$$

$$N_2 = \frac{e_2^2 R_g \mid Z_{12} \mid^2}{\mid (Z_{11} + Z_{T1})(Z_{22} + Z_{T2}^*) - Z_{12}Z_{21} \mid^2}. \tag{3.80}$$

The noise figure is given by

$$F = \frac{N_1 + N_2}{g_s k T_o B} = \frac{1}{4kT_o B R_g}\left\{e_1^2 + \frac{\mid Z_{12} \mid^2}{\mid Z_{22} + Z_{T2}^* \mid^2} e_2^2\right\}. \tag{3.81}$$

Note that up to this point the noise figure formulation is similar to that for the up-converter. For the particular case of the negative-resistance parametric amplifier, we must insert the following values:

$$\begin{aligned} e_1^2 &= 4kB(T_o R_g + T_d R_s + T_1 R_1) \\ e_2^2 &= 4kB(T_d R_s + T_2 R_2) \\ Z_{22} + Z_{T2}^* &= R_{T2} \quad \text{at resonance} \\ Z_{12} &= -\frac{\gamma}{j\omega_2 C}. \end{aligned} \tag{3.82}$$

Inserting these values, we obtain for the noise figure at resonance:

$$F = 1 + \frac{T_1}{T_0}\frac{R_1}{R_g} + \frac{T_d R_s}{T_0 R_g} + \frac{\omega_1}{\omega_2}\frac{R}{R_g}\frac{1}{T_0}\left(\frac{T_d R_s + T_2 R_2}{R_{T2}}\right). \tag{3.83}$$

Assuming that all amplifier loss is at the same temperature, $\bar{T}$, and recalling that $R \approx R_{T1}$ according to our high-gain approximation, we can simplify Eq. (3.83) considerably.

$$F = 1 + \frac{\bar{T}}{T_0}\left\{\frac{R_{T1}}{R_g}\frac{\omega_3}{\omega_2} - 1\right\} \tag{3.84}$$

The effective input noise temperature can be immediately written as

$$T_e = \bar{T}\left\{\frac{R_{T1}}{R_g}\frac{\omega_3}{\omega_2} - 1\right\}. \tag{3.85}$$

We may ask what the mimimum value of noise figure is when we are constrained to a finite diode series resistance, R_s. It is clearly desirable to make the excess circuit loss at the signal frequency, R_1, as small as possible. It is not immediately clear whether or not we want to make R_2 as small as possible when $T < T_d$; in other words, do we gain in noise figure by adding a cool external idler loading? It is clear that we should make R_g as large as possible. The limit of R_g occurs when loading is so heavy that high gain is no longer possible. It would appear from Eq. (3.85) that we should make the idler frequency, ω_2, as high as possible. In reality, this is not so, as will be shown below.

To derive the minimum noise figure, let us assume that $R_1 \approx 0$. Then $R_{T1} = R_g + R_s$, while $R_{T2} = R_2 + R_s$. For the moment, let us assume that the external idler loading, R_2, is at a temperature of absolute zero. Using this assumption, it will be easy to see that cooled external idler loading does not give the minimum noise figure. Under these conditions, Eq. (3.83) becomes

$$F = 1 + \frac{T_d}{T_0}\frac{R_s}{R_g} + \frac{T_d}{T_0}\frac{\omega_1}{\omega_2}\left[1 + \frac{R_s}{R_g}\right]\frac{R_s}{R_2 + R_s}. \tag{3.86}$$

To evaluate the minimum noise figure, we make use of Eq. (3.67):

$$\frac{\gamma^2}{\omega_1\omega_2 C^2 R_{T1} R_{T2}} \approx 1. \tag{3.87}$$

We may write this in terms of the diode Q at ω_1:

$$\frac{\omega_1}{\omega_2}(\gamma Q)^2 \frac{R_s}{R_2 + R_s}\frac{R_s}{R_g + R_s} \approx 1. \tag{3.88}$$

We can solve this equation for the generator resistance, R_g, and use this value in the expression for noise figure, Eq. (3.86). It is mathematically convenient to express this relation in terms of a normalized effective input temperature:

$$(F - 1)\frac{T_0}{T_d} = \frac{\left[\frac{\omega_1}{\omega_2}\frac{R_s}{R_2 + R_s}\gamma Q\right]^2 + 1}{\frac{\omega_1}{\omega_2}\frac{R_s}{R_s + R_2}(\gamma Q)^2 - 1}. \tag{3.89}$$

We may now optimize this noise figure by the proper choice of pump frequency and idler loading. By differentiation of Eq. (3.89), we find that the optimum condition for minimum noise figure is obtained when

$$\frac{\omega_1}{\omega_2}\frac{R_s}{R_2 + R_s} = \frac{1 + \sqrt{1 + (\gamma Q)^2}}{(\gamma Q)^2}. \tag{3.90}$$

The corresponding optimum noise figure is

$$F = 1 + \frac{T_0}{T_d} \frac{2[1 + \sqrt{1 + (\gamma Q)^2}]}{(\gamma Q)^2}$$

$$\approx 1 + 2\frac{T_0}{T_d}\left[\frac{1}{(\gamma Q)} + \frac{1}{(\gamma Q)^2}\right]. \tag{3.91}$$

There are several points worth noting. First, the result is independent of the external idler circuit loading, *for this special case of* $T = 0°K$. With any degree of idler loading, we can choose the proper idler frequency so that Eq. (3.90) remains satisfied. Thus, in this ideal case, we can reduce the required pump frequency by increasing the external idler loading without changing the noise figure. Or, we may increase the pump frequency and reduce R_2 to zero, without increasing the noise figure above that given by Eq. (3.91). As we pass into the world of reality, however, where absolute zero cannot be reached, we see that whenever $R_2 \neq 0$, the optimum noise figure will always be higher than that given by Eq. (3.91) since R_2 will now contribute some noise power to the amplifier. In reality, only when $R_2 = 0$ (no external idler loading) can the optimum noise figure of Eq. (3.91) be reached. Therefore, it must be concluded that the optimum condition for noise performance occurs when there is no external loading of the idler circuit. On the other hand, for reasons of practicality, it may be desirable to reduce the required pump frequency. The so-called degenerate parametric amplifier, for example, has external idler loading which is cooled to the antenna temperature.

Another point of interest is that the optimum noise figure of the negative-resistance amplifier as given by Eq. (3.91) is identical with that for the up-converter, Eq. (3.45). Since the negative-resistance amplifier can always have higher gain than the up-converter, it follows that second-stage noise contributions will be less for the negative-resistance amplifier and, hence, the negative-resistance amplifier should theoretically have the lower overall system noise figure.

This analysis is directly applicable to the case of lower-frequency or harmonic pumping. For example, if third-harmonic pumping is used, with the fundamental pump frequency of $\omega_p/3$, the appropriate value of γ used in Eq. (3.91) would be given by the Fourier coefficient for the component of capacitance variation at ω_p. For equal voltage swings, direct pumping will always yield larger values of γ than harmonic pumping, and, hence, direct pumping will result in the lowest noise figure. However, if sufficient power were not available at ω_p to drive the diode to its full voltage swing, one might choose to harmonically pump the

What's harmonic pumping?

amplifier at higher power and perhaps obtain a greater value of γ, and, hence, a lower noise figure.

Several interesting bits of design information can be obtained from these results for the optimum negative-resistance amplifier. From Eq. (3.90) with $R_2 = 0$, we can obtain the optimum pump frequency:

$$\frac{\omega_p}{\omega_s} = \sqrt{1 + (\gamma Q)^2}. \tag{3.92}$$

Since γQ will be of the order of three or greater in most practical applications, to a very good approximation we have

$$\frac{\omega_p}{\omega_s} \approx \gamma Q. \tag{3.93}$$

In this case the optimum pump frequency is a function of the diode characteristics alone, and is independent of the signal frequency. If we define a diode cutoff frequency, *evaluated at the effective diode bias point*, as $\omega_{co} = 1/CR_s$, the optimum pump frequency can be written as

$$\omega_p \approx \gamma\omega_{co}. \tag{3.94}$$

Not only must the proper pump frequency be used to minimize noise figure, but also the proper generator loading must be used. The effective generator resistance which one must use can be obtained from Eq. (3.88) with $R_2 = 0$. The result is

$$\begin{aligned} R_g &= R_s\sqrt{1 + (\gamma Q)^2} \\ &\approx R_s\gamma Q. \end{aligned} \tag{3.95}$$

In terms of microwave circuitry, this means we must overcouple the input with VSWR at resonance equal to approximately γQ.

The relation between γQ, pump frequency, and noise figure can be displayed in a useful nomograph when we set $T_d = T_0$. With this diode temperature, the noise figure can be written in the following form:

$$F = \frac{(\gamma Q)^2}{\left[1 - \dfrac{\omega_s}{\omega_p}\right]\left[(\gamma Q)^2 - \dfrac{\omega_p}{\omega_s} + 1\right]}. \tag{3.96}$$

This relation is plotted in the nomograph, Fig. 3.8. Notice that the noise figure is not a strong function of the pump frequency when γQ is above about four and the ratio of pump to signal frequency is greater than about three.

When no circulator is used with the negative-resistance amplifier, the situation can become complicated. The concept of available power

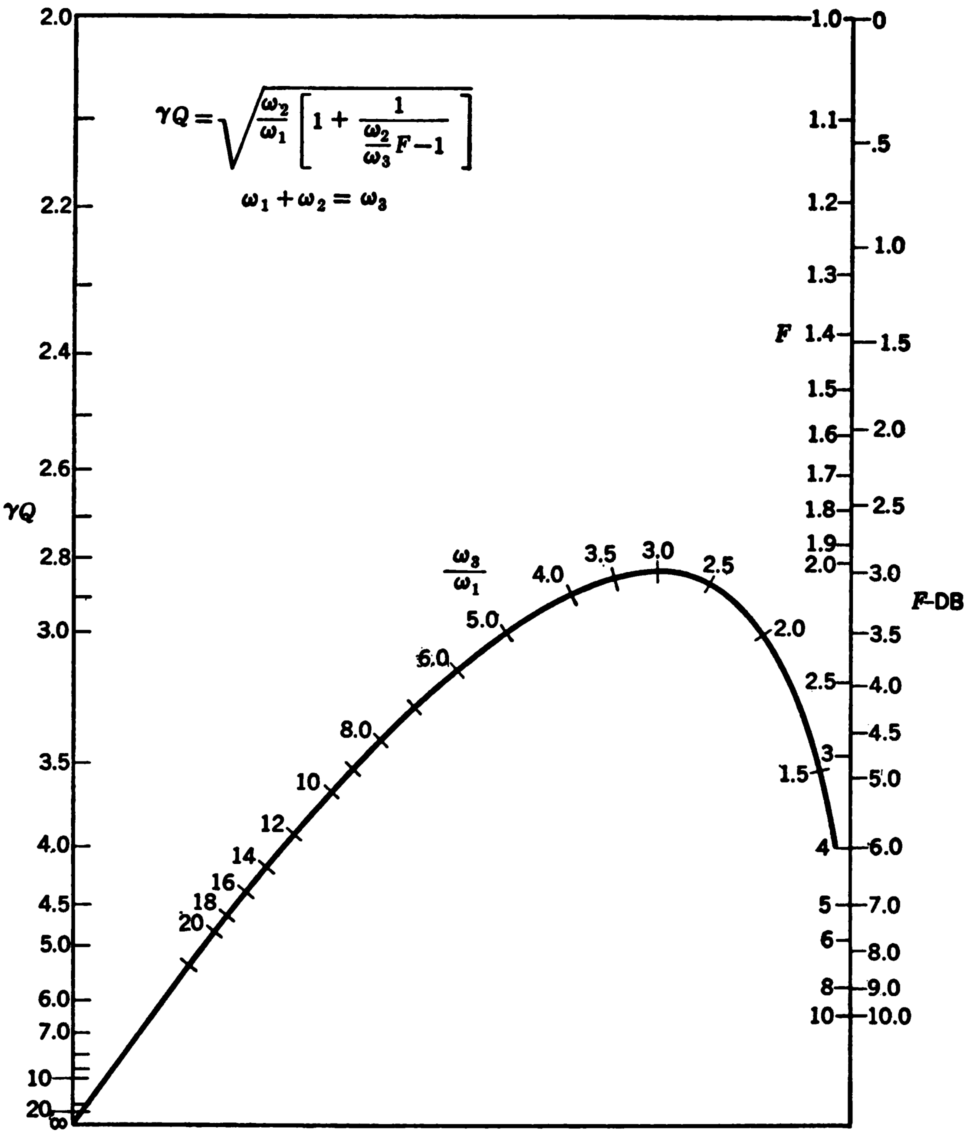

Fig. 3.8. Nomograph for noise figure of the negative-resistance amplifier.

breaks down, so strictly speaking noise figure according to IRE standards is not defined. We can make a logical modification and speak in terms of transducer gain instead of available gain. Even then, all is not well. It is customary to not include noise contributed by the load termination in the evaluation of the noise figure of the amplifier. This is a reasonable practice for most amplifiers since the relative noise contribution of the amplifier is usually independent of the noise contribution of the load. (Of course the load noise must ultimately be counted in the evaluation of *overall* system performance.) When we use a negative-resistance parametric amplifier without a circulator, however, any noise originating in the load will be amplified in the parametric amplifier and returned to the load. Thus the noise contributed by the first stage (parametric amplifier) is *not* independent of the second-stage noise. To further complicate the problem, this amplified load noise will be *coherent* with the initial load noise since they have a common source.

This coherency means that the effective noise contribution of the parametric amplifier arising from load noise is a function of the magnitude and phase of the output reflection coefficient. For example, if $R_g = | -R |$, the output impedance will appear as a short circuit, reflecting the noise power originating in the load. If $R_g - R = R_l$, the output will appear matched and no load noise will be reflected from the parametric amplifier.

Many of these rather bewildering problems can be overcome by including an isolator in the amplifier output. The output impedance becomes positive, and the source of the "load noise" becomes the isolator, which is not coherent with the noise in the actual load termination. Under these conditions, one can calculate the noise figure in the same manner as for the circulator case. The result for this case is:

$$F = 1 + \frac{T_1}{T_0}\frac{R_1}{R_g} + \frac{T_d}{T_0}\frac{R_s}{R_g} + \frac{T_l}{T_0}\frac{(R_{T1} - 2R_l - R)^2}{4R_gR_l} + \frac{\omega_1}{\omega_2}\frac{R}{R_g}\frac{1}{T_0}\frac{T_dR_s + T_2R_2}{R_{T2}}. \tag{3.97}$$

At high gain and uniform amplifier temperature, we have

$$F = 1 + \frac{\bar{T}}{T_0}\left\{\frac{R_{T1}}{R_g}\frac{\omega_3}{\omega_2} - 1\right\} \tag{3.98}$$

where now $R_{T1} = R_g + R_l + R_1 + R_s$. Comparing the above expression with the analogous relation derived for the circulator, we see that the noise figure is increased when no circulator is used. This increase can be looked upon as resulting from the additional loading of the circuit by the output load resistance. One may approach the circulator figure by sufficiently decoupling the load resistance; a penalty must be paid, however, in the form of a reduced gain-bandwidth product and reduced stability of operation.

3.3 The Degenerate Amplifier

The degenerate parametric amplifier will be defined as a negative-resistance parametric amplifier with both signal and idler frequencies contained within the pass-band of the amplifier and with the signal frequency approximately equal to the idler frequency. For convenience in analysis it will be assumed that the pass-band is symmetric about half-pump frequency.

There are two cases of interest in the analysis of the degenerate parametric amplifier: where signal and idler frequencies are separate, and where the signal and idler frequencies are identical. This latter case, which we shall denote as the phase-coherent case, is not one which would ordinarily be used in communication, for perfect knowledge of the signal is necessary in order to make signal and idler coincide at every instant in time. However, it is of interest to investigate its characteristics, since it may well have useful properties in some applications. To build a phase-coherent degenerate amplifier, we merely have to double the *signal* and use it as the pump. But first, let us investigate the non-coherent degenerate amplifier.

The formulation of the gain and bandwidth characteristics of the degenerate parametric amplifier is exactly the same as for the general case. All we need to do is set $\omega_1 \approx \omega_2$ in the expressions previously developed. One possible change in the concept of gain should be mentioned here. We usually think of gain as being the ratio of output power to input power *at the same frequency*. In the case of the degenerate amplifier the idler falls within the pass-band of the amplifier, and we have the possibility of detecting this idler power in addition to the amplified signal power. From the Manley-Rowe relations [see Eq. (1.11) and (1.12)] we know that the power transferred from pump to signal frequency is equal to the power transferred from pump to idler frequency. Thus at high gain the total power at the signal frequency is very nearly equal to the power at the idler frequency, and if we detect the total power in the pass-band which is due to the signal input, we will in effect have 3 db more gain. Going one step further, we can mix signal and idler with a local oscillator at one-half the pump frequency. At i-f frequencies signal and idler will then become identical and we can add their *amplitudes*, obtaining a 6 db increase in gain. This latter technique is sometimes called synchronous pumping.

Noise Figure

The degenerate amplifier possesses the distinction of having two noise figures, much like the broadband microwave mixer, which has a narrow-band and a broadband noise figure. The reason for this situation lies in the definition of average noise figure. This definition states in part: "For heterodyne systems the *input* noise power . . . includes only that noise from the input termination which appears at the output via the principal-frequency transformation of the system. . . ."* As applied to the degenerate parametric amplifier this implies that only noise power *at the signal channel* should be counted as the input noise power. The noise figure which results from this interpretation has often been called the *single-sideband noise figure*. We may ask, though, what happens if there are *two* principal-frequency transformations of the system. For example, suppose that we have information coming into our device at both the signal and idler frequencies of our degenerate parametric amplifier. The information at the signal frequency will be amplified, and the information at the idler frequency will be amplified and *converted* to the signal frequency. Thus, we have two useful frequency transformations between the input and output of our device: one being signal frequency to signal frequency, and the other idler frequency to signal frequency. Under this interpretation we should count noise power at both signal frequency and idler frequency as the source of the output noise power at the signal frequency. The noise figure which results from this interpretation has often been called the *double-sideband noise figure*. The single-sideband noise figure may be computed directly from Eq. (3.83) by setting $\omega_1 = \omega_2$, $T_2 = T_0$, and $R_2 = R_g$. When the gain is high and the circuit loss is small we may write the result in the following simple form:

$$F_{ssb} = 2\left[1 + \frac{\bar{T}}{T_0}\frac{R_s}{R_g}\right]. \tag{3.99}$$

The desired value of R_g when a circulator is used can be obtained from Eq. (3.67), which in this case becomes

$$\gamma Q \frac{R_s}{R_g + R_s} \approx 1. \tag{3.100}$$

Therefore

$$R_g = R_s[\gamma Q - 1]. \tag{3.101}$$

Substituting this value into Eq. (3.99), we obtain

$$\begin{aligned} F_{ssb} &= 2\left[1 + \frac{\bar{T}}{T_0}\frac{1}{\gamma Q - 1}\right] \\ &\approx 2\left[1 + \frac{\bar{T}}{T_0}\left(\frac{1}{\gamma Q} + \frac{1}{(\gamma Q)^2}\right)\right]. \end{aligned} \tag{3.102}$$

It is interesting to note that the minimum noise figure in this case is 3 db. This is a direct result of the restriction to single-sideband operation. We may illustrate this by reference to Fig. 3.9. Here we have schematically

*"IRE Standards on Electron Tubes: Definition of Terms, 1957;" *Proc IRE*, vol. 45, p 1000; July 1957.

illustrated the pass-band of a degenerate amplifier centered about half-pump frequency. For single-sideband operation we will arbitrarily define the signal input channel as that portion of the pass-band which is below $\omega_p/2$. Let us compute the noise figure of this amplifier under the assumption of no internal noise contribution. The total output noise in this case will consist of $2g_tkT_0B$ where g_t is the transducer power gain at signal frequency; *i.e.*, the ratio of output signal power to available input signal power. The factor of 2 arises in the following manner: input noise power in the signal band $B/2$ produces output noise power of $g_tkT_0B/2$ in the signal band and also produces an equal amount of noise power in the idler band due to the frequency-mixing action. The equality of signal and idler noise power at high gain is a direct consequence of the Manley-Rowe relations as was stated earlier. (We shall also derive this on page

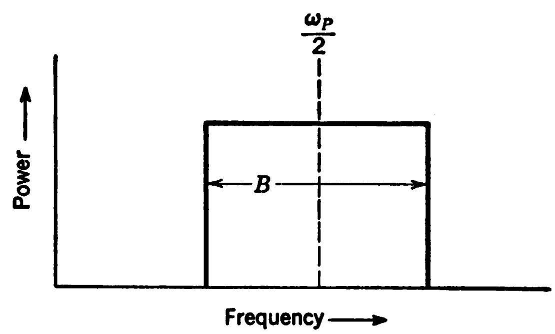

Fig. 3.9. Pass-band of idealized degenerate amplifier.

75.) In exactly the same manner noise power of value $kT_0B/2$ enters the idler pass-band and contributes $g_tkT_0B/2$ of noise power to both signal and idler output pass-bands. Adding these four non-coherent noise powers we obtain a total noise power of $2gkT_0B$. The noise figure of this ideal amplifier is not a function of its bandwidth; let us for convenience focus our attention only on the signal pass-band of width $B/2$ and very carefully compute the signal-sideband noise figure. We must take the *total* output noise power in $B/2$ (no matter from what source) and divide this by the gain at the signal frequency multiplied by the noise from the input termination at 290°K *which appears at the output via the principal-frequency transformation of the system*. The principal-frequency transformation is defined in single-sideband applications as that which does not change frequency; *i.e.*, idler-to-signal transformation is excluded. The total output power in $B/2$ is g_tkT_0B, and the input *signal* noise power in $B/2$ is $kT_0B/2$. Therefore

$$F_{ssb} = \frac{g_tkT_0B}{g_tkT_0B/2} = 2. \tag{3.103}$$

We can now rather easily evaluate the corresponding double-sideband noise figure. According to the previously stated definition of double-sideband noise figure, we now have *two* pincipal-frequency transformations: signal-to-signal and idler-to-signal. Since input at the idler channel is now considered as part of the signal channel, we must include noise *at the input* over the full bandwidth, B, of the device. However, since any information arriving at either signal or idler frequencies will be contained in a bandwidth of only $B/2$ at the output, it is still valid to restrict our attention to an output bandwidth of $B/2$. The applicable input noise is kT_0B and the output noise in bandwidth $B/2$ is $g_t kT_0B$; hence the noise figure is unity.

At first it appears that some illegal "sleight-of-hand" has been employed here to obtain a double-sideband noise figure. It should be emphasized that we are in a sense just defining it by the above "derivation." It so happens that it is this noise figure which one measures for a degenerate parametric amplifier in practice with a standard broadband noise source; in addition it is this noise figure (and corresponding operating noise temperature) which may be convenient to use in the evaluation of the sensitivity of some systems. In this double-sideband mode of operation we are essentially taking information over a band B and converting it so all the information is contained in a band $B/2$. If this can be done without degradation of the desired information upon detection, the double-sideband operating noise temperature may be a useful measure of system sensitivity. (See Section 6.3.)

To compute the double-sideband noise figure for the general case of the lossy degenerate parametric amplifier, we can use the same procedure as for the single-sideband noise figure except that in this case the applicable input noise power is *twice* that for the single-sideband case. The output noise power is the same, regardless of whether a single-sideband or double-sideband operation is involved. It must then follow that the double-sideband noise figure of the degenerate parametric amplifier is one-half the single-sideband noise figure. Therefore:

$$F_{dsb} = 1 + \frac{\bar{T}}{T_0}\frac{R_s}{R_g}. \tag{3.104}$$

Recall that for operation with a circulator,

$$R_g = R_s[\gamma Q - 1]. \tag{3.101}$$

Therefore the double-sideband noise figure becomes

$$F_{dsb} = 1 + \frac{\bar{T}}{T_0}\frac{1}{\gamma Q - 1} \approx 1 + \frac{\bar{T}}{T_0}\left[\frac{1}{\gamma Q} + \frac{1}{(\gamma Q)^2}\right]. \tag{3.105}$$

We will next derive the expressions for the operating noise temperature of both the single-sideband and double-sideband modes. Recall that the operating noise temperature has been defined as the ratio of the actual noise power output of the device under operating conditions to the product of transducer gain, Boltzmann's constant, and the actual signal-channel noise bandwidth. In terms of the example of Fig. 3.9 the signal-channel noise bandwidth for single-sideband operation is $B/2$, while the signal-channel noise bandwidth for double-sideband operation is B. So again we see that the operating noise temperature for double-sideband operation is precisely one-half that for single-sideband operation.

We will follow the same derivation for operating noise temperature as for the non-degenerate amplifier. From Eq. (3.80) we see that at high gain the noise output power for the degenerate amplifier can be written as

$$N_0 = \frac{e_1^2}{4R_g} g_t + \frac{R_l e_2^2}{(R_{T1} - R)^2} \tag{3.106}$$

where

$$e_1^2 = e_2^2 = 4kB/2[T_a R_g + T R_s].$$

The operating noise temperature for single-sideband operation can thus be written as

$$(T_{op})_{ssb} = 2\left[T_a + \bar{T}\frac{R_s}{R_g}\right]. \tag{3.107}$$

Comparing Eq. (3.105) and (3.107), we see that the operating noise temperature can be readily expressed in terms of the single-sideband noise figure.

$$(T_{op})_{ssb} = (F_{ssb} - 2)T_0 + 2T_a. \tag{3.108}$$

By definition, if you will, the double-sideband operating noise temperature then is

$$(T_{op})_{dsb} = \tfrac{1}{2}[(F_{ssb} - 2)T_0 + 2T_a] = (F_{dsb} - 1)T_0 + T_a. \tag{3.109}$$

It is of interest to compare the operating noise temperatures of the optimum up-converter and non-degenerate parametric amplifier with that of the degenerate amplifier. Recall that for the optimum up-converter and non-degenerate parametric amplifier the operating noise temperature is

$$T_{op} = 2\bar{T}\left[\frac{1}{\gamma Q} + \frac{1}{(\gamma Q)^2}\right] + T_a.$$

Using Eq. (3.105) and (3.108), the corresponding expression for the single-sideband degenerate parametric amplifier is found to be

$$(T_{op})_{ssb} = 2\bar{T}\left[\frac{1}{\gamma Q} + \frac{1}{(\gamma Q)^2}\right] + 2T_a. \tag{3.110}$$

For double-sideband operation we therefore have

$$(T_{op})_{dsb} = \bar{T}\left[\frac{1}{\gamma Q} + \frac{1}{(\gamma Q)^2}\right] + T_a. \tag{3.111}$$

Comparing the three expressions for operating noise temperature, we see that the double-sideband degenerate figure is the lowest, and the single-sideband degenerate figure is the highest. For systems where the double-sideband operating noise temperature is appropriate it is thus seen that the degenerate parametric amplifier is the logical choice for best sensitivity; for systems where the single-sideband operating noise temperature is appropriate, the choice would be either an up-converter or non-degenerate negative-resistance amplifier. This comparison will be discussed in terms of specific system applications in Chapter 6.

The Phase-coherent Degenerate Amplifier

We will next consider the special case where the pump frequency is *exactly* twice the signal frequency of the degenerate parametric amplifier. A simple method of accomplishing this is indicated schematically in Fig. 3.10. Here we have a signal generator which is simultaneously fed to the input of the degenerate parametric amplifier and to a frequency doubler. The output of the frequency doubler is then used as a pump source for the parametric amplifier. Under this condition the signal and idler frequencies are identical and therefore coherent.

Such a device is by its nature a single-frequency device since no departure from coherence with the pump is allowed. Bandwidth is therefore of little interest. Also, strictly speaking, noise figure is not defined for this case since the signal bandwidth is essentially ~~zero~~. In

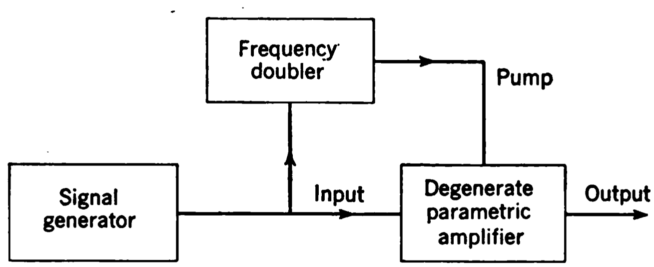

Fig. 3.10. Possible configuration for a phase-coherent degenerate amplifier.

amazing!!!

fact, if we attempt to define noise figure as is often done on the basis of input signal-to-noise ratio relative to output signal-to-noise ratio, we will find that a noise figure of -3 db is possible. This implies that a 3 db improvement in signal-to-noise ratio can be obtained by passing a signal through a perfect phase-coherent degenerate amplifier! Before one jumps to any conclusions regarding possible practical applications of this seemingly wonderous property, it should be pointed out that the signal frequency must be *exactly* half the pump frequency. This in turn means that the signal frequency (or carrier frequency) must be known completely at every instant of time so that we can know how to pump the amplifier. This point will be discussed further in the chapter on system applications, with particular reference to phase-lock systems and AM systems.

is the coefficient of varactor Fourier series

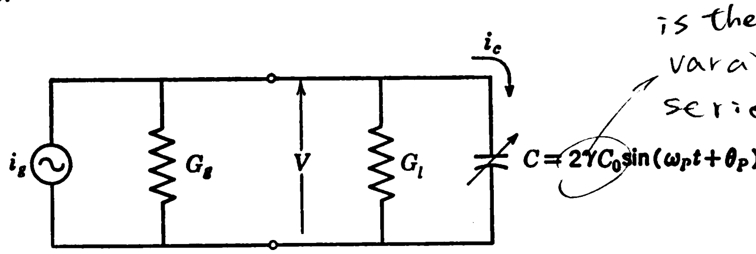

Why?

Fig. 3.11 Circuit model used in the analysis of the phase-coherent degenerate amplifier.

In the analysis of the phase-coherent degenerate parametric amplifier we will depart from the use of the impedance matrix technique and use a shunt circuit for analysis. This is done so that phase relations are explicitely stated in a manner which is convenient in subsequent analysis for possible system applications. The circuit model to be used is as shown in Fig. 3.11. For convenience the circuit is assumed to be resonant at the signal frequency, hence only the time-varying portion of capacitance is indicated. No results of consequence are lost by this assumption; off-resonance operation merely introduces a phase shift into the results. For generality we will first assume signal and idler frequencies are not identical, and then later impose the condition of coherence. Using the linear time-varying capacitance approach, we can express the current flow in the capacitor by the following equation:

How to make a paramp oscillate?

$$i_c = \frac{d}{dt}[Cv] = C\frac{dv}{dt} + v\frac{dC}{dt}. \tag{3.112}$$

We will assume that

$$C = 2\gamma C_o \sin(\omega_p t + \theta_p)$$

$$v = V_1 \sin(\omega_1 t + \theta_1) + V_2 \sin(\omega_2 t + \theta_2)$$

$$\omega_1 + \omega_2 = \omega_p. \tag{3.113}$$

input small

$\bar{i}_c = \bar{i}_c(\omega_1) + \bar{i}_c(\omega_2)$

The capacitor current thus becomes, for the components at ω_1 and ω_2:

$$i_c \approx \overbrace{\omega_1\gamma C_0 V_2 \sin(\omega_1 t + \theta_p - \theta_2)}^{\bar{i}_c(\omega_1)} + \overbrace{\omega_2\gamma C_0 V_1 \sin(\omega_2 t + \theta_p - \theta_1)}^{\bar{i}_c(\omega_2)}. \tag{3.114}$$

For ~~the on-reso~~nance circuit model used, the current at a given frequency must be in phase with the voltage at that frequency. Therefore

What does on-resonance mean?

$$\theta_1 = \theta_p - \theta_2, \qquad \theta_2 = \theta_p - \theta_1 \tag{3.115}$$

or simply

$$\theta_1 + \theta_2 = \theta_p. \tag{3.116}$$

From the circuit model,

$$-i_c(\omega_2) = V_2(G_g + G_l)\sin(\omega_2 t + \theta_2). \tag{3.117}$$

Combining the res~~ults of Eq. (3.117) and~~ (3.114) we obtain

$$-\frac{\omega_2\gamma C_o}{G_g + G_l}V_1 \sin(\omega_2 t + \theta_2) = V_2 \sin(\omega_2 t + \theta_2). \tag{3.118}$$

Therefore

$$i_c(\omega_1) = -\frac{\omega_1\omega_2(\gamma C_0)^2}{G_g + G_l}V_1 \sin(\omega_1 t + \theta_1). \tag{3.119}$$

The transducer gain at ω_1 is given by

① $\frac{V_1^2}{4R_g}$ ② $R_L|i_g(\omega_1)|^2$ power

$$g_t = \frac{4G_gG_l}{|i_g(\omega_1)|^2}V_1^2 \tag{3.120}$$

and

$$i_g(\omega_1) = V_1(G_g + G_l)\sin(\omega_1 t + \theta_1) - \underbrace{\frac{\omega_1\omega_2(\gamma C_0)^2}{G_g + G_l}V_1 \sin(\omega_1 t + \theta_1)}_{\bar{i}_c(\omega_1)}. \tag{3.121}$$

Therefore

the i_g current at frequency ω_1

$$g_t = \frac{4G_gG_l}{\left[G_g + G_l - \frac{\omega_1\omega_2(\gamma C_0)^2}{G_g + G_l}\right]^2}. \tag{3.122}$$

When the gain is high, the negative conductance term will be approximately equal to the total passive circuit conductance.

$$G_g + G_l \approx \frac{\omega_1\omega_2(\gamma C_0)^2}{G_g + G_l}. \tag{3.123}$$

Since $\omega_1 \approx \omega_2$ we can further approximate Eq. (3.123) by

$$\omega_1\gamma C_0 \approx \omega_2\gamma C_0 \approx G_g + G_l. \tag{3.124}$$

$r_n = \frac{C''}{2C_1}$

Combining Eqs. (3.124) and (3.118), we find

$$V_1 \approx V_2 \tag{3.125}$$

which in turn implies that equal power ~~output is~~ obtained from either the signal frequency or the idler frequency. As was previously mentioned, this property can sometimes ~~be used~~ to advantage in certain system applications. This point will be discussed further in Chapter 6.

Let us now consider the phase-coherent case. Set $\omega_1 = \omega_2 = \frac{1}{2}\omega_p$. We therefore assume that

$$\begin{aligned} C &= 2\gamma C_0 \sin(2\omega_1 t + \theta_p) \quad \text{pump phase} \\ v &= V_1 \sin(\omega_1 t + \theta_1). \quad \text{signal phase} \end{aligned} \tag{3.126}$$

The capacitor current at ω_1 is

$$i_c(\omega_1) = -\,\omega\gamma C_0 V_1 \sin(\omega_1 t + \theta_p - \theta_l). \tag{3.127}$$

The expression for the generator current then becomes $I_c(\omega_1)$

$$i_g = V_1(G_g + G_l)\sin(\omega_1 t + \theta_l) - \omega\gamma C_0 V_1 \sin(\omega_1 t + \theta_p - \theta_l). \tag{3.128}$$

V Note that in this case the two components are not necessarily in phase. Because of this phase difference, it is convenient to now use the exponential representation of sinusoids. In such complex notation we can write

$$i_g = v_1(G_g + G_l)e^{j\theta_l} - \omega\gamma C_0 V_1 e^{j(\theta_p - \theta_l)}. \tag{3.129}$$

The transducer gain is then given by

$$\begin{aligned} g_t &= \frac{4G_g G_l V_1^2}{i_g i_g{}^*} \\ &= \frac{4G_g G_l}{(G_g + G_l)^2[1 + \beta^2 - 2\beta\cos(2\theta_l - \theta_p)]} \end{aligned} \tag{3.130}$$

where $$\beta = \frac{\omega\gamma C_0}{G_g + G_l}.$$

We therefore see that the gain of the phase-coherent degenerate parametric amplifier is phase-dependent. The maximum gain occurs when $2\theta_1 = \theta_p$ and has the value

$$(g_t)_{\max} = \frac{4G_g G_l}{(G_g + G_l)^2(1 - \beta)^2}. \tag{3.131}$$

Going back to the expression for the gain of the non-phase-coherent degenerate amplifier, Eq. (3.122), we see that this gain can be written as

$$g_t = \frac{4G_g G_l}{(G_g + G_l)^2(1 - \beta^2)^2}. \tag{3.132}$$

The ratio of the value of the two gains for equal values of β is

$$\text{ratio} = \left[\frac{1 - \beta^2}{1 - \beta}\right]^2 = (1 + \beta)^2 \approx 4 \qquad (3.133)$$

since for high gain $\beta \approx 1$. We thus see that the phase-coherent amplifier has 6 db more gain than the non-phase-coherent amplifier. We can picture this result as arising from the fact that now signal and idler are coherent so we can add the voltages in phase, doubling the output voltage for 6

How to ensure phase coherent?

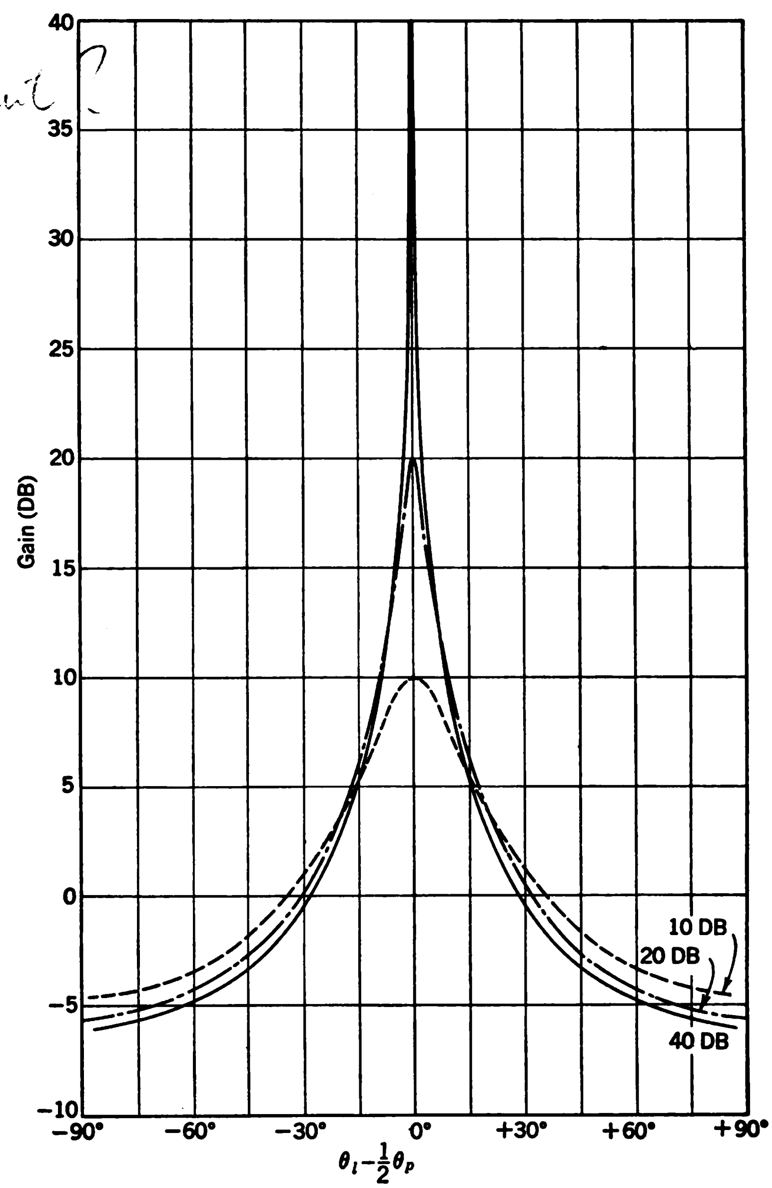

Fig. 3.12. Gain characteristic of a phase-coherent degenerate parametric amplifier.

db more gain. If signal and idler add out of phase, these two voltages approximately cancel and we get loss instead of gain.

This phase-sensitive gain characteristic is illustrated in Fig. 3.12, which is a plot of Eq. (3.130) with $G_g = G_l$. Notice that the abscissa is essentially the output phase relative to the pump phase. A quite different curve is obtained when the gain as a function of the *input* phase is determined. This is because there is a phase shift between input and output which is a function of the output phase relative to the pump. To compute this phase shift we can make use of Eq. (3.129). Expressing i_g in terms of the quantity β, we have

$$i_g = V_1(G_g + G_l)\,[e^{j\theta_l} - \beta e^{j(\theta_p - \theta_l)}]. \tag{3.134}$$

The load current is simply

$$i_l = V_1 G_l e^{j\theta_l}. \tag{3.135}$$

The ratio is then

$$\frac{i_g}{i_l} = \frac{G_g + G_l}{G_l}\,[1 - \beta e^{j(\theta_p - 2\theta_l)}]. \tag{3.136}$$

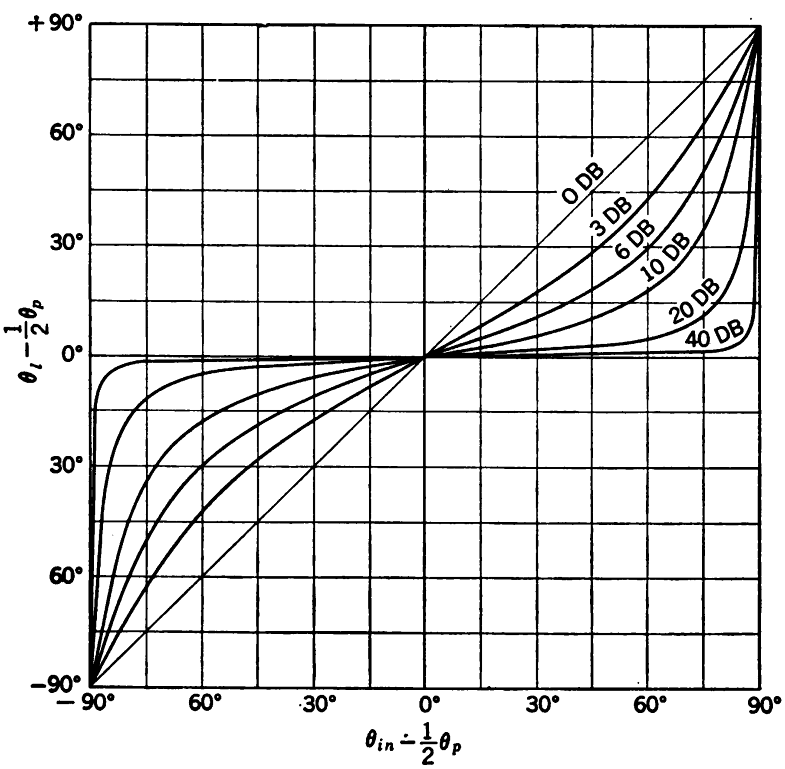

Fig. 3.13. Phase shift characteristic of a phase-coherent degenerate parametric amplifier.

To obtain the argument of Eq. (3.136) we will rewrite it as

$$\frac{i_g}{i_l} = \frac{G_g + G_l}{G_l} \{1 - \beta[\cos(\theta_p - 2\theta_l) + j \sin(\theta_p - 2\theta_l)]\} \tag{3.137}$$

Therefore

$$\text{argument}\left(\frac{i_g}{i_l}\right) = \tan^{-1}\left[\frac{\beta \sin(\theta_p - 2\theta_l)}{1 - \beta \cos(\theta_p - 2\theta_l)}\right] = \theta_{\text{in}} - \theta_l. \tag{3.138}$$

A plot of Eq. (3.138) for several values of gain (with $G_g = G_l$) is shown in Fig. 3.13). It is interesting to note that at high gain the input phase can vary quite drastically relative to the pump phase without greatly affecting the output phase.

Combining the results of Eq. (3.130) and (3.138), we can compute the gain characteristic as a function of input phase; the result is shown in Fig. 3.14. Here we see that a phase excursion of $\pm 45°$ will decrease the

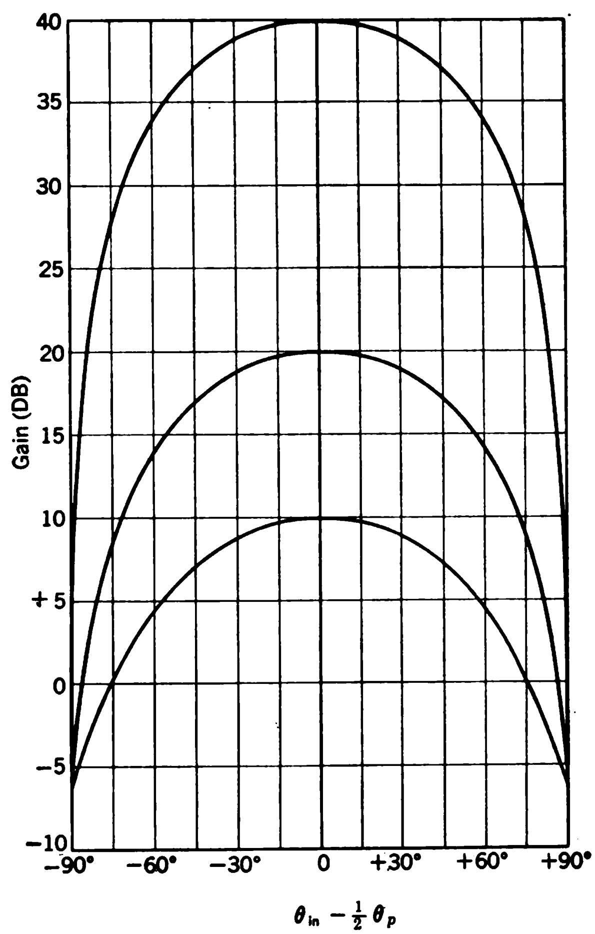

Fig. 3.14. Gain of a phase-coherent degenerate parametric amplifier as a function of input phase.

gain by only about 3 db. This is precisely the shape of gain response one would obtain experimentally using the arrangement indicated in Figure 3.10, using a phase shifter between the signal generator and degenerate amplifier. Because of the very sharp null which can be obtained at high gain with $\theta_{in} - \frac{1}{2}\theta_p = \pm 90°$, such a scheme could have possible application as a sensitive microwave phase indicator.

The result shown in Fig. (3.14) can be directly obtained in another fashion. The load current can be expressed in the following form:

$$i_l = \frac{|i_g|}{1 - \beta^2} \frac{G_l}{G_g + G_l} [e^{j\theta_{\text{in}}} + \beta e^{j(\theta_p - \theta_{\text{in}})}] \tag{3.139}$$

The power gain thus becomes

$$g_t = \frac{4|i_l|^2 G_g}{|i_g|^2 G_l} = \frac{4G_g G_l}{(G_g + G_l)^2} \frac{1 + \beta^2 + 2\beta \cos\,(2\theta_{\text{in}} - \theta_p)}{[(1 + \beta)(1 - \beta)]^2} \tag{3.140}$$

which is plotted in Fig. (3.14) with $G_g = G_l$.

4

Additional Theory of Parametric Devices

Now that we have formulated the basic characteristics of the two fundamental parametric amplifiers, the up-converter and the negative-resistance amplifier, we will consider a variety of more specialized topics which are of interest. The problem of broadbanding the negative-resistance amplifier will be discussed, and some of its large-signal characteristics determined. A theory of harmonic generation will be developed which indicates the efficiency of higher-harmonic generation with semiconductor diodes. The chapter will conclude with a very brief description of several examples of more sophisticated or more specialized parametric devices which can be constructed.

4.1 Broadbanding the Negative-resistance Parametric Amplifier

One of the disadvantages of negative-resistance parametric amplifiers using single-tuned circuits is narrow bandwidth. Typical bandwidths of experimental amplifiers at useful values of gain have often been on the order of 1%. The theory developed in Section 3.2 indicates that even if we have a perfect amplifier we could not hope for bandwidths much greater than about 5% at 20 db gain when single-tuned circuits are used. Two approaches have been used in an attempt to increase the bandwidth of these devices: the use of traveling-wave circuits, and the use of multiple-tuned circuits. The traveling-wave parametric amplifier consists typically of a multitude of parametric diodes periodically placed in a propagating structure. Bandwidths of the order of 25% with modest gain have been obtained from such amplifiers. The traveling-wave approach to broadbanding will be discussed in Section 4.2; in this section we will briefly examine the multiple-tuned circuit approach, which uses but a single diode in a suitably designed circuit.

It was previously pointed out that an amplifier which can be characterized by a negative resistance in a single-tuned resonant structure possesses a voltage-gain bandwidth product which is a constant determined by the parameters of the resonant structure. For low-loss amplifiers, the expression can be written approximately as

$$g^{1/2}b = 1/Q_l \tag{4.1}$$

where g = transducer power gain,

b = fractional bandwidth,

Q_l = loaded Q of amplifier resonant circuit.

We can graphically derive this relation in a manner which is useful in explaining, in qualitative terms at least, how it is possible to increase the bandwidth of such a negative-resistance amplifier.

The gain of a general negative-resistance amplifier can be expressed in the following form:

$$g = \frac{K^2}{|R_a - R + jX_a|^2}$$

or

$$g^{1/2} = \frac{K}{|R_a - R + jX_a|} \tag{4.2}$$

where K = a constant independent of frequency,

R = negative resistance of amplifier,

R_a = circuit resistance of amplifier,

X_a = circuit reactance of amplifier.

For high-Q single-tuned circuits, the impedance $R_a + jX_a$ can be approximated as $R_a(1 + j2\ (\Delta f/f_0)\ Q)$. The locus of this impedance as a function of frequency is a straight line as is shown in Fig. 4.1. The gain of a negative-resistance amplifier can be conveniently plotted on such an

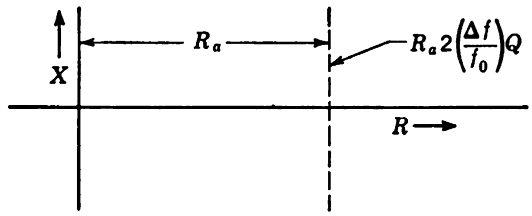

Fig. 4.1. Impedance plot of a high-Q single-tuned circuit.

impedance plane, as shown in Fig. 4.2. The length l_1 is seen to be equal to $|R_a - R + jX_a|$, and therefore the square root of the power gain is equal to

$$g^{1/2} = \frac{K}{l_1}. \tag{4.3}$$

When the angle θ in Fig. 4.2 is equal to 45°, the length l_1 is equal to $\sqrt{2}$ times its length when $\theta = 0°$. Therefore, when $\theta = 45°$ the gain is 3 db

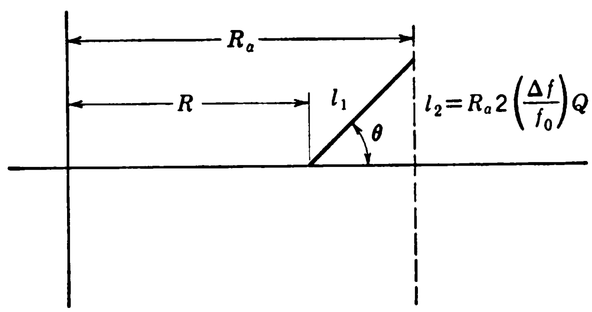

Fig. 4.2. Impedance plot illustrating gain of a negative-resistance amplifier.

less than the mid-band gain ($\theta = 0°$). The fractional bandwidth at this point is then proportional to the length l_2. We see then that the gain-bandwidth product is proportional to the ratio of l_2 to l_1 with $\theta = 45°$.

$$g^{1/2}b \propto \frac{l_2}{l_1}. \tag{4.4}$$

If we increase the gain of the amplifier, the length l_1 will decrease, but so will l_2, since θ is constrained to be 45° in this example. The ratio l_2/l_1 will remain constant; therefore the gain-bandwidth product is a constant for a given (single-tuned) circuit.

From this graphical explanation of gain-bandwidth product, we can readily see the effect of the shape of the impedance function on the bandwidth of negative-resistance amplifiers. The existence of a constant gain-bandwidth product, is seen, for example, to depend solely upon the straight-line locus which characterizes the high-Q single-tuned circuit. We may radically alter the gain-bandwidth characteristics of negative-resistance amplifiers then by changing the shape of the circuit impedance function. If it were possible to obtain a circular impedance locus as in Fig. 4.3, we would have an amplifier approaching infinite bandwidth. Of course we cannot obtain such functions, nor can we obtain a constant negative resistance over extreme frequency ranges, but we can certainly do better than with simple single-tuned circuits. For example, it has been shown experimentally that large bandwidths can be obtained with double-tuned circuits. A possible impedance plot of such a circuit is indicated in Fig. 4.4.

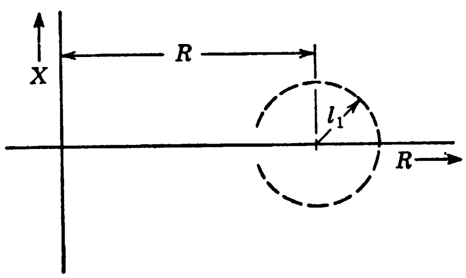

Fig. 4.3. Impedance plot of "ideal" wide-band negative-resistance amplifier.

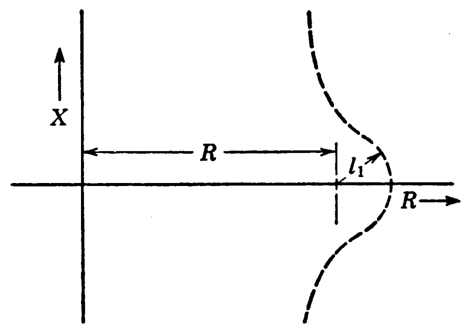

Fig. 4.4. Possible impedance plot of a double-tuned negative-resistance amplifier.

The above qualitative reasoning indicates the general philosophy involved in the broadbanding of single-diode, negative-resistance parametric amplifiers. As one becomes quantitative, however, the discovery is soon made that broadbanding of parametric amplifiers is not as straightforward as is implied by the above qualitative arguments. This is because in the general parametric amplifier we have not one, but two circuits to worry about: the signal circuit and the idler circuit. Moreover, these two circuits cannot be treated independently, for they interact with each other through the mixing action in the nonlinear reactance. The problem is somewhat analogous to the construction of a wideband filter to match a load impedance when this load impedance is a function of the characteristics of the filter under consideration.

The detailed analysis of such amplifiers unfortunately is rather complex, and consequently no attempt will be made to pursue the subject much further. We can, however, make some brief qualitative comments regarding this technique. Matthaei[96] has shown, for example, that in order to avoid excessive variations in gain the filter circuit used for broadbanding must have only very small variations in impedance over the pass-band. This is perhaps obvious from our previous discussion of the negative-resistance amplifier which pointed out that for gain stability the amplifier loading must be constant. Another interesting result of Matthaei's work is that the maximum theoretical bandwidth obtainable from multiple-tuned circuits is directly proportional to γ, a result which has previously been stated in Section 3.2 in connection with single-tuned amplifiers. Thus it is again highly desirable to pump the diode as hard as possible.

There appears to be no theoretical reason why a multiple-tuned *degenerate* parametric amplifier should have a higher noise figure than a comparable single-tuned amplifier. However, in practice one must work with circuits of finite loss, and a complex multi-stage filter structure will have higher loss than a comparable single-tuned circuit. Such loss will deteriorate noise figure, hence care must be taken in the circuit design to minimize this loss. Even if it were possible to eliminate all loss, however, the single-sideband noise figure of the degenerate parametric amplifier can never be less than 3 db. Often in order to realize the inherent low-noise properties of parametric amplifiers, it is necessary to use pump frequencies several times higher than the signal frequency. When this is done, separate circuits for signal and idler frequencies must be provided. To broadband a non-degenerate amplifier, a broadband filter structure could be provided at the idler frequency, as well as a filter structure at the signal frequency. Such an arrangement necessitates the use of a resistive termination of the idler filter circuit if the diode is to see a constant real impedance, R_{o2}, looking into the idler filter. (See Fig. 4.5.) From the standpoint of noise performance, the addition of resistive loss to the idler circuit is definitely undesirable.

One possible approach which would avoid this loading would be to use a simple single-tuned resonant circuit at the idler frequency with no added loss, and to compensate for the resulting impedance variation at the signal frequency with a suitable circuit. By such a method some broadbanding should be possible without degradation of noise figure.

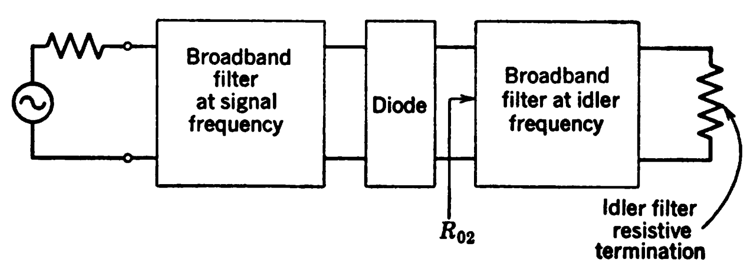

Fig. 4.5. A possible configuration for a broadband non-degenerate parametric amplifier.

4.2 The Traveling-wave Parametric Amplifier

Up to now we have considered parametric devices which utilize essentially resonant structures. Such circuits suffer from certain drawbacks which can be minimized by resorting to nonresonant propagating circuits. For example, the negative-resistance parametric amplifier was shown to be a potentially unstable device with bilateral characteristics. However, if we replace the resonant structure by a suitable propagating structure, it is possible to achieve a measure of unilateral gain with improved stability and bandwidth. A variety of configurations are possible, each with its own characteristics. Perhaps the simplest is the case where all three traveling waves—signal, idler, and pump—have positive phase and group velocities. In the following section such an amplifier will be analyzed for the case where the propagating structure, including the associated nonlinear reactive medium, is lossless and uniform in the direction of propagation, following the method of Tien and Suhl.[128] This is the simplest case to analyze, but is perhaps not the most useful case since quite often the nonlinear reactance is concentrated at discrete intervals along an otherwise linear transmission line. A coaxial line periodically loaded by semiconductor diodes is an example of such a configuration. Several analyses of such periodic structures are in the literature.[77–79] Following the analysis of the uniform line we will present in abbreviated form the analysis of Bell and Wade[7] for the iterated parametric amplifier. Finally we will simply state some of the characteristics of allied traveling-wave amplifiers with other combinations of phase and group velocities.

The Uniform Traveling-wave Parametric Amplifier Without Loss

The circuit model of the uniform traveling-wave parametric amplifier is shown in Fig. 4.6. It is essentially a transmission line with a distributed nonlinear dielectric. If we impress a strong traveling-wave on the structure at the pump frequency we will effectively have a capacitance which varies with time and distance. Using the small-signal approximation we may thus replace the nonlinear capacitance at signal and idler frequencies

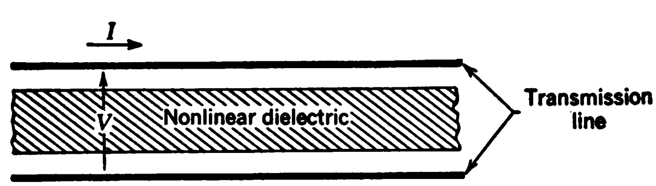

Fig. 4.6. Schematic representation of the distributed parametric amplifier.

by an equivalent linear time-varying capacitance. We may then write the governing differential equations for the traveling waves which exist at the signal and idler frequencies. It will be assumed that no frequencies above the pump frequency propagate in phase with the pump; in fact, Boyd and Roe[11] and Landauer[79] have shown that the gain will be seriously impaired if such components are allowed to propagate in synchronism. The equations for the waves at ω_1 and $\omega_2 = \omega_p - \omega_1$, are:

$$\frac{\partial i_1(z, t)}{\partial z} = -\frac{\partial}{\partial t}[(C_1 + C(z, t))v_1(z, t)]$$

$$\frac{\partial v_1(z, t)}{\partial z} = -L_1 \frac{\partial i_1(z, t)}{\partial t}$$

$$\frac{\partial i_2(z, t)}{\partial z} = -\frac{\partial}{\partial t}[(C_2 + C(z, t))v_2(z_1 t)]$$

$$\frac{\partial v_2(z, t)}{\partial z} = -L_2 \frac{\partial i_2(z, t)}{\partial t}. \tag{4.5}$$

Combining these equations, we have

$$\frac{\partial^2 v_1(z, t)}{\partial z^2} = C_1 L_1 \frac{\partial^2 v_1(z, t)}{\partial t^2} + L_1 \frac{\partial^2}{\partial t^2}[C(z, t)v_2(z, t)]$$

$$\frac{\partial^2 v_2(z, t)}{\partial z^2} = C_2 L_2 \frac{\partial^2 v_2(z, t)}{\partial t^2} + L_2 \frac{\partial^2}{\partial t^2}[C(z, t)v_1(z, t)]. \tag{4.6}$$

Let us now assume that the voltages v_1 and v_2 are traveling waves with propagation constants β_1 and β_2 respectively. That is,

$$v_1 = V_1 e^{j(\omega_1 t - \beta_1 z)} + V_1^* e^{-j(\omega_1 t - \beta_1 z)}$$

$$v_2 = V_2 e^{j(\omega_2 t - \beta_2 z)} + V_2^* e^{-j(\omega_2 t - \beta_2 z)}. \tag{4.7}$$

The quantities V_1 and V_2 are thus the amplitudes of the voltage traveling waves at the signal and idler frequencies. As we expect to have growing waves, we will assume that V_1 and V_2 are slowly-varying functions of z. It will be further assumed that the capacitance varies in a like manner:

$$C = C_0[e^{j(\omega_p t - \beta z)} + e^{-j(\omega_p t - \beta z)}]. \tag{4.8}$$

The simplest case and the one which results in the maximum gain is when

$$\beta_1 + \beta_2 = \beta. \tag{4.9}$$

Using these assumptions and neglecting terms involving $\partial^2 v/\partial z^2$ Eq. (4.6) can be written as

$$-2j\beta_1 \frac{\partial V_1}{\partial z} - \beta_1^2 V_1 = -\omega_1^2 L_1 C_1 V_1 - \omega_1^2 C L_1 V_2^*$$

$$2j_1\beta_2 \frac{\partial V_2^*}{\partial z} - \beta_2^2 V_2^* = -\omega_2^2 C_2 L_2 V_2^* - \omega_2^2 C L_2 V_1 \qquad (4.10)$$

and similar equations for V_1^* and V_2. It is convenient to define

$$C = \gamma_1 C_1 = \gamma_2 C_2. \qquad (4.11)$$

Noting that the propagation constant of a uniform transmission line is given by $\beta = \omega\sqrt{LC}$, we can now write Eq. (4.10) as

$$\frac{\partial V_1}{\partial z} = -\tfrac{1}{2}j\gamma_1\beta_1 V_2^*$$

$$\frac{\partial V_2^*}{\partial z} = \tfrac{1}{2}j\gamma_2\beta_2 V_1. \qquad (4.12)$$

Combining these equations we have

$$\frac{\partial_2 V_1}{\partial z^2} - \tfrac{1}{4}\gamma_1\gamma_2\beta_1\beta_2 V_1 = 0 \qquad (4.13)$$

which has the following exponential solution:

$$V_1 = a_1 e^{\alpha z} + b_1 e^{-\alpha z} \qquad (4.14)$$

where $\alpha = \tfrac{1}{2}(\gamma_1\gamma_2\beta_1\beta_2)^{1/2}$.

Exactly the same solution is obtained for V_2^*. It is thus seen that exponentially growing and decaying waves will exist on this transmission line. The gain per unit length of the dominant growing wave is given by

$$\text{gain of growing wave} = \tfrac{1}{2}(\gamma_1\gamma_2\beta_1\beta_2)^{1/2} \quad \text{nepers/meter} \qquad (4.15)$$

If we impose the boundary conditions at the input of the line

$$v_1 = a \cos(\omega_1 t + \phi)$$

$$v_2 = 0 \qquad (4.16)$$

we obtain the following relations for the voltage at signal and idler frequencies:

$$v_1(z, t) = a \cosh \alpha z[\cos(\omega_1 t - \beta_1 z + \phi)]$$

$$v_2(z, t) = a\sqrt{\frac{\gamma_2}{\gamma_1}\frac{\beta_2}{\beta_1}} \sinh \alpha z[\sin(\omega_2 t - \beta_2 z - \phi)]. \qquad (4.17)$$

The power gain at ω_1 is then given by

$$\text{Power gain} = \cosh^2 \alpha z \tag{4.18}$$

When the gain is high, the decreasing wave can be ignored and we can write the gain in a somewhat simpler manner.

$$\text{Power gain} \approx \tfrac{1}{4} e^{2\alpha z}. \tag{4.19}$$

Bandwidth

The bandwidth of the traveling-wave parametric amplifier is determined in large measure by the range in frequency over which Eq. (4.9) remains approximately satisfied. It is useful to have some measure of what deviation from synchronism will produce a given decrease in gain. Tien[127] has shown that for the case just treated, a deviation from synchronism by the amount $\Delta\beta$ results in a gain constant given by

$$\begin{aligned} \alpha L &= \tfrac{1}{2}\left[\gamma_1\gamma_2\beta_1\beta_2 - \Delta\beta^2\right]^{1/2} L \quad \text{nepers} \\ &= 4.34\left[\gamma_1\gamma_2\beta_1\beta_2 - \Delta\beta^2\right]^{1/2} L \quad \text{db} \\ &\approx 4.34\left[\gamma_1\gamma_2\beta_1\beta_2\right]^{1/2}\left[1 - \frac{1}{2}\left(\frac{\Delta\beta^2}{\gamma_1\gamma_2\beta_1\beta_2}\right)\right] L \quad \text{db} \end{aligned} \tag{4.20}$$

where L is the length of the amplifier. A 3 db decrease in gain will thus occur when the following relation is satisfied:

$$3 \text{ db} = 2.17\,\frac{\Delta\beta^2 L}{\sqrt{\gamma_1\gamma_2\beta_1\beta_2}} \quad \text{db}. \tag{4.21}$$

Solving for $\Delta\beta$ we obtain

$$\Delta\beta = 1.18\sqrt{\frac{\overline{\gamma\beta}}{L}} \tag{4.22}$$

where $\overline{\gamma\beta} = \sqrt{\gamma_1\gamma_2\beta_1\beta_2}$.

For large bandwidth it is desirable to have $\Delta\beta$ as large as possible, since this means that we can then depart an appreciable amount from synchronism without suffering loss in gain. Therefore it is desirable from bandwidth considerations to pump the amplifier as hard as possible, a result again in agreement with that obtained for resonant-circuit parametric amplifiers.

The Iterated Traveling-wave Parametric Amplifier

The circuit model used by Bell and Wade[7] consists of a uniform transmission line periodically loaded with shunt admittances, Fig. 4.7. From our previous experience with the negative-resistance parametric

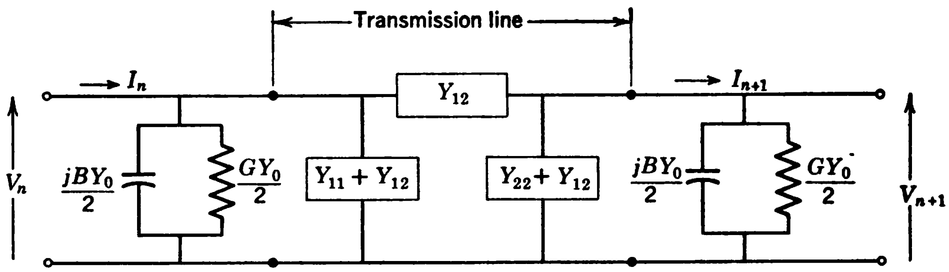

Fig. 4.7. Circuit model for one section of the iterated traveling-wave parametric amplifier (after Bell and Wade).

amplifier we might anticipate that the real part of this shunt admittance will be negative for the lossless case. The method of analysis to be used will be to evaluate the gain of an infinite line in terms of such an admittance, and then calculate the value of this effective admittance which the nonlinear mixing process creates.

The model of Fig. 4.7 can be described by the following equations:

$$I_n = \left[Y_{11} + (G + jB)\frac{Y_o}{2}\right]V_n + Y_{12}V_{n+1}$$

$$I_{n+1} = -\,Y_{12}V_n - [Y_{22} + (G + jB)\,Y_o/2]V_{n+1}. \qquad (4.23)$$

We can now employ a simple but very powerful theorem which is indispensable in the analysis of periodic structures. This is the theorem of Floquet which states that in a given mode of propagation in a periodic structure at a given steady-state frequency, the fields at one cross section differ from those a period away only by a complex constant. The real part of this constant will denote the change in amplitude of the fields while the imaginary part will denote the change in phase between sections. It will be convenient to write this complex constant as $e^{-\Gamma L}$, where L is the period of the periodic structure. We can thus write an expression for the voltage and current at the nth section of line in terms of the input voltage and current:

$$V_n = V_0e^{-\Gamma Ln}$$

$$I_n = I_0e^{-\Gamma Ln}. \qquad (4.24)$$

Substituting these relations into Eq. (4.23) we obtain

$$\frac{I_0}{V_0} = Y_{11} + (G + jB)\frac{Y_o}{2} + Y_{12}e^{-\Gamma L}$$

$$= -\left[Y_{12}e^{\Gamma L} + Y_{22} + (G + jB)\,\frac{Y_o}{2}\right]. \qquad (4.25)$$

Combining these two equations for I_0/V_0 and rearranging the terms, we arrive at a transcendental equation for ΓL.

$$\cosh \Gamma L = \frac{Y_{11} + Y_{22} + (G + jB)Y_o}{-2Y_{12}}. \tag{4.26}$$

For a uniform transmission line of characteristic admittance Y_o, and propagation constant β_o the admittance parameters are

$$Y_{11} = Y_{22} = -jY_o \cot \beta_o L$$
$$Y_{12} = jY_o \csc \beta_o L. \tag{4.27}$$

Substituting these values into Eq. (4.26), we arrive at the following result:

$$\cosh \Gamma L = \cos \beta_o L + \frac{jG - B}{2} \sin \beta_o L. \tag{4.28}$$

So far we have not specified the nature of the constant Γ. In general Γ will be a complex number; to explicitly express this fact, let us write Γ as

$$\Gamma = \alpha + j\beta \tag{4.29}$$

where now α and β are real quantities. Using this definition we can write Eq. (4.28) as two equations, one obtained by equating all the real quantities, and one obtained by equating all the imaginary quantities.

$$\cosh \alpha L \cos \beta L = \cos \beta_o L - B/2 \sin \beta_o L$$
$$\sinh \alpha L \sin \beta L = G/2 \sin \beta_o L. \tag{4.30}$$

These are the general equations for the propagation constant of an infinite uniform transmission line which is periodically loaded by the general admittance $Y_0(G + jB)$. The real part of the propagation constant, αL, gives the gain or loss of the line per period, while the imaginary part, βL, gives the phase shift of the line per section.

In order to use Eq. (4.30) in the analysis of the iterated parametric amplifier, it is necessary to evaluate the effective admittance $G + jB$. Assuming that we allow voltages only at frequencies ω_1, ω_2, and $\omega_p = \omega_1 + \omega_2$ to propagate, we can use the small-signal admittance matrix, Eq. (1.33) to determine G and B. We have by Eq. (1.33)

$$Y_{o_1}(G_1 + jB_1) = \frac{I_1}{V_1} = j\omega_1 C_0 + j\omega_1 \gamma C_0 \frac{V_2^*}{V_1}$$
$$Y_{o_2}(G_2 + jB_2) = \frac{I_2}{V_2} = j\omega_2 C_0 + j\omega_2 \gamma C_0 \frac{V_1^*}{V_2}. \tag{4.31}$$

In order to obtain gain, we will need a negative real part of Eq. (4.31). This requirement means physically that we must have the proper phase relation between signal and idler frequencies at all times. We can express the required phase as

$$\frac{V_2^*}{V_1} = Ae^{j\pi/2}$$

$$\frac{V_1^*}{V_2} = De^{j\pi/2} \tag{4.32}$$

where A and D are real quantities. Just as in the single-diode case, the mixing process automatically insures the correct phase for gain *at the input to the line.** Thereafter the phase velocity of the transmission line must be proper in order to maintain this correct phase, relative to the pump phase. Recall that in the case of the single-diode amplifier, the phase relation was

$$\theta_1 + \theta_2 = \theta_3. \tag{3.114}$$

The analogous relation here is

$$e^{j(\beta_1 L + \beta_2 L)} = e^{j\beta_3 L}. \tag{4.33}$$

Therefore

$$\beta_1 + \beta_2 = \beta_3 \tag{4.34}$$

must be satisfied for maximum gain in the traveling-wave amplifier.

There remains to be evaluated the magnitude of the voltage ratio V_1/V_2. This can be done on physical grounds with the aid of the Manley-Rowe relations. The Manley-Rowe relations tell us that the ratio of the power flow from the nonlinear reactance at signal and idler frequencies is dependent *only* on the frequency ratio ω_1/ω_2. This ratio must be the *same* for every diode along our iterated parametric amplifier. Let P_n^1 be the power flow from the nth diode at ω_1 and P_n^2 be the power flow from the nth diode at ω_2. For this infinite periodic line all the power will flow in the forward direction and be increased by the additional power at the $n + 1$ diode. We can express this mathematically as

$$P_{n+1}^1 = P_n^1 e^{2\alpha_1 L}$$

$$P_{n+1}^2 = P_n^2 e^{2\alpha_2 L}. \tag{4.35}$$

* This phase relation is a result of the assumption of a real iterative impedance as seen by the time-varying portion of the capacitance.

But from the Manley-Rowe relations we have

$$\frac{P_{n+1}^1}{P_{n+1}^2} = \frac{P_n^1}{P_n^2} \tag{4.36}$$

since the ratio must be independent of which diode we are considering. This can only be true if $\alpha_1 = \alpha_2$.

We can now use the additional information that $\alpha_1 = \alpha_2$ to eliminate the remaining unknown, V_1/V_2. Assuming that the gain per unit length is small, we can say that $\sinh \alpha L \approx \alpha L$. Eq. (4.30) then becomes

$$\alpha L = \frac{G}{2} \frac{\sin \beta_o L}{\sin \beta L}. \tag{4.37}$$

Using the derived value of G, we obtain

$$\alpha_1 L = \alpha_2 L = \frac{\omega_1 \gamma C_0}{2} \left| \frac{V_2}{V_1} \right| \left[\frac{\sin \beta_o L}{\sin \beta L} \right]_1 Z_{o1}$$

$$= \frac{\omega_2 \gamma C_0}{2} \left| \frac{V_1}{V_2} \right| \left[\frac{\sin \beta_0 L}{\sin \beta L} \right]_2 Z_{o2}. \tag{4.38}$$

For convenience let us introduce the image impedance of the loaded line, Z_a:

$$Z_a = Z_o \frac{\sin \beta_o L}{\sin \beta L}. \tag{4.39}$$

Eliminating the voltage ratio $| V_1/V_2 |$ from Eq. (4.38) we obtain

$$\alpha L = \pm \frac{\gamma C_0}{2} \sqrt{\omega_1 \omega_2} \sqrt{Z_{a1} Z_{a2}}. \tag{4.40}$$

We therefore will have both a growing and a decaying wave on the line. To obtain an expression for the power gain of a finite line, we must impose boundry conditions. Let us assume that the line is perfectly terminated at input and output, and that the idler voltage is zero at the input before the first diode. Under these assumptions the power gain becomes

$$\text{gain} = \cosh^2 |\alpha| LN \tag{4.41}$$

where N is the number of diodes used. We thus see that there is great similarity between the uniformly-distributed traveling-wave parametric amplifier and the iterated traveling-wave amplifier.

The use of an array of discrete diodes does introduce another parameter, however: the spacing of the diodes. One effect of this discrete loading is to alter slightly the phase requirement between pump, signal, and idler frequencies. In the continuously-distributed amplifier the phase must be correct at every point along the amplifier; for the iterated amplifier the phase need be correct *only* at the points where the diodes are located. Mathematically this means that for the distributed amplifier we have

$$\beta_1 + \beta_2 = \beta_3 \tag{4.34}$$

while for the iterated amplifier we have

$$\beta_1 + \beta_2 = \beta_3 + \frac{2n\pi}{L} \tag{4.42}$$

where n is an integer. We see that Eq. (4.42) is equivalent to Eq. (4.34) only when the distance z is a multiple of L, the spacing between diodes.

Another consequence of the discrete nature of the iterated amplifier is that the reverse gain will be a function of the diode spacing. Bell and Wade show that the minimum reverse gain for a lossless amplifier is unity, and is obtained when the phase shift between diodes at the pump frequency is equal to an odd number of quarter cycles.

The Iterated Amplifier with Loss

The previous treatment of the traveling-wave parametric amplifier has ignored all loss in the line and diodes. In practice, diode loss cannot usually be ignored; both gain and noise figure will be altered because of such loss. In the model used by Bell and Wade it is convenient to represent loss as a shunt conductance which then becomes a part of GY_0. (See page 96 for a discussion of the error involved in this approximation.) With this approximation it is a relatively straightforward but tedious matter to derive an expression for gain in exactly the same manner as before. The result is:

$$\text{gain} = e^{-2\alpha_a LN}\left[\cosh \alpha_b\, LN + \frac{\alpha_2 - \alpha_a}{\alpha_b}\sinh \alpha_b\, LN\right]^2 \tag{4.43}$$

where $\alpha_1 L$ = attenuation constant of line at signal frequency,

$\alpha_2 L$ = attenuation constant of line at idler frequency,

$\alpha_a L = \frac{1}{2}(\alpha_2 L + \alpha_1 L)$ = average of attenuation at signal and idler frequencies,

$\alpha_b L = \frac{1}{2}\sqrt{(\alpha_1 L - \alpha_2 L)^2 + 4(\alpha L)^2}$.

We can obtain a useful approximation by assuming that the gain per unit length is large compared to the loss per unit length, or that $\omega_1 \approx \omega_2$. In either case we have approximately the following expression for gain:

$$\text{gain} \approx e^{-2\alpha_a LN} \cosh^2 \alpha LN \tag{4.44}$$

which states that the net gain is equal to the lossless gain minus the average *cold loss* of the actual line.

Noise Figure

Four noise contributions must be considered in the evaluation of the noise figure of the traveling-wave parametric amplifier. They are:

1. noise at the signal frequency due to input noise at the signal frequency,
2. noise at the signal frequency due to input noise at the idler frequency,
3. noise at the signal frequency due to internal noise generated at the signal frequency,
4. noise at signal frequency due to internal noise generated at the idler frequency.

The first two contributions are readily evaluated, for they are simply the available noise power at the generator multiplied by the power gain and conversion gain, respectively. In the evaluation of the last two contributions, we will assume that all internal loss consists of lumped shunt loss, which we will relate in an approximate manner to the loss in semiconductor diodes. This internal noise contribution can thus be represented by a noise current generator with mean square current

$$\overline{i^2} = 4kTBG_s \tag{4.45}$$

where G_s is the passive shunt conductance periodically loading the line. It is then a straightforward process to compute the output noise power from the amplifier due to this current generator. The result is simply the available noise power of the current generator multiplied by the power gain (or conversion gain for the idler contribution) for $N-n$ sections of line. N is the total number of diodes in the amplifier and n is the position of the current generator being considered. The total noise output due to the internal loss is then obtained by summing over all the N independent current generators. Since little is gained from going through the somewhat tedious algebra, the full derivation of these contributions will be omitted. The resulting expression for noise figure is

$$F = 1 + \frac{T_2}{T_0}\frac{\omega_1}{\omega_2}\left(\frac{\alpha}{\alpha_b}\right)^2 \frac{\sinh^2 \alpha_b LN}{\left[\cosh \alpha_b LN - \frac{\alpha_2 - \alpha_1}{2\alpha_b}\sinh \alpha_b LN\right]^2}$$

$$+ \frac{T_d}{T_0}\sum_{n=1}^{N} 2\alpha_1 L e^{(\alpha_2+\alpha_1)LN}$$

$$\cdot \frac{\left[\cosh \alpha_b L(N-n) + \frac{\alpha_2 - \alpha_1}{2\alpha_b}\sinh \alpha_b L(N-n)\right]^2}{\left[\cosh \alpha_b LN + \frac{\alpha_2 - \alpha_1}{2\alpha_b}\sinh \alpha_b LN\right]^2}$$

$$+ \frac{\omega_1}{\omega_2}\frac{T_d}{T_0}\sum_{n=1}^{N} 2\alpha_2 L\left(\frac{\alpha}{\alpha_b}\right)^2 e^{(\alpha_1+\alpha_2)LN}$$

$$\cdot \frac{\sinh^2 \alpha_b L(N-n)}{\left[\cosh \alpha_b LN + \frac{\alpha_2 - \alpha_1}{2\alpha_b}\sinh \alpha_b LN\right]^2}. \tag{4.46}$$

This is indeed a rather formidable expression. To obtain a simpler and hopefully more useful expression, we will make three further assumptions:

1. the amplifier gain is high,
2. the Q of the diodes used is relatively high,
3. the image impedance of the line does not change radically with frequency over the pass-band.

With these assumptions we can show that

$$\frac{\alpha_2 - \alpha_1}{2\alpha_b} < \gamma Q \tag{4.47}$$

for $\omega_2/\omega_1 \leq 2$. We are saying in effect that the gain is large compared to the difference in line attenuation at idler and signal frequencies. The high gain assumption allows us to say that

$$\cosh \theta \approx \sinh \theta \approx e^{\theta}. \tag{4.48}$$

With these two approximations the expression for noise figure becomes:

$$F \approx 1 + \frac{T_2}{T_0}\frac{\omega_1}{\omega_2} + \frac{2T_d}{T_0}\left[\alpha_1 L + \frac{\omega_1}{\omega_2}\alpha_2 L\right]\sum_{n=1}^{N} e^{2n(\alpha_a - \alpha_b)L}. \tag{4.49}$$

The sum can now be readily evaluated since it is a simple geometric series.

$$\sum_{n=1}^{N} e^{2n(\alpha_a-\alpha_b)L} = \frac{1 - e^{-2NL(\alpha_b-\alpha_a)}}{e^{2(\alpha_b-\alpha_a)L} - 1}. \tag{4.50}$$

Because the overall gain is high, the numerator is approximately unity. The gain per section will be relatively low, however, so we can approximate the exponential in the denominator by the first two terms of its series expansion.

$$e^{2(\alpha_b-\alpha_a)L} \approx 1 + 2(\alpha_b - \alpha_a)L. \tag{4.51}$$

Incorporating these expressions into Eq. (4.49), we have finally

$$F \approx 1 + \frac{T_2}{T_0}\frac{\omega_1}{\omega_2} + \frac{T_d}{T_0}\left\{\frac{\alpha_1 L + \dfrac{\omega_1}{\omega_2}\alpha_2 L}{(\alpha_b L - \alpha_a L)}\right\}. \tag{4.52}$$

At this point we should recall the physical significance of the various quantities which comprise the last term of this expression:

$\alpha_1 L$ = attentuation per unit length at signal frequency,

$\alpha_2 L$ = attenuation per unit length at idler frequency,

$\alpha_b L \approx$ gain per unit length,

$\alpha_a L = (\alpha_1 L + \alpha_2 L)/2$ = average of attenuation per unit length.

Through further approximation we can relate noise figure directly to the diode characteristics. We will make the approximation that the shunt line loss can be related to the diode series loss by the standard transformation between series and shunt equivalent circuits.*

$$G_s \approx \frac{(\omega C_0)^2 R_s}{1 + (\omega C_0 R_s)^2} \approx \frac{1}{R_s Q^2}. \tag{4.53}$$

* We can evaluate the error involved in using this approximation by taking the matrix of Eq. (3.46), adding a series resistance, and reinverting to form an admittance matrix. In so doing we find, for example, that the effective capacitance which we should use is not C, but $C(1 + \gamma^2)$ while the effective series resistance should be $R_s[1 + (\omega_2/\omega_1)\gamma^2]$. Of more importance is the fact that the off-diagonal elements of the "exact" admittance matrix contain a real component which is smaller than the imaginary component by the factor $2/\bar{Q}$, where $\bar{Q}$ is the diode Q evaluated at half-pump frequency. Thus, we can say that the approximation used in Eq. (4.53) is valid when $\omega_1 \approx \omega_2$ and the diode Q is moderately high.

The attenuation constant is related to the shunt loss as in Eq. (4.54).

$$\alpha_L = \frac{G_s Z_a}{2} \tag{4.54}$$

If we now invoke the assumption that the image impedance does not change radically over the frequency range of interest, the expression for noise figure can be written approximately as

$$F \approx 1 + \frac{T_2}{T_0}\frac{\omega_1}{\omega_2} + \frac{2T_d}{T_0}\left\{\frac{1 + \dfrac{\omega_2}{\omega_1}}{2\gamma Q\sqrt{\dfrac{\omega_2}{\omega_1}} - \left[1 + \left(\dfrac{\omega_2}{\omega_1}\right)^2\right]}\right\}. \tag{4.55}$$

It is of interest to note that for degenerate operation, Eq. (4.55) reduces to

$$F \approx 2\left[1 + \frac{1}{\gamma Q - 1}\right] \tag{4.56}$$

which is identical to the expression obtained for the resonant-circuit degenerate parametric amplifier.

Note that Eq. (4.55) shows that if the idler channel of the amplifier is terminated by the antenna, the noise figure will be a function of antenna temperature. The proper expression for the operating noise temperature will be

$$T_{op} = \frac{\omega_3}{\omega_2}T_a + T_d\left\{\frac{\alpha_1 L + \dfrac{\omega_1}{\omega_2}\alpha_2 L}{\alpha_b L - \alpha_a L}\right\}. \tag{4.57}$$

Since noise figure is measured at room temperature, it is useful to express T_{op} in terms of measured noise figure.

$$T_{op} = (F_{T_0} - 1)T_0 + T_a + \frac{\omega_1}{\omega_2}[T_a - T_0] \tag{4.58}$$

where F_{T_0} = spot noise figure measured with idler terminated at 290°K. Equation (4.58) applies only for single-sideband application with the idler matched into the antenna. Also note that F_{T_0} is the *spot* noise figure, which is essentially the noise figure measured at a particular frequency, rather than an average over a large range of frequencies. When $\omega_1 = \omega_2$, Eq. (4.58) reduces to Eq. (3.108) which was obtained for the resonant-circuit degenerate parametric amplifier.

Other Types of Traveling-wave Parametric Amplifiers

In the case of resonant-circuit parametric devices, several modes of operation are possible; the same is true for the traveling-wave version of parametric devices. For example, it is possible to obtain a different mode of operation merely by introducing the signal power into the *output* of the amplifier. This reverses the direction of propagation of the signal with respect to the pump and in so doing completely changes the operating characteristics of the amplifier. In the investigation of such devices it is of interest to determine the existence and nature of gain, together with the bandwidth characteristics which they may have. A detailed picture of the gain behavior can be obtained only from an analysis of the particular case, but it is possible to make some useful generalizations. If the direction of energy propagation in the signal and idler waves is in the same direction, for example, we would expect that regeneration could not occur, and hence the device would be stable. If the direction of energy propagation is *not* the same for signal and idler, the idler can form a feedback loop which causes regeneration, instability, and even oscillation. We may illustrate these two possible modes of operation conveniently with the aid of a Brillouin diagram, which is simply a plot of the phase-shift characteristics of the circuit as a function of frequency. The Brillouin diagram conveniently displays both the phase velocity and group velocity of the structure as a function of frequency. We recall that the phase velocity is given by

$$v_p = \frac{\omega}{\beta} \tag{4.59}$$

while the group velocity, which is the velocity of energy propagation, is given by

$$v_g = \frac{d\omega}{d\beta}. \tag{4.60}$$

Thus on the Brillouin diagram the phase velocity is given by the ratio of ordinate to abscissa while the group velocity is given by the slope of the curve.

In Fig. 4.8 we show a possible Brillouin diagram for the traveling-wave parametric amplifier which we have analyzed in some detail. We recall that for operation at maximum gain we must simultaneously satisfy the two relations

$$\omega_1 + \omega_2 = \omega_3, \qquad \beta_1 + \beta_2 = \beta_3. \tag{4.61}$$

We may indicate this relation graphically on the Brillouin diagram by insisting that the points of operation at signal, idler, and pump frequencies, together with the origin, must form a parallelogram. That is, we must vectorially add the points corresponding to signal and idler to obtain the point corresponding to the pump. This restriction will indicate very quickly what the bandwidth capabilities of the device can be. It is obvious that the circuit of Fig. 4.8 is broadband, for we may change the signal

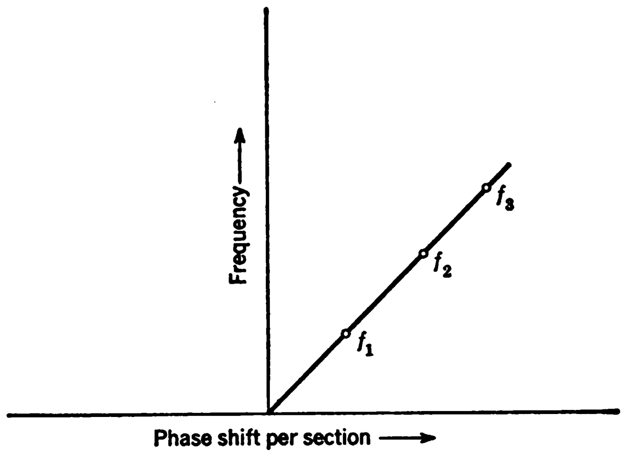

Fig. 4.8. Brillouin diagram of a broadband forward-wave parametric amplifier.

vector to a new position along the line forming the locus of the propagation characteristics of the structure, and still find a new idler vector along this same locus which adds vectorially to the *original* pump vector. Fig. 4.9 shows another example of this same mode of operation which is *not* broadband, for here the pump frequency must be changed when the signal frequency is changed in order to arrive at a condition satisfying the vector addition requirement.

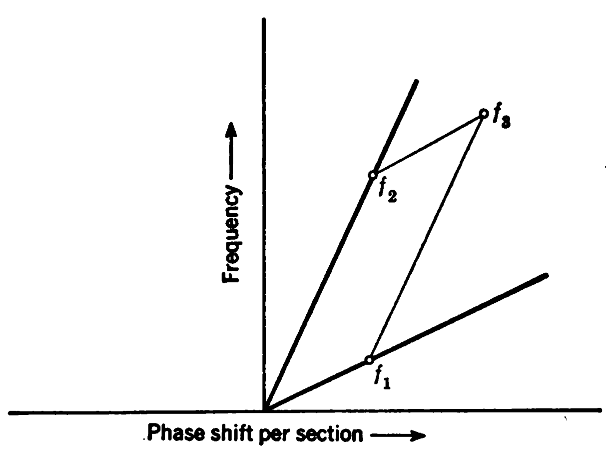

Fig. 4.9. Brillouin diagram of a narrow-band forward-wave parametric amplifier.

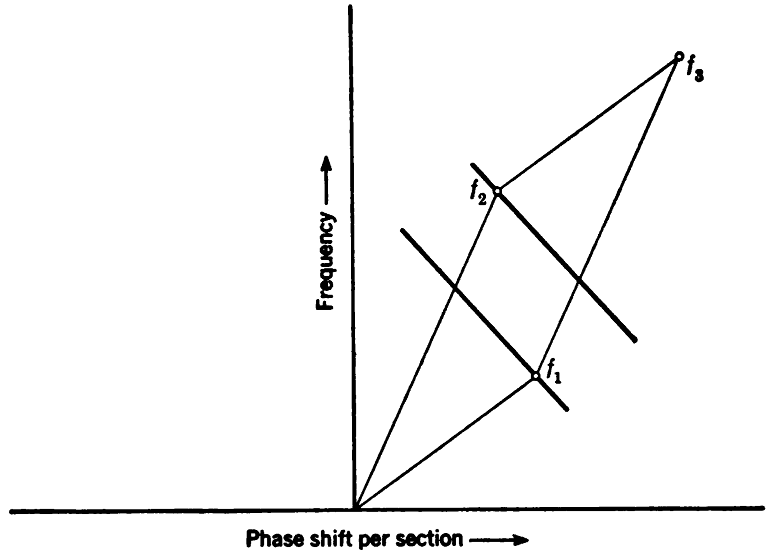

Fig. 4.10. Brillouin diagram of a broadband backward-wave parametric amplifier.

In Fig. 4.10 we show another mode of operation closely related to the one we have studied above. Here the signal and idler circuits use so-called backward waves; waves which have group and phase velocities in opposite directions. Since energy propagation is in the same direction for signal and idler, we would expect no regeneration of the type leading to oscillation. This mode can also be broadband if the Brillouin diagrams of the signal and idler circuits are approximately parallel lines.

Another possible mode is shown in Fig. 4.11. Here we have signal and idler energy propagation in opposite directions, hence instability is possible. The device is also narrow-band as is indicated the vector addi-

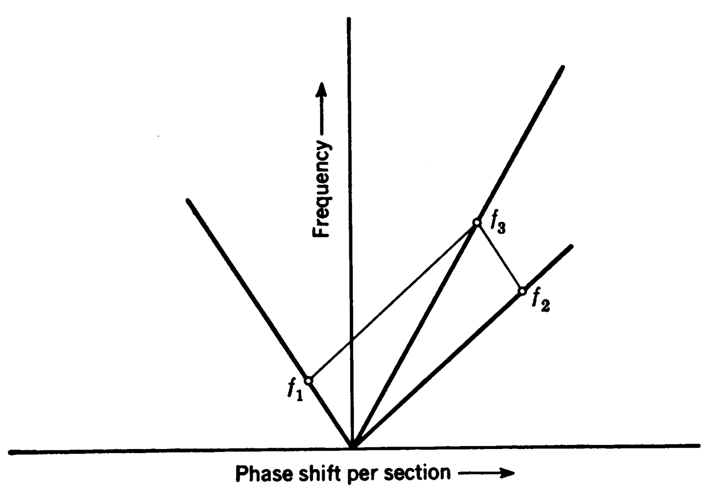

Fig. 4.11. Brillouin diagram of a regenerative traveling-wave parametric amplifier.

tion test. This mode could be used in the construction of a tunable amplifier since synchronism could be maintained over a wide range of frequencies merely by changing the pump frequency.

4.3 Some Large-signal Properties of the Two-port Negative-resistance Parametric Amplifier

The method of analysis which has been used to this point has employed the assumption that the signal level is small compared to the pump level. With this assumption it is possible to separate the pump and signal circuits. At the pump frequency the effect is simply one of changing capacitance with any mixing effects due to the signal circuit ignored. This changing capacitance is then treated as a linear time-varying capacitance at the signal and idler frequencies. With the circuit reduced to such a linear approximation it is impossible to predict what happens to the amplifier performance when the signal level becomes significant. However, by taking a somewhat different approach it is possible to obtain some large-signal properties without any additional mathematical complexity. This method was briefly discussed in Section 1.3 as the so-called large-signal approach. Let us apply this method to the analysis of the negative-resistance parametric amplifier.

For convenience as well as variety we will analyze the shunt version of the two-port negative-resistance amplifier. This type of amplifier is essentially three parallel-resonant circuits placed in series with a nonlinear capacitance, as indicated in Fig. 4.12.

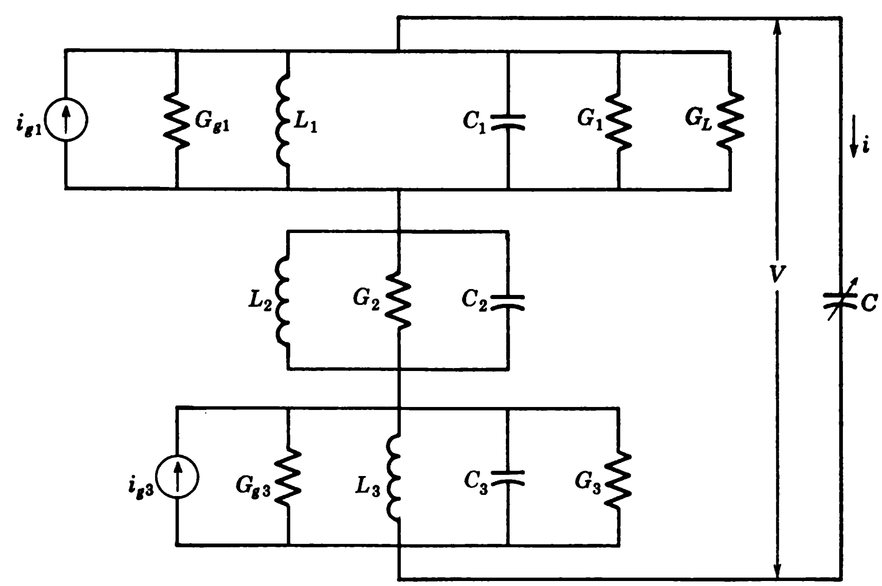

Fig. 4.12. Equivalent circuit for the large-signal analysis of the negative-resistance parametric amplifier.

One circuit is resonant at $\omega_1 (\omega_1 = 2\pi f_1)$, the signal frequency; one at ω_2, the idler frequency; and one at ω_3, the pump frequency. For regenerative gain at ω_1, the three frequencies must satisfy the usual relation

$$\omega_1 + \omega_2 = \omega_3. \tag{4.62}$$

It is assumed that all resonant circuits are high-Q so that significant voltages are developed across them only at frequencies close to their resonant frequencies. Input power sources are indicated at the signal frequency and the pump frequency by constant-current generators and associated-shunt conductances.

The defining relation between current and voltage which will be used in this analysis is as given in Eq. (4.63).

$$i = \frac{dq}{dt} = \frac{dq}{dv}\frac{dv}{dt} = C(v)\frac{dv}{dt} \tag{4.63}$$

where $$C(v) = dq/dv.$$

As will be shown in Sec. 5.1, the small-signal dynamic capacitance, $C(v)$, is directly applicable to the case of the back-biased semiconductor diode where the capacitance as defined and measured is $C = dq/dv$. For the planar abrupt-junction diode, for example,

$$C(v) = C_0\left(1 - \frac{v}{\phi}\right)^{-1/2}. \tag{4.64}$$

It is assumed that the voltage across the nonlinear capacitor consists of a d-c bias voltage, V_0, and of r-f voltages at frequencies ω_1, ω_2, and ω_3. Assuming that the r-f voltages are small compared to the bias voltage, we can expand the quantity $C(v)$ in a Taylor series about V_0 and retain only the first few terms.

$$C(v) = C(V_0) + \frac{\partial C(V_0)}{\partial v} v_{\text{r-f}} + \frac{1}{2}\frac{\partial^2 C(V_0)}{\partial v^2}(v_{\text{r-f}})^2 + \cdots. \tag{4.65}$$

It should be noted that in this expansion no assumption is necessary regarding the magnitude of the voltage at the pump frequency relative to the voltages at the signal or idler frequencies. However, the analysis is still mathematically a small-signal analysis since the restriction is made that $v_{rf} \ll V_0$.

First-order Effects

a The first term of Eq. (4.65) is a constant linear capacitance and does not contribute to any large-signal effects. The second term yields the mixing effects which result in parametric amplification, while the third term contributes an effective capacitance whose magnitude is a function of the magnitudes of the voltages present across the capacitance. To facilitate the analysis the approximation is made that this last term of Eq. (4.65) may initially be neglected and introduced later as a perturbation. The mixing effects can then be shown to be equivalent to the introduction of additional admittances in the circuit as indicated schematically in Fig. 4.13. These admittances are calculated by evaluating the current flowing through the capacitor with the aid of Eqs. (4.63) and (4.65), assuming that the only voltages present are at frequencies ω_1, ω_2, and ω_3. The resultant current at a particular frequency is then divided by the assumed voltage at that frequency, giving an effective admittance.

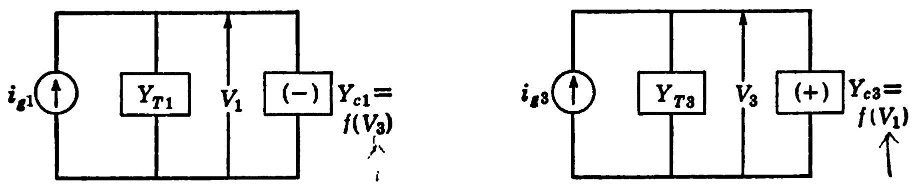

(*a*) Equivalent circuit at signal frequency (*b*) Equivalent circuit at pump frequency

Fig. 4.13. Effective equivalent circuits at signal frequency and pump frequency.

The admittance at the signal frequency introduced by parametric mixing is seen to possess a negative real part (*i.e.*, a negative conductance). At the pump frequency, however, a similar admittance is introduced which possesses a *positive* real part. This is of course to be expected from simple energy considerations as stated by the Manley and Rowe relations: the power introduced at the signal frequency (*produced* by the negative conductance) is derived from the pump power (*absorbed* by the positive conductance), these two powers having a ratio equal to the ratio of their respective frequencies. The signal circuit and the pump circuit are thus inevitably related, and it is this interrelation which produces a first-order saturation effect.

Why?

Why?

How this interplay of admittances causes saturation can be seen by again referring to Fig. 4.13. The gain of the device at ω_1 depends on the magnitude of the negative conductance at ω_1, which in turn depends on the magnitude of the pump voltage V_3. If V_3 were to decrease only slightly under conditions of high gain, the gain would drop appreciably. Referring to the schematic circuit at ω_3 shown in Fig. 4.13, it is seen that with a constant available pump power (constant i_{g3}), the voltage V_3 will indeed drop as more admittance is introduced to the circuit through the presence of voltage V_1. Hence, the gain of the parametric amplifier will decrease as the signal level increases; that is, the amplifier will exhibit saturation effects.

The effective conductance introduced in the signal circuit at resonance by the action of the nonlinear capacitance is given by the following expression.

$$G = \frac{\omega_1\omega_2K^2P_p}{\dfrac{G_{T2}}{G_{g3}}\left[G_{T3} + \dfrac{\omega_2\omega_3K^2P(\omega_1)}{4G_{T2}G_l}\right]^2} \tag{4.66}$$

where
$$K = \partial C(V_0)/\partial v,$$
$$P_p = \text{available pump power},$$
$$P(\omega_1) = \text{power output at } \omega_1,$$
$$G_{T2} = G_2 = \text{total circuit loss at } \omega_2,$$
$$G_{T3} = G_{g3} + G_3.$$

With the aid of Eq. (4.66) for the effective negative conductance, it is now a straightforward matter to obtain the power gain of the amplifier under conditions where the signal power level is significant.

Defining transducer gain as the ratio of power output to available power input, the following expression is obtained:

$$g = \frac{4G_{g1}G_l}{\left\{G_{T1} - \dfrac{G_o}{[1 + aP(\omega_1)]^2}\right\}} \tag{4.67}$$

where g = transducer gain,
$$G_{T1} = G_{g1} + G_1 + G_l = \text{total circuit loading at } \omega_1,$$
$$G_o = \text{small-signal value of negative conductance},$$
$$= (\omega_1\omega_2K^2G_{g3}P_p)/(G_{T2}G_{T3}^2),$$
$$a = (\omega_2\omega_3K^2)/(4G_lG_{T2}G_{T3}).$$

A plot of Eq. (4.67) for a constant value of a and several values of small signal-gain is shown in Fig. 4.14. It is useful to define a quantity which will be called the saturated power output. A convenient definition is that value of $P(\omega_1)$ at which $aP(\omega_1) = 1$. For this value of $P(\omega_1)$ the negative conductance is decreased to $\frac{1}{4}$ its small-signal value, at which point the power gain is always less than 2.5 db, regardless of the value of the small-signal gain. Using this criterion for defining the saturated power output, the following result is obtained:

$$P_{\text{sat}} = \frac{4G_{T2}G_{T3}G_l}{\omega_2\omega_3K^2}. \tag{4.68}$$

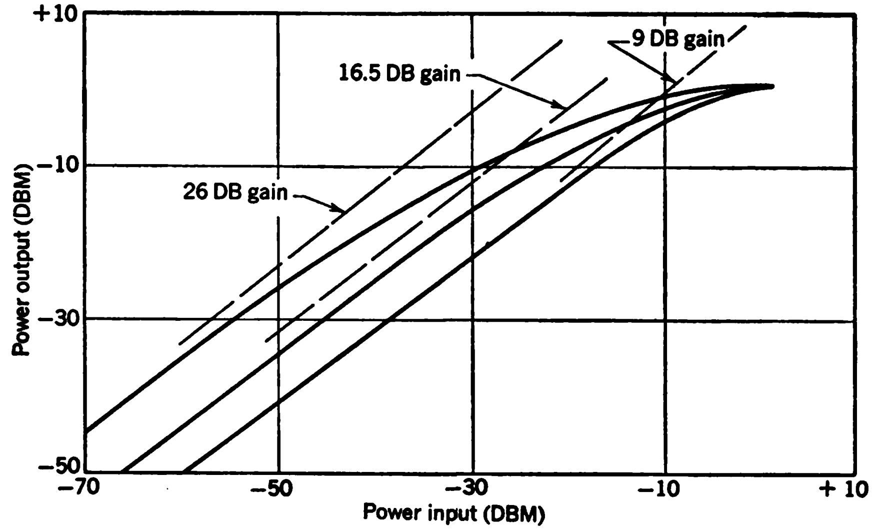

Fig. 4.14. Some theoretical first-order gain-saturation curves.

To achieve a high saturated power output, we thus see that it is desirable to do the following:

1. Load the circuits heavily.
2. Decrease the degree of nonlinearity, K, such as by increasing the reverse bias on a semiconductor diode:

An increase in saturated power output, however, is accompanied by a corresponding increase in the pump power required for a given value of gain as well as an increase in noise figure. To see this, consider Eq. (4.67). For a given value of small-signal gain, the negative conductance will be some definite fraction of G_{T1}, the total passive circuit loading at ω_1. Therefore, we can write the relation:

$$G = bG_{T1} \tag{4.69}$$

where b is a parameter ranging from zero to one, corresponding to conditions of no gain and oscillation, respectively. Using (4.67) and (4.69), we can solve for the available pump power, P_p, required to give a specified value of small signal-gain by setting $P(\omega_1) = 0$.

$$P_p = \frac{bG_{T1}G_{T2}G_{T3}}{\omega_1\omega_2K^2}\left(\frac{G_{T3}}{G_{g3}}\right). \tag{4.70}$$

The ratio of the saturated power output to the required available pump power is a quantity of some interest. For cases of interest, $b = 1$, this ratio becomes

$$\frac{P_{\text{sat}}}{P_p} = 4\,\frac{\omega_1G_lG_{g3}}{\omega_3G_{T1}G_{T3}}. \tag{4.71}$$

Operation As an Oscillator

As the pump power supplied to the device increases, oscillation will occur. It is of interest to determine what limits the level of the resulting oscillation. Again, Eq. (4.67) can be used to yield a first-order approximation to the answer. The condition for oscillation at resonance is

$$G = G_{T1} \tag{4.72}$$

Under this condition, Eq. (4.67) can be solved for the resultant power output, $P(\omega_1)$.

$$P(\omega_1) = \frac{4G_{T2}G_l}{\omega_2\omega_3K^2}\left[\left(\frac{\omega_1\omega_2K^2G_{g3}}{G_{T1}G_{T2}}P_p\right)^{1/2} - G_{T3}\right]. \tag{4.73}$$

The physical explanation of the existence of such a first-order limit on the oscillation level is similar to that used to explain saturation: The pump produces a voltage resulting in sufficient capacitance swing to cause the effective negative conductance to equal (or momentarily exceed) the total positive conductance at the signal frequency. The thermal voltages present start a buildup of oscillation, but as the oscillation increases, the effective negative conductance decreases because of the same interaction between signal and pump described earlier. As a result, the oscillation will reach an equilibrium value which is sufficient to cause the negative conductance to precisely equal the positive conductance.

Second-order Effects

The foregoing analysis would explain most on-resonance, large-signal, steady-state phenomena of the cavity-type parametric amplifier if the capacitance variation were linearly proportional to the pump voltage. In practice, however, the relation between capacitance and voltage is usually not a linear one. Because of this nonlinearity, it is necessary to examine the next term in the Taylor series expansion, Eq. (4.65). Under the assumption that ω_1, ω_2, and ω_3 are the only frequencies at which significant voltages are produced, analysis shows that the effect of this term is to introduce an additional capacitance into each of the tuned circuits. The value of this capacitance is a function of the magnitude of the voltages present across it. This effect is analogous to the shift in d-c bias across a nonlinear resistor (such as a diode or vacuum tube) due to the presence of an a-c voltage. The magnitude of this capacitance is given by the following relation:

$$C_i = \frac{1}{4}\frac{\partial^2 C(V_0)}{\partial v^2}\left(\tfrac{1}{2}V_i^2 + V_j^2 + V_k^2\right) \quad \text{why?} \tag{4.74}$$

where V_i is the magnitude of the voltage at frequency ω_i.

The effect of this capacitance is to detune the resonant circuits. If high-Q circuits are used in the device, the effect can be quite pronounced, causing saturation at power levels lower than predicted by the first-order analysis. To compute the magnitude of this detuning capacitance, it is of some assistance to evaluate the voltages present in terms of the available pump power and signal power output. A somewhat tedious algebraic computation yields the following result.

$$V_1^2 = \frac{P(\omega_1)}{G_l}$$

$$V_2^2 = \frac{\omega_2^2 K^2 G_{g3} P(\omega_1) P_p}{G_l G_{T2}^2 \left[G_{T3} + \dfrac{\omega_2 \omega_3 K^2 P(\omega_1)}{4 G_l G_{T2}} \right]^2}$$

$$V_3^2 = \frac{4 G_{g3} P_p}{G_{T3} + \dfrac{\omega_2 \omega_3 K^2 P(\omega_1)}{4 G_l G_{T2}}}. \tag{4.75}$$

A plot of a typical variation in circuit voltages as a function of power output for an experimental microwave parametric amplifier is shown in Fig. 4.15. It should be pointed out that in practice the use of Eq. (4.74) is difficult and laborious. It is laborious because a trial and error procedure is necessary: the amount of detuning capacitance present depends on the magnitude of the voltages present, and conversely the magnitude of the voltages depends on the amount of detuning capacitance present. In addition, the voltages present depend on the power output, which is in turn dependent on the amount of detuning present. However, Eq. (4.74) is useful in estimating to what extent detuning capacitance is a factor in parametric amplification. The concept of detuning capacitance itself is also useful in helping to qualitatively explain experimental results.

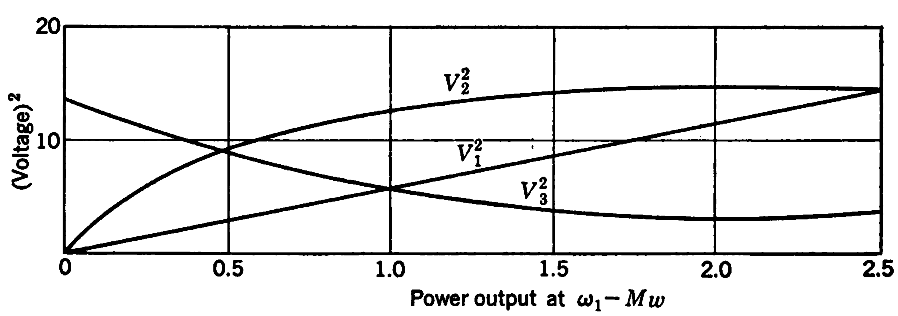

Fig. 4.15. Typical variations in circuit voltages with change in power output.

4.4 Harmonic Generation by Nonlinear Reactance

The subject of harmonic generation is in a sense out of place in a book on amplifiers. From a practical standpoint, however, the consideration here of harmonic generation by nonlinear reactance is appropriate for at least three reasons:

1. The methods of analysis are quite similar to those used in the analysis of parametric devices.
2. Harmonic conversion by this method provides a means of constructing an all-solid-state pump source for parametric devices.
3. Such harmonic generation appears to be an important method of generating moderate amounts of microwave power efficiently and reliably from a small all-solid-state package.

It seems reasonable that harmonic generation by nonlinear reactance should have high efficiency, for a perfect reactance can only transfer or store energy.

Indeed, it can be shown from the Manley-Rowe relations that the efficiency of generation of any harmonic can approach unity. For example, let us assume that we have a perfect nonlinear reactance with power flow allowed only at the fundamental frequency, f, and the nth harmonic, nf. The Manley-Rowe relation, Eq. (1.9) then becomes

$$\frac{P_o}{f} + \frac{nP_n}{nf} = 0 \qquad (4.76)$$

where P_o = power flow in at f,

P_n = power flow in at nf.

Therefore

$$\frac{P_n}{P_o} = -1 \qquad (4.77)$$

which indicates a conversion efficiency of 100%, *regardless of the order of the harmonic involved.*

In practice, however, power flow at unwanted frequencies, and the inevitable loss of realizable circuit elements, will reduce the efficiency. It is desirable to have a suitable theory for harmonic generation to indicate how much conversion loss we can expect in a given circuit when semiconductor diodes are used as the nonlinear reactance.

An approximate solution for the conversion loss of a nonlinear reactance harmonic generator is not too difficult to obtain, provided we restrict ourselves sufficiently. Even though high efficiencies can be expected in many instances, we will use a small-signal analysis in order to keep the mathematics under control. Experimental results indicate that the error involved will normally be small in designs of practical interest. We will start with the fundamental equation for current:

$$i = \frac{dq}{dt} = \frac{dq}{dv}\frac{dv}{dt}$$

$$= C(v)\,\frac{dv}{dt}. \tag{4.78}$$

We will assume that the a-c voltage is composed of a large fundamental voltage, v_1, and small harmonic voltages, v_2. With this assumption we can expand the capacitance function, $C(v)$, in a Taylor series about v_1:

$$C(v) = C(v_1) + \frac{dC}{dv}(v_1)v_2 + \cdots. \tag{4.79}$$

We can also write the identity

$$\frac{dC}{dt} = \frac{dC}{dv}\frac{dv}{dt}; \tag{4.80}$$

therefore,

$$\frac{dC}{dv}(v_1) = \frac{\dfrac{dC}{dt}(v_1)}{\dfrac{dv}{dt}(v_1)}. \tag{4.81}$$

Substituting Eqs. (4.81) and (4.79) into Eq. (4.78), we get

$$i = C(v_1)\left[\frac{dv_1}{dt} + \frac{dv_2}{dt}\right] + \frac{dC(v_1)}{dt}\,v_2\left[1 + \frac{dv_2/dt}{dv_1/dt}\right] + \cdots. \tag{4.82}$$

To obtain linear equations, we assume that $dv_2/dt \big/ dv_1/dt$ is small compared to unity. With this approximation, the expression for current becomes

$$i = C(v_1)\left[\frac{dv_1}{dt} + \frac{dv_2}{dt}\right] + \frac{dC(v_1)}{dt}\,v_2. \tag{4.83}$$

In the evaluation of Eq. (4.83) we will use exponential representations. Let

$$v_1 = V_1 e^{j\omega_1 t} + V_1^* e^{-j\omega_1 t}, \qquad V_1 = V_1^*$$

$$v_2 = \sum_{\substack{n=-\infty \\ \mp\pm 1}}^{\infty} V_n e^{jn\omega_1 t}$$

$$C(v_1) = C_0 \sum_{n=-\infty}^{\infty} \gamma_n e^{jn\omega_1 t}, \qquad \gamma_n = \gamma_{-n}$$

$$i = \sum_{n=-\infty}^{\infty} I_n e^{jn\omega_1 t}. \tag{4.84}$$

Substituting these values into Eq. (4.83), we obtain the following expression for the nth harmonic current:

$$I_n = j\omega C_0[\gamma_{n-1} - \gamma_{n+1}]V_1 + jn\omega C_0 \sum_{\substack{k=-\infty \\ \mp\pm 1}}^{\infty} \gamma_{n-k} V_k. \tag{4.85}$$

From this equation we can construct an admittance matrix which will describe the *small-signal* harmonic generator. Before carrying the analysis further, let us assume that our circuit is so constructed as to allow significant voltages to exist across the capacitor only at the fundamental and nth harmonic. This is a reasonable assumption for many practical circuits, since the diodes will be of relatively high Q. With only V_1 and V_n not equal to zero, we can then obtain from Eq. (4.85) the following equations for I_1 and I_n:

$$I_1 = j\omega C_0[1 - \gamma_2]V_1 + j\omega C_0 \gamma_{n-1} V_n$$

$$I_n = j\omega C_0[\gamma_{n-1} - \gamma_{n+1}]V_1 + jn\omega C_0 V_n. \tag{4.86}$$

In matrix notation we have,

$$\begin{bmatrix} I_1 \\ I_n \end{bmatrix} = j\omega C_0 \begin{bmatrix} 1 - \gamma_2 & \gamma_{n-1} \\ \gamma_{n-1} - \gamma_{n+1} & n \end{bmatrix} \begin{bmatrix} V_1 \\ V_n \end{bmatrix}. \tag{4.87}$$

This matrix represents the admittance of the lossless, small-signal harmonic generator. We will approximate the effect of series loss by inverting the admittance matrix and by adding a series resistance. The *lossless* inverted matrix equation is:

$$\begin{bmatrix} V_1 \\ V_n \end{bmatrix} = \begin{bmatrix} Z_{11} & Z_{12} \\ Z_{21} & Z_{22} \end{bmatrix} \begin{bmatrix} I_1 \\ I_n \end{bmatrix} \tag{4.88}$$

where

$$Z_{11} = \frac{n}{j\omega C_0 D},$$

$$Z_{12} = -\frac{\gamma_{n-1}}{j\omega C_0 D},$$

$$Z_{21} = -\frac{\gamma_{n-1} - \gamma_{n+1}}{j\omega C_0 D},$$

$$Z_{22} = \frac{1 - \gamma_2}{j\omega C_0 D},$$

$$D = n(1 - \gamma_2) - \gamma_{n-1}(\gamma_{n-1} - \gamma_{n+1}),$$

$$\approx n(1 - \gamma_2).$$

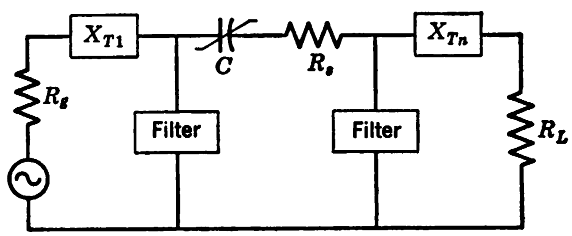

Fig. 4.16. Circuit model for harmonic generation.

The circuit model for Equation (4.88) is shown in Figure 4.16. We can now write down the transducer gain for this circuit as

$$g_t = \frac{4R_g R_l \,|\, Z_{21} \,|^2}{|\,(Z_{11} + Z_{T1})(Z_{22} + Z_{Tn}) - Z_{12}Z_{21}\,|^2}. \tag{4.89}$$

Substituting the matrix values we have,

$$g_t = \frac{4R_g R_l \left(\dfrac{\gamma_{n-1} - \gamma_{n+1}}{1 - \gamma_2}\right)^2 \dfrac{1}{(n\omega C_0)^2}}{\left|\left(\dfrac{1}{j\omega C_0(1 - \gamma_2)} + Z_{T1}\right)\left(\dfrac{1}{j\omega n C_0} + Z_{Tn}\right) + \dfrac{\gamma_{n-1}(\gamma_{n-1} - \gamma_{n+1})}{(1 - \gamma_2)^2} \dfrac{1}{(n\omega C_0)^2}\right|^2}. \tag{4.90}$$

CONVERSION EFFICIENCY OF HARMONIC GENERATION USING PARAMETRIC DIODES, (FIGS 4.17–4.20)

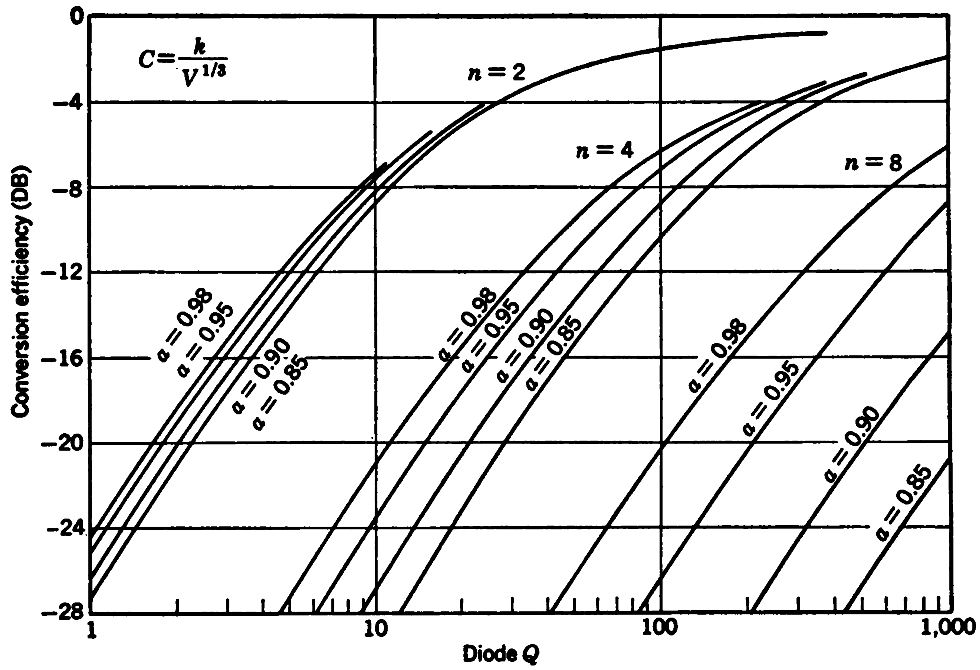

Figure 4.17

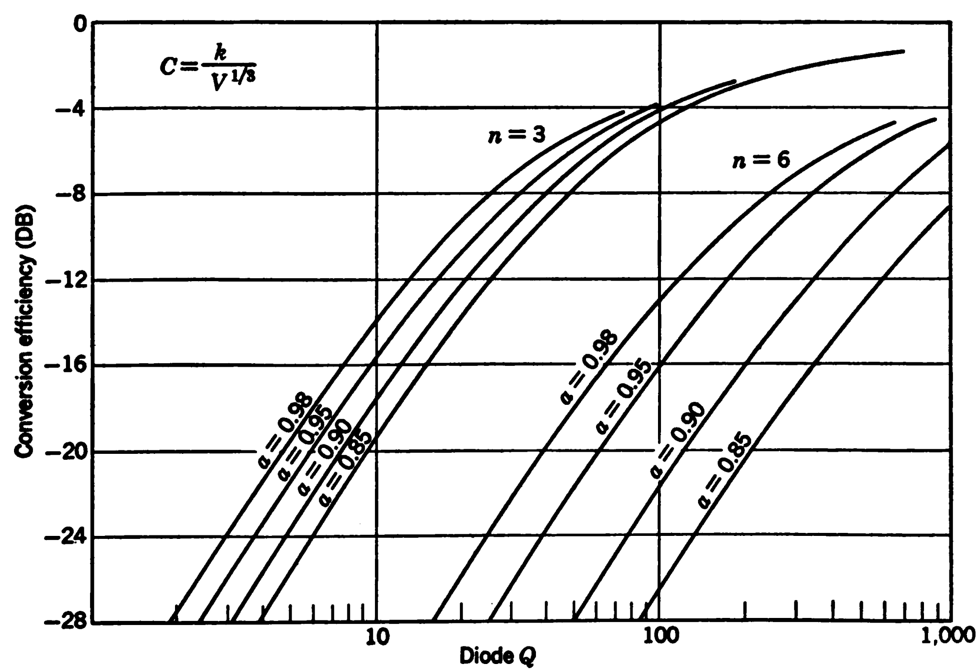

Figure 4.18

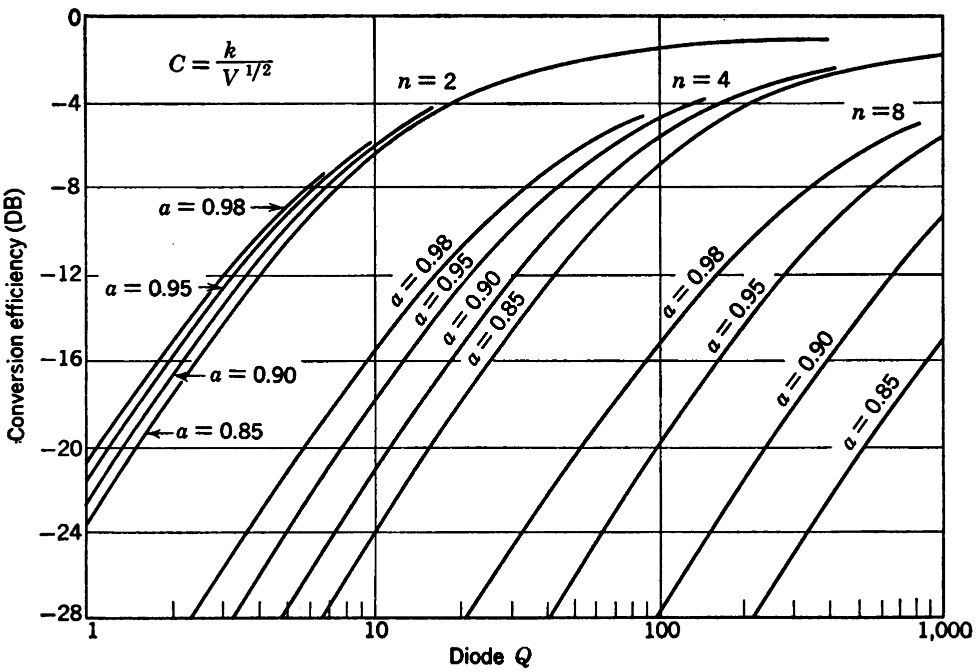

Figure 4.19

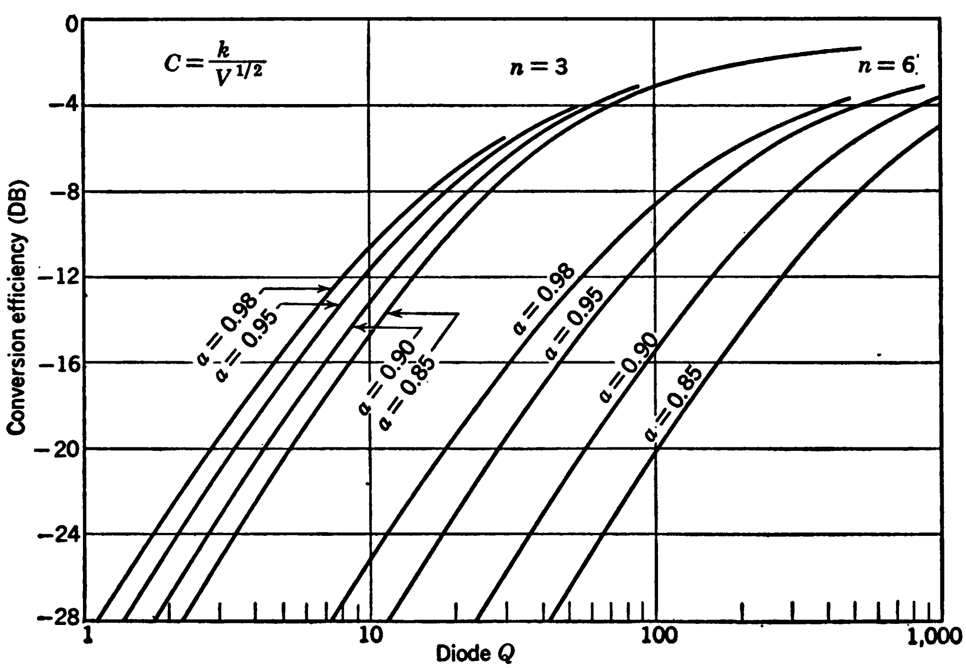

Figure 4.20

Now, let us assume that we impose the tuning conditions

$$X_{T1} = \frac{1}{\omega C_0(1 - \gamma_2)} \quad \text{and} \quad X_{Tn} = \frac{1}{n\omega C_0}. \tag{4.91}$$

Further, let us assume that all circuit loss, exlusive of source or load resistance, is series loss associated with the nonlinear capacitor. Therefore,

$$R_{T1} = R_g + R_s \quad \text{and} \quad R_{Tn} = R_l + R_s$$

Equation (4.90) then becomes

$$g_t = \frac{4R_gR_l\left(\dfrac{\gamma_{n-1} - \gamma_{n+1}}{1 - \gamma_2}\right)^2 \dfrac{1}{(n\omega C_0)^2}}{\left[(R_g + R_s)(R_l + R_s) + \dfrac{\gamma_{n-1}(\gamma_{n-1} - \gamma_{n+1})}{(1 - \gamma_2)^2}\dfrac{1}{(n\omega C_0)^2}\right]^2}. \tag{4.92}$$

We can maximize the gain by choosing the proper values for the source and load resistances. A little calculus will show the values to be

$$R_g = R_l = R_s\sqrt{1 + \bar{\gamma}^2Q_n^2} \tag{4.93}$$

where

$$\bar{\gamma}^2 = \frac{\gamma_{n-1}(\gamma_{n-1} - \gamma_{n+1})}{(1 - \gamma_2)^2}$$

and

$$Q_n = \frac{1}{n\omega C_0R_s}.$$

Substituting this optimum value into the expression for transducer gain we get, after some manipulation,

$$g_t = \frac{\gamma_{n-1} - \gamma_{n+1}}{\gamma_{n-1}} \frac{\bar{\gamma}^2Q_n^2}{[1 + \sqrt{1 + \bar{\gamma}^2Q_n^2}]^2}. \tag{4.94}$$

Notice that as we allow the loss to approach zero (by making Q larger), the transducer gain approaches unity. That it will never quite reach unity may be attributed to our initial small-signal approximations.

Using computed values for the capacitance Fourier coefficients, we can readily obtain curves which show how much loss can be expected in harmonic generators using semiconductor diodes. The actual capacitance Fourier coefficients for the sinusoidal pumping of such semiconductor diodes are presented in Sec. 5.1. Here we will merely make use of these results in order to obtain the desired design curves. In Figs. 4.17 through

4.20 we show curves of conversion loss as a function of diode Q at the fundamental frequency for various harmonics using both abrupt-junction diodes and linearly-graded junction diodes. The parameter a is the ratio of a-c voltage amplitude to d-c bias (including contact potential). The maximum value of a cannot at this time be stated precisely; however, a combination of theory and experiment indicates that $a \leq 0.98$ is appropriate. Notice that these results indicate that an abrupt-junction diode will have a somewhat better conversion efficiency than a diffused-junction diode. This assumes that such diodes have capacitance variations as noted on the figures. In practice these diodes are driven into forward conduction where the so-called diffusion capacitance may become important. The difference is often small, however, and a small improvement in diode Q will often be sufficient to compensate for this predicted difference in conversion efficiency.

Several useful conclusions may be drawn from Figs. 4.17 through 4.20. One is that for efficient generation, particularly at the higher harmonics, diode and circuit Q's must be quite high. It should be noted here that the generation of higher harmonics with this type of circuit is best accomplished in stages. As an example of this, let us assume that we wish to generate the sixth harmonic with an abrupt-junction diode of $Q = 100$ at the fundamental frequency in circuits having negligible losses. Figs. 4.19 and 4.20 show that if we go directly to the sixth harmonic we should expect a conversion loss of 15.5 db when $a = 0.90$. If we choose to double and then to triple with two diodes of same quality used in the previous example, we find a conversion loss of 1.8 db in doubling, and 4.5 db in tripling ($Q = 50$ for the tripler), which gives a total conversion loss of only 6.3 db, an improvement of 9.2 db over the single-stage conversion efficiency. If we triple first and then double, we get even better efficiency: only a 5.4-db conversion loss. This is an order of magnitude improvement over the single-stage conversion efficiency.

4.5 Other Parametric Devices

There are many parametric devices in existence other than those treated in the previous sections, and the number is certain to increase greatly with the passage of time. It would be a hopeless task to attempt to include full treatments of all the devices which have been built or proposed; on the other hand the techniques and results already at hand are sufficient to enable one to analyze the large majority of these devices. The intent of this section will be to discuss briefly several such parametric devices and to point out how the methods previously used can be employed in their analysis.

Four-frequency Parametric Devices

One can conceive of innumerable complex parametric amplifiers with power flow allowed at various frequencies other than the usual sum and difference frequencies encountered in the operation of up-converters and negative-resistance amplifiers. While these may be of some interest, devices of significantly greater interest can be obtained by simply combining the up-converter and negative-resistance amplifier to obtain so-called four-frequency devices. These devices allow power transfer among four frequencies: the signal frequency, ω_1; the difference frequency, ω_2; the pump frequency, ω_3; and the sum frequency, ω_4. Without resorting to any mathematics we can deduce some of the important properties of this device. We would expect, for example, that the conversion gain from ω_1 to ω_4 could be greater than ω_4/ω_1, since the power dissipation at the difference frequency introduces a negative resistance at the signal frequency, causing regeneration. On the other hand we would expect that the stability of such a converter would be better than that of the negative-resistance amplifier since power dissipation at the sum frequency introduces an effective positive resistance.

The appropriate Manley-Rowe relation for this situation is

$$\frac{P_1}{\omega_1} + \frac{P_4}{\omega_4} - \frac{P_2}{\omega_2} = 0 \tag{4.95}$$

Recalling that the sign convention is such that positive power is power flowing *into* the nonlinear reactance, we have that the power gain between ω_1 and ω_4 is

$$g_{14} = -\frac{P_4}{P_1} = \frac{\omega_4}{\omega_1} - \frac{P_2\omega_2}{P_1\omega_1}. \tag{4.96}$$

P_1 will be positive since we are supplying energy (the signal) to the reactance at ω_1. If we have a passive resistive termination at ω_2, P_2 will be negative. Therefore we see that the gain is indeed increased by the presence of dissipation at f_2, which is the condition for regeneration.

To compute the gain of this parametric device we can use the small-signal matrix, Eq. (1.31). Note that in this case the second harmonic of capacitance variation is important. The physical reason for this can be illustrated with the aid of Fig. 4.21. Here we show the significant frequency spectrum, together with a dotted line reminding us of a second-harmonic component of the capacitance variation at ω_3. For convenience, we will artificially divide the amplification process into two phases: one due to the capacitance variation at ω_3 alone, and one due to the capacitance variation at $2\omega_3$ alone. The former gives rise to up-conversion gain and regenerative gain, as has just been discussed. For the *second phase* of amplification, let us ignore the signal frequency and the capacitance variation at ω_3. What remains is seen to be simply another negative-resistance amplifier pumped at $2\omega_3$. (The fact that there is no resonant circuit at $2\omega_3$ is of no concern since it is only the capacitance variation which is significant, *not* any voltage or current which might be present at $2\omega_3$.) This second negative-resistance parametric amplifier will produce additional gain, hence it must be considered whenever the nonlinear reactance is such that a significant second harmonic component exists. A glance at Figs. 5.4 and 5.5 will show that when semiconductor diodes are used as the nonlinear reactance significant second harmonic will be present.

Many different devices can be constructed using this four-frequency principle. We can consider, for example, amplifiers at ω_1, ω_2, or ω_4, as well as up-converters and down-converters. In some cases interesting combinations can be formed by cascading two or more different devices[1].

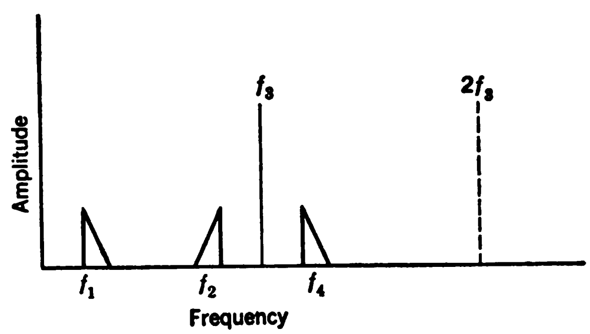

Fig. 4.21. Frequency spectrum of a four-frequency parametric amplifier.

Harmonic Pumping of Parametric Devices

It was pointed out that pump power supplied to a parametric device need not be at the effective pump frequency if harmonic capacitance components are present. For example, suppose we have a negative-resistance parametric amplifier with signal, idler, and pump frequencies ω_1, ω_2, and $\omega_3 = \omega_1 + \omega_2$. In practice, it is not necessary that we supply pump power to the amplifier at ω_3, for we can alternatively supply power at $\omega_3/2$ and rely upon the second harmonic of capacitance to give us our effective pump at ω_3. No change in any of the small-signal analysis is needed for such harmonic pumping; we need only remember to use the correct value of γ appropriate to the harmonic being used. Since the harmonic components of capacitance for a given value of a decrease with increasing harmonic number, the optimum harmonically-pumped amplifier can theoretically never have as good a performance as the corresponding amplifier pumped directly.

Parametric Limiting

The negative-resistance parametric amplifier has a definite threshold characteristic since it will suddenly break into oscillation as the pump level is increased. This phenomenon can be used to build a passive limiter, where the signal being limited is the pump supplied to the amplifier. Such a device could consist of a conventional one-port negative-resistance parametric amplifier with the pump circuit modified so as to have external loading. This loading will represent the output of our limiter, with the input of the limiter being the conventional pump input. If we introduce no signal into the amplifier at ω_1 or ω_2, the presence of the nonlinear capacitance in the pump circuit will produce only a constant load independent of pump power, whenever we stay below the point of oscillation (neglecting detuning effects and the presence of noise voltage). It therefore follows that in this region the output of our limiter will be directly proportional to the input. As we continue to supply pump power however, the effective negative resistance will increase until the point of oscillation will occur. At this point the loading of the pump circuit will change since the power at ω_1 will increase from noise level to oscillation level. As the pump power is further increased, the effective loading will increase. This additional loading represents pump power which is being parametrically converted into oscillation power at ω_1 and ω_2. The consequence of this increasing loading is to tend to stabilize the output power of our limiter as the input power is raised above the oscillation point. The ideal and actual characteristic of one such limiter[149] is shown in Fig. 4.22. To control the power at which limiting occurs we need only control the external loading at ω_1 and ω_2 as is indicated in Eq. (4.70).

Another type of parametric limiter is possible. This limiter is again essentially a negative-resistance parametric amplifier, except that now

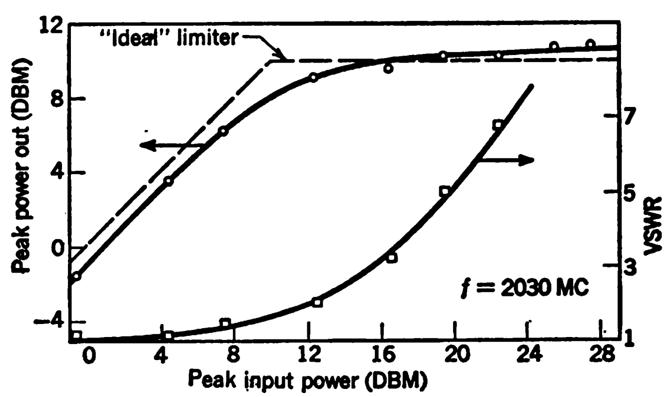

Fig. 4.22. Ideal and actual characteristics of a passive parametric limiter (after Wolf and Pippen).

ω_1 is the signal to be limited. The mechanism of limiting is precisely the same as described in the section on gain limiting. To avoid the straight-through transfer of signal power which will occur above gain saturation, this limiter is operated as a frequency converter with the output taken at ω_2. To come back to ω_2, a second down-converting negative-resistance stage can be used with additional limiting. This type of limiter has the advantage of giving gain as well as limiting, but has the disadvantage of requiring a separate pump for operation. The experimental characteristic of such a limiter is shown in Fig. 4.23[102].

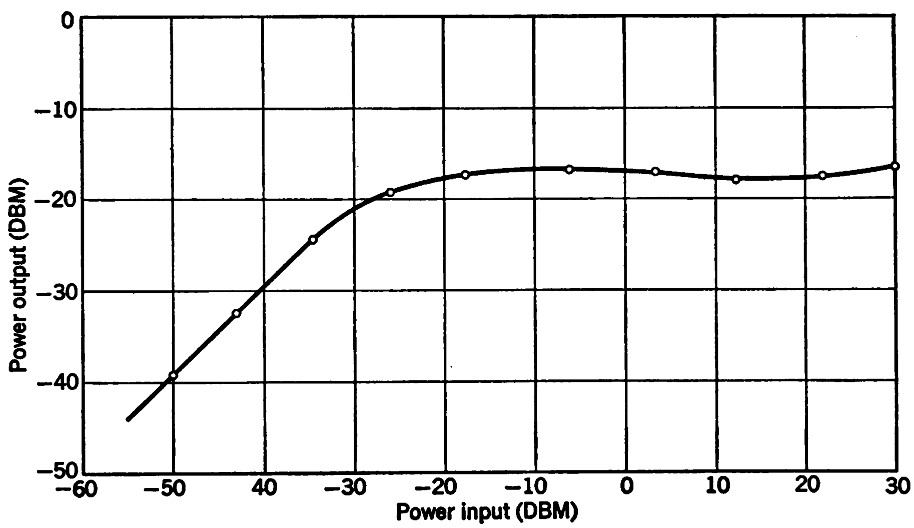

Fig. 4.23. Measured saturation characteristics of a parametric limiter (after Olson and Wade).

A Possible Frequency Stabilizer or Q Multiplier

We can use the oscillation characteristic of the negative-resistance amplifier in yet another fashion. One condition for oscillation which we have more or less ignored is the phase relation involved. From Eq. (3.49) we can see that the condition for oscillation is

$$Z_{11} + Z_{T1} = \frac{\gamma^2}{\omega_1\omega_2(Z_{22} + Z_{T2}^*)}. \tag{4.97}$$

Employing the high-Q approximation of Eq. (4.97), we can express this as

$$R_{T1}(1 + j2\delta_1 Q_1) = \frac{\gamma^2/\omega_1\omega_2}{R_{T2}(1 - j2\delta_2 Q_2)} \approx \frac{\gamma^2}{\omega_1\omega_2 R_{T2}}(1 + j2\delta_2 Q_2). \tag{4.98}$$

Equating the real and imaginary parts of Eq. (4.98) we arrive at the two conditions for oscillation:

$$R_{T1} = \frac{\gamma^2}{\omega_1\omega_2 R_{T2}}, \qquad \delta_1 Q_1 \approx \delta_2 Q_2. \tag{4.99}$$

For convenience let us assume that we are pumping at the correct frequency so that oscillation is occuring at ω_1 and ω_2 at precisely the resonant frequencies of the tuned circuits. Therefore $\delta_1 = \delta_2 = 0$. Now let the pump frequency change from ω_3 to $\omega_3 + \Delta\omega$. The oscillation frequencies must also change, say to $\omega_1 + \Delta\omega_1$ and $\omega_2 + \Delta\omega_2$. We still must maintain the relation

$$\omega_3 + \Delta\omega = \omega_1 + \Delta\omega_1 + \omega_2 + \Delta\omega_2 \tag{4.100}$$

therefore

$$\Delta\omega = \Delta\omega_1 + \Delta\omega_2. \tag{4.101}$$

We also have the relations

$$\delta_1 = \frac{\Delta\omega_1}{\omega_1}, \qquad \delta_2 = \frac{\Delta\omega_2}{\omega_2}. \tag{4.102}$$

Using Eq. (4.99), (4.101), and (4.102), we can solve for $\Delta\omega_1$ in terms of $\Delta\omega$.

$$\Delta\omega_1 = \Delta\omega \frac{\omega_1}{\omega_1 + \omega_2(Q_1/Q_2)}. \tag{4.103}$$

Of more interest is the fractional change in frequency. Rearranging, we have

$$\frac{\Delta\omega_1}{\omega_1} = \frac{\Delta\omega}{\omega_3} \frac{\omega_1 + \omega_2}{\omega_1 + \omega_2(Q_1/Q_2)}. \tag{4.104}$$

For any net "frequency stabilization" we thus require that

$$\omega_1 + \omega_2 < \omega_1 + \omega_2(Q_1/Q_2) \tag{4.105}$$

or therefore

$$Q_1 > Q_2. \tag{4.106}$$

This inequality can be satisfied by the addition of external loading to the "idler" circuit, and only lightly loading the signal circuit. As an example, assume $\omega_2 = 2\omega_1$ and $Q_1 = 20Q_2$. Then Eq. (4.104) becomes

$$\frac{\Delta\omega_1}{\omega_1} = 0.073 \frac{\Delta\omega}{\omega_3}. \tag{4.107}$$

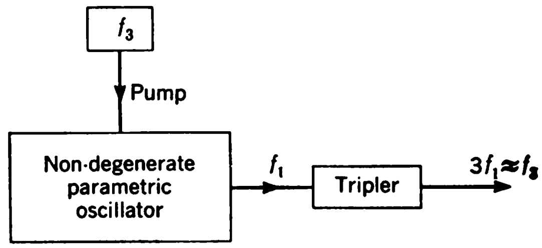

Fig. 4.24. A possible parametric frequency stabilizer.

In Fig. 4.24 we show a hypothetical arrangement for using this principle to increase the frequency stability of a signal. The input signal is used as the pump of a negative-resistance oscillator tuned so that

$$\omega_2 \approx 2\omega_1. \tag{4.108}$$

A small amount of power is removed at ω_1 and tripled. The result is a signal approximately equal to the input signal, but with increased stability. In practice this increased stability might not be easily realized, however, because of detuning effects caused by amplitude variation.

5

Semiconductor Diodes

We have thus far tacitly assumed the existence of a nonlinear capacitor characterized by a Q and a quantity called γ which was defined as the fractional change in capacitance due to the pump voltage. Until the discovery that a back-biased p–n junction could be made to perform as an almost ideal electronically-variable capacitor even at microwave frequencies, discussions of parametric amplification remained largely academic. Since semiconductor diodes have been and are likely to remain the heart of most parametric amplifiers, this chapter will present a brief discussion of the theory of their operation, the influence of semiconductor properties on their performance and techniques for measuring their quality.

5.1 Elementary Theory of *p-n* Junctions

It would perhaps be in order before beginning a discussion of semiconductor diodes to review in a qualitative way the physics of a p-n junction. A physical picture of the processes involved will be quite helpful. The reader, however, may want to refer to one of the many excellent books on semiconductor physics or transistor technology for a more detailed and quantitative treatment of this important subject.

Electrons in all crystalline solids may, as a consequence of certain quantum-mechanical principles which need not concern us here, be identified with energy bands within the crystal. There are three types of energy bands: empty, partially filled, and completely filled. The regions between these allowed bands are energetically forbidden to the electrons. The highest occupied band may, therefore, be either partially filled or completely filled. The former is called a conduction band because when an external electric field is applied, these electrons are free to drift, creating an electric current. In the highest completely filled band, known as the valence band, there can be no net flow of electrons in an electric field and consequently no current. If the highest occupied band is a valence band, the material is either an insulator or a semiconductor. A semiconductor differs from an insulator in the energy required to elevate an electron from the valence band across the energy gap of the forbidden region to the conduction band. In an insulator, this gap may be several electron volts so that at room temperature virtually no electrons may make this transition. In many semiconductors this gap is less than an electron volt, so that there is a high probability that thermal agitation will elevate sufficient numbers of electrons into the conduction band to make the material a fair conductor. This qualitative description predicts, for example, that the resistance of a semiconductor decreases with an increase in temperature while it is well known that the resistance of normal conductors increases with temperature.

In the intrinsic semiconductor described above, there are two processes which contribute to the conduction of current. The first is the normal drift of the electrons in the conduction band when an electric field is applied, and the second is the drift of positive charge carriers (called holes) in the now incompletely filled valence band. In the intrinsic semiconductor referred to here, for every electron that enters the conduction band, a hole is created which moves in a direction opposite to the electron under the influence of the applied field (not necessarily, however, with the same average velocity). This phenomenon of having two kinds of carriers is responsible for many of the unique and highly useful electrical properties of semiconductors.

Elemental semiconductors such as silicon and germanium, with a valence of four, and some of the III-V intermetallic compounds have found the widest application in semiconductor devices. Let us consider now the effect of adding an element of valence five such as arsenic or antimony to a pure semiconductor such as germanium. Let us assume that the impurity concentration is small, say one part in 10^5 so that the band structure of the original perfect semiconductor remains essentially the same. The effect of the impurity atoms is to introduce new energy levels in the forbidden region near the conduction band. At room temperature these impurity atoms are easily ionized, giving off an electron to the conduction band and leaving behind a fixed ionized positive charge.

Here we have one important difference between the intrinsic semiconductor discussed previously and the impurity semiconductor considered here. In the impurity semiconductor no hole is created when an electron moves into the conduction band, but rather a fixed charge which cannot contribute to conduction is produced. The impurities mentioned above donate electrons and hence are called *donor* impurities. Since electrons are primarily responsible for the conduction process, the material is called n-type. Even for small impurity concentrations the electrons far outnumber the holes and are therefore sometimes called *majority carriers.*

When an impurity of valence three such as gallium is introduced into a germanium crystal, impurity levels near the valence band are created. These *acceptors* as they are called have an affinity for electrons and at normal temperatures, electrons are thermally excited from the valence band, becoming attached to these impurity centers. Fixed centers of negative charge within the lattice are thus created, leaving hole carriers within the valence band. This type of semiconductor is called p-type.

Although p-n junctions in practice are not formed in this manner, let us visualize what would happen if two pieces of semiconductor, one of p-type the other of n-type, were brought into intimate contact. We would expect that upon contact electrons would diffuse from a region of high concentration (n-type material) to the region of low concentration (p-type material). Similarly, holes would diffuse from the p-region into the n-region. Remembering the presence of the fixed positive charges of the donor impurities in the previously neutral n-region and the negative acceptor impurities in the p-region we can see that as the diffusion proceeds, an electric field is set up at the junction which retards and finally stops the diffusion of charge carriers across the junction. After this equilibrium is established, a narrow region called the *depletion layer* is left at the junction which is swept completely free of carriers by the electric field. We now have all the essentials of a parallel-plate capacitor, with the depletion layer forming the separation between two conductive regions.

If a small reverse bias voltage is now applied across the junction, the electron distribution and the hole distribution will be pulled in opposite directions, widening the depletion layer. A small voltage of opposite polarity applied to the junction would push the two regions together, narrowing the depletion layer. We have then an easy means of varying the width of the depletion layer and consequentially the capacitance of the junction.

The discussion above gives a fairly accurate physical picture of how a p-n junction behaves as a voltage variable capacitor. It would be useful, however, to have a more quantitative relationship between the voltage across a junction and its capacitance for the several types of impurity distributions. Such information is necessary in order to predict how this and other properties of the semiconductor influence the quantity γ.

There are two fundamental types of impurity distributions which are characteristic of most *p-n* junctions. They are the abrupt or step junction and the linearly-graded junction. The former is a good approximation to the impurity gradient of an alloyed junction. The linearly, or uniformly-graded junction is, strictly speaking, that pictured in Fig. 5.1 where the difference in the acceptor and donor population changes linearly with distance. Practically, however, this is very nearly the

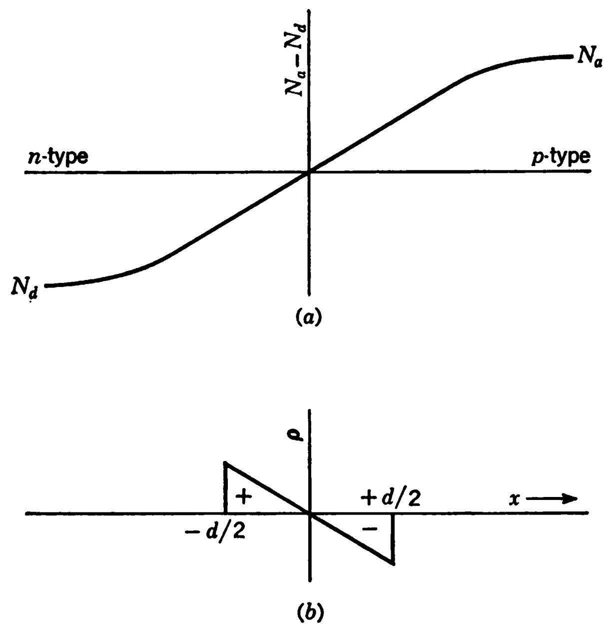

Fig. 5.1. Impurity and idealized space charge distribution for a linearly graded junction.

situation at the depletion region whether the distribution be exponential, hyperbolic, or any smooth function of distance. To a very good approximation then this is the distribution for grown or diffused junctions.

Referring to Fig. 5.1(a) for a uniformly-graded junction in which the impurity concentration is assumed to vary linearly with distance, we have

$$N_a - N_d = kx \tag{5.1}$$

where N_a and N_d are the excess acceptor and donor concentrations, respectively, and k is a constant. We will further assume that the charge density ρ varies linearly with distance over the depletion layer of thickness d as shown in Fig. 5.1(b). Therefore

$$\rho = -qkx, \qquad -\frac{d}{2} < x < \frac{d}{2} \tag{5.2}$$

where q is the elementary charge. Poisson's equation then becomes

$$\frac{d^2\varphi}{dx^2} = \frac{\rho}{\epsilon} = \frac{qk}{\epsilon}x \tag{5.3}$$

where $\varphi(x)$ is the electric potential and ϵ is the permittivity of the semiconductor. Integrating Eq. (5.3) twice and using the boundary conditions,

$$\frac{d\varphi}{dx} = 0 \quad \text{at} \quad x = \pm\frac{d}{2} \tag{5.4}$$

and

$$\varphi = 0 \quad \text{at} \quad x = 0 \tag{5.5}$$

we obtain

$$\varphi = \frac{qkx}{2\epsilon}\left(\frac{x^2}{3} - \frac{d^2}{4}\right). \tag{5.6}$$

The total potential difference across the junction is the sum of the negative bias $-V$ and the contact potential ϕ_0. Equating this quantity to the difference in potential across the depletion layer given by Eq. (5.6), we get

$$\phi_0 - V = \varphi\,|_{x=-d/2} - \varphi\,|_{x=d/2}$$

which becomes

$$\phi_0 - V = \frac{qkd^3}{12\epsilon}. \tag{5.7}$$

The total charge Q on either side of the origin may be found by integration

$$Q = \int_0^{d/2} - qkx\,dx = \frac{qkx^2}{2}\bigg|_{d/2} = q\,\frac{kd^2}{8}. \tag{5.8}$$

Using Eq. (5.7) d may be found and substituted into Eq. (5.8) yielding

$$Q = \frac{qk}{8}\left[\frac{12\epsilon(\phi_0 - V)}{qk}\right]^{2/3}. \tag{5.9}$$

The capacitance per unit area C' may now be found by differentiation

$$C' = \frac{dQ}{d(\phi_0 - V)} = \epsilon\left[\frac{qk}{12\epsilon(\phi_0 - V)}\right]^{1/3}. \tag{5.10}$$

We have the important result then that for a linearly-graded junction the capacitance varies inversely as the cube root of the applied bias.

An analysis similar to that given above yields for the capacitance per unit area of an abrupt junction

$$C' = \left[\frac{\epsilon q N_d}{2(\phi_0 - V)}\right]^{1/2} \tag{5.11}$$

where $N_d \ll N_a$. We have then an inverse square root variation of capacitance with voltage for the abrupt junction. Differentiation will show that for a given voltage change this relationship will produce a greater capacitance change than Eq. (5.10) for the linearly-graded junction. This may be more easily seen by the expression of the respective capacitance functions in Fourier series and an examination of the coefficients.

Let us write Eq. (5.11) in the form

$$C = \frac{A}{\sqrt{V_0 + v_{a\text{-}c}}} = \frac{A}{\sqrt{V_0}} \frac{1}{\sqrt{1 + v_{a\text{-}c}/V_0}} \tag{5.12}$$

where V_0 is the "total" d-c bias including contact potential and ~~self bias~~ and ~~$v_{a\text{-}c} = V \cos \omega t$ the applied a-c or pump voltage. If~~ we let $a = V/V_0$ Eq. (5.12) becomes

pump voltage to DC bias of varactor

$$C = \frac{A}{\sqrt{V_0}} \frac{1}{\sqrt{1 + a \cos \omega t}}. \tag{5.13}$$

Expanding into a Fourier series we get

$$C = C_0 - C_1 \cos \omega t + C_2 \cos 2\omega t - C_3 \cos 3\omega t + \cdots \tag{5.14}$$

where

$$C_n = C(V_0) \left| \frac{1}{\pi} \int_{-\pi}^{\pi} \frac{\cos nx}{\sqrt{1 + a \cos x}} \, dx \right|$$

and

$$C(V_0) = \frac{A}{\sqrt{V_0}}.$$

⇒ C_n is related to the pump voltage.

Figures 5.2 to 5.5 show the results of the computation of the capacitance coefficients for both the inverse square-root and the inverse

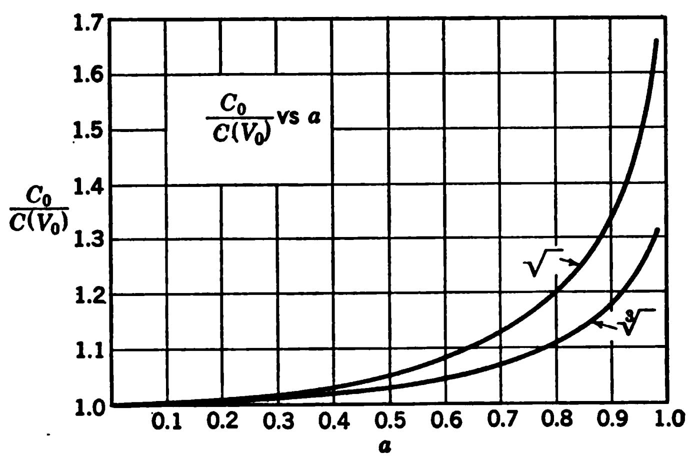

Fig. 5.2. Ratio of first Fourier Coefficient to d-c capacitance as a function of a.

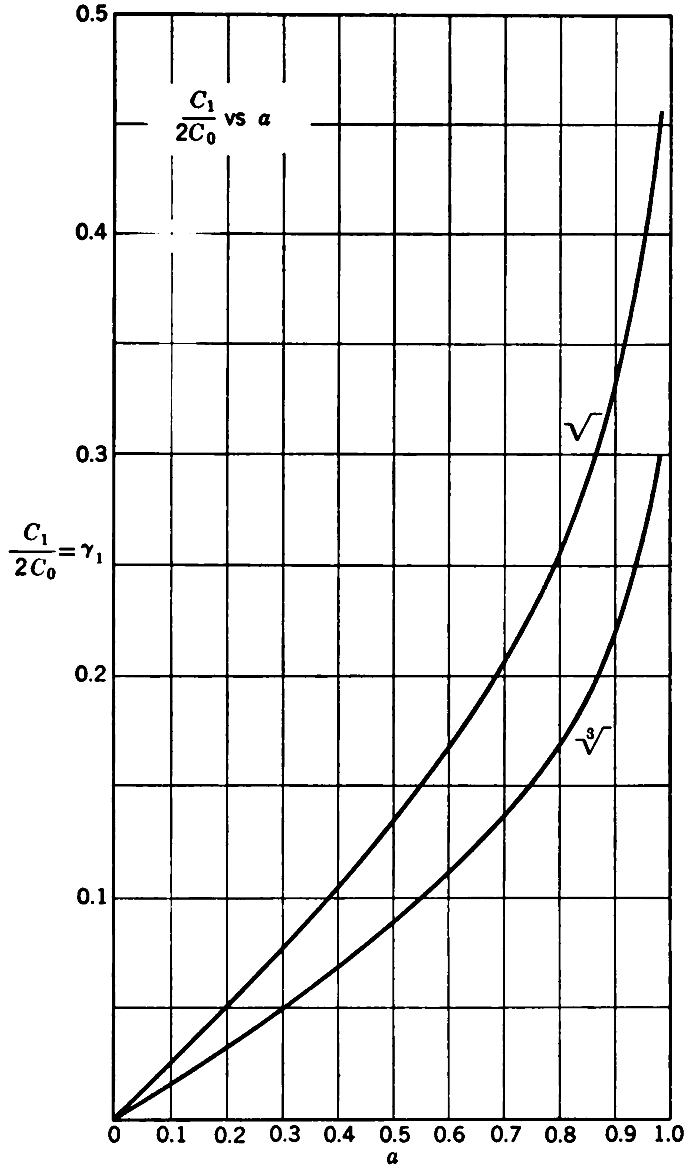

Fig. 5.3. Ratio of the second Fourier Coefficient as a function of a.

cube-root variation. The normalized coefficients are plotted against a. It can be easily seen that the square-root variation produces greater capacitance change for a given pump voltage swing.

Let us now consider an encapsulated semiconductor diode and the factors which influence its performance in a parametric amplifier.

For high frequency operation it is assumed that the high reverse leakage resistance shunting the junction capacitance can be neglected. The package capacitance C_p and inductance L are parasitics whose

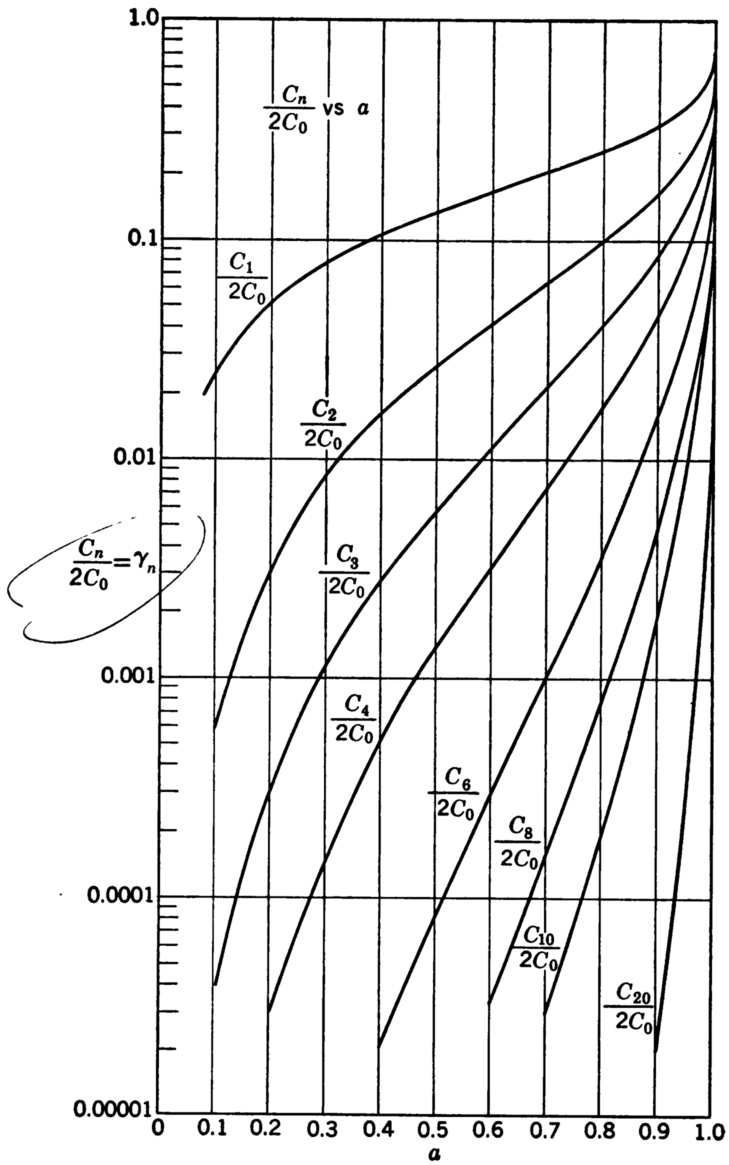

Fig. 5.4. Normalized higher-order Fourier Coefficients for an abrupt junction.

effect can sometimes be minimized but not completely removed. They may be in principle completely tuned out by the addition of a suitable matching network but the reactance added to the circuit will in general further restrict its bandwidth. Proper design of the diode package to minimize parasitics, as will be discussed later, appears the only practical solution to this problem short of eliminating the package entirely.

In order to determine the effect of the parasitic case capacitance of a particular diode on the performance of an amplifier, consider the equiva-

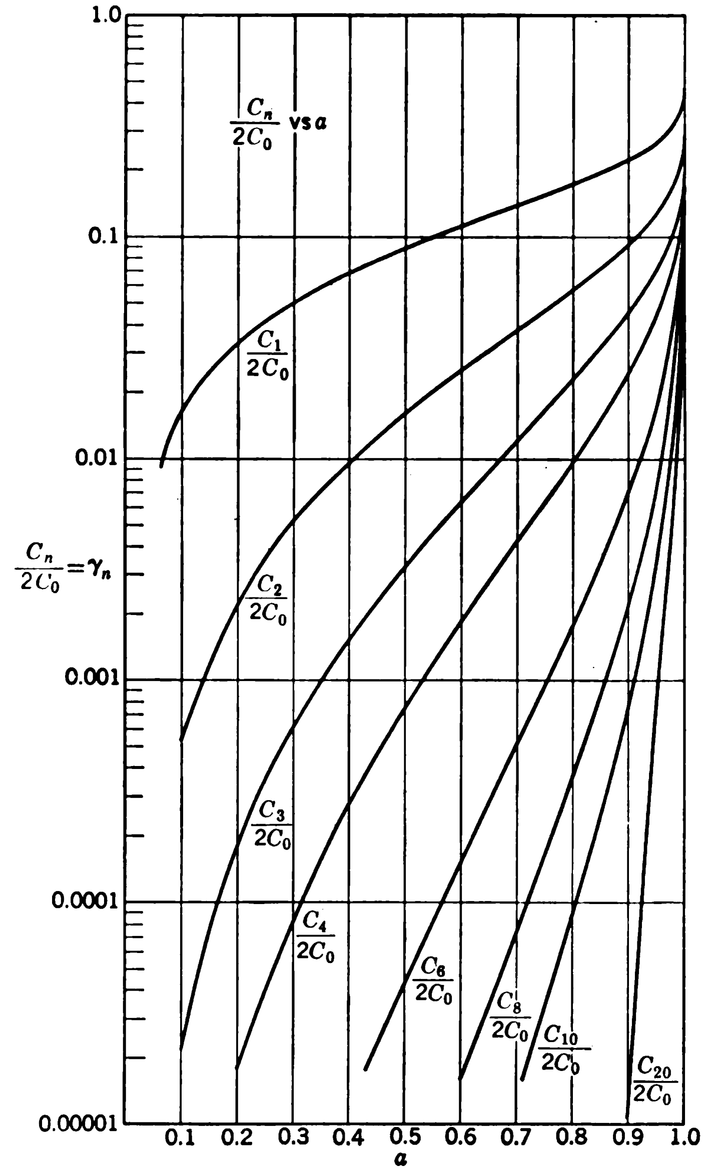

Fig. 5.5. Normalized higher-order Fourier Coefficients for a linearly-graded function.

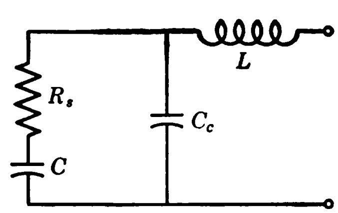

Fig. 5.6. Equivalent circuit of parametric diode.

lent circuit shown in Fig. 5.6. This representation which is slightly different from that which is usually assumed was found by careful measurement to be quite accurate throughout the microwave region. The cartridge capacitance C_c was 0.4 pf and the inductance L was 0.7 nh for this diode.

It is useful to transform the circuit of Fig. 5.6 to a series equivalent and to neglect for the moment the inductance. We obtain then

$$R' = \frac{C^2 R_s}{(R_s \omega C C_c)^2 + (C + C_c)^2} \tag{5.15}$$

and

$$X' = \frac{(\omega R_s C)^2 C_c + C + C_c}{\omega(\omega R_s C C_c)^2 + \omega(C + C_c)^2}. \tag{5.16}$$

We will define Q' as

$$Q' = \frac{X'}{R'} = \frac{\omega^2 R^2 C^2 C_c + C + C_c}{\omega C^2 R_s} = \omega R_s C_c + \frac{1}{\omega C R_s} + \frac{1}{\omega C R_s}\frac{C_c}{C}. \tag{5.17}$$

Assuming that $\omega R C_c \ll 1$, Eq. (5.17) becomes

$$Q' = Q\left(1 + \frac{C_c}{C}\right) = Q\left(\frac{C + C_c}{C}\right) \tag{5.18}$$

where Q is the junction $Q[Q = (1/\omega R_s C)]$.

We see therefore that the presence of the cartridge capacitance C_c has effectively increased the diode Q by the factor $(C + C_c)/C$. The capacitance variation factor $C_1'/C_0 = \gamma'$ has become

$$\gamma' \approx \frac{C_1}{C_0 + C_c} = \frac{C_1}{C_0}\frac{C_0}{C_0 + C_c} \approx \gamma_1 \frac{C}{C + C_c}. \tag{5.19}$$

We see then that in this example the parasitic cartridge capacitance C_c has increased the Q of the diode and decreased γ_1 by the same factor so that the figure of merit γQ remains unchanged.

This leaves then for our discussion the inevitable junction losses characterized by a series resistance R_s. For the usual semiconductor diode designed for parametric amplifier applications the series resistance is almost completely due to the bulk resistivity of the base region. The series resistance for a simple planar structure would be

$$R_s = \frac{t}{q\mu N_d A} \tag{5.20}$$

where t is the thickness of the base, μ is the electron mobility, N_d the donor impurity concentration in the base region, and A is the area of the junction.

Since the junction capacitance given by Eq. (5.11) is proportional to A, the Q of the junction is independent of area and is

$$Q = \frac{1}{\omega R_s C} = \frac{2q^{1/2}\mu N_d^{1/2}(\phi_0 - V)^{1/2}}{\omega t \epsilon^{1/2}} \tag{5.21}$$

at the operating bias for an abrupt junction diode. One might be tempted at this point to define a figure of merit as the product of the Q at breakdown voltage and the ratio of maximum to minimum junction capacitance. The product of these two quantities might be expected to be proportional to the quantity γQ and be useful as a guide to materials, doping levels, etc. Unfortunately, the ratio C_{max}/C_{min} is not directly related to γ and the value of such a figure of merit is questionable.

By inspection of Eq. (5.21), however, a material figure of merit can be written:

$$M = \frac{\mu N_d^{1/2}}{\epsilon^{1/2}}. \tag{5.22}$$

For highly doped materials, μ is related to N_d but the product $\mu N_d{}^{1/2}$ generally increases with impurity concentrations. In the light of Eq. (5.22) little can be said in favor of either silicon or germanium over each other. However some of the intermetallic semiconductors such as indium antimonide and gallium arsenide look particularly attractive on the basis of these considerations.

While the Q of a planar junction may be assumed to be independent of area, the quantity γ may not be when pump power is limited. For simplicity, let us consider the case where the diode is matched to the pump guide and all the pump power is dissipated in the series resistance. Under these conditions the voltage developed across the junction is

$$V_{\text{a-c}} = \left(\frac{2P}{R_s}\right)^{1/2} \frac{1}{\omega C} = (2PR_s)^{1/2} Q. \tag{5.23}$$

Two conclusions may be drawn from Eq. (5.23). In the first place, for a given voltage across the capacitance the required power increases as the square of the frequency. Secondly, for a given Q, a large value of R_s and consequentially a small capacitance is desirable.

5.2 Diode Fabrication

Thus far silicon, germanium, and gallium arsenide have received the most attention as materials for parametric diodes, and it has been demonstrated that high quality diodes can be fabricated using any of them. Gallium arsenide has been shown to be particularly useful for extremely-low-noise applications when operated a reduced temperatures,[132] in spite of the fact that it is still a relatively unfamiliar material whose technology has not reached the point of either silicon or germanium. Nevertheless gallium arsenide diodes are commercially available with cutoff frequencies greater than 150 Gc (Gigacycles) at a 2V bias.

Two fundamentally different techniques have been used successfully to construct high frequency parametric diodes. They are sometimes called the mesa and the point contact methods. In the first, a wafer which has been properly doped either n- or p-type is subjected to a diffusion which forms a region of the opposite type near the upper surface. A small area is masked in some fashion and the remaining surface etched away forming a mesa structure with the junction near its base. This technique has the advantage that the abruptness of the junction, which has been shown to significantly affect the microwave properties of the diode, can be varied over wide limits. In addition the size and geometry of the junction can be carefully controlled. After the mesa has been formed, the wafer is mounted in a suitable microwave package. Contacting the mesa is often accomplished by providing a flexible diaphragm on the end of a stud and carefully bringing this in contact with the mesa.

The second and somewhat simpler method for producing parametric diodes is to form the junction with a metal contact. In practice, a sharpened metal alloy wire is first brought into contact with a low-resistivity semiconductor wafer. The junction is then usually formed by pulsing the diode with low voltage a-c current and observing the d-c characteristic on a curve tracer. The junction is formed by the diffusion of atoms from the whisker into the semiconductor due to local heating at the point of contact by the forming current. While the mechanisms involved in this forming are not completely understood, the technique has been widely used to make high quality parametric diodes and mixer diodes.

After the specification of the Q and the capacitance variation of a diode, properties which depend on the semiconductor junction itself, the characteristics of the package remain as the only other important consideration of the circuit designer. Unlike the conventional microwave mixer crystal, whose encapsulation has been standardized for some time, the parametric diode package has taken a variety of forms. In general, package designs have been evolved with the idea of keeping their physical size small and yet minimizing stray capacitance and series inductance which, of course, play a more significant role in amplifiers than they do in mixers.

5.3 Diode Measurement Techniques

As we have said, there are two diode parameters of particular interest in the design of parametric devices: the degree of nonlinearity of the capacitance, and the effective Q of the diode junction. At the present time there exists no satisfactory method of dynamically and directly measuring the nonlinearity of the capacitance under operating conditions. On the other hand, it is a straightforward matter to measure the small-signal capacitance of the diode junction as a function of voltage. From this, one can compute the Fourier coefficients of capacitance, (which we have called γ_n), assuming a sinusoidal pump voltage, as was done in Section 5.1. This is not the ideal method, for in practice the pump voltage cannot be directly determined, either in magnitude or in waveform. Such a static determination of γ, however, does result in values which appear reasonable in the light of experimental results.

The second parameter of interest, the Q of the diode junction, can be measured under small-signal conditions. Unfortunately the Q of interest is the effective Q under actual conditions of large-signal drive, so again we must enlist the aid of some theoretical approximations to help us. These approximations are that the effective series resistance remains constant under large-signal conditions, and that the effective junction capacitance is as given by the first Fourier capacitance coefficient C_0.*

The measurement of the junction capacitance and resistance is in theory quite straightforward, and in practice somewhat difficult. The difficulty in measurement centers around two characteristics of the diode: 1) The diode is of very low capacitance and high Q, and 2) The diode is usually operated at microwave frequencies. The first characteristic presents a problem in that ordinary low frequency impedance measuring devices do not have the required range and resolution to determine the Q. The second characteristic presents a problem in that the device parameters should be measured at frequencies close to their actual operating frequencies, thereby necessitating the use of more difficult microwave measuring techniques.

The measurement of the diode junction Q at microwave frequencies is most accurately accomplished by measuring the input impedance of some fixture containing the diode as the bias applied to the diode is varied. By suitable methods this input impedance is then converted to obtain the actual junction impedance of the diode. To make this conversion, we make use of the fact that at a fixed frequency an arbitrary microwave network can be represented by an array of lumped elements. For example, a "T" network can be used to represent such a network, as shown in Fig. 5.7. A more useful representation is that termed the canonical circuit by Felsen and Oliner,† which represents the observed behavior of the network with a minimum number of elements.

* In a sense it *is* possible to make a dynamic measurement of the figure of merit γQ, providing we are willing to accept the validity of the foregoing analysis of parametric devices. For example we could build a tunable degenerate amplifier, and determine the highest frequency at which it will oscillate without any external loading. By Eq. (3.98) we see that at this point, $\gamma Q = 1$.

† L. B. Felsen and A. A. Oliner, "Determination of Equivalent Circuit Parameters for Dissipative Microwave Structures," *Proc IRE* vol. 42, pp. 477–483, 1954.

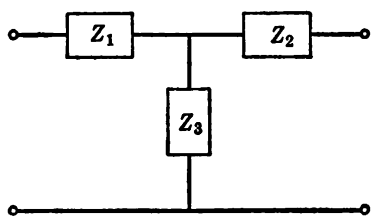

Fig. 5.7. A "T" network representation of a general microwave coupling network.

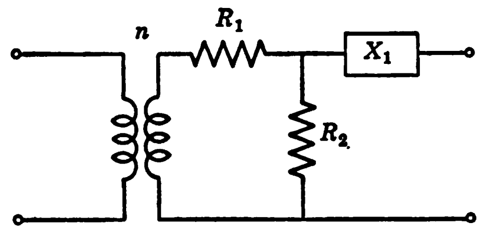

Fig. 5.8. A canonical representation of a microwave coupling network.

One such representation is shown in Fig. 5.8. Let us use this representation and place our diode junction impedance on the output of this circuit. If we knew the values of the parameters of our coupling circuit, it would then be a simple matter to convert our measured values of input impedance to obtain a value for the junction impedance, Z_j.

The equivalent circuit of Fig. 5.9 becomes particularly convenient when it is possible to neglect the coupling loss as represented by R_1 and R_2. Experiment shows that with well-designed fixtures, this can indeed be done; in fact, one criteria for good fixture design should be such low loss. Using this lossless circuit as shown in Fig. 5.9, we can now readily imagine how the parameters can be evaluated. One method is the use of standard impedances. This method involves the construction of known impedances in standard diode packages. In this manner we have known values of Z_j which enable us to calibrate the fixture. Let us assume that we first use an open-circuit standard, $Z_j = \infty$. The input impedance to our fixture will also be infinite *at the correct reference* plane. Hence, this experiment determines the reference plane for our fixture. Next, let us use a short-circuit standard, $Z_j = 0$. The input impedance will now be n^2X_1, evaluated with respect to the reference plane. The remaining parameter to be evaluated is thus n^2, the transformation ratio. To evaluate this quantity we need another impedance, such as a known resistance or capacitance. A method of fabricating a standard resistance has been described by Waltz[144]. Since the diode capacitance is independent of frequency in the range of interest, the diode itself can be used as a standard capacitance. To measure Q, however, it is not necessary to evaluate n^2, since Q is the *ratio* of reactance to resistance.

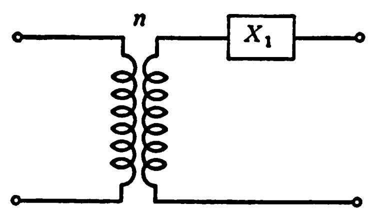

Fig. 5.9. A canonical representation of a lossless microwave coupling network.

The measurement of impedance at microwave frequencies is often done on a slotted line by observing the position and magnitude of the standing-wave pattern. It will be perhaps instructive to outline a simple "recipe" for the measurement of diode Q, using a slotted line in conjunction with a Smith chart.

1. Place an open-circuit impedance standard in the fixture and measure the standing-wave ratio (VSWR) and the position of a voltage *maximum*. This measurement establishes the reference plane at which the load is effectively located. (We measure the location of a *maximum* since such a maximum exists at an open circuit.) Place this point on the Smith chart as shown in Fig. 5.10. The radial position of the point 1 is given by the VSWR; for a good fixture, this VSWR should be high, say in excess of 200.

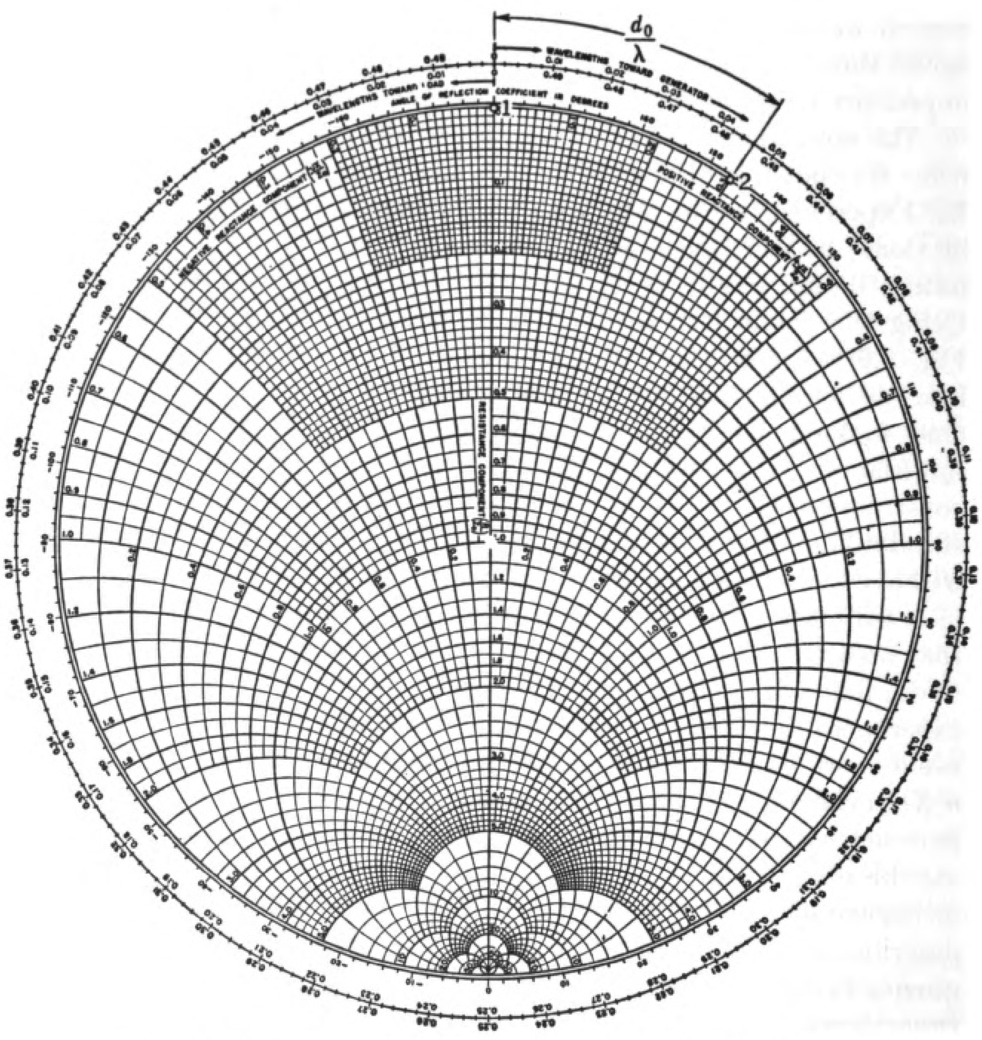

Fig. 5.10. Placement of the open-circuit and short-circuit standards on the Smith Chart. (Courtesy P. H. Smith, Bell Telephone Laboratories.)

2. Place a short-circuit standard in the fixture. Measure the VSWR and the distance between the reference plane and the position of a voltage *minimum*. Plot this point on the Smith chart as shown in Fig. 5.10, point 2. Again the VSWR should be high. Positive distance is measured from the reference plane toward the signal generator and plotted in a counter-clockwise direction on the Smith chart. Point 2 as plotted implies that X_1 is an inductance.
3. Place the diode in the fixture and again measure VSWR and the position of a minimum. Plot this on the Smith chart in the same manner as in Step 2.
4. To obtain the normalized impedance of the diode junction, read the normalized reactance value of the short-circuit point on the Smith chart and algebraically subtract from the value of reactance measured in Step 3. The resultant reactance is the normalized junction impedance. The normalized junction resistance is read directly without alteration. The diode Q is then simply the ratio of the normalized reactance to resistance.

This method is simply a graphical evaluation of the following equations which express load impedance in terms of the VSWR, and the position of a minimum with respect to a reference plane:

$$R_j = \frac{Z_o}{n^2} \frac{r\left(1 + \tan^2 \dfrac{2\pi d}{\lambda}\right)}{r^2 + \tan^2 \dfrac{2\pi d}{\lambda}} \tag{5.24}$$

$$X_j = -\frac{Z_o}{n^2} \frac{(r^2 - 1) \tan \dfrac{2\pi d}{\lambda}}{r^2 + \tan^2 \dfrac{2\pi d}{\lambda}} + \frac{Z_o}{n^2} \tan \frac{2\pi d_o}{\lambda} \tag{5.25}$$

where r = VSWR,

d_0 = position of voltage minimum of a standard short circuit with respect to the reference plane,

d = position of voltage minimum of the diode under test with respect to the reference plane.

There are two main sources of error in such a procedure: measurement errors, and errors in the standard impedances. Measurement errors mainly occur because of high VSWR, too high a signal level to the diode, and fixture losses. High VSWR can be measured by using the double-minimum technique. With this technique the two positions are found at which the detected power is twice the minimum power. The VSWR is then given by

$$\mathrm{VSWR} = \frac{\lambda}{\pi x} \tag{5.26}$$

where x = total distance between double-minimum. While quite high VSWR can be measured in this fashion, it is often more desirable to deliberately introduce some lossless circuit transformation to reduce the VSWR and make the measurements more convenient and perhaps more accurate.

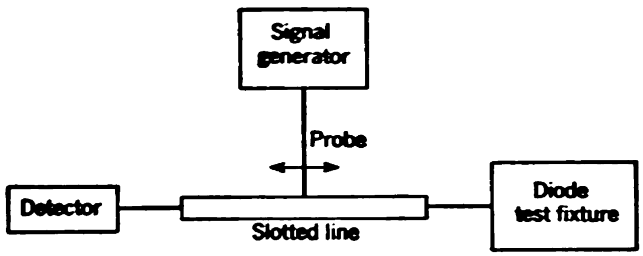

Fig. 5.11. Suggested experimental use of a slotted line in the measurement of diode impedance.

The signal level can be reduced to a safe level by using the experimental configuration shown in Fig. 5.11. If the measured impedance changes with signal level, the drive should be reduced until no change is noted. Fixture losses can be minimized by measuring the minimum as close to the diode as possible, and by placing the necessary d-c bias isolation before the slotted line. In Fig. 5.12 a possible test fixture is indicated.

The accuracy of the impedance standards can be determined by cross-checking the results in a number of different ways. (It should be

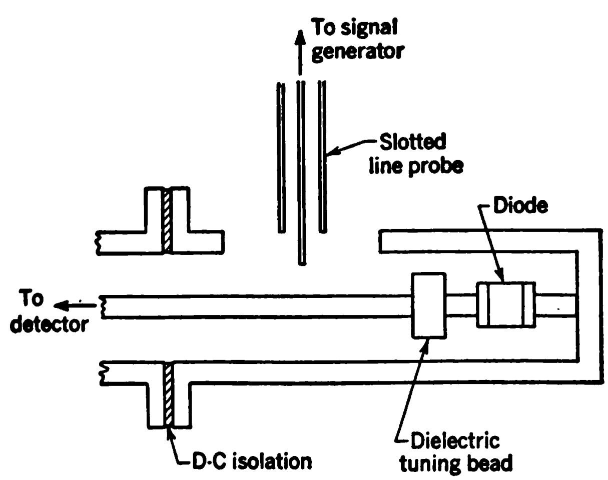

Fig. 5.12. Cross-section of a possible diode test fixture.

pointed out that diode packaging has to be consistent before a "standard" can be fabricated and evaluated.) The open-circuit standard should be electrically equivalent to a diode which has the junction removed; in fact, successful open standards have been produced by sending a large current surge through the diode and vaporizing the junction. If it is not possible to visually observe the results, however, one might wonder how much of the diode package has been similarly removed. Another method is to mount a wafer without a junction in a package and bring the connecting pin to precisely the same position as when a junction is present. This can be checked by measuring the low-frequency capacitance of the standard and comparing it with package shunt capacitance, if this is known. (One method of determining the package capacitance

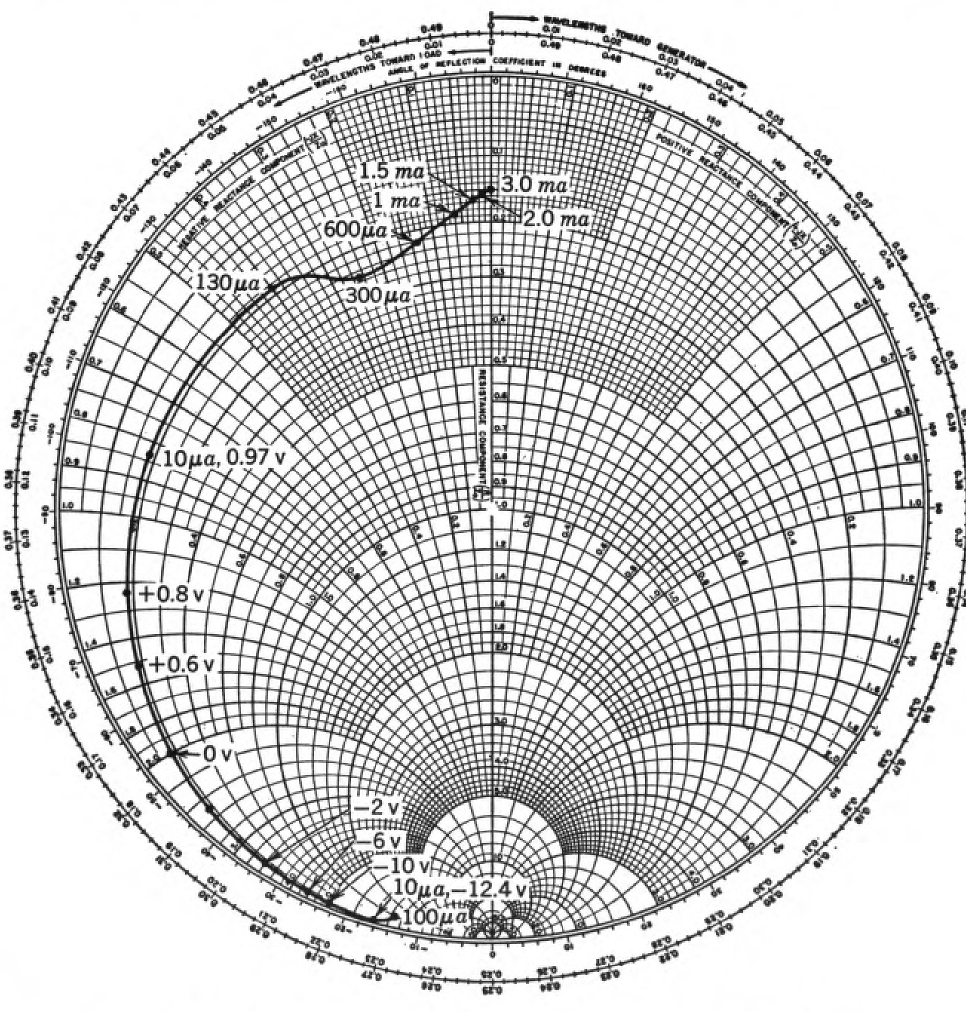

Fig. 5.13. Equivalent series impedance versus d-c bias for a typical parametric diode. (Courtesy P. H. Smith, Bell Telephone Laboratories.)

is to measure the total low-frequency capacitance of a number of diodes over a wide range of bias, plot the variation on log-log graph paper, and experimentally determine what value of capacitance has to be subtracted from all the capacitance measurements to yield the best fit to a straight line. This non-varying capacitance is then the effective package shunt capacitance).

Perhaps the most convincing evidence of a correct open-circuit standard is the experimental results of a number of diode measurements. If the series resistance is truly independent of bias, a plot of the impedance on a Smith chart should yield a segment of a circle. When the reference plane is properly determined by the open standard, this circle should coincide with a contour of constant resistance. Figure 5.13 shows an actual experimental result, vividly demonstrating this fact.

A short-circuit standard can be fabricated by replacing the semiconductor wafer and junction by a wafer of metal. The accuracy of this standard is somewhat more difficult to check. One possible method is to forward bias several diodes until no further change in the position of the voltage minimum is observed. This value of reactance should closely correspond to that obtained for the shorted standard because, at high forward bias, the junction capacitance increases to a large value, becoming an effective short-circuit. In some cases this procedure may damage the diodes, but the sacrifice of two or three diodes may not be too high a price to pay. Another method is to use a measured low-frequency capacitance-voltage characteristic as a calibration aid. For example, we could pick three points on such a curve, Fig. 5.14, so that the *junction*

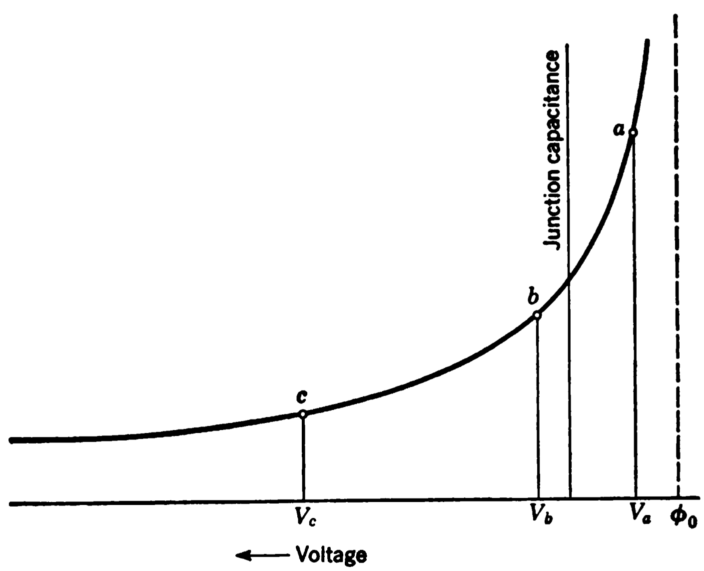

Fig. 5.14. Illustration of diode capacitance-voltage curve used in calibration of the short-circuit standard.

capacitance at bias V_b is half that at bias V_a, and that at bias V_c is half that at bias V_b. This same diode is then measured at microwave frequencies at the same bias values V_a, V_b, and V_c. The normalized reactance values are computed as previously described. If the position of the short circuit is accurate, the normalized net reactance obtained at bias a should be half that at b, and that at bias b should be half that obtained at c. Many such measurements could be made with diodes of widely varying capacitance. The consistency of the results would then be a good indication of the validity of the impedance standard used.

As has been previously pointed out, the value of the transformation ratio, n^2, need not be determined in order to evaluate diode Q. On the other hand, it is a simple matter to obtain the transformation if the diode junction capacitance has been accurately measured in a separate experiment. Computing the diode reactance at the frequency at which the Q is determined, we can then compare this reactance to the normalized reactance, obtaining the constant of proportionality. Another method of obtaining the transformation ratio is to construct a number of standard resistances. Assuming that the resistance at microwave frequencies is the same as that measured at d-c, the transformation ratio can be evaluated. At the same time the accuracy of the short circuit can be checked, for the standard resistors should all show a reactive component equal to that of the short circuit reactance, when measured with respect to the established reference plane.

6

Applications

6.1 Design Considerations

The choice of what type of parametric amplifier to use will depend upon the details of the system requirements. Several such examples will be discussed in Section 6.2. At this point we will content ourselves with a few general remarks which will be somewhat in the nature of a summary of what has already been presented.

As we have seen, there are two main types of parametric amplifiers: the up-converter and the negative-resistance amplifier. The analysis has shown that the optimum noise figures of these two devices are identical. The negative-resistance amplifier is inherently bilateral and unstable, requiring a circulator for best performance. It is capable of high gain at the expense of stability, but it usually has rather limited bandwidth. The up-converter is a unilateral stable device. It is capable of wider bandwidth than the negative-resistance amplifier, but it has rather limited gain.

The choice between the up-converter and the negative-resistance amplifier is in large measure determined by the frequency of operation. The output frequency of an up-converter will be around ten times or so higher than the signal frequency in order to achieve sufficient gain. Since the second stage following the up-converter will often be a resistive mixer, rather high first-stage gain is needed in order to minimize the high second-stage noise contribution. With typical mixer noise figures, it is probably

@ impractical to operate such a "pure" up-converter much above 1000 mc. This situation can be improved in practice by using the so-called four-frequency up-converter as described in Section 4.5. This device employs a degree of regeneration to augment gain at the expense of a somewhat higher first-stage noise figure and reduced stability of operation.

@ At higher frequencies where the up-converter is no longer practical, the negative-resistance parametric amplifier operated with a circulator becomes of interest. As we have seen, the use of a circulator is desirable from almost every aspect: stability, bandwidth, noise figure, and unilateral gain. The disadvantages are the added size, weight, and complexity, added insertion loss, and in some instances narrow bandwidth.

The choice between a degenerate or a non-degenerate parametric amplifier is a function of the system characteristics. This will be discussed in some detail in Section 6.3. It will suffice to say here that in some instances it may be possible to realize system sensitivities calculated from the double-sideband noise figure of the degenerate parametric amplifier. @ When this is so, the degenerate amplifier would be the logical choice since its double-sideband operating noise temperature is less than the optimum operating noise temperature of the non-degenerate negative-resistance amplifier or up-converter. Even if the single-sideband figure must be used, with its corresponding higher operating noise temperature, there may well be practical considerations which would make the degenerate amplifier the better choice. The degenerate amplifier offers the advantages of being a much simpler device to build, and uses a relatively low pump frequency. Broadbanding is also much easier for the degenerate amplifier. When the antenna temperature is low, little will be lost in sensitivity, and in some instances equal or even better sensitivity perhaps can be obtained. This is because a high idler frequency must be used for the nondegenerate amplifier and it may be impossible to reduce cavity loss to a point where it can be neglected compared to the diode loss. All such additional loss will increase the noise figure. It may therefore be preferable to operate in the degenerate mode to minimize such circuit loss. One disadvantage of the degenerate amplifier is the nearby idler frequency which would in many cases restrict the useful bandwidth to one side of half-pump frequency. It is possible to eliminate the idler by using a balanced arrangement with two identical amplifiers. (See Section 6.3.)

If wide bandwidth is needed, it will be necessary to use either a traveling-wave parametric amplifier or a multiple-tuned negative-resistance amplifier. Such devices are more difficult to construct and present added challenge to the circuit designer.

Once the type of amplifier has been selected, it is of interest to know what performance can be obtained. Table 6.1 gives a summary of the

TABLE 6.1

	Up-converter	Negative-resistance amplifier with circulator	Degenerate amplifier with circulator
Minimum operating noise temperature....	$2T_d\left[\frac{1}{\gamma Q} + \frac{1}{(\gamma Q)^2}\right] + T_a$	$2T_d\left[\frac{1}{\gamma Q} + \frac{1}{(\gamma Q)^2}\right] + T_a$	$T_d\left[\frac{1}{\gamma Q} + \frac{1}{(\gamma Q)^2}\right] + T_a$*
Maximum gain........................	$(1/4)(\gamma Q)^2$	∞	∞
Maximum bandwidth, single-tuned circuits	$b = \frac{2}{Q_1} < 2\gamma\sqrt{\omega_4/\omega_1}$	$b = g^{-1/2}\gamma\sqrt{\omega_2/\omega_1}$	$b = g^{-1/2}\gamma$
Optimum loading for maximum gain......	$R_g = R_l = R_s\sqrt{1 + \omega_1/\omega_4(\gamma Q)^2}$		
Optimum loading for minimum noise figure.	$R_g = R_l = R_s\sqrt{1 + (\gamma Q)^2}$	$R_g = R_l = R_s\sqrt{1 + (\gamma Q)^2}$	$R_g = R_l = R_s(\gamma Q - 1)$
Optimum pump frequency for minimum noise figure.........................		$\omega_3 = \omega_1\sqrt{1 + (\gamma Q)^2}$	$2\omega_1$

* Double-sideband case

best results that one can hope to attain with up-converters and negative-resistance amplifiers, together with pertinent design values.

The results presented here are not meaningful unless they can be related to the physical properties of the semiconductor diode used in the parametric amplifier. Two questions which need to be answered are: 1) What is a reasonable design value for γ_1? 2) What value of diode capacitance should be used in the evaluation of the diode Q? A combination of experiment and theory provides approximate answers to these questions. The fractional change in capacitance was shown to be a function of the shape of the capacitance-voltage curve and of the ratio of the a-c voltage swing to the effective d-c bias voltage, which includes the built-in contact potential. If we can specify these parameters, and if we assume sinusoidal pumping, it is a straightforward matter to evaluate γ_1. We *can* specify the shape of the capacitance as a function of voltage. The question of a-c voltage swing cannot be answered precisely. Obviously one cannot carry the a-c swing all the way to the effective contact potential because of the onset of forward conduction. Such conduction reduces the effective Q of the diode and introduces shot noise. At the present time there is no theoretical analysis which shows what the maximum permissible voltage swing should be. Experimentally the maximum ratio of peak a-c voltage to d-c bias appears to be around 0.90 to 0.95 for diodes with reverse breakdown voltages around 10 volts. A value of 0.90 will be assumed here as a reasonable design standard. With this assumption, the appropriate value of γ_1 can be computed. The design value of capacitance can also now be specified, at least to first-order. The optimum bias point will be about mid-way between the points of significant forward or reverse conduction. This specifies the static capacitance but does not give the effective capacitance which exists at large a-c capacitance swings. Again this can be computed using the above assumptions. The resulting estimated design values are indicated in Table 6.2. $C(V_b)$ is the small-signal capacitance at operating bias.

TABLE 6.2

	γ_1	C_0
Abrupt junction	1/3	$1.3C(V_b)$
Linearly-graded junction	1/4	$1.2C(V_b)$

As an example, let us assume that we have available an abrupt-junction diode with 1 pf capacitance at operating bias and a series resistance of 3 ohms. It is desired to design a negative-resistance amplifier at 3 Gc.

For this case, γQ would be about 4.5. The optimum pump frequency would be about 13.5 Gc. No external idler loading would be used, and a circulator would be incorporated. The diode would be pumped as hard as possible to achieve the design value of γ_1, and the input coupling would be adjusted to load the amplifier as heavily as possible and still achieve significant gain. The input VSWR at resonance before the inclusion of the circulator would be about 4.5 in this case. The minimum value of noise figure thus obtained would be about 1.8 db with the amplifier at room temperature. If the amplifier could be cooled to liquid nitrogen temperature without change in diode Q, the minimum noise figure would decrease to 0.6 db, or an effective input noise temperature of about 44°K.

6.2 Specific Examples

The design guides discussed in the previous section are useful in predicting the expected performance of a parametric amplifier in terms of diode parameters and in choosing the optimum pump frequency to signal frequency ratio for a non-degenerate amplifier. The reduction to practice of the equivalent circuits assumed in the analyses in Chapters 3 and 4 however, is not always a simple task and in most cases compromises must be made which inevitably have their effect on amplifier performance. This is most apparent when one compares the gain bandwidth products which have been actually achieved with that predicted by theory. The narrow bandwidths often obtained are due to parasitic reactances which may or may not be associated with the diode itself. Fortunately the picture is brighter when one compares achievable noise figures with theoretical values. The agreement is often quite good.

In this section some design details of a few parametric amplifiers of various types will be given. These amplifiers are not necessarily represented as the ultimate but are certainly typical of the present state of the art.

Degenerate Parametric Amplifiers

Since it does not require a separate signal and idler circuit coupled by the diode, the degenerate amplifier is the least complex type of parametric amplifier. It is easily tunable, puts the least demands on the pump source and, in some applications, may perform as well or better than a non-degenerate amplifier employing a diode of equal quality. Perhaps the simplest embodiment of a degenerate amplifier is a crossed-waveguide structure. In this type of circuit, the pump is introduced through an appropriately dimensioned waveguide and matched into the diode, which is coupled to the signal cavity formed in the second guide by a movable short and a coupling iris. This type of circuit can generally be operated

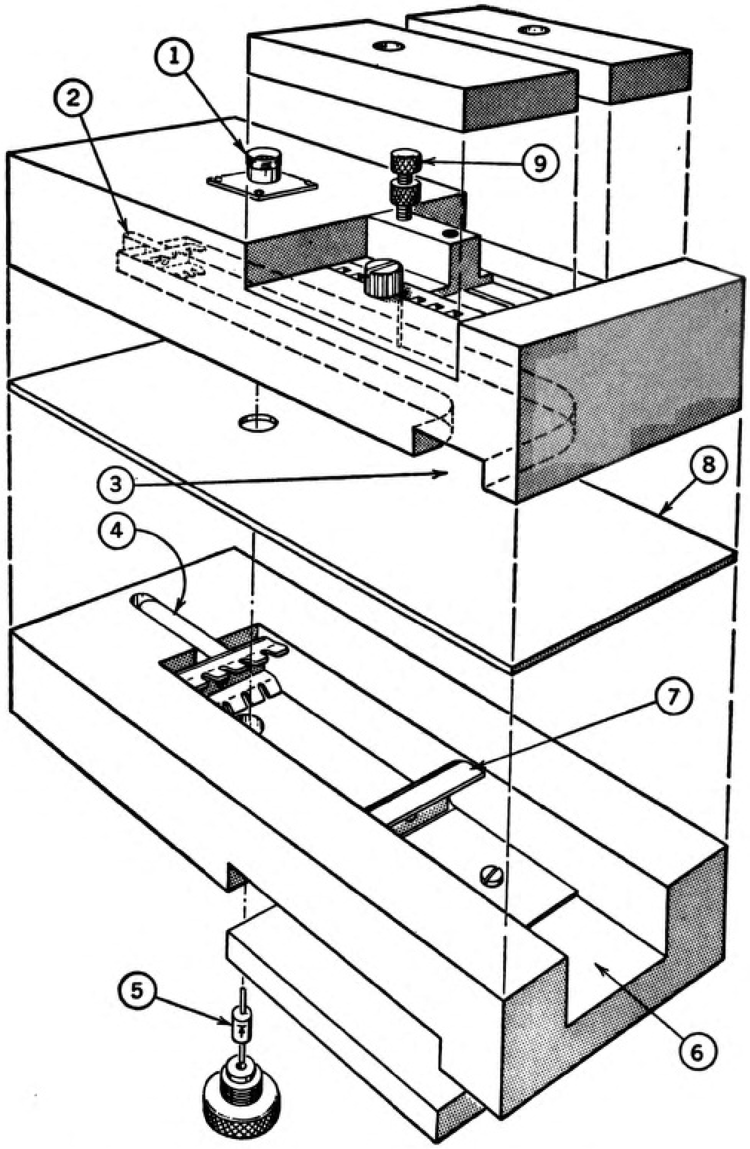

Fig. 6.1. A degenerate X-band parametric amplifier.

with diodes exhibiting a fairly wide range of characteristics. The bandwidths achieved, however, are usually measured in tenths of a per cent. An X-band amplifier of this design is shown in Fig. 6.1. A voltage gain bandwidth product of 50 mc and a double-sideband noise figure of 0.85 db were achieved using a diode having a cutoff frequency of 147 Gc at -2 V bias.

The simplest way to remove the bandwidth restrictions imposed by parasitic reactances associated with the diode and matching elements is to use the self-resonance of the diode as the principal signal resonance.

In order to illustrate how this might be accomplished, let us consider the design of an X-band amplifier. If the equivalent circuit of Fig. 5.6 is transformed to a series representation, the equivalent series resistance and capacitance will be given by Eqs. (6.1) and (6.2) respectively.

$$R' = \frac{C^2 R_s}{\left(\frac{C_c}{Q}\right)^2 + (C + C_c)^2} \tag{6.1}$$

$$C' = \frac{\left(\frac{C_c}{Q}\right)^2 + (C + C_c)^2}{\frac{C_c}{Q^2} + C + C_c}. \tag{6.2}$$

For $Q \gg 1$ these expressions reduce to

$$R' \approx R_s \left(\frac{C}{C + C_c}\right)^2 \tag{6.3}$$

and

$$C' \approx C + C_c. \tag{6.4}$$

For a series inductance of 0.6 nh, a package capacitance $C_c = 0.4$ pf and a junction capacitance of 0.1 pf the diode will become self-resonant at

$$f = \frac{1}{2\pi} \frac{1}{\sqrt{L(C + C_c)}} = \frac{1}{2\pi} \frac{1}{[(0.6)(10^{-9})(0.5)(10^{-12})]^{1/2}} \approx 10 \text{ Gc.}$$

The optimum source resistance may be found from Eqs. (3.101) and (6.3)

$$R_g = R_s \left(\frac{C}{C + C_c}\right)^2 (\gamma Q - 1). \tag{6.5}$$

If we assume that the diode above has a cutoff frequency between 150 and 200 Gc at the operating bias, the optimum value of R_g from Eq. (6.5) is about 3 ohms. The amplifier consists then of a short coaxial taper from the 50 ohm input to a 3 ohm line terminated in the diode. The pump was coupled to the coaxial line by a probe from a short section of waveguide. A 250 mc bandwidth at 20 db gain was typical and at 39 db gain a voltage gain bandwidth product exceeding 10,000 mc was measured. The double-sideband noise figure of the amplifier was about 2 db. Figure 6.2 shows one version of this amplifier.

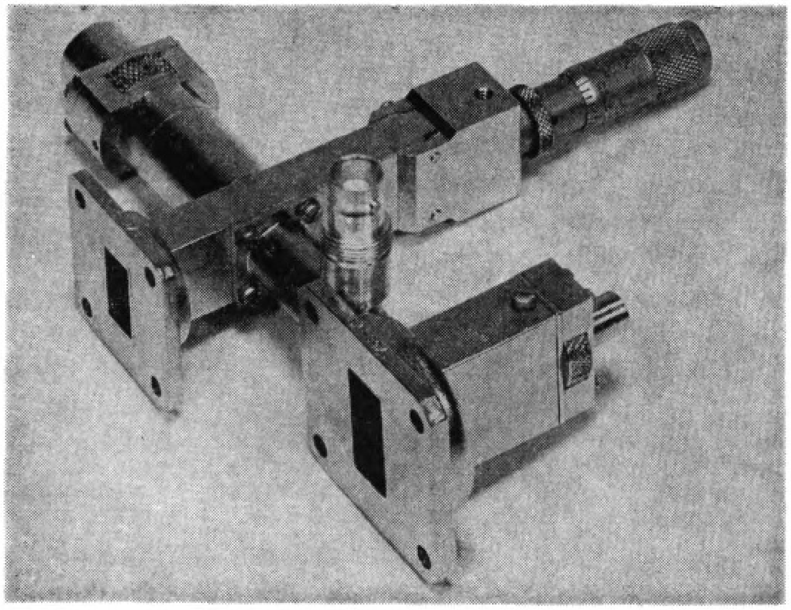

Fig. 6.2. An X-band parametric amplifier. (Courtesy Texas Instruments, Inc.)

A Non-degenerate Amplifier

The design of a low-noise non-degenerate parametric amplifier is not always as straightforward as the design of its degenerate counterpart. In practice the most difficult problem encountered is the simultaneous coupling of the diode to three resonant circuits at the pump, the idler, and the signal frequency. In order to achieve significant bandwidth it is further necessary to keep the Q of the signal and idler circuits low without introducing significant losses other than those due to the diode series resistance. This implies that parasitic reactances either associated with the diode itself or with matching devices be kept to a minimum. Further complications arise when it is desired to make the amplifier tunable over say a 20% band. If the tuning of the signal and idler resonances are not independent, retuning can be a tedious procedure. When the figure of merit of the diode is sufficiently high at the signal frequency, however, the optimum ratio of pump to signal will be high, and consequently the idler frequency will be high relative to the signal. Under these conditions the Q of the idler resonance can sometimes be made low enough so that an appreciable bandwidth can be covered by tuning the signal resonance but leaving the idler resonance fixed tuned.

Since the non-degenerate diode parametric amplifier first made its appearance several rather flexible designs have evolved which perform adequately for most applications. A version of one such design is illustrated in Fig. 6.3. This amplifier was designed to operate in the S-band

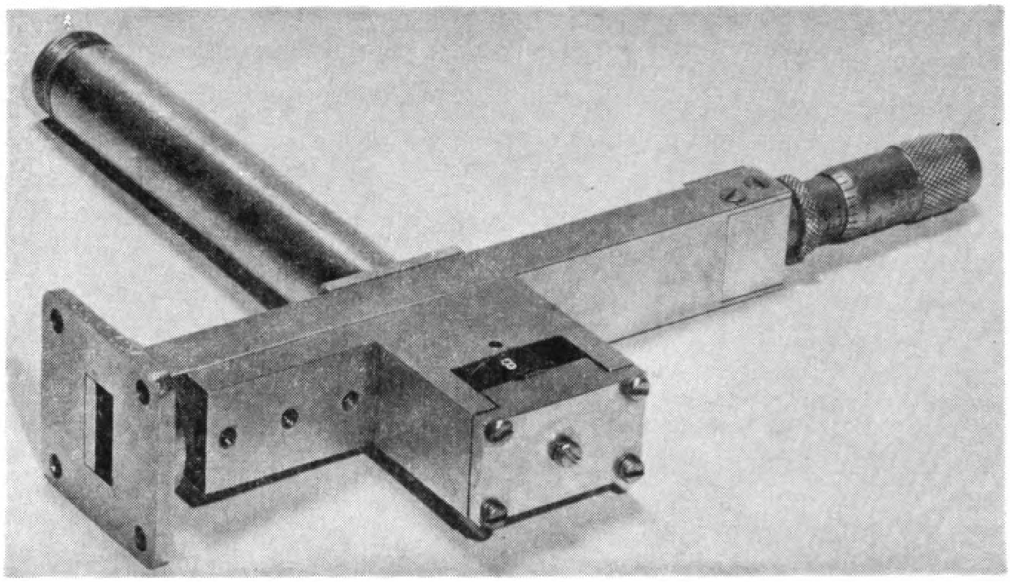

Fig. 6.3. A tunable S-band amplifier. (Courtesy Texas Instruments, Inc.)

region and be tunable over a 200 mc range. The diodes available at the time of design had a Q of about 20 at the operating bias and nominal operating frequency of 2.8 Gc. If we assume a value of $\gamma = 0.25$, which is fairly conservative for the diodes used, the optimum ratio of pump to signal frequency for minimum noise figure becomes

$$\left(\frac{\omega_p}{\omega_s}\right) = \sqrt{1 + (\gamma Q^2)} = \sqrt{1 + (5)^2} \approx 5$$

which yields a pump frequency of 14 Gc.

The pump power is supplied to the amplifier by a section of RG 91/U K_u band waveguide through a stepped transformer to reduced-height waveguide at the diode. Another step in the broad dimension of the guide confines the idler resonance (at approximately 11 Gc) to the amplifier. Idler tuning is provided by a movable short behind the diode. The signal tuning is accomplished by the adjustable stub at the bottom of the amplifier. The signal is introduced coaxially through a low-pass filter to the diode. The proper impedance transformation to the diode from the 50 ohm line is provided for minimum noise figure.

For the optimum source resistance and pump to signal ratio the minimum theoretical noise figure for the diode used is given by

$$F = 1 + 2\left[\frac{1}{\gamma Q} + \frac{1}{(\gamma Q)^2}\right] = 1 + 2\left[\frac{1}{5} + \frac{1}{(25)^2}\right] = 1.44.$$

The measured noise figure excluding circulator and second stage contribution was 2.2 db. The maximum bandwidth attainable was 70 mc at 15 db gain.

An Up-converter

Although it was shown in Section 3.1 and 3.2 that the minimum noise figure obtainable with a given diode is approximately the same for both the up-converter and the optimum non-degenerate parametric amplifier, extremely low noise up-converters are limited to L-band and below in frequency. This is because of the increasing noise figures of conventional mixers with increasing frequency. It can, in fact, be shown that for a given input frequency, the overall noise figure of an up-converter-mixer combination is practically independent of the pump frequency since the conversion loss of the mixer increases with frequency at about the same rate as the gain of the up-converter for pump frequencies above X-band. The real usefulness of the "pure" up-converter is therefore limited primarily by high frequency mixer performance rather than by parametric diodes. Although the technology of microwave mixer diodes is not young, significant improvements in diode quality are still being made. Recent work on materials such as gallium arsenide has shown considerable promise for improved diodes, especially at the higher microwave frequencies.

In spite of the limitations discussed above, the up-converter has advantages over the negative-resistance parametric amplifier of:

1. having a positive input impedance,
2. being unilateral and as a consequence unconditionally stable,
3. requiring no circulator,
4. having gain virtually independent of changes in its source impedance, and
5. having a typical bandwidth of the order of 5 per cent.

As an example of an up-converter of fairly simple design and good performance let us consider such a device developed by Jones and Honda[65] which can be operated as either a "pure" up-converter or as a regenerative up-converter by allowing power to be dissipated at the difference frequency. In this amplifier the diode is situated in the center of a symmetrical "Y" junction with provision for supplying external bias. The signal at around 400 mc is introduced in series with the diode by a coaxial line through a low-pass filter section. In addition to the filtering action provided by the waveguide to the signal frequency, bandpass filters are placed in the pump guide and output guide at the appropriate frequencies and positioned so that a high impedance is presented to the diode throughout their respective stop bands. For operation in the up-converter mode, the third arm of the "Y" is shorted by an adjustable plunger positioned so as to present a low impedance across the diode at the difference frequency and a high impedance at the pump and upper sideband frequencies. To achieve regenerative operation a variable attenuator and bandpass filter was inserted in this arm between the diode and the short and was used to vary the impedance across the diode at the difference frequency.

The conversion gain for a 410 mc input signal and 9227 mc output was 12.4 db without regeneration and 20.7 db with a large amount of power dissipated at the lower sideband. The bandwidth in these two modes of operation was about 3.8 mc and 1.7 mc respectively and the noise figure slightly less than one db in either case.

The Traveling-wave Parametric Amplifier

We have seen that single-tuned cavity type parametric amplifiers are limited to bandwidths of a few per cent, while if passive filter structures are used to replace the resonant cavities bandwidths greater than 10 per cent are possible. Both types are of course bilateral and require the use of a circulator for best operation. It was shown in Section 4.2 that considerably greater bandwidths are possible if the variable reactance can be distributed either periodically or continuously in a non-resonant structure. In addition such an amplifier is unilateral without the use of non-reciprocal devices. Several interated traveling-wave parametric amplifiers using semiconductor diodes have been successfully operated. The one pictured in Fig. 6.4 is a balanced type consisting of 16 pairs of diodes.[37] The balanced arrangement permits independent adjustment of the pump and signal velocities. In this amplifier the line is constructed of printed circuit board and the diodes are self-biased. The structure required 10 mw of pump power and had 8 to 10 db of gain over a 200 mc bandwidth centered about 700 mc. The reverse gain was between $+1$ and -2 db depending on frequency; the single-sideband noise figure was 3.5 db.

Harmonic Generators

Harmonic generation with reactance diodes appears to have a number of useful applications. With relatively inexpensive diodes conversion efficiencies and power handling capabilities are high enough to make practical fairly efficient low-level microwave sources using transistor oscillators as the primary source. Another important use is in the generation of millimeter waves. For example, using the curves of Figs. 4.17 to 4.20 we can expect less than a 10 db conversion loss in tripling from 11 to 33 Gc or doubling from 35 to 70 Gc with a diode having a 200 Gc cutoff frequency. In view of the voltage requirements and expense of some of the millimeter wave klystrons, it may sometimes be desirable to use a less expensive klystron at X-band, for example, and multiply the output to the desired output if sufficient efficiency can be retained.

Transistor-driven reactance diode microwave sources may be useful in such applications as local oscillators and parametric amplifier pump

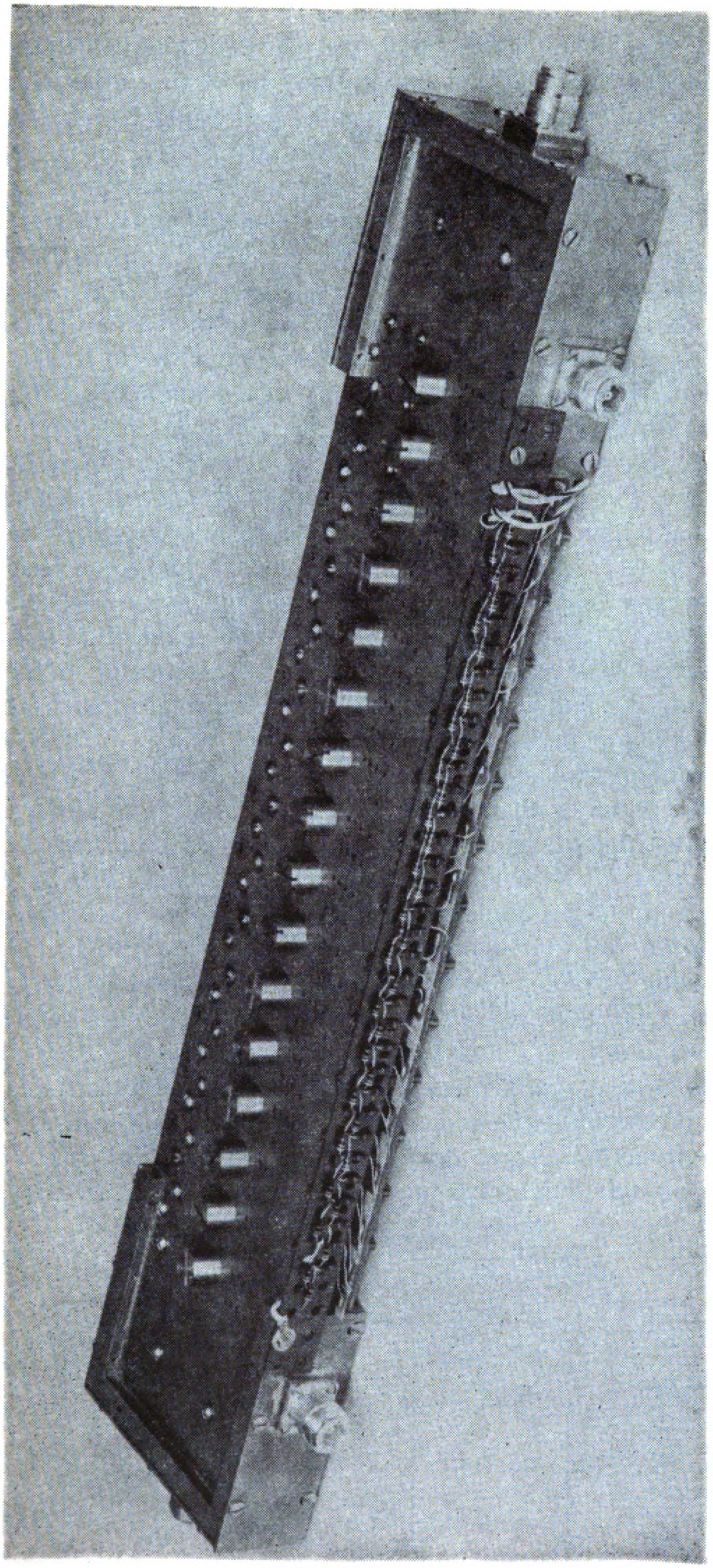

Fig. 6.4. A traveling-wave parametric amplifier. (Courtesy Bell Telephone Laboratories, Inc.)

sources. The efficiency of these devices may be of the order of only a per cent or so, but still competitive with low-power klystrons.

As an example of a reactance diode microwave source let us consider the design of an oscillator, which was developed to supply 10 mw at 2520 mc. The source consists of a crystal-controlled transistor oscillator at 70 mc and a transistor doubler and power amplifier followed by three stages of reactance multiplication. In Section 4.4 it was shown that harmonic generation can be more efficiently accomplished in several stages of doublers or triplers rather than a single higher-order multiplication. To best utilize the reactance diodes available at the time of design, the sequence of multiplication chosen was: to triple from 140 to 420 mc, to double from 420 to 840 mc and, finally, to triple again from 840 to 2520 mc. The output of the final transistor stage was at a level of 200 mw so that a high breakdown-voltage diode was required in the first tripler. This diode, a diffused junction silicon device, had a reverse breakdown of approximately 80 volts, a capacitance of 4 picofarads, and a 2.5 ohm series resistance. The circuit for this tripler is suggested by the circuit model used in the analysis and is shown schematically in Fig. 6.5. After optimum coupling was achieved, 80 mw was produced at the output frequency of 420 mc for a 4 db conversion loss.

The circuits for the doubler to 840 mc and the tripler to 2520 mc are essentially the same of that of Fig. 6.5 except that a combination of lumped and distributed elements are used in their construction. The design of these stages was largely empirical. The procedure was to breadboard the circuit using standard coaxial components and adjustable stubs and, after the desired performance was obtained, to reconstruct the circuit using Microdot cable of the appropriate lengths for the resonators. Stripline filters were used in the final two stages to remove unwanted harmonics.

The performance obtained from these harmonic generators was very close to that predicted by the design curves given in Chapter 4. An input power of 1.3 watts was required for an output power of 6.5 mw. Figure 6.6 shows a similar harmonic generator which produces 10 mw at C band.

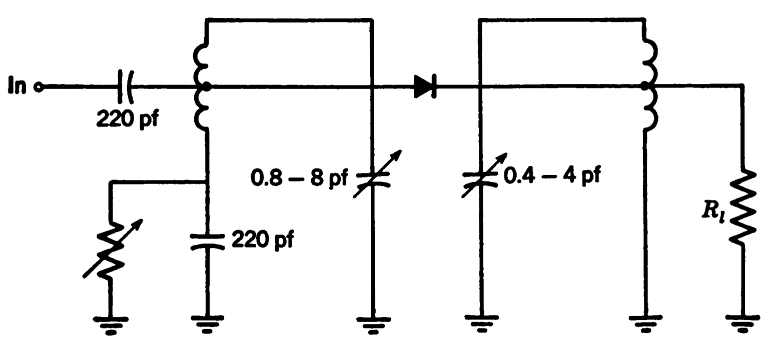

Fig. 6.5. Schematic of tripler from 140 to 420 mc.

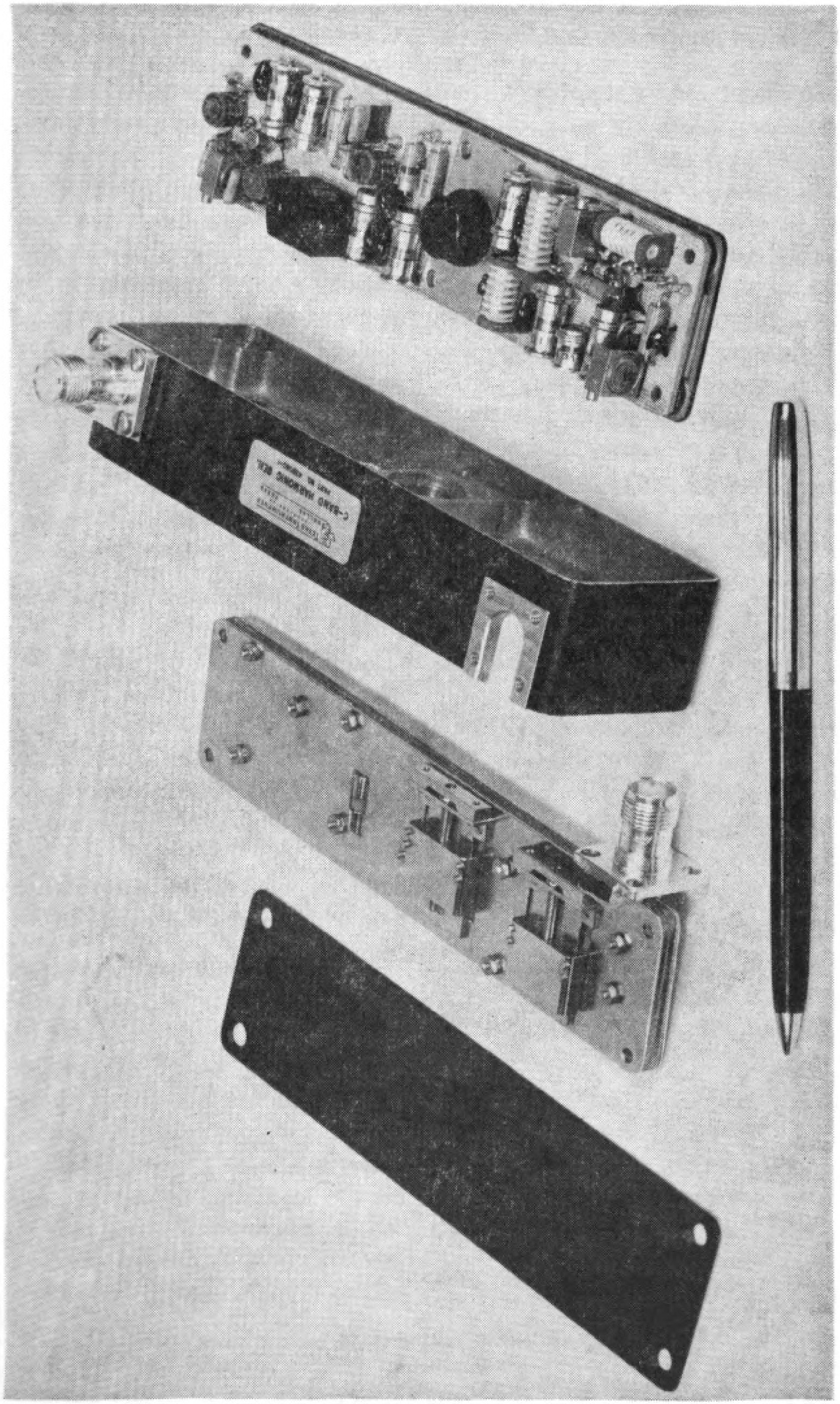

Fig. 6.6. A *C*-band harmonic generator. (Courtesy Texas Instruments, Inc.)

6.3 System Applications

In the preceding chapters we have seen that while parametric amplifiers are capable of low-noise amplification, this performance is sometimes achieved at a sacrifice in bandwidth, stability, and possibly simplicity relative to other devices. In Chapter 2 the fact was further brought out that in some situations improvement in receiver noise figure may be relatively unimportant because of the effect of a high level of external noise on a system, while in other applications modest improvement in noise figure may yield significant improvement in system performance. The system designer is therefore often faced with the question of whether the improvement in receiver sensitivity by incorporation of a parametric amplifier is really worth the trouble. In order to partly answer this question it is necessary to consider in more detail some of the applications where the use of parametric amplifiers might be considered.

Radar

Radar is perhaps the ideal application for parametric amplifiers: First, the bandwidth requirements for most radar receivers are quite modest and within the limitations of simple cavity-type amplifiers. Secondly, operating frequencies for most systems are in the spectral region where external noise is low and a low noise figure can be fully utilized. Furthermore, the usual receiver front-end, a resistive mixer, is a device with a fairly high noise figure because of the conversion loss associated with this type of mixing and, in addition, is no less complex than a well designed parametric amplifier.

The effect of the noise figure of a radar receiver on its performance may be seen by examination of Eq. (6.6) which gives the range of an ideal pulse radar in terms of its system parameters.

$$R = \sqrt[4]{\frac{P\sigma A^2\tau}{\lambda^2 k T_0 F_{op}}} \tag{6.6}$$

where P = peak transmitted power

σ = effective target area

A = effective antenna area

τ = pulse duration

λ = wavelength

F_{op} = operating noise figure.

While it may be seen that the range of such a system is a slowly-varying function of noise figure (for example, a 6 db improvement in F_{op} produces only a 40 per cent increase in range), Eq. (6.6) does show that a given reduction in noise figure can be as effective as an increase in transmitter power or antenna aperture. Often a 3 db improvement in operating noise figure may be more economical than doubling the transmitter power or increasing the antenna area by 40 per cent. This is especially true for large, long-range systems. In Fig. 2.15 is plotted operating noise figure and normalized range against noise figure with antenna temperatue as the parameter. It can be seen from this figure how significant small improvements in noise figure can be when the antenna temperature is low. For example, assuming an antenna temperature close to zero, a 1 db reduction in noise figure from 2 db to 1 db produces a 3 db improvement in operating noise figure and a 10 per cent increase in range.

The incorporation of a non-degenerate parametric amplifier or a degenerate amplifier under the conditions of single-sideband operation into a conventional pulse radar is relatively straightforward. Usually the amplifier can be installed just prior to the mixer. Three-port circulators of the "Y" or "T" variety can be used but, where space permits, the four-port circulator is usually more desirable because of the excess noise generated by the mixer which, if not directed into a matched load, often finds its way back into the amplifier due to the high standing wave ratio of the T-R device.

The application of the degenerate parametric amplifier to any system which uses both the signal and idler response is certainly of interest. Unfortunately, when both signal and idler are detected the amplifier can no longer be considered as a linear transducer. One consequence of this fact is that it is not possible in general to compare in any simple manner the minimum detectable signal of a system with and without a degenerate parametric amplifier. This is because the minimum detectable signal for a given system is not necessarily related in a simple manner to the quantity which we called sensitivity in Eq. (2.44). The quantity defined in Eq. (2.44) is that input signal power which gives rise to a unity signal-to-noise power ratio *prior to detection*. The effects of detection, signal processing, display, etc. have not been considered.*

Little theoretical and experimental work has been done to date in this area, and a full treatment of such a subject is certainly beyond the scope of this book. The remarks to be made in the remainder of this book on systems applications of degenerate amplifiers are therefore of necessity somewhat incomplete and qualitative. The experimental evidence which

* For a discussion of some of these factors, see J. L. Lawson and G. E. Uhlenbeck, "Threshold Signals," *M.I.T. Radiation Laboratory Series*, vol. 24, New York, McGraw-Hill Book Company, Inc., 1950.

is presently available, however, substantially agrees with the results to be presented.

To indicate some of the complexities which can arise in the analysis of system performance when a degenerate parametric amplifier is used, let us briefly look at two simple receivers: one using a noiseless linear amplifier, and one using a noiseless degenerate parametric amplifier. Assume that we have an input signal of the form

$$V(t) \sin (\omega_s t + \theta_s). \tag{6.7}$$

This represents an amplitude-modulated wave with an envelope of $V(t)$. For example, $V(t)$ could be a square wave, or a series of pulses at frequencies small compared to ω_s. Let us assume that we have an incoming noise wave represented by

$$n(t) = N(t) \sin (\omega_0 t + \phi(t)) \tag{6.8}$$

where $N(t)$ and $\phi(t)$ are slowly varying random functions of time. We will now examine the case of an ideal noiseless linear amplifier followed by a square-law device and output low-pass filter. The filter is assumed to pass all of the frequency components in $V(t)$ except for d-c. With a normalized amplifier gain of unity, the input to the square-law device is of course just

$$e_1(t) = V(t) \sin (\omega_s t + \theta_s) + N(t) \sin (\omega_0 t + \phi(t)). \tag{6.9}$$

The output of the square-law device is then, neglecting high-frequency components, a *voltage* (or current) equal to

$$e_2(t) = \tfrac{1}{2}[V(t)]^2 + \tfrac{1}{2}[N(t)]^2 + V(t)N(t) \cos [(\omega_0 - \omega_s)t + \phi(t) - \theta_s]. \tag{6.10}$$

The first term can be considered as signal, while the last two terms may be considered as noise.

Let us now perform the same calculation with a degenerate parametric amplifier before the square-law detector. With the same input of signal and noise as before, the normalized output at high gain will be

$$\begin{aligned} e_1(t) = {} & V(t)\{\sin (\omega_s t + \theta_s) + \sin [(2\omega_0 - \omega_s)t + \theta_p - \theta_s]\} \\ & + N(t)\{\sin (\omega_0 t + \phi(t)) + \sin (\omega_0 t + \theta_p - \phi(t))\} \end{aligned} \tag{6.11}$$

where for convenience the pump frequency has been taken to be $2\omega_0$. (This does *not* imply any special relation between noise and pump.)

Eq. (6.11) can be written in the following more convenient form:

$$\begin{aligned} e_1(t) = 2\{ & V(t) \cos [(\omega_0 - \omega_s)t + \tfrac{1}{2}\theta_p - \theta_s] + N(t) \cos [\tfrac{1}{2}\theta_p - \phi(t)]\} \\ & \cdot \sin (\omega_0 t + \tfrac{1}{2}\theta_p). \end{aligned} \tag{6.12}$$

When this voltage is squared and filtered, we get

$$
\begin{aligned}
e_2(t) = {} & \tfrac{1}{2}[V(t)]^2 \{1 + \cos [2(\omega_0 - \omega_s)t + \theta_p - 2\theta_s]\} \\
& + \tfrac{1}{2}[N(t)]^2 \{1 + \cos [\theta_p - 2\phi(t)]\} \\
& + V(t)N(t)\{\cos [(\omega_0 - \omega_s)t + \theta_p - \theta_s - \phi(t)] \\
& + \cos [(\omega_0 - \omega_s)t - \theta_s + \phi(t)]\}
\end{aligned} \tag{6.13}
$$

Let us now compare Eqs. (6.10) and (6.13), and see what they imply with regard to minimum detectable signal. For the ordinary amplifier the output signal voltage is proportional to the square of the input envelope, a result which is probably not too surprising. For the degenerate amplifier, the output is also proportional to the square of the input envelope, but is modulated at the beat frequency $2(\omega_0 - \omega_s)$. On comparing the noise, we see that where one noise term was present for the ordinary amplifier, now *two* such noise terms are present for the degenerate amplifier. These two similar noise terms are of the same power; when added in a statistical sense their total *amplitude* (rms value) is higher by the factor $\sqrt{2}$. These results can be schematically illustrated as shown in Fig. 6.7.

How, then, do these two systems compare with regard to the minimum detectable signal? There is no precise answer to this question for we have yet to consider the characteristics of the indicating instrument or display device. Let us assume for this idealized system that the display device gives an indication corresponding to average amplitude. For the ordinary amplifier the noise level could then be defined as proportional to N_1, with the signal level defined as S_1. For the degenerate parametric amplifier, the noise level would then be proportional to $\sqrt{2}\, N_1$, with the *average* signal level proportional to S_1. In this hypothetical system, then, the degenerate parametric amplifier would have to have a double-sideband operating noise temperature lower than that for an ordinary amplifier by $\sqrt{2}$ in order to have equal minimum detectable signal levels.

The above example is intended only as a qualitative illustration, for actual systems probably cannot be represented in such a simple manner. (There is, however, some experimental evidence which is roughly in agreement with the results presented above.*)

It appears that the foregoing system does not make optimum use of the peculiarities of the degenerate parametric amplifier. For example, the beat frequency component was averaged out and not used in any

* See R. Adler, "Electron-Beam Parametric Amplifiers with Synchronous Pumping," *Proc. Symposium on the Application of Low Noise Receivers to Radar and Allied Equipment*, vol. 3, pp. 177–197, November 1960.

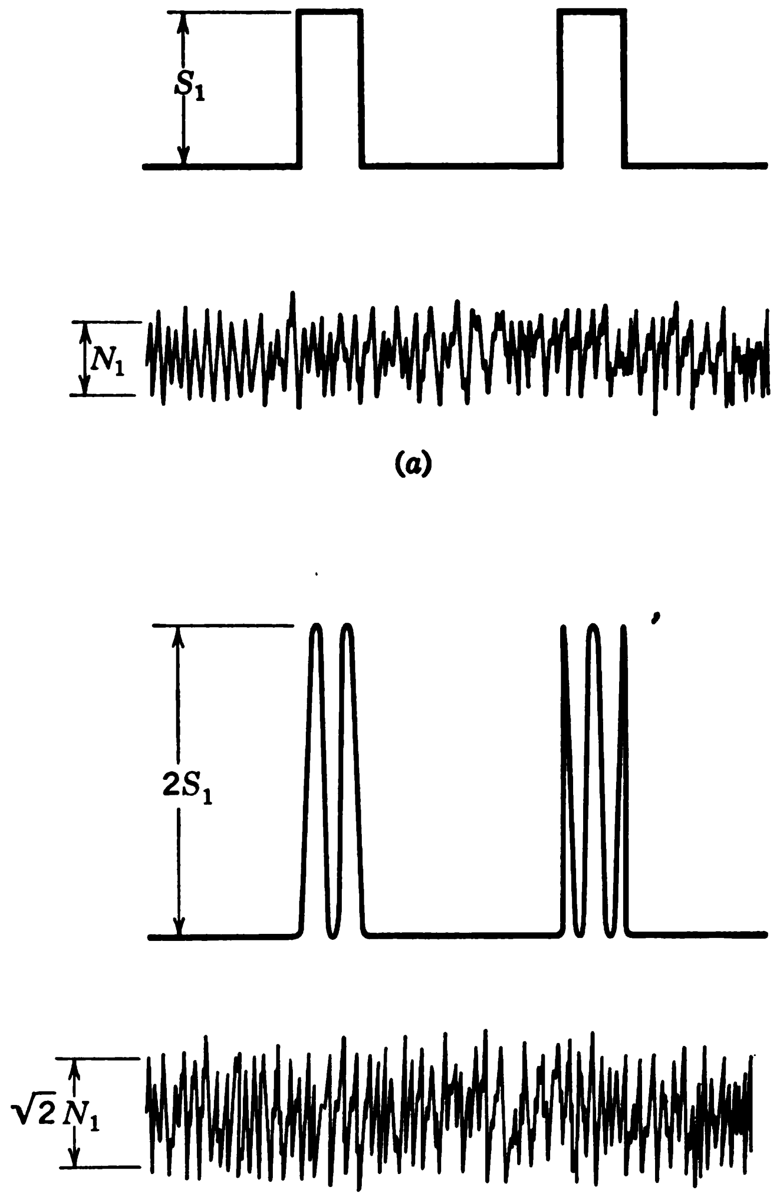

(b)

Fig. 6.7. (a) Representation of signal and noise output for a square-law detector. (b) Representation of signal and noise output for a degenerate parametric amplifier and square-law detector.

way. One modification could be the use of a linear envelope detector instead of a square-law detector. At high input signal-to-noise ratio (say around 10 db) a linear envelope detector can give a somewhat better output signal-to-noise ratio than a square-law detector, and hence might be more sensitive in some applications using degenerate amplifiers. On the other hand, near unity input signal-to-noise ratio or below, the performance of the linear envelope detector closely approaches that of the square-law detector.

There may well exist other detection schemes which use the degenerate amplifier more effectively. One such method which has been used is called *synchronous pumping*.* The so-called synchronously-pumped degenerate parametric amplifier may be useful in certain types of MTI and pulse doppler radars. In order to understand the principles of operation consider the circuit pictured in Fig. 6.8. The essential elements are a degenerate parametric amplifier followed by a synchronous

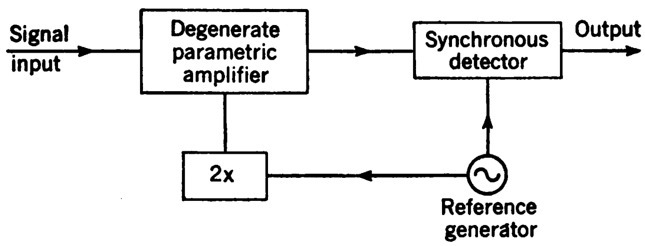

Fig. 6.8. Circuit arrangement for synchronous pumping.

detector. The reference signal for the synchronous detector, which is coherent with the transmitter frequency, is doubled and used to pump the amplifier. Now consider what happens if a returning pulse is shifted in frequency due to the doppler effect by an amount Δf. The output of the degenerate amplifier will consist of the original amplified return and its image at the idler frequency. For high gain these symmetrical outputs, sometimes called coherent sidebands, are equal in magnitude. In addition to the amplified signal and idler outputs the amplifier will have a noise power output due to the finite antenna noise temperature, and internally generated noise due to losses within the amplifier. As was discussed in Section 3.3, the noise is composed of symmetrical components about $\omega_p/2$. This follows from the fact that at at any two symmetrical frequencies about $\omega_p/2$ the noise is actually made up of two equal and identical components, one converted and another unconverted. Through the action of the synchronous detector these components, both signal and noise, are folded about $\omega_p/2$ and added coherently. We can see this by taking Eq. (6.12) and multiplying by sin $(\omega_0 t + \frac{1}{2}\theta_p)$. The low-frequency component of signal is seen to be at the doppler frequency.

If one in fact compares the synchronously-pumped degenerate para-

* R. Adler, *loc. cit.*

metric amplifier with a *similar system* using a conventional amplifier, and if we assume that both amplifiers are perfect and introduce no noise themselves, then it appears that the minimum detectable signal will be comparable for the two cases.* When the parametric amplifier is used, however, the information as to whether the target is closing or opening is lost. This may not be of interest in an MTI radar but in a pulse doppler system with a zero frequency i-f it may be necessary to retain this information.

like mixer

image cancellation

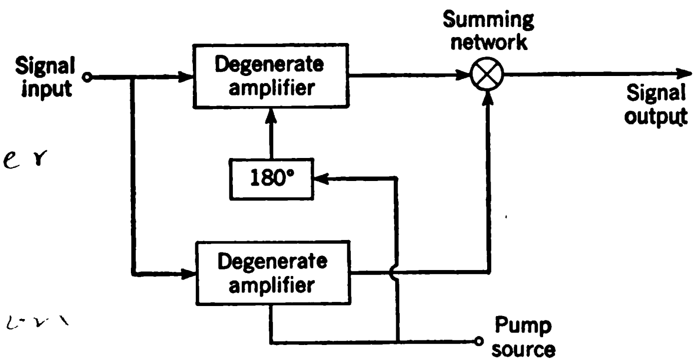

Fig. 6.9. Idler cancellation scheme.

Another scheme for using the degenerate parametric amplifier which eliminates the sometimes bothersome idler response and enables the complete bandwidth of the amplifier to be used is illustrated in Fig. 6.9. Here two identical amplifiers are used. The pump for one of the amplifiers is shifted 180° from the pump supplying the second. In practice the amplifiers might be located at the colinear arms of a "Magic Tee" and the signal introduced into the shunt arm and the pump into the series arm. If the outputs at the signal frequency are summed they will add in phase while the idler component will cancel since they are 180° out of phase. In principle the noise properties are not greatly altered; however since the idler is no longer present, double-sideband operation is not possible.

Radiometry

The detection of microwave radiation of either thermal or nonthermal origin is important in both radio astronomy and in certain passive surveillance systems. In radio astronomy two types of observations are commonly made. The first is the observation of the continuum discussed in Chapter 2 which is of galactic origin. This radiation does not vary

* R. Adler, *loc. cit.*

rapidly with frequency and wideband receivers are usually used in order to reduce noise fluctuations. The second type of measurement is the observation of line sources such as arise from the hyperfine transition of neutral hydrogen in the ground state at 1420 mc.

For the observation of any continuous source the minimum detectable temperature has been given for a comparison radiometer by Drake and Ewen[32] in terms of the noise figure, bandwidth, and gain stability of the receiver. In this type of radiometer, the receiver is switched alternately between the antenna and a matched load at a known temperature. The minimum detectable temperature is given by

$$\overline{\Delta T} = K\left[\frac{T_{op}}{(B\tau)^{1/2}} + \left(\frac{\overline{G(t) - G_o}}{G_o}\right)(T_a - T_l)\right] \tag{6.14}$$

where K is a constant having a value near unity

T_{op} = operating noise temperature

B = bandwidth

τ = integration time constant

G_o = average amplifier gain

$G(t)$ = instantaneous gain

T_a = antenna temperature

T_l = temperature of comparison load.

It is apparent from the first term of Eq. (6.14) that the minimum detectable signal is directly proportional to the operating noise temperature and inversely proportional to the square root of the r-f bandwidth. Although a given improvement in bandwidth is not as significant as an equivalent improvement in noise figure, it must be remembered that with presently attainable parametric amplifiers noise figures are approaching the physical limitations of the device, while the gain bandwidth products usually achieved are considerably smaller than theoretically possible. For example, the theory for single-tuned circuits shows that the gain-bandwidth product of a degenerate amplifier has an upper bound approximately equal to γ. If we assume a reasonable value of γ to be 0.25, we find that

$$g^{1/2}b \leq 25\% \tag{6.15}$$

where g = power gain

b = percentage bandwidth.

Thus, for a power gain of 10 db we would have $b \leq 8$ per cent. This value of b is substantially higher than the usual results for single-tuned amplifiers. The theory for multiple-tuned amplifiers predicts considerably larger gain-bandwidth products but again practical circuit difficulties, especially at the higher microwave frequencies, can severely limit actual performance.

Another approach to the problem of improving bandwidth is to cascade or stagger-tune a number of similar amplifiers. Each amplifier may be operated at a relatively low gain, say 6 db, and the overall bandwidth of the combination may be calculated from computed or measured gain curves for the specific amplifier and a knowledge of the characteristics of the circulators used to isolate the amplifiers.

When the signal input to a radiometer is broadband noise, it seems reasonable that the proper noise temperature to use in computing sensitivity is that noise temperature experimentally obtained with a broadband noise source, which for the degenerate amplifier is the double-sideband effective input noise temperature. Assuming this to be so, we can see that a degenerate amplifier would be the logical choice for this application since the double-sideband operating noise temperature of the degenerate amplifier is lower than the operating noise temperature of the optimum non-degenerate amplifier or up-converter. From table 6.1 we have:

$$(T_{op})_{\text{d}} = T_d\left[\frac{1}{\gamma Q} + \frac{1}{(\gamma Q)^2}\right] + T_a \tag{6.16}$$

$$(T_{op})_{\text{n.d.}} = 2T_d\left[\frac{1}{\gamma Q} + \frac{1}{(\gamma Q)^2}\right] + T_a. \tag{6.17}$$

In addition to the advantage over the non-degenerate amplifier of improved sensitivity, the degenerate amplifier does not put as severe demands on the pump frequency and power, is easier to tune, and, since the same resonance is used for both the signal and idler, broadbanding through the use of multiple-tuned coupling networks is more easily achieved.

As an example of what might be theoretically achieved in a particular situation, let us examine the case where the operating frequency is 15 Gc and a diode having a cutoff at operating bias of 150 Gc is available. The minimum theoretical noise figure assuming the diode is operated near room temperature and $\gamma = 0.25$ is

$$\begin{aligned} F &= 1 + \left[\frac{1}{\gamma Q} + \frac{1}{(\gamma Q)^2}\right] \\ &= 1 + \left[\frac{1}{2.5} + \frac{1}{(2.5)^2}\right] = 1.56 \approx 2\ db. \end{aligned} \tag{6.18}$$

If we are able to refrigerate the diode to the temperature of boiling liquid nitrogen and if the mobility of the material remains approximately constant, the noise figure becomes

$$F = 1 + \frac{77}{290}\left[\frac{1}{2.5} + \frac{1}{(2.5)^2}\right] = 1.15 \approx 0.6\ db \qquad (6.19)$$

or $T_e = 45°\mathrm{K}$.

As far as noise figure and, to a lesser degree, bandwidth are concerned the parametric amplifier compares quite well with other potential preamplifiers such as the traveling-wave tube and the traveling-wave maser.

Since its operation depends on the existence of an effective negative resistance at the signal frequency, the negative-resistance amplifier is susceptable to gain instability. In any but the most carefully designed and regulated systems, gain variations may limit its usefulness for this application. Most radiometer systems depend for their calibration on a comparison source or load at a known temperature. In operation, the radiometer is switched between the antenna and the comparison source at a rate depending on the integration time. Since the antenna and the comparison source may appear as different source impedances at the amplifier, the gain of the amplifier may change. Unless this variation can be kept below a certain level, depending on the application and other system parameters, the amplifier cannot be used. It is important therefore that considerable attention be given to matching the antenna and comparison source to the amplifier over the operating frequency of the receiver and providing maximum isolation between the terminals of the switch and the input to the amplifier. It may be necessary to use both a ferrite isolator and circulator at the input to adequately minimize impedance variations. The effects of residual impedance variations may be minimized by operating the amplifier at low gain if possible, and by using several amplifiers in cascade. The effect of pump power variations on the gain may be reduced by providing amplitude regulation to the pump source and self-bias for the diodes.

Radiometric techniques are not only used for observations of continuous sources; since the discovery of discrete line radiation from outside the galaxy, narrow-band observations have become an important tool to radio astronomers.

The frequency of interest is 1420 mc, which arises from the hyperfine transition of neutral hydrogen in the ground state. The desired information is usually a detailed measurement of intensity as a function of frequency after subtracting the continuum. Since integration times of several minutes are not uncommon for this type of measurement, long term gain stability becomes important for good temperature resolution. Although only the degenerate parametric amplifier has been considered up to now in this discussion, the up-converter has a number of advantages which make it more attractive for operation around 1400 mc. Recall that the minimum theoretical noise figure of an up-converter in terms of the diode figure of merit γQ is given by

$$F = 1 + 2\frac{T_d}{T_0}\left[\frac{1}{\gamma Q} + \frac{1}{(\gamma Q)^2}\right]$$

or

$$T_e = T_0(F - 1) = 2T_d\left[\frac{1}{\gamma Q} + \frac{1}{(\gamma Q)^2}\right]. \tag{6.20}$$

If we assume $\gamma = 0.25$ and a cutoff frequency at operating bias of 140 Gc the minimum first stage noise figure for unrefrigerated operation becomes

$$F = 1 + 2\left[\frac{1}{25} + \frac{1}{25^2}\right] = 1.08 \tag{6.21}$$

or $T_e = 23°$K.

If we assume a pump frequency of 70 Gc the gain of the first stage will be about 17 db. If the up-converter is followed by a mixer using a a 1N2792 crystal for example, a second stage noise figure as low as 11 db might be expected. The overall system noise figure becomes

$$F_{12} = F_1 + \frac{F_2 - 1}{G_1} = 1.08 + \frac{12.6 - 1}{50} = 1.3 \tag{6.22}$$

or $T_e = 87°$K. An overall effective input noise temperature this low is adequate for most hydrogen line observations. As a consequence of the net positive resistance transformed into the signal circuit, the gain of the up-converter is highly stable with respect to changes in source impedance caused by switching between the antenna and the comparison source. Furthermore, it is a two-port unilateral amplifier and does not require a circulator for its operation.

Still another scheme which has been proposed to overcome the problem of gain instability is to use an up-converter operating at a relatively low gain followed by a conventional degenerate parametric amplifier operated at some convenient frequency where a reasonably low noise figure can be achieved, as for example, at X-band. Most of the gain is provided by the degenerate amplifier, and the up-converter acts as an isolator with gain between the source and the amplifier. Such a hybrid scheme should provide a low overall noise figure, adequate gain, and low sensitivity to changes in source impedances.

Radiometric systems have also found important application in passive surveillance. One such application is in passive airborne mapping

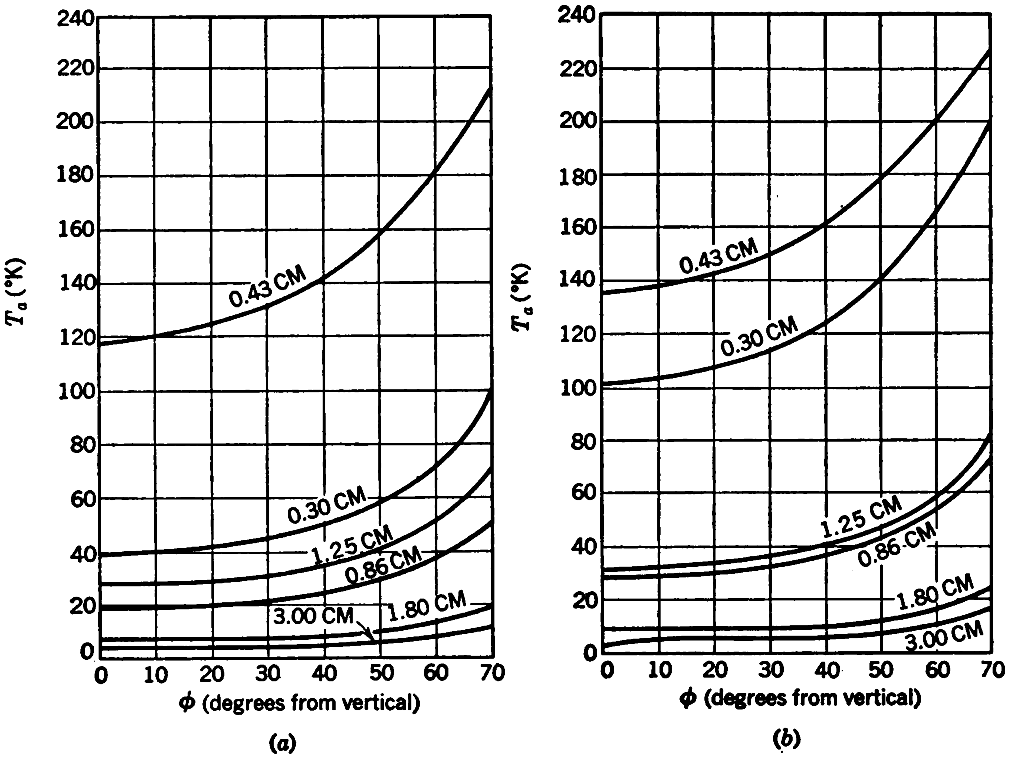

Fig. 6.10. Atmospheric contribution to the antenna temperature of an airborne antenna, as a function of wavelength and angle from the vertical (after Weger).

systems. There are several points of difference in such a system and a radiometer used in radio astronomy. Since resolution is often of primary importance and high speed aircraft and space vehicles are generally limited to small antennas, operation in the millimeter region is often desirable. However, sensitivity may be sacrificed due to atmospheric absorption and scattering. Figures 6.10(a) and 6.10(b) illustrate this point.[146] They show the calculated antenna temperature contributions [second term of Eq. (2.42)] due to the intervening atmosphere between sea level and 32,000 feet as a function of wavelength and angle from the vertical. The conditions for Fig. 6.10(a) are a clear sky, 1% absolute humidity at sea level, and a surface temperature of 290°K and, for Fig. 6.10(b) a moderate cloud cover between 3000 and 6000 feet, 1% absolute humidity and a surface temperature of 290°K. The total antenna temperature may be found by adding to this contribution the apparent surface temperature, reduced by the atmospheric loss between the surface and the antenna. The apparent surface temperature T_g consists of a reflected and an emitted contribution given by

$$T_g = \epsilon T_a + \rho T_s \tag{6.23}$$

where ϵ and ρ are the surface emissivity and reflectivity respectively and are both functions of angle, polarization of the antenna, surface composition, and roughness as well as wavelength. T_a is the actual thermodynamic temperature of the surface and T_s is the sky temperature. Relatively rough surfaces such as concrete, asphalt, or grass may differ in apparent temperature by up to ten degrees, while water or polished metal may differ in apparent temperature by 100 degrees or more. Since the signal level under these conditions is relatively large, high scanning rates and correspondingly shorter integration times are characteristics of such systems. With presently achievable noise figures and bandwidths, parametric amplifiers should be able to compete quite well with other thermal sensors and will, in general, be affected very little by atmospheric conditions.

Communications

It should be apparent that the incorporation of a parametric amplifier into any communication equipment where sensitivity is of importance can in general improve the performance. However, it should be pointed out that in addition to providing low noise amplification, the parametric amplifier may be used to perform other useful circuit functions such as frequency shifting, inversion, filtering, and limiting as well.

The Phase-coherent Degenerate Amplifier. It was shown in Section 3.3 that a degenerate amplifier has phase-dependent gain for the special case of signal at exactly half the pump frequency. Furthermore, it was shown that under conditions of high gain, the maximum gain was 6 db greater than that for a signal which is not at half-pump frequency. This interesting property could cause one to speculate whether or not it would be possible to use this property to advantage in a communication system to increase sensitivity. We might reason that if we could somehow cause the pump phase to track the incoming signal phase, the signal-to-noise ratio could be improved as much as 6 db over ordinary degenerate operation since non-coherent noise would receive 6 db less gain than the signal. One problem in such a system would be how to make the pump track the signal. We can imagine three ways in which this could be accomplished:

1. By having signal and pump derived from the same source,
2. By using some of the signal for a pump,
3. By tracking the incoming signal with a servo loop.

As an example of the first possibility, we could consider a simple radar designed to detect stationary targets. Such a hypothetical system could have a CW reference oscillator to drive both a transmitter and a doubler for use as the pump for the degenerate parametric amplifier. A target

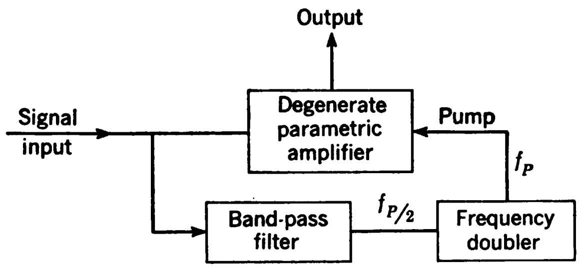

Fig. 6.11. A hypothetical method of phase-locking to an AM signal.

echo of the proper phase would then receive the additional 6 db gain, while an echo of the incorrect phase would be attenuated.

As an example of the second possibility, let us consider a receiving system for double-sideband amplitude modulation. Such a signal possesses a frequency spectrum which is symmetric about the carrier in frequency, amplitude, and phase. If we can lock to the carrier of such a signal so as to obtain our 6 db increase in gain, we will also increase the gain of each sideband by 6 db. This will occur since we would be putting signal in at both the signal frequency and its image (the idler). Each signal generates its own image which then adds coherently to the original signal, doubling the amplitude of each sideband and giving 6 db more gain.

A possible scheme of this type is shown in Fig. 6.11. The signal is fed through a narrow bandpass filter which passes only the carrier. This signal is then amplified, doubled, and used as a pump to drive the parametric amplifier. In theory, it appears that such an amplifier would have the same sensitivity as an ordinary amplifier using synchronous detection when the double-sideband noise figure of the degenerate parametric amplifier equals the noise figure of the ordinary amplifier. In practice, however, such a scheme may not be too attractive, for the incoming signal-to-noise ratio may have to be high to avoid the effects of noise pumping the amplifier.

An example of the third possible method of tracking the signal phase is the so-called *phase-lock* system, shown schematically in Fig. 6.12. This system uses a locally-generated signal which is compared to the incoming signal by a phase detector. Any phase difference produces an error signal

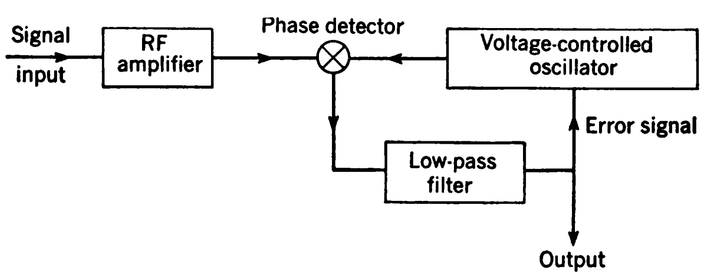

Fig. 6.12. Schematic diagram of a phase-lock system.

which is used to correct the phase of the locally-generated signal to more closely match the incoming signal. The phase error for good locking will in practice be on the order of 10°.

Let us briefly investigate the operation of a phase-lock system in order to see how a degenerate parametric amplifier could be used. For the case of an ordinary amplifier of gain g, the input to the phase detector can be written as

$$e_1(t) = g \sin [\omega_s t + \theta_s(t)] + g \sum_i \alpha_i \sin [(\omega_s + \omega_i)t + \theta_i]. \tag{6.24}$$

The first term is the signal with time-varying phase $\theta_s(t)$, while the second term is a representation of the incoming noise. We will represent the phase detector as a voltage multiplier and low-pass filter. The reference signal is assumed to be of the form

$$e_2(t) = \cos [\omega_s t + \phi(t)]. \tag{6.25}$$

The low-frequency component of the product $e_1(t)e_2(t)$ is

$$e_3(t) = \tfrac{1}{2}g \sin [\theta_s(t) - \phi(t)] + \tfrac{1}{2}g \sum_i \alpha_i \sin [\omega_i t + \theta_i - \phi(t)]. \tag{6.26}$$

This voltage is then used to control the frequency of the voltage-controlled oscillator so that the phase difference $\theta_s(t) - \phi(t)$ is kept small.

Let us now place a degenerate parametric amplifier in the system as shown in Fig. 6.13. With the same input signal as before, the output of

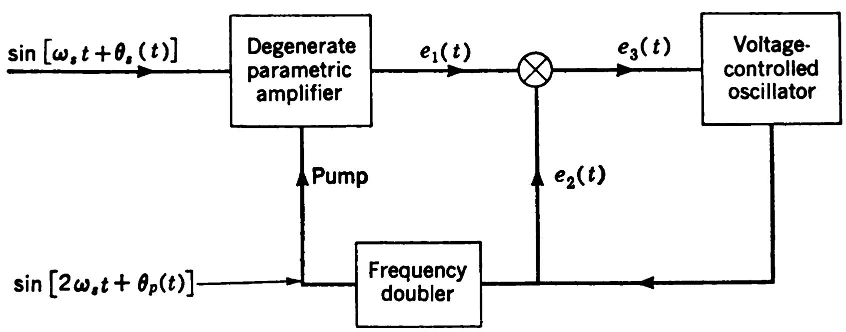

Fig. 6.13. Schematic diagram of a phase-lock loop, using a degenerate parametric amplifier.

the degenerate amplifier will be

$$e_1(t) = \frac{1}{(1+\beta)(1-\beta)} \Big[\sin [\omega_s t + \theta_s(t)] + \beta \sin [\omega_s t + \theta_p(t) - \theta_s(t)]$$
$$+ \sum_i \{\alpha_i \sin [(\omega_s + \omega_i)t + \theta_i] + \beta\alpha_i \sin [(\omega_s - \omega_i)t + \theta_p(t) - \theta_i]\}\Big] \tag{6.27}$$

This result follows from Eq. (3.137). Let us assume that the multiplying voltage is $\cos[\omega_s t + \frac{1}{2}\theta_p(t)]$. The low-frequency component of the multiplier output will then be

$$e_3(t) = \frac{1-\beta}{2(1+\beta)(1-\beta)}\,[\{\sin\theta_s(t) - \tfrac{1}{2}\theta_p(t)] + \sum_i \alpha_i \sin[\omega_i t + \theta_i - \tfrac{1}{2}\theta_p(t)]\}. \tag{6.28}$$

On comparing Eq. (6.26) and (6.28), we see that they are of identical form. For the degenerate amplifier case, however, the effective gain is $1/1 + \beta$, which is a loss since $\beta \approx 1$. The implication of this result is that noise contributions from any amplifiers between the degenerate parametric amplifier and phase detector will be significant, resulting in system performance described by the noise figure of the succeeding stages after the parametric amplifier. We can modify this situation by changing the relative phase between the pump and the reference voltage for the phase detector. Let

$$e_2(t) = \sin[\omega_s t + \tfrac{1}{2}\theta_p(t)]. \tag{6.29}$$

The output of the multiplier is now

$$e_3(t) = \frac{1+\beta}{2(1+\beta)(1-\beta)}\,\{\cos[\theta_s(t) - \tfrac{1}{2}\theta_p(t)] + \sum_i \alpha_i \cos[\omega_i t + \theta_i - \tfrac{1}{2}\theta_p(t)]\}. \tag{6.30}$$

This time the effective gain $1/1 - \beta$, which can be very high. Since for this phase relation between reference and pump the output is a cosine function of the difference between the signal phase and pump phase, the feedback loop will introduce an additional constant phase shift of $\pi/2$ as compared to the ordinary phase-lock loop. Such a constant phase offset is probably of no consequence in actual system performance since the information is contained in the time-varying portion of the phase.

In summary, then, it appears that a degenerate parametric amplifier may be compatible with a phase-lock system and will have sensitivity proportional to the double-sideband operating noise temperature.

Space Communications

A chapter on applications of parametric amplifiers would not be complete unless some mention were made of the very important application of these devices in space communications. Parametric amplifiers have already significantly increased the range of several receiving stations used to track the first American deep space probes. The magnitude of the problem of maintaining contact with such vehicles over periods ranging over months and perhaps even years and distances of tens and eventually hundreds of millions of miles can best be appreciated by examination of the range equation

$$R = \sqrt{\frac{P_t A_t A_r}{\lambda^2 k T_o B F_{op}}} \tag{6.31}$$

P_t = transmitted power

A_t = effective area of transmitting antenna

A_r = effective area of receiving antenna

λ = wavelength

B = bandwidth

F_{op} = operating noise figure.

A number of factors affect the optimum transmitter frequency. Some of these factors are: the conversion efficiency between primary power and the transmitted frequency, natural and man-made noise levels, atmospheric absorption, and capabilities of existing tracking installations. Since for power levels above 10 watts the efficiency of conventional transmitters is nearly constant with frequency, the term of importance for a given antenna area and information bandwidth in Eq. (6.31) is the product $\lambda^2 F_{op}$. For a given diode and under conditions of minimum noise figure F_{op} may be written

$$F_{op} \propto \left[\frac{2T_d}{\gamma Q} + T_a(f)\right] \tag{6.32}$$

so that

$$\lambda^2 F_{op} \propto \frac{1}{f^2}\left[\frac{4\pi T_d RCf}{\gamma} + T_a(f)\right]. \tag{6.33}$$

If one further assumes that the diode has an RC product equal to 10^{-12} psec and a $\gamma = 0.25$ this function will be found to have a minimum in the X-band region for a typical variation of T_a with frequency.

In extremely long range telemetry, one more factor of the range equation should be considered. This is the bandwidth B. Even though a typical space vehicle is traveling quite fast, the elapsed time between significant events may be quite slow so that the information bandwidth may be quite low. Through the use of phase-locked loops, bandwidths of the order of a few cycles per second may be maintained.

APPENDIX

The Manley-Rowe Power Relations

The circuit model used by Manley and Rowe in their original derivation of power flow relations for nonlinear reactances is shown in Fig. A.1.

Here we have two voltage generators at frequencies f_1 and f_2 together with associated series resistances and bandpass filters, placed across a nonlinear capacitor. These filters are designed to reject power at all frequencies other than their respective signal frequencies. In addition to the two signal generators, an infinite array of load resistances and bandpass filters are also connected to the nonlinear capacitor. These filters are tuned to the various sum and difference frequencies which will arise because of the nonlinear reactance. The sign convention will be used that power flowing *into* the nonlinear capacitance is positive (*e.g.*, the power coming from the two signal generators), while power flowing *from* the capacitance (*e.g.*, the power flowing into the load resistances) will be negative in sign.

As stated in Eq. (1.1), a capacitive reactance may be defined as a circuit element for which a functional relation between charge and voltage can be written.

$$q = f(v). \tag{A.1}$$

The inverse function will do just as well in defining capacitance; that is, we may also write

$$v = h(q). \tag{A.2}$$

The only restriction placed on the function $h(q)$ is that it be single-valued, *i.e.*, free from hysteresis.

It is next of interest to investigate the time-dependence of the charge q in the circuit described by Fig. A.1. With impressed frequencies of f_1 and f_2, there will certainly be variations in charge across the nonlinear capacitor at frequencies f_1 and f_2. In addition, because of the mixing action in the nonlinear capacitor, there will be generated charge variations at all the possible sum and difference frequencies $f_{mn} = mf_1 + nf_2$, where m and n take on all integral values.

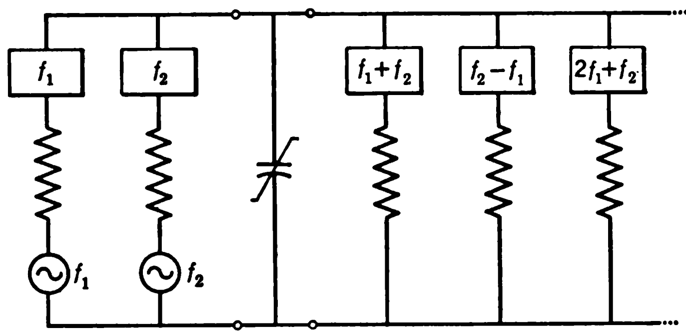

Figure A.1

As in usual circuit analysis, it is convenient here to use the exponential representation of sinusoids so that differentiation with respect to time reduces to multiplication by $j\omega$. However, since we will here be interested in products involving current and voltage, we must exercise care in dealing with complex quantities. It will be most convenient to use only real quantities, expressing them in complex form. For example,

$$A \cos (\omega t) = \frac{A}{2} [e^{j\omega t} + e^{-j\omega t}]. \tag{A.3}$$

Using this artifice, we can express the total charge flowing into the nonlinear capacitor in the following form:

$$q = \sum_{m=-\infty}^{\infty} \sum_{n=-\infty}^{\infty} Q_{m,n} e^{j(m\omega_1 t + n\omega_2 t)} \tag{A.4}$$

$$\omega_1 = 2\pi f_1$$

$$\omega_2 = 2\pi f_2.$$

For q to be real, we require only that

$$Q_{m,n} = Q^*_{-m,-n} \tag{A.5}$$

We may immediately find the total current i flowing through the non-linear capacitor by taking the total derivative of (A.4) with respect to time.

$$i = \frac{dq}{dt} = \sum_{m=-\infty}^{\infty} \sum_{n=-\infty}^{\infty} j(m\omega_1 + n\omega_2) Q_{m,n} e^{j(m\omega_1 + n\omega_2)t} \qquad \text{(A.6)}$$

$$= \sum_{m=-\infty}^{\infty} \sum_{n=-\infty}^{\infty} I_{m,n} e^{j(m\omega_1 + n\omega_2)t}$$

where $j(m\omega_1 + n\omega_2)Q_{m,n} = I_{m,n}$, and $I_{m,n} = I^*_{-m,-n}$.

From (A.2) we see that the voltage may be expressed as a function of q, and consequently it may also be expressed as a function of $(m\omega_1 t + n\omega_2 t)$. That is, we may also represent v in a double Fourier series, just as we did for q.

$$v = \sum_{m=-\infty}^{\infty} \sum_{n=-\infty}^{\infty} V_{m,n} e^{j(m\omega_1 t + n\omega_2 t)} \qquad \text{(A.7)}$$

where $V_{m,n} = V^*_{-m,-n}$.

The Fourier coefficients can be expressed by the usual integral expression

$$V_{m,n} = \frac{1}{4\pi^2} \int_0^{2\pi} \int_0^{2\pi} v e^{-j(m\omega_1 t + n\omega_2 t)} \, d(\omega_1 t) \, d(\omega_2 t). \qquad \text{(A.8)}$$

At this point some mathematical sleight-of-hand is necessary. We are after an expression involving power; therefore, we need to form products involving $I_{m,n}$ and $V_{m,n}$. As a first step toward this goal, let us multiply (A.8) by $jmQ_{m,n}{}^*$ and sum over m and n.

$$\sum_{m=-\infty}^{\infty} \sum_{n=-\infty}^{\infty} jmQ_{m,n}{}^* V_{m,n} = \sum_{m=-\infty}^{\infty} \sum_{n=-\infty}^{\infty} jmQ_{m,n}{}^*$$

$$\cdot \frac{1}{4\pi^2} \int_0^{2\pi} \int_0^{2\pi} v e^{-j(m\omega_1 t + n\omega_2 t)} \, d(\omega_1 t) \, d(\omega_2 t). \qquad \text{(A.9)}$$

If we interchange the order of summation and integration, we obtain

$$\sum_{m=-\infty}^{\infty} \sum_{n=-\infty}^{\infty} jmQ_{m,n}{}^* V_{m,n}$$

$$= \frac{1}{4\pi^2} \int_0^{2\pi} \int_0^{2\pi} v \sum_{m=-\infty}^{\infty} \sum_{n=-\infty}^{\infty} jmQ_{m,n}{}^* e^{-j(m\omega_1 t + n\omega_2 t)} \, d(\omega_1 t) \, d(\omega_2 t). \qquad \text{(A.10)}$$

The double sum inside the integral is reminiscent of the expression for charge, Eq. (A.4). In fact we obtain this sum by taking $\partial q / \partial(\omega_1 t)$.

$$\frac{\partial q}{\partial(\omega_1 t)} = \sum_{m=-\infty}^{\infty} \sum_{n=-\infty}^{\infty} jmQ_{m,n} e^{j(m\omega_1 t + n\omega_2 t)}. \qquad \text{(A.11)}$$

Since q is real, we may take the complex conjugate of (A.11) without changing its value.

$$\frac{\partial q}{\partial(\omega_1 t)} = -\sum_{m=-\infty}^{\infty} \sum_{n=-\infty}^{\infty} jmQ_{m,n}{}^* e^{-j(m\omega_1 t + n\omega_2 t)}. \tag{A.12}$$

Similarly, the left side of (A.10) is strongly reminiscent of products of current and voltage. Remembering that

$$I_{m,n} = j(m\omega_1 + n\omega_2)Q_{m,n}$$

we may express the left side of (A.10) as

$$\sum_{m=-\infty}^{\infty} \sum_{n=-\infty}^{\infty} jmQ_{m,n}{}^* V_{m,n} = -\sum_{m=-\infty}^{\infty} \sum_{n=-\infty}^{\infty} \frac{mV_{m,n}I_{m,n}{}^*}{m\omega_1 + n\omega_2}. \tag{A.13}$$

Hence we may re-write Eq. (A. 10) in the following form:

$$\sum_{m=-\infty}^{\infty} \sum_{n=-\infty}^{\infty} \frac{mV_{m,n}I_{m,n}{}^*}{mf_1 + nf_2} = \frac{1}{2\pi} \int_0^{2\pi} \int_0^{2\pi} v \frac{\partial q}{\partial(\omega_1 t)} \, d(\omega_1 t) \, d(\omega_2 t). \tag{A.14}$$

Now

$$\frac{\partial q}{\partial(\omega_1 t)} = \left.\frac{dq}{d(w_1 t)}\right|_{\omega_2 t = \text{constant}}. \tag{A.15}$$

Hence we can write the integral over $d(\omega_1 t)$ as

$$\int_{\omega_1 t=0}^{2\pi} v \frac{\partial q}{\partial(\omega_1 t)} \, d(\omega_1 t) = \int_{\omega_1 t=0}^{2\pi} v \frac{dq}{d(\omega_1 t)} \, d(\omega_1 t) = \int_{q(\omega_1 t=0)}^{q(\omega_1 t=2\pi)} v(q) \, dq \tag{A.16}$$

with $\omega_2 t$ held constant. Therefore (A.14) can be simplified even further to obtain

$$\sum_{m=-\infty}^{\infty} \sum_{n=-\infty}^{\infty} \frac{mV_{m,n}I_{m,n}{}^*}{mf_1 + nf_2} = \frac{1}{2\pi} \int_{\omega_2 t=0}^{2\pi} d(\omega_2 t) \int_{q(0,\omega_2 t)}^{q(2\pi,\omega_2 t)} v(q) \, dq. \tag{A.17}$$

With the mathematical manipulation now almost complete, it is time to stop and consider how the products of current and voltage as expressed by (A.17) are related to the power flow in the nonlinear capacitor. We know from circuit theory that if we express current and voltage in exponential form, we can obtain the average power flow by taking the real part of the product of VI^*. Since Eq. (A.17) consists of such products the real portion of (A.17) will give us the desired information regarding power flow in a nonlinear reactance. Let us break the summation over

m into two parts, one a summation form 0 to ∞, and one a summation from 0 to $-\infty$.

$$\sum_{m=-\infty}^{\infty} \sum_{n=-\infty}^{\infty} \frac{mV_{m,n}I_{m,n}{}^*}{mf_1 + nf_2}$$

$$= \sum_{m=0}^{\infty} \sum_{n=-\infty}^{\infty} \frac{mV_{m,n}I_{m,n}{}^*}{mf_1 + nf_2} + \sum_{m=0}^{-\infty} \sum_{n=-\infty}^{\infty} \frac{mV_{m,n}I_{m,n}{}^*}{mf_1 + nf_2}. \quad \text{(A.18)}$$

Recalling that

$$I_{m,n} = I^*_{-m,-n} \quad \text{(A.6)}$$

$$V_{m,n} = V^*_{-m,-n} \quad \text{(A.7)}$$

we can effectively change the summation over the negative values of m into a summation over the positive values by simply replacing $V_{m,n}$ and $I^*_{m,n}$ by their complex conjugates. Hence (A.18) becomes

$$\sum_{m=-\infty}^{\infty} \sum_{n=-\infty}^{\infty} \frac{mV_{m,n}I_{m,n}{}^*}{mf_1 + nf_2} = \sum_{m=0}^{\infty} \sum_{n=-\infty}^{\infty} \frac{m[V_{m,n}I_{m,n}{}^* + V_{m,n}{}^*I_{m,n}]}{mf_1 + nf_2}. \quad \text{(A.19)}$$

The right side of (A.19) is seen to consist of a quantity plus its complex conjugate, which is equal to twice the real part of that quantity. So (A.19) can be written as

$$\sum_{m=-\infty}^{\infty} \sum_{n=-\infty}^{\infty} \frac{mV_{m,n}I_{m,n}{}^*}{mf_1 + nf_2} = \sum_{m=0}^{\infty} \sum_{n=-\infty}^{\infty} \frac{m2Re[V_{m,n}I_{m,n}{}^*]}{mf_1 + nf_2} \quad \text{(A.20)}$$

$$= \sum_{m=0}^{\infty} \sum_{n=-\infty}^{\infty} \frac{mP_{m,n}}{mf_1 + nf_2}$$

where $P_{m,n}$ is the power flowing into the nonlinear capacitor at frequency $mf_1 + nf_2$. (Here the magnitudes of V and I have been defined so that $P_{m,n} = 2Re[V_{m,n}I^*_{m,n}]$.)

All that now remains is the evaluation of the double integral in Eq. (A.17). Fortunately this is trivial for the case when hysteresis effects are excluded. Since q is periodic in both $\omega_1 t$ and $\omega_2 t$ with period 2π, the integrals over the range 0 to 2π will be identically equal to zero, as $v(q)$ is single-valued. The desired result for the power flow in a nonlinear reactance is thus

$$\sum_{m=0}^{\infty} \sum_{n=-\infty}^{\infty} \frac{mP_{m,n}}{mf_1 + nf_2} = 0. \quad \text{(A.21)}$$

In exactly the same manner, a second result can be obtained involving the index n instead of m.

$$\sum_{n=0}^{\infty} \sum_{m=-\infty}^{\infty} \frac{nP_{m,n}}{mf_1 + nf_2} = 0. \quad \text{(A.22)}$$

Bibliography

1. Adams, D. K., "An Analysis of Four-frequency Nonlinear Reactance Circuits," *IRE Trans. on Microwave Theory and Techniques*, Vol. MTT-8, pp. 274–283, May 1960.

2. Barrow, W. L., Smith, D. B., and Baumann, F. W., "A Further Study of Oscillatory Circuits Having Periodically Varying Parameters," *J. Franklin Inst.*, Vol. 221, pt. I, pp. 403–416; pt. II, pp. 509–529; March 1936.

3. Bateman, R., and Bain, W. F., "New Thresholds in VHF and UHF Reception, the World Below KTB," *QST*, Vol. 42, p. 30, December 1958.

4. Bateman, R., and Bain, W. F., "New Thresholds in VHF and UHF Reception, Devices and Diodes," *QST*, Vol. 43, p. 11, January 1959.

5. Bateman, R., and Bain, W. F., "New Thresholds in VHF and UHF Reception, Circuit Theory and Diode Details," *QST*, Vol. 43, pp. 28–35, February 1959.

6. Bateman, R., and Bain, W. F., "New Thresholds in VHF and UHF Reception, Practical Results," *QST*, Vol. 43, pp. 35–39, March 1959.

7. Bell, C. V., and Wade, G., "Circuit Considerations in Traveling-wave Parametric Amplifiers," *1959 IRE WESCON Convention Record*, pt. 2, pp. 75–82.

8. Bennett, W. R., "A General Review of Linear Varying Parameter and Nonlinear Circuit Analysis," *Proc. IRE*, Vol. 38, pp. 259–263, March 1950.

9. Bloom, S., and Chang, K. K. N., "Parametric Amplification Using Low-frequency Pumping," *J. Applied Phys.*, Vol. 29, p. 594, March 1958.

10. Bossard, B. B., "Superregenerative Reactance Amplifier," *Proc. IRE*, Vol. 47, pp. 1269–1271, July 1959.

11. Boyd, M. R., and Roe, G. M., "Parametric Energy Conversion in Distributed Systems," *Proc. IRE*, Vol. 47, pp. 1213–1218, July 1959.

12. Boyet, H., and Fleri, D., "A Method for Broadbanding Synchronism in Traveling-wave Parametric Devices," *Proc. IRE*, Vol. 48, pp. 1331–1333, July 1960.

13. Brand, F. A., Matthei, W. K., and Saad, T., "The Reactatron—A Low-noise Semiconductor Diode Microwave Amplifier," *Proc. IRE*, Vol. 47, pp. 42–44, January 1959.

14. Breitzer, D. I., and Sard, E. W., "Low Frequency Prototype Backward-wave Reactance Amplifier," *Microwave Journal*, Vol. 2, pp. 34–37, August 1959.

15. Bossard, B. B., Frost, E., and Fishbein, W., "X-Band Super-regenerative Parametric Amplifier," *Proc. IRE*, Vol. 48, pp. 1229–1230, July 1960.

16. Chang, K. K. N., "Harmonic Generation With Nonlinear Reactances," *RCA Rev.*, Vol. 19, pp. 455–464, September 1958.

17. Chang, K. K. N., "Four-terminal Parametric Amplifier," *Proc. IRE*, Vol. 47, pp. 81–82, January 1959.

18. Chang, K. K. N., "Analysis of a Four-terminal Parametric Amplifier," *RCA Rev.*, Vol. 20, pp. 205–221, June 1959.

19. Chang, N. C., "Parametric Amplification and Conversion in Propagating Circuits Using Nonlinear Reactances," *Proc. IRE*, Vol. 47, p. 2117, December 1959.

20. Chang, K. K. N., and Bloom, S., "Parametric Amplifier Using Lower-frequency Pumping," *Proc. IRE*, Vol. 46, pp. 1383–1386, July 1958.

21. Chang, K. K. N., and Bloom, S., "A Parametric Amplifier Using Lower-frequency Pumping," *1958 IRE WESCON Convention Record*, pt. 3, pp. 23–27.

22. Chang, K. K. N., and Bloom, S., "A Parametric Amplifier Using Lower-frequency Pumping," *Proc. IEE*, 105B (supplement 11), pp. 680–683, May 1958.

23. Clovier, P. A., "The Manley-Rowe Relations," *Proc. IRE*, Vol. 47, pp. 1781–1782, October 1959.

24. Cohen, Seymour, "Experimental Verification of Parametric Amplifier Excess Noise Using Transformer Coupling," *Proc. IRE*, Vol. 48, p. 108, January 1960.

25. Cohn, S. B., "The Noise Figure Muddle," *Microwave Journal*, Vol. 2, pp. 7, 9, 11, March 1959.

26. Conrad, G., Chang, K. K. N., and Hughes, R., "The Diode-loaded Helix as a Microwave Amplifier," *Proc. IRE*, Vol. 48, pp. 939–940, May 1960.

27. Cullen, A. L., "A Traveling-wave Parametric Amplifier," *Nature*, Vol. 181, p. 332, February 1, 1958.

28. Danielson, W. E., "Low Noise in Solid State Parametric Amplifiers at Microwave Frequencies," *J. Applied Phys.*, Vol. 30, pp. 8–16, January 1959.

29. DeLoach, B. C., "17.35 and 30 KMC Parametric Amplifiers," *Proc. IRE*, Vol. 48, p. 1323, July 1960.

30. DeLoach, B. C., and Sharpless, W. M., "An X-Band Parametric Amplifier," *Proc. IRE*, Vol. 47, p. 1664, September 1959.

31. DeLoach, B. C., and Sharpless, W. M., "X-Band Parametric Amplifier Noise Figure," *Proc. IRE*, Vol. 47, p. 2115, December 1959.

32. Drake, F. D., and Ewen, H. I., "A Broadband Microwave Source Comparison Radiometer for Advanced Research in Radio Astronomy," *Proc. IRE*, Vol. 46, pp. 53–60, January 1958.

33. Duinker, S., "General Properties of Frequency Converting Networks," *Phillips Research Repts.*, Vol. 13, pp. 37–78, February 1958, pp. 101–148, April 1958.

34. Edwards, C. E., "Frequency Conversion by Means of a Nonlinear Admittance," *Bell System Technical Journal*, Vol. 35, pp. 1403–1416, November 1956.

35. Endler, H., Berk, A. D., and Whirry, W. L., "Relaxation Phenomena in Diode Parametric Amplifiers," *Proc. IRE*, Vol. 47, pp. 1375–1376, August 1959.

36. Eng, S. T., and Solomon, R., "Frequency Dependence of the Equivalent Series Resistance for a Germanium Parametric Amplifier Diode," *Proc. IRE*, Vol. 48, p. 358, March 1960.

37. Engelbrecht, R. S., "Nonlinear-reactance (Parametric) Traveling-wave Amplifiers for UHF," *Digest of Technical Papers, 1959 Solid-State Circuits Conf., Philadelphia, Pa.*, February 12, 1959.

38. Engelbrecht, R. S., "A Low-noise Nonlinear Reactance Traveling-wave Amplifier," *Proc. IRE*, Vol. 46, p. 1655, September 1958.

39. Ewen, H. I., "A Thermodynamic Analysis of Maser Systems," *Microwave Journal*, Vol. 2, pp. 41–46, March 1959.

40. Faraday, M., "On a Peculiar Class of Acoustical Figures; and Certain Forms Assumed by a Group of Particles Upon Vibrating Elastic Surfaces," *Phil. Trans. Roy. Soc., London*, Vol. 121, pp. 299–318, May 1831.

41. Fisher, S. T., "Bandwidth of Lower Sideband Parametric Up-converters and Parametric Amplifiers," *Proc. IRE*, Vol. 48, p. 946, May 1960.

42. Fisher, S. T., "Theory of Single-resonance Parametric Amplifiers," *Proc. IRE*, Vol. 48, pp. 1227–1232, July 1960.

43. Fleri, D., and Sie, J., "The Effect of Parasitic Diode Elements on Traveling-wave Parametric Amplification," *Proc. IRE*, Vol. 48, pp. 1330–1331, July 1960.

44. Frost, A. D., "Parametric Amplifier Antenna," *Proc. IRE*, Vol. 48, pp. 1163–1164, June 1960.

45. Giacoletto, L. J., "Junction Capacitance and Related Characteristics Using Graded Impurity Semiconductors," *IRE Trans. on Electron Devices*, Vol. ED–4, pp. 207–214, July 1957.

46. Giacoletto, L. J., and O'Connell, J., "A Variable-Capacitance Germanium Diode for UHF," *RCA Rev.*, March 1956.

47. Greene, J. C., and Lombardo, P. P., "Low Noise 400-MC Reactance Amplifiers," *Microwave Journal*, Vol. 2, pp. 28–31, May 1959.

48. Harris, S. F., "The Parametric Amplifier," *CQ*, Vol. 14, p. 74, November 1958.

49. Hartley, R. V. L., "Oscillations in Systems With Nonlinear Reactance," *Bell System Technical Journal*, Vol. 15, pp. 424–440, July 1936.

50. Haus, H. A., "Power Flow Relations in Nonlinear Media," *IRE Trans. on Microwave Theory and Techniques*, Vol. MTT–3, pp. 317–324, July 1958.

51. Haus, H. A., and Adler, R. B., "Circuit Theory of Linear Noisy Networks," Technology Press and John Wiley & Sons, New York 1959.

52. Heffner, H., "Solid-state Microwave Amplifiers," *IRE Trans. on Microwave Theory and Techniques*, Vol. MTT-7, pp. 83–91, January 1959.

53. Heffner, H., and Kotzebue, K., "Experimental Characteristics of a Microwave Parametric Amplifier Using a Semiconductor Diode," *Proc. IRE*, Vol. 46, p. 1301, June 1958.

54. Heffner, H., and Wade, G., "Minimum Noise Figure of a Parametric Amplifier," *J. Applied Phys.*, Vol. 29, p. 1262, August 1958.

55. Heffner, H., and Wade, G., "Gain, Bandwidth, and Noise Characteristics of a Variable-parameter Amplifier," *J. Applied Phys.*, Vol. 29, pp. 1321–1331, September 1958.

56. Herrmann, G. F., Uenohara, M., and Uhlir, A., Jr., "Noise Figure Measurements on Two Types of Variable Reactance Amplifiers Using Semiconductor Diodes," *Proc. IRE*, Vol. 46, pp. 1301–1303, June 1958.

57. Heilmeier, G. H., "An Analysis of Parametric Amplification in Periodically Loaded Transmission Lines," *RCA Rev.*, Vol. 20, pp. 442–454, September 1959.

58. Heilmeier, G. H., "Millimeter Wave Generation by Parametric Methods," *Proc. IRE*, Vol. 48, p. 1326, July 1960.

59. Hilibrand, J., and Beam, W. R., "Semiconductor Diodes in Parametric Subharmonic Oscillators," *RCA Rev.*, Vol. 20, pp. 229–253, June 1959.

60. Hogg, D. C., "Effective Antenna Temperatures Due to Oxygen and Water Vapor in the Atmosphere," *J. Applied Phys.*, Vol. 30, pp. 1417–1418, September 1959.

61. Honey R. C., and Jones, E. M. T., "A Wide-band UHF Traveling-wave Variable Reactance Amplifier," *IRE Trans. on Microwave Theory and Techniques*, Vol. MTT-8, pp. 351–361, May 1960.

62. Houlding, N., "Low-noise Parametric Amplifier," *Proc. IRE*, Vol. 47, p. 2025, November 1959.

63. Hsiung, Hsu, "Multiple Frequency Parametric Devices," *Digest of Technical Papers, 1959 Solid-State Circuits Conf., Philadelphia, Pa.*, February 12, 1959.

64. Johnson, K. M., "Effect of a Generator or Load Mismatch on the Operation of a Parametric Amplifier," *Proc. IRE*, Vol. 48, pp. 1327–1328, July 1960.

65. Jones, E. M. T., and Honda, J. S., "A Low Noise Up-converter Parametric Amplifier," *1959 IRE WESCON Convention Record*, pt. 1, pp. 99–107.

66. Kaufman, I., and Douthett, D., "Harmonic Generation Using Idling Circuits," *Proc. IRE*, Vol. 48, p. 790, April 1960.

67. Kibler, L. U., "Directional Bridge Parametric Amplifier," *Proc. IRE*, Vol. 47, pp. 583–584, April 1959.

68. Kibler, L. U., "Parametric Oscillations With Point Contact Diodes at Frequencies Higher Than Pumping Frequencies," *Proc. IRE*, Vol. 48, p. 239, February 1960.

69. Kim, C. S., "Four-terminal Equivalent Circuits of Parametric Diodes," *1959 IRE WESCON Convention Record*, pt. 2, pp. 91–101.

70. Kita, S., and Fujii, T., "Microwave Amplification by Use of Crystal Diode," *Annual Convention Inst. of Elec. Commun. Engrs.*, Japan, October 1954.

71. Kita, S., "A Harmonic Generator by Use of the Nonlinear Capacitance of Germanium Diode," *Proc. IRE*, Vol. 46, p. 1307, June 1958.

72. Kotzebue, K. L., "Large-signal Characteristics of Three-frequency Cavity Parametric Amplifiers," *Digest of Papers, 1959 Solid-State Circuits Conf., Philadelphia, Pa.*, February 12, 1959.

73. Kotzebue, K. L., "Optimum Noise Performance of Parametric Amplifiers," *Proc. IRE*, Vol. 48, p. 1324, July 1960.

74. Klotzbaugh, G. A., "Phase Considerations in Degenerate Parametric Amplifier Circuits," *Proc. IRE*, Vol. 47, pp. 1782–1783, October 1959.

75. Knechtli, R. C. and Weglein, R. D., "Low-noise Parametric Amplifier," *Proc. IRE*, Vol. 47, pp. 584–585, April 1959.

76. Knechtli, R. C., and Weglein, R. D., "Low-noise Parametric Amplifier," *Proc. IRE*, Vol. 48, pp. 1218–1226, July 1960.

77. Kurokawa, K., and Hamasaki, J., "Mode Theory of Lossless Periodically Distributed Parametric Amplifiers," *IRE Trans. on Microwave Theory and Techniques*, Vol. MTT–7, pp. 360–365, July 1959.

78. Kurokawa, K., and Hamasaki, J., "An Extension of the Mode Theory to Periodically Distributed Parametric Amplifiers with Losses," *IRE Trans. on Microwave Theory and Techniques*, Vol. MTT–8, pp. 10–18, January 1960.

79. Landauer, R., "Parametric Amplification Along Nonlinear Transmission Lines," *J. Applied Phys.*, Vol. 31, pp. 479–484, March 1960.

80. Landauer, R., "Parametric Standing-wave Amplifiers," *Proc. IRE*, Vol. 48, pp. 1328–1329, July 1960.

81. Landon, V. D., "The Use of Ferrite Cored Coils as Converters, Amplifiers, and Oscillators," *RCA Rev.*, Vol. 10, pp. 387–396, September 1949.

82. Leenov, D., and Rood, J. W., "VHF Harmonic Generation With Silicon Diodes," *Proc. IRE*, Vol. 48, p. 1335, July 1960.

83. Leenov, D., "Gain and Noise Figure of a Variable-capacitance Up-converter," *Bell System Technical Journal*, Vol. 37, pp. 989–1008, July 1958.

84. Leenov, D., and Uhlir, A., "Generation of Harmonics and Subharmonics at Microwave Frequencies With P-N Junction Diodes," *Proc. IRE*, Vol. 74, pp. 1724–1729, October 1959.

85. Leeson, D. B., and Weinreb, S., "Frequency Multiplication With Nonlinear Capacitors—A Circuit Analysis," *Proc. IRE*, Vol. 47, pp. 2076–2084, December 1959.

86. Lombardo, P. P., "Low-noise 400 mc Reactance Amplifier," *Digest of Technical Papers, 1959 Solid-State Circuits Conf., Philadelphia, Pa.*, February 12, 1959.

87. Lombardo, P. P., and Sard, E. W., "Low-frequency Prototype Traveling-wave Reactance Amplifier," *Proc. IRE*, Vol. 47, pp. 995–996, May 1959.

88. Lombardo, P. P., and Sard, E. W., "Low-noise Microwave Reactance Amplifiers With Large Gain-bandwidth Products," *1959 IRE WESCON Convention Record*, pt. 1, pp. 83–98.

89. Lowell, R., and Kiss, J. J., "Solid-state Microwave Power Sources Using Harmonic Generation," *Proc. IRE*, Vol. 48, pp. 1334–1335, July 1960.

90. Macpherson, A. C., "An Analysis of the Diode Mixer Consisting of Nonlinear Capacitance and Conductance and Ohmic-Spreading Resistance," *IRE Trans. on Microwave Theory and Techniques*, Vol. MTT–5, pp. 43–51, January 1957.

91. Manley, J. M., "Some General Properties of Magnetic Amplifiers," *Proc. IRE*, Vol. 39, pp. 242–251, March 1951.

92. Manley, J. M., and Peterson, E., "Negative Resistance Effects in Saturable Reactor Circuits," *Trans. Am. Inst. Elec. Eng.*, Vol. 56, pp. 870–881, December 1946.

93. Manley, J. M., and Rowe, H. E., "Some General Properties of Nonlinear Elements—Part I, General Energy Relations," *Proc. IRE*, Vol. 44, pp. 904–913, July 1956.

94. Manley, J. M., and Rowe, H. E., "General Energy Relations in Nonlinear Reactances," *Proc. IRE*, Vol. 47, pp. 2115–2116, December 1959.

95. Mason, W. P., and Wick, R. F., "Ferroelectrics and the Dielectric Amplifier," *Proc. IRE*, Vol. 42, pp. 1606–1620; November 1954.

96. Matthaei, G. L., "A Study of the Optimum Design of Wideband Parametric Amplifiers and Up-converters," *PGMTT National Symposium*, Coronado, California, May 9–11, 1960.

97. Minorski, N., "On Parametric Excitation," *J. Franklin Inst.*, Vol. 240, pp. 25–46, July 1945.

98. North, H. Q., "Properties of Welded Contact Germanium Rectifiers," *J. Applied Phys.*, Vol. 19, pp. 912–923, November 1946.

99. Mumford, W. W., "Some Notes on the History of Parametric Transducers," *Proc. IRE*, Vol. 48, pp. 847–853, May 1960.

100. Nergaard, L. S., "Nonlinear-capacitance Amplifiers," *RCA Rev.*, Vol. 20, pp· 3–17, March 1959.

101. Oguchi, B., Kita, S., Inage, N., and Okajima, T., "Microwave Parametric Amplifier by Means of Germanium Diode," *Proc. IRE*, Vol. 47, pp. 77–78, January 1959.

102. Olson, F. A., and Wade, G., "A Cavity-type Parametric Circuit as a Phase-distortionless Limiter," *PGMTT National Symposium*, Coronado, California, May 9–11, 1960.

103. Olson, F. A., Wang, C. P., and Wade, G., "Parametric Devices Tested for Phase-distortionless Limiting," *Proc. IRE*, Vol. 47, pp. 587–588, April 1959.

104. Page, C. H., "Frequency Conversion With Nonlinear Reactances," *J. Research Natl. Bur. Standards*, Vol. 58, pp. 227–236, May 1957.

105. Pettai, R., Bossard, B., and Weisbaum, S., "Single-diode Parametric Up-converter With Large Gain-bandwidth Products," *Proc. IRE*, Vol. 48, p. 1323, July 1960.

106. Peterson, L. C., and Llewellyn, F. B., "The Performance and Measurements of Mixers in Terms of Linear Network Theory," *Proc. IRE*, Vol. 33, pp. 458–476, July 1945.

107. Pierce, J. R., "Use of the Principle of Conservation of Energy and Momentum in Connection with the Operation of Wave-type Parametric Amplifiers," *J. Applied Phys.*, Vol. 30, pp. 1341–1346, September 1959.

108. Pittman, W. C., "A Parametric Amplifier in Space-probe Tracking," *Astronautics*, Vol. 4, pp. 40, 44, August 1959.

109. Pound, R. V., "Microwave Mixers," *M.I.T. Rad. Lab. Ser.*, McGraw-Hill Book Co., Inc., New York, N. Y., Vol. 16, 1948.

110. Reed, E. D., "The Variable Capacitance Parametric Amplifier," *IRE Trans. on Electron Devices*, Vol. ED–6, pp. 216–224, April 1959.

111. Rowe, H. E., "Some General Properties of Nonlinear Elements—Part II, Small-signal Theory," *Proc. IRE*, Vol. 46, pp. 850–860, May 1958.

112. Salzberg, B., and Sard, E. W., "Low-noise Wide-band Reactance Amplifier," *Proc. IRE*, Vol. 46, p. 1303, June 1958.

113. Sard, E. W., "Analysis of a Negative Conductance Amplifier Operated With a Non-ideal Circulator," *IRE Trans. on Microwave Theory and Techniques*, Vol. MTT–7, pp. 288–294, April 1959.

114. Seidel, H., and Herrmann, G. E., "Circuit Aspects of Parametric Amplifiers," *1959 IRE WESCON Convention Record*, pt. 2, pp. 83–90.

115. Shafer, C. G., "Noise Figure for a Traveling-wave Parametric Amplifier of the Coupled-mode Type," *Proc. IRE*, Vol. 47, pp. 2117–2118, December 1959.

116. Shunaman, F., "The Variable Reactance Amplifier," *Radio Electronics*, Vol. 30, pp. 78–80, 82, February 1959.

117. Sie, J., and Weisbaum, S., "Noise Figure of Receiver Systems Using Parametric Amplifiers," *1959 IRE National Convention Record*, pt. 3, pp. 141–157.

118. Siegel, K., "Anomalous Reverse Current in Varactor Diodes," *Proc. IRE*, Vol. 48, p. 1159, June 1960.

119. Solomon, A. H., and Sterzer, F., "A Parametric Sub-harmonic Oscillator Pumped at 34.3 KMC," *Proc. IRE*, Vol. 48, p. 1322, July 1960.

120. Sterzer, F., "Microwave Parametric Subharmonic Oscillators for Digital Computing," *Proc. IRE*, Vol. 47, pp. 1317–1324, August 1959.

121. Stevens, K. W. H., "Circuit Analogues of Suhl-Type Masers," *Journal of Electronics and Control*, Vol. 4, pp. 275–279, March 1958.

122. Stockman, H. E., "Parametric Oscillatory and Rotary Motion," *Proc. IRE*, Vol. 48, pp. 1157–1158, June 1960.

123. Strutt, J. W., Lord Rayleigh, "On The Crispations of Fluid Resting Upon a Vibrating Support," *Phil. Mag.*, vol. 16, pp. 50–53; July 1883.

124. Strutt, J. W., Lord Rayleigh, "On the Maintenance of Vibrations by Forces of Double Frequency, and on the Propagation of Waves Through a Medium Endowed with a Periodic Structure, *Phil. Mag.*, Ser. 5, Vol. 24, pp. 145–159, August 1887.

125. Suhl, H., "Proposal for a Ferromagnetic Amplifier in the Microwave Range," *Phys. Rev.*, Vol. 106, pp. 384–385, April 15, 1957.

126. Sutherland, A. D., and Countiss, D. E., "Parametric Phase Distortionless L-band Limiter," *Proc. IRE*, Vol. 48, p. 938, May 1960.

127. Tien, P. K., "Parametric Amplification and Frequency Mixing in Propagating Circuits," *J. Applied Phys.*, Vol. 29, pp. 1347–1357, September 1958.

128. Tien, P. K., and Suhl, H., "A Traveling-wave Ferromagnetic Amplifier," *Proc. IRE*, Vol. 46, pp. 700–706, April 1958.

129. Torrey, H. C., and Whitmer, C. A., "Crystal Rectifiers," *M.I.T. Radiation Lab. Series*, McGraw-Hill Book Co., Inc., New York, N. Y., Vol. 15, 1948.

130. Uenohara, M., and Bakanowski, A. E., "Low-noise Parametric Amplifier Using Germanium *p-n* Junction Diode at 6 kmc, *Proc. IRE*, Vol. 47, pp. 2113–2114, December 1959.

131. Uenohara, M., and Sharpless, W. M., "An Extremely Low-noise 6 KMC Parametric Amplifier Using Gallium Arsenide Point-contact Diodes," *Proc. IRE*' Vol. 47, pp. 2114–2115, December 1959.

132. Uenohara, M., "Noise Considerations of the Variable Capacitance Parametric Amplifier," *Proc. IRE*, Vol. 48, pp. 169–179, February 1960.

133. Uhlir, A., Jr., "Junction Diodes in Microwave Circuits," *Proc. IEE*, 105B (Supplement 11), pp. 661, 672, 673, May 1958.

134. Uhlir, A., Jr., "The Potential of Semiconductor Diodes in High-frequency Communications," *Proc. IRE*, Vol. 46, pp. 1099–1115, June 1958.

135. Uhlir, A., Jr., "Shot Noise in *p-n* Junction Frequency Converters," *The Bell System Technical Journal*, Vol. 37, pp. 951–987, July 1958.

136. Uhlir, A., Jr., "Junction Diode Amplifiers," *Scientific American*, Vol. 200, pp. 118 ff., June 1959.

137. Valdes, L. B., "Circuit Conditions for Parametric Amplification," *J. Electron. and Control*, Vol. 5, pp. 129–141, August 1958.

138. Van der Pol, B., "Nonlinear Theory of Electric Oscillations," *Proc. IRE*, Vol. 22, pp. 1051–1086, September 1934.

139. van der Ziel, A., "On the Mixing Properties of Nonlinear Capacitances," *J. Applied Phys.*, Vol. 19, pp. 999–1006, November 1948.

140. van der Ziel, A., "Noise Figure of Reactance Converters and Parametric Amplifiers," *J. Applied Phys.*, Vol. 30, p. 1449, September 1959.

141. van der Ziel, A., and Tamiya, J., "Note on the Noise Figure of Negative Conductance Amplifiers," *Proc. IRE*, Vol. 48, p. 796, April 1960.

142. Wade, G., and Heffner, H., "Microwave Parametric Amplifiers and Converters," *Proc. IEE*, 105B, (supplement 11) pp. 667–679, May 1958.

143. Waltz, M. C., "A Technique for the Measurement of Microwave Impedance in the Junction Region of a Semiconductor Device," *Microwave Journal*, Vol. 2, No. 5, pp. 23–27, May 1959.

144. Warren, T. B., "Low-noise Parametric Amplifiers and Converters," *1959 IRE National Convention Record*, pt. 3, p. 158.

145. Weber, S., "The MAVAR: A Low-noise Microwave Amplifier," *Electronics*, Vol. 31, pp. 65–71, September 26, 1958.

146. Weger, E., "Apparent Thermal Noise Temperatures in the Microwave Region," *IRE Trans. on Antennas and Propagation*, Vol. AP–8, pp. 213–217, March 1960.

147. Weiss, M. T., "A Solid-state Microwave Amplifier and Oscillator Using Ferrites," *Phys. Rev.*, Vol. 107, p. 317, July 1957.

148. Weiss, M. T., "Quantum Derivation of Energy Relations Analogous to Those for Nonlinear Reactances," *Proc. IRE*, Vol. 45, pp. 1012–1013, July 1957.

149. Wolf, A. A., and Pippen, J. E., "A Passive Parametric Limiter," *Digest of Technical Papers, 1960 Solid-State Circuits Conference, Philadelphia, Pa.*, February 10–12, 1960.

150. Younger, J. J., Little, A. G., Heffner, H., and Wade, G., "Parametric Amplifiers as Superregenerative Detectors," *Proc. IRE*, Vol. 47, pp. 1271–1272, July 1959.

151. Younger, J. J., Little, A. G., Heffner, H., and Wade, G., "Superregenerative Operation of Parametric Amplifiers," *1959 IRE WESCON Convention Record*, pt. 1, pp. 108–111.

Index

Copy 2